

# **Gas Phase Infrared Spectra of some PAHs and Diols: Experiment and Theory**

A Thesis

Submitted for the Degree of

*Doctor of Philosophy*

In the Faculty of Science

by

**Prasanta Das**



**Department of Inorganic and Physical Chemistry**

**Indian Institute of Science**

**Bangalore - 560012, INDIA**

**July 2010**

*Dedicated to*  
*My Parents*

## **STATEMENT**

I hereby declare that the research work described in this thesis is the result of investigation carried out by me in the Department of Inorganic and Physical Chemistry, Indian Institute of Science, Bangalore, India, under the supervision of **Prof. Puspendu K. Das and Prof. E. Arunan.**

In keeping with the general practice of reporting scientific observations, due acknowledgements have been made wherever the work described in this thesis is based on the findings of other investigators. Any omission that might have occurred due to oversight or error is regretted.

**July, 2010**




**Prasanta Das**

**Department of Inorganic and Physical Chemistry  
Indian Institute of Science, Bangalore-560012**

# **CERTIFICATE**

This is to certify that the work presented in the thesis titled “**Gas Phase Infrared Spectra of some PAHs and Diols: Experiment and Theory**” has been carried out by Mr. Prasanta Das under our supervision and the same has not been submitted elsewhere for a degree.



**Prof. Puspendu K. Das**



**Prof. E. Arunan**

**P. K. Das**  
Professor  
Department of Inorganic & Physical Chemistry  
Indian Institute Of Science  
Bangalore - 560 012, India

**E. ARUNAN**  
Professor  
Dept. of Inorganic and Physical Chemistry  
Indian Institute of Science  
BANGALORE-560 012

## **ACKNOWLEDGEMENT**

It is a great pleasure to express my gratitude and words of appreciation to the people who have been the source of help, inspiration and encouragement.

I express my heartfelt gratitude to Prof. Puspendu K. Das and Prof. E. Arunan for giving me an opportunity to work in their groups. I thank them for their guidance and enormous freedom they have given me to work independently. I particularly appreciate Prof. Puspendu K. Das's efforts throughout the tenure of my stay to help grow scientific inquisitiveness and analytical thinking in me. His extreme co-operation and patience, particularly, during the preparation of manuscripts is deeply appreciated. I also thank Prof. E. Arunan for valuable discussions and help in data analysis. It has been a good learning experience to work with them.

I am thankful to Prof. K. P. J. Reddy in the Department of Aerospace Engineering for allowing me to use the FT-IR spectrometer in initial days in his laboratory and for providing the lab facility. I am thankful to Prof. S. Monogaran in the Department of Chemistry at Indian Institute of Technology, Kanpur for educating me on vibrational spectra analysis and providing me the modified version of UMAT program in the QCPE package. I thank the past and present chairman Prof. A. R. Chakravarthy, Prof. K. L. Sebastian and Prof. A. G. Samuelson of the IPC Dept. for providing the necessary facilities in the department. I thank Prof. S. Umapathy, Prof. K. L. Sebastian and the students of Chemical Dynamics Group for all the stimulating and rigorous discussions in our Saturday group meetings.

I thank all the supporting staff of the IPC office and workshop for their help whenever needed. Special thanks to Mr. Logonathan, Mr. Thomas, and Mr. Samuel for their prompt help during the hours of urgent need. I also thank Mr. Ashoka in the Department of Aerospace

Engineering for his cooperation to make detachable gas cell and cell holder for multi-pass long-path gas cell in the initial days.

I thank Mr. Kiran (SERC) and Prof. Jemmis's group for their help to carry out the calculations in SERC. I thank Dr. Amit Pathak for many helpful discussions and for teaching me about the Linux operating system and latex software. I take this opportunity to thank Mr. Morrison of Laser Spectra Services, Mr. Sandip Maiti of GE, and Mr. Surendra from Optoelectronics for their prompt services.

I thank all my senior labmates, Dr. Dulal Senapati, Dr. A. Sri Ranjini, Dr. Pankaj Mandal, Dr. Mily Bhattacharya, Dr. Sampa Ghosh, Dr. Manabendra Chandra, Dr. Mousumi Goswami, Dr. Abdul Wahab, and Dr. M. Britto Dhas from whom I have learned many things in my initial days. Special thanks to Mily, Sampa and Manabendra for their critical suggestions and remarks which added value to my work. I am indebted to all my juniors Ravindra, Harish, Soumi, Debendra, Shubhadip, Manisha, and Abhishek for their immense help and cooperation to maintain a friendly environment in the lab. The valuable academic discussions with them, apart from my own project, have greatly enriched my science and life. I appreciate their every effort to help me in my experiments, in my work presentations and in preparation of this thesis.

I thank my batchmates Dipak, Sangeeta, Aiswarya, Musthafa, Ramkumar, Debojoyti, Sovan, Mithun, Deepa, Vikrant, Viswanathan, and Akshay for the time I have spent with them in various academic and nonacademic associations. I thank all my friends in IISc, Nupur, Anirudha and Paromita (CES), Pijus, Krishna, Moinak (MCBL), Joydeep (OC), Chakravarty (BC), Rekha, Puja, Pallavi, Sanchari (MBU) for many memorable moments I spent with them.

I express my deep sense of gratitude to a set of very special people in my life, without whose guidance, encouragement and moral support it would have been impossible for me to reach IISc. They are Mr. Gouranga Sasmal (my neighbor, uncle), Dr. Chittaranjan Das (one of my relatives), Dr. Dulal Maity and Panchanan Pandit (my chemistry and physics teachers from school), Prof. S. K. Sengupta, Prof. Lal Bahadur and Prof. R. A. Singh (my university teachers).

Words are less to thank my parents whose sacrifice, support, encouragement and love have made me going. I also thank my brother, sister, sister-in-law, brother-in-law, one nephew and a niece for their love and affection.

# Thesis Synopsis

In this thesis, I report the gas phase infrared spectra of some polycyclic aromatic hydrocarbons (PAHs) namely 1, 5-, 1, 6-, and 2, 6-dimethyl naphthalenes (DMNs); 2, 4-, 2, 6-, 2, 7-, and 2,8-dimethyl quinolines (DMQs); and 1, 9-, 2, 4-, and 3, 9-dimethyl phenanthrenes (DMPs) and diols such as 1, 2-ethylene glycol (1,2-EG) and 1, 4-butanediol (1,4-BD). Assignment of the IR spectra has been done with the help of DFT calculations followed by scaled quantum mechanical force field calculations.

*Chapter 1* gives a brief introduction to PAHs and diols. A brief survey of literature pertinent to their sources, their importance, experimental techniques for identification of PAHs and different conformers of diols and intramolecular interactions between the two hydroxyl groups in the diols are presented. The scope and motivation of the present investigation have been described at the end of the chapter.

*In Chapter 2*, I have discussed all the methods used in carrying out this work. The details of the experimental FT IR set-up and quantum-chemical calculations employed in this work have been elaborated in this chapter.

The subsequent chapters 3 - 5 deal with the experimental and theoretical results obtained for DMNs, DMQs, and DMPs. *In chapter 3*, infrared spectra of 1,5-, 1,6-, and 2,6-DMN have been described. The spectra have been recorded using a multi-pass gas cell coupled with Nexus-870 spectrometer (Thermonicolet, US). Qualitatively, spectral assignments have been made with the help of calculated doubly scaled (one scaling factor for the C-H stretching and another factor for the non C-H stretching frequencies) harmonic frequencies at the B3LYP/6-31G\* level of theory. The spectral features to distinguish three different isomers of DMN have



been identified. *In chapter 4*, IR spectra of 2,4-, 2,6-, 2,7-, and 2,8-DMQ in the gas phase have been recorded using a high resolution Vertex-70 (Bruker Optics, Germany) FT-IR spectrometer. DFT calculations have been carried out in order to get harmonic and anharmonic frequencies and their intensities at the B3LYP/6-31G\* level of theory. Unambiguous assignments of IR bands could not be made with the help of anharmonic or selectively scaled harmonic frequencies. Therefore, scaled quantum mechanical (SQM) force field calculations were performed where force fields in local coordinates were scaled for getting frequencies in close agreement with experiment. Potential energy distributions (PEDs) of the normal modes in terms of the local coordinates of the molecule using a modified UMAT program in the QCPE package were also obtained in order to identify the nature of the fundamental vibration modes. *In chapter 5*, I have presented the gas phase IR spectra of 1,9-, 2,4-, and 3,9-DMP. The harmonic and anharmonic frequencies and their intensities were obtained at the B3LYP/6-31G\* and B3LYP/6-311G\*\* levels of theory. I have carried out SQM calculations for the assignment of the experimental frequencies in a similar fashion as was done for the DMQs.

*In chapter 6*, IR spectra of two diols namely 1,2-ethylene glycol and 1,4-butane diol are reported and discussed. DFT calculations have been carried out for the harmonic fundamental frequencies and intensities at the experimental temperatures with 10 unique chosen conformers of the diols at the B3LYP/6-311++G\*\* level of theory. Gas phase equilibrium population analysis has been done in order to generate the theoretical spectrum with the weighted average contributions from the 10 conformers to match the experimental spectrum. The hydrogen bond enthalpy, strength and nature have been investigated in details. From this experimental and theoretical studies, it has been concluded that the intramolecular hydrogen bond is absent in 1,2-EG at ordinary temperatures whereas it is present in 1,4-BD.

*Chapter 7* is the concluding chapter where the main work done in this thesis is summarized and future direction is presented.

# Table of Contents

Acknowledgement	i
Thesis Synopsis	v
Table of Contents	ix
List of Abbreviations	xiii
<b>Chapter 1 An Introduction to PAHs, Diols and Infrared Spectroscopy</b>	<b>1</b>
1.1 Introduction	3
1.1.1 Definition of PAHs and Diols	3
1.1.2 Sources and importance of PAHs	3
1.1.3 Diols and intramolecular hydrogen bonding	5
1.2 Experimental techniques for identification of PAHs	5
1.3 Experimental techniques for the conformational analysis and characterization of hydrogen bonding in diols	6
1.4 Infrared Spectroscopy	7
1.5 Infrared Spectroscopy of PAHs and Diols	10
1.6 Scope and motivation of this thesis work	13
1.7 References	15
<b>Chapter 2 Methods: Experimental and Theoretical</b>	<b>23</b>
2.1 Introduction	25
2.2 Experimental technique	25
2.2.1 Principle of FT-IR spectrometry: Michelson interferometer	25
2.2.2 Continuous-Scan Interferometry	27
2.2.3 Variable Path-length Long Path Gas Cell	28
2.3 Experimental set-up	29
2.3.1 Set-up for PAHs and diols	29
2.3.2 Standardization of multi-pass gas cell of 7.2 meter path-length coupled with Nexus-870 (Thermonicolet, US) spectrometer	32
2.3.3 Standardization of the multi-pass gas cell of 8.0 meter coupled with	34

	Vertex-70 (Bruker Optics, Germany) spectrometer	
2.4	Theoretical methods	36
2.4.1	Harmonic and anharmonic frequency calculations	36
2.4.2	Scaled quantum mechanical (SQM) force field calculation	37
2.4.3	Error analysis	39
2.5	IR band intensity calculation	40
2.5.1	Intensity	40
2.5.2	Vapor pressure calculation	41
2.6	Simulated spectra	41
2.7	References	42
<b>Chapter 3</b>	<b>Infrared Spectroscopic Studies of Dimethylnaphthalenes (DMNs) in the Gas Phase</b>	<b>45</b>
3.1	Introduction	47
3.2	Materials and methods	47
3.2.1	Materials	47
3.2.2	Experimental method	48
3.2.3	Theoretical calculation	48
3.2.4	Vapor pressure and absolute intensity calculation	50
3.3	Results and discussion	52
3.4	Conclusion	65
3.5	References	67
<b>Chapter 4</b>	<b>Infrared Spectra of Dimethylquinolines (DMQs) in the Gas Phase: Experiment and Theory</b>	<b>69</b>
4.1	Introduction	71
4.2	Experimental: Materials and Methods	72
4.2.1	Materials	72
4.2.2	Methods	72
4.3	Theoretical calculation	73

4.3.1	Harmonic and anharmonic calculation	73
4.3.2	Force field calculation	73
4.4	Results and discussion	79
4.4.1	C-H stretching Vibrations	81
4.4.2	Non C-H stretching Vibrations	82
4.4.3	Non-fundamental bands	96
4.5	Conclusion	98
4.6	References	100
<b>Chapter 5</b>	<b>An Experimental and Theoretical investigation of Infrared Spectra of Dimethylphenanthrenes (DMPs) in the Gas Phase</b>	<b>103</b>
5.1	Introduction	105
5.2	Experimental section	106
5.2.1	Materials	106
5.2.2	Methods	106
5.3	Theoretical calculation	107
5.4	Results and discussion	112
5.4.1	Spectral region of 2800 – 3200 cm <sup>-1</sup>	113
5.4.2	Spectral region 1700 – 2800 cm <sup>-1</sup> : Non-fundamental bands	127
5.4.3	Spectral region 1200 – 1700 cm <sup>-1</sup>	129
5.4.4	Spectral region 500 – 1200 cm <sup>-1</sup>	132
5.5	Conclusion	136
5.6	References	137
<b>Chapter 6</b>	<b>Is there Intramolecular Hydrogen Bonding in Diols? An FT-IR and DFT investigation</b>	<b>139</b>
6.1	Introduction	141
6.2	Experimental section	142
6.3	Computational methods	142
6.4	Results and discussion	145

6.4.1	Gas phase infrared spectra of 1,2-EG and 1,4-BDO	145
6.4.2	Population analysis	147
6.4.3	Identification of conformers	150
6.4.4	Estimation of the hydrogen bond energy	155
6.4.5	Nature of hydrogen bond in diols	158
6.5	Conclusion	162
6.6	References	163
<b>Chapter 7</b>	<b>Concluding remarks and future directions</b>	<b>165</b>
7.1	Concluding remarks	167
7.2	Future Directions : Photochemistry of PAHs and time-resolved FT-IR spectroscopy	167
<b>Appendix:</b>	<b>Symbolic Force constant matrix, unscaled and scaled Force constants in terms of nonredundant local coordinates</b>	<b>171</b>

## List of Abbreviations

<b>BCP</b>	: <b>Bond Critical Point</b>
<b>BD</b>	: <b>Butanediol</b>
<b>BO</b>	: <b>Born Oppenheimer</b>
<b>BS</b>	: <b>Beamsplitter</b>
<b>D</b>	: <b>Detector</b>
<b>DFT</b>	: <b>Density Functional Theory</b>
<b>DMN</b>	: <b>Dimethyl naphthalene</b>
<b>DMP</b>	: <b>Dimethyl phenanthrene</b>
<b>DMQ</b>	: <b>Dimethyl quinoline</b>
<b>DTGS</b>	: <b>Deuterated Triglycine Sulfate</b>
<b>EG</b>	: <b>Ethylene glycol</b>
<b>ESI-MS</b>	: <b>Electrospray Ionization Mass Spectrometry</b>
<b>FT-IR</b>	: <b>Fourier Transform Infrared Spectroscopy</b>
<b>GC-FID</b>	: <b>Gas chromatography with flame ionization detection</b>
<b>GC-MS</b>	: <b>Gas Chromatography Mass Spectrometry</b>
<b>HB</b>	: <b>Hydrogen bond</b>
<b>HPLC</b>	: <b>High performance liquid chromatography</b>
<b>IHB</b>	: <b>Intramolecular hydrogen bonding</b>
<b>InSb</b>	: <b>Indium Antimonide</b>
<b>IDP</b>	: <b>Interplanetary dust particles</b>
<b>LD</b>	: <b>Laser Detector</b>

**LN - MCT** : Liquid N<sub>2</sub> cooled Mercury Cadmium Telluride

**MCT** : Mercury Cadmium Telluride

**MMP** : Mono-methyl phenanthrene

**MN** : Methyl naphthalene

**MQ** : Methyl quinoline

**NBO** : Natural Bond Orbital

**NMR** : Nuclear Magnetic Resonance

**OPL** : Optical path lengths

**PAH:** : Polycyclic Aromatic Hydrocarbon

**PD** : Propanediol

**PED** : Potential energy distribution

**QCPE** : Quantum Chemistry Program Exchange

**QDMC** : Quantum Diffusion Monte Carlo

**UHP** : Ultra High Pure

**UIR** : Unidentified Infrared

**UV** : Ultraviolet

**SQM** : Scaled Quantum Mechanical

**TMQ** : Tri-methyl quinoline

**ZPVE** : Zero point vibrational energy



# **Chapter-1**

## **An Introduction to PAHs, Diols and Infrared Spectroscopy**

## **1.1 Introduction**

### **1.1.1 Definition of PAHs and diols**

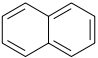
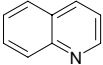
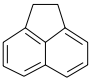
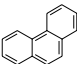
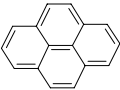
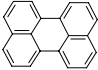

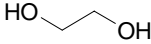
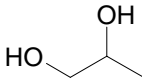
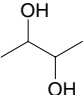
Polycyclic aromatic hydrocarbons (PAHs) are a family of aromatic compounds containing more than one benzene or heterocyclic (O, N, S) benzene rings whereas diols belongs to a class of compounds containing two hydroxyl groups separated by a  $(-CH_2-)_n$  (where  $n=2, 3, 4, \dots$ ) backbone. Methylated polycyclic aromatic compounds belong to the PAHs. A few representative structures and some physical properties of PAHs<sup>1a,b</sup> and diols<sup>2</sup> are listed in Table 1.1.

### **1.1.2 Sources and importance of PAHs**

There are several sources which are responsible for the presence of PAHs in the gas phase and in particulates in the atmosphere. These hydrocarbons are mostly formed during incomplete combustion and pyrolysis of fossil fuels or wood, and petroleum products. Terrestrial sources of PAHs are from non-anthropogenic burning of forests, woodland and moorland due to lightning strikes, and volcanic eruptions.<sup>3,4</sup> Furthermore, some cosmic sources such as carbonaceous chondrites, which originate in the main asteroid belt, have also been proposed.<sup>5a-c</sup> Other sources of PAHs include petroleum spills, oil seepage, and organic matter in anoxic sediments. In general, there are five major emission sources of PAHs i.e., domestic,<sup>6,7</sup> mobile,<sup>8a-d</sup> industrial,<sup>9a-d</sup> agricultural,<sup>10a-c</sup> and natural. PAHs are the most stable hydrocarbons present in atmosphere in the gas phase (containing 2 - 3 rings) or as particulate matters (containing more than 4 rings). PAHs having two to three rings show higher vapor pressures at room temperature compared to their higher analogs (see Table 1.1).

*Chapter 1: An Introduction to PAHs, Diols and Infrared Spectroscopy*

**Table 1.1: Structure and vapor pressure of a few representative PAHs and Diols**

Name of PAHs and Diols	Structure	P(mmHg) @25 °C
1. Naphthalene		$7.80 \times 10^{-2}$
2. Quinoline		$9.12 \times 10^{-2}$
3. Acenaphthene		$2.10 \times 10^{-3}$
4. Phenanthrene		$1.20 \times 10^{-4}$
5. Pyrene		$4.50 \times 10^{-6}$
6. Perylene		$4.12 \times 10^{-9}$
7. Coronen		$2.51 \times 10^{-12}$
8. Ethanediol		$*6.0 \times 10^{-2}$
9. Propan-1,2-diol		$12.9 \times 10^{-2}$
10. Butane-2,3-diol		$26.0 \times 10^{-2}$

**\*Vapor pressure at 20 °C.**

PAHs are known to be carriers of unidentified IR band (UIR) in the interstellar medium (ISM).<sup>11</sup> Many are carcinogenic,<sup>12,13</sup> mutagenic,<sup>14,15</sup> toxic,<sup>13,16</sup> and hence cause health hazard to human being and aquatic lives. Some of them are used in medicine or to make dyes, plastics

and pesticides.<sup>17a-e</sup> Therefore, it is necessary to identify/distinguish them and find out some way of removal from the lower and upper atmospheres.

### **1.1.3 Diols and intramolecular hydrogen bonding**

Diols exist in a mixture of conformers with several possibilities of intramolecular and intermolecular interactions between the two hydroxyl groups depending on the temperature and the physical state. The extent of the latter kind of interaction is dependent on the concentration of the compound, while the former is concentration independent. Intramolecular hydrogen bonding is particularly sensitive to changes in the molecular geometry.

Ethandiol or 1,2-ethylene glycol (1,2-EG) is one of the simplest molecules with two vicinal hydroxyl groups which serves as a simple model for understanding the influence of hydrogen bonding on the conformation of biological molecules such as sugars. In EG, the intramolecular hydrogen bond (IHB) conformation will form a five-member quasi-ring. The hydrogen bond angle in such a five member ring is far from an optimal  $180^\circ$  and thus the hydrogen bond is expected to be weak. On the otherhand, butanediol isomers are compound with numerous applications in biochemical fields such as protein-stabilizing agents. Butane-1,4-diol or 1,4-butanediol (1,4-BD) represents an interesting diol with many possibilities of intramolecular interactions between the two hydroxyl groups.

## **1.2 Experimental techniques for identification of PAHs**

Many experimental techniques have been employed for the separation and identification of PAHs in a complex mixture. The GC/MS spectrometry is one of the popular techniques

## *Chapter 1: An Introduction to PAHs, Diols and Infrared Spectroscopy*

---

which has been used for the analysis of PAHs. Gas chromatography with flame ionization detection (GC-FID) and GC-MS has been used for the qualitative and quantitative analysis of PAHs in cigarette smoke,<sup>18</sup> diesel engine soot,<sup>8c,19</sup> synthetic fuel,<sup>20</sup> coke oven and wood combustion,<sup>21</sup> biodiesel,<sup>22,23</sup> coal derived liquid,<sup>24</sup> and in sugar cane soot.<sup>25</sup> Furthermore, high-performance liquid chromatographic (HPLC) and GC-MS have been employed for the separation and identification of PAHs.<sup>26</sup> Identification of PAHs has been done by the Programmed-Temperature Capillary-Column Gas Chromatography technique.<sup>27,28</sup> Bate et al. reported the analysis of particle bound PAHs with the help of a Thermal Desorption (TD) – GC/MS technique.<sup>29</sup> In 2004, Porter et al. used Electrospray Ionization Mass Spectrometry (ESI-MS) for the analysis of petroleum resins.<sup>30</sup> Recently, mars organic analyzer microchip capillary electrophoresis system has been used by Stockton et al. for the analysis of PAHs.<sup>31</sup> In addition to mass spectrometric techniques, FT-IR spectroscopy has been used by Wornat et al. for the analysis of substituted PAHs present in bituminous coal.<sup>32</sup> GC/FT-IR & GC/FT-IR/MS techniques have also been employed for the isomeric identification of PAHs.<sup>33a-c</sup> IR spectroscopic identification and discrimination of PAHs will be presented separately below.

### **1.3 Experimental techniques for the conformational analysis and characterization of hydrogen bonding in diols**

In section 1.1.3, I have discussed that diols exist in a mixture of conformers. Whether or not 1,2-EG form an IHB has large significance since this molecule has been used as a part of the training set for parametrizing molecular mechanics programs.<sup>34</sup> It is used in pharmacologically active materials<sup>35</sup> and in polymer synthesis.<sup>36</sup> In the past, structure of diols

## *Chapter 1: An Introduction to PAHs, Diols and Infrared Spectroscopy*

---

including 1,2-EG and 1,4-BD in the gas, liquid and solid phases have been studied extensively by different experimental methods such as x-ray<sup>37a,b</sup> and electron diffractions<sup>38a,b</sup> and microwave,<sup>39a-d</sup> NMR<sup>40a-c</sup> and FT-IR<sup>41a,b</sup> spectroscopy. The electron and x-ray diffraction studies on 1,2-EG indicate that the *gauche* conformer is considerably more stable than the *trans* in the gas phase<sup>38b</sup> because of the presence of the H-bonding in the *gauche* conformer. The NMR investigation of 1,2-EG by Roberts and co-workers led the authors to conclude that “the bulk of the NMR evidence indicates that intramolecular hydrogen bonding between the hydroxyl groups is unlikely to be a significant factor in determining that preference, except possibly in fairly non-polar solvents. The ‘*gauche* effect’ is clearly very important, especially in aqueous solution”.<sup>40c</sup> Recent X-ray crystallographic studies on crystalline 1,2-EG suggests that the intramolecular hydrogen bond (IHB) does not exist in this molecule.<sup>42</sup> IR spectroscopy is one of the simple methods for the identification and characterization of hydrogen bonding. Generally, hydrogen bonding manifests in a red shift of the X-H-stretching frequency. For the hydroxyl group, increase in the IR band intensity and a red-shift of the O–H stretching frequency are spectroscopic signatures of hydrogen bond formation. The magnitude of both the intensity and frequency shift increase with increasing hydrogen bond strength.<sup>43</sup> Since IR spectroscopy has been widely used for studying the IHB in diols, it will be discussed separately below.

### **1.4 Infrared spectroscopy**

Infrared spectroscopy is a branch of spectroscopy that deals with the interaction of molecules with infrared radiation. IR spectra result from the transitions between two quantized

## *Chapter 1: An Introduction to PAHs, Diols and Infrared Spectroscopy*

---

vibrational energy states in a molecule. Molecular vibrations can range from the simple coupled motion of two atoms in a diatomic molecule to the much more complex motion of many atoms in a large polyatomic molecule. Molecules with  $N$  atoms have  $3N$  degrees of freedom of which  $3N-6$  degrees of freedom give the number of ways that the atoms in a non-linear molecule can vibrate whereas for linear molecules the number of vibrational modes is  $3N-5$ .

Each vibrational mode,  $i$  in a molecule involves displacements of the atoms from their equilibrium positions such that all the atoms vibrate at a certain characteristic frequency,  $\nu_i$ . The potential energy,  $V(r)$  of such an oscillator is shown by the green line in Figure 1.1 as a function of the distance between the atoms,  $r$  assuming harmonic motion. For any mode in which the atoms vibrate with simple harmonic motion (i. e., obeying Hook's law), the vibrational energy,  $V_{iv}$  can be described by the equation

$$V_{iv} = h\nu_i\left(\nu_i + \frac{1}{2}\right) \text{ --- --- --- --- --- (1.1)}$$

where  $h$  is the Plank's constant,  $\nu_i$ , the fundamental frequency and  $\nu_i$  is the vibrational quantum number of the  $i$ -th mode. The energy difference for transitions between the ground state ( $\nu_i = 0$ ) and the first excited state ( $\nu_i = 1$ ) for most molecular vibrations fall in the mid-infrared region (between  $400$  to  $4000 \text{ cm}^{-1}$ ). The motion of the atoms during the vibration can also be described in terms of the normal modes,  $Q_i$  of vibration. The molecule is promoted to the excited state only if its dipole moment,  $\mu$ , changes during that normal mode vibration i.e.,  $(\partial\mu / \partial Q_i) \neq 0$ .

The actual variation of the potential energy as a function of the displacement of the atoms from their equilibrium position is shown in Figure 1.1 as the blue line.

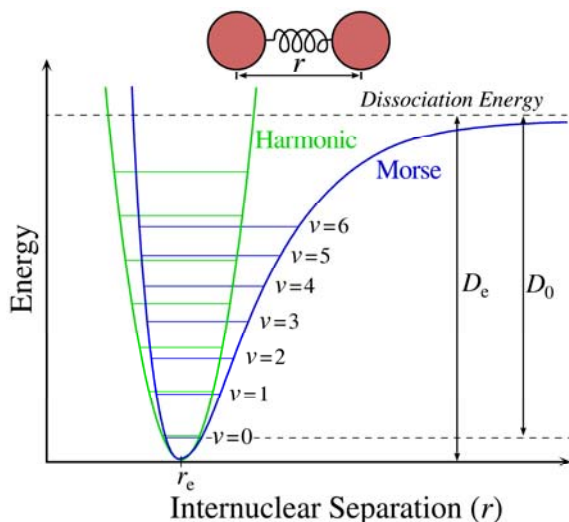


Figure 1.1. The harmonic (green line) and anharmonic (Morse type, blue line) potentials of a diatomic molecule as a function of the internuclear separation.

From the curve it can be seen that equation 1.1 is valid only for low vibrational quantum number. In practice,  $V_{iv}$  must be described using an anharmonic (Morse-type) potential function.<sup>44,45</sup> This behavior is shown in Figure 1.1 as the blue line, and the potential energy is given to a first approximation by the expression

$$V_{iv} = h\nu_i\left(\nu_i + \frac{1}{2}\right) + h\nu_i x_i \left(\nu_i + \frac{1}{2}\right)^2 \text{ --- (1.2)}$$

where  $x_i$  is the anharmonicity constant.

For polyatomic molecules, accurate representation of potential energy becomes more difficult, since more coordinates and potential parameters are required. Therefore, to describe



the potential energy either conceptually or mathematically, it is convenient to use internal coordinates such as bond stretches and angle bends. A nonlinear polyatomic molecule consisting of  $N$  atoms has  $3N-6$  ( $3N-5$  for linear molecule) independent internal coordinates. Additional internal coordinates are called “redundant coordinates.” The representation of a potential energy surface is often facilitated by including redundant internal coordinates. In general, no difficulty arises in including redundant internal coordinates in a potential energy function as long as the function correctly represents the molecular symmetry.

### **1.5 Infrared Spectroscopy of PAHs and Diols**

IR spectroscopy is a classical experimental technique for the determination of fundamental vibrational frequencies in a molecule and for the identification of various positional isomers of a molecule in the gas phase. Due to their low vapor pressures at room temperature (see Table 1.1), vibrational spectroscopy of PAHs namely naphthalene, phenanthrene, anthracene, 1-methylanthracene, 9-methyanthracene, 9-cyanoanthracene, 2-aminoanthracene, acridine, 1,2-benzanthracene, chrysene, pyrene, tetracene, pentacene, perylene, triphenylene, coronene, fluoranthene, benzo[a]fluoranthene, benzo[b]fluoranthene, benzo[z]fluoranthene, and benzo[k]fluoranthene and their cations have been carried out mostly in rare gas matrices.<sup>46</sup> There are a few literature reports on the gas-phase IR studies of PAHs with vibrational mode assignment. Jobline et al. recorded IR spectra of gas-phase pyrene, coronene and ovalene at a high temperature with the help of a  $7.0\text{ cm}^3$  oven made of nickel-chromium alloy and fitted with IR transparent diamond windows at a spectral resolution of  $1\text{ cm}^{-1}$  or lower.<sup>47,48</sup> They compared the gas phase spectra with the solid and matrix phase

## Chapter 1: An Introduction to PAHs, Diols and Infrared Spectroscopy

---

spectra and found that the matrix spectrum was much sharper. They identified the bands by comparing the gas phase spectra with previously assigned matrix spectra. In 1997, Cane et al. recorded the gas phase IR spectra of anthracene and phenanthrene, and their deuterated analogs with the help of a multi-pass gas cell of 4.8 and 5.6 meter, respectively, at a resolution of  $0.2\text{ cm}^{-1}$  at  $100\text{ }^{\circ}\text{C}$ .<sup>49a,b</sup> They assigned the vibrational bands using DFT and scaled self-consistent force fields and found that both theoretical methods reproduce the sequence of the experimental frequencies well. The room temperature IR spectra of naphthalene in the gas phase have been reported by Pirali et al. recently using an 8 meter path-length gas cell at a resolution of  $0.005\text{ cm}^{-1}$ .<sup>50</sup> At this high resolution they saw rotational structure in the spectra. The vibrational assignments were made using anharmonic DFT calculations.

Generally both harmonic and anharmonic DFT calculations have been carried out to assign the experimental IR spectra of polycyclic aromatic compounds.<sup>51a-d</sup> Calculated harmonic frequencies deviate by several hundreds of wavenumbers from the observed frequencies and thus one or more scaling factors have been used to multiply the calculated frequencies in order to get a close agreement with experiment. In 1996, Langhoff carried out the harmonic frequency and intensity calculation of 13 PAHs using the DFT method. He found that the harmonic frequencies, when uniformly scaled agree with the matrix isolation IR fundamentals with an average error of about  $10\text{ cm}^{-1}$ .<sup>51a</sup> In the same year, Martin et al. did harmonic calculation for naphthalene, azulene, phenanthrene, and anthracene using B3LYP functional and basis sets of *spd* and *spdf* quality. They have used three scaling factors for the harmonic frequencies of C-H stretching, in-plane-bending and rest of the vibrations to find agreement with the observed bands within  $10 - 20\text{ cm}^{-1}$ .<sup>51b</sup> In 1997, Bauschlicher et al. carried

## *Chapter 1: An Introduction to PAHs, Diols and Infrared Spectroscopy*

---

out DFT calculation to determine the harmonic frequencies and intensities of perdeuterated naphthalene, phenanthrene, pyrene, and chrysene.<sup>51c</sup> They performed the calculations with two different basis sets, 4-31G\* and 6-31G\* and found maximum mismatch of frequencies by about 12.4 and 36.6  $\text{cm}^{-1}$ , respectively, when harmonic frequencies were scaled uniformly by a factor of 0.958. In 2007, Cane et al. did DFT calculations in order to get the cubic and the quartic semidiagonal anharmonic force fields of naphthalene and deuterated naphthalene.<sup>51d</sup> They found that the fundamental frequencies computed by second-order vibrational perturbation are in good agreement with the experimental frequencies with a mean deviation of 4  $\text{cm}^{-1}$ . However, in the case of aromatic C–H stretching vibrations deviation is more  $\sim 10 \text{ cm}^{-1}$  due to the possible presence of Fermi resonances. We have found earlier that for methyl C–H stretching vibrations the differences between scaled harmonic DFT and experimental frequencies are even more than 30  $\text{cm}^{-1}$ .<sup>52</sup> McKean et al. have pointed out that even for methyl C-H symmetric and antisymmetric stretches, different scaling factors for calculated harmonic frequencies are necessary to match the experimental frequencies.<sup>53</sup>

IR spectroscopy has also been used for the identification of different conformers and characterization of hydrogen bonding in diols as discussed in section 1.3. Conformational isomers of ethylene glycol have been investigated by IR spectroscopy in the gas (up to 125 °C), liquid and solid phases in 1967 by Buckle et al.<sup>41a</sup> Normally two closely spaced IR absorption peaks are seen in these molecules. The peaks correspond to a free O–H and a H-bonded O–H stretching frequencies. The difference in frequency between these two peaks are known as the red shift between bound and free OHs. The gas phase result of Buckle et al. shows a 33  $\text{cm}^{-1}$  red-shift. The red shift is believed to be an evidence for the presence of the

*gauche* conformer in the gas phase which is stabilized by IHB. IR spectroscopy of 1,2-, 1,3-, 2,3-, and 1,4-BD have been studied by Fishman et al. in the gas and liquid phases at  $\pm 2 \text{ cm}^{-1}$ .<sup>41b</sup> They found a large red-shift of  $110 \text{ cm}^{-1}$  in 1,4-BD. Their results also show that the enthalpies of IHB formation in these isomers depend strongly on their conformation. In 2003, Jesus et al. did conformational analysis of BD isomers by means of DFT calculations and matrix isolation IR spectroscopic studies.<sup>54</sup> They have also characterized the HB strength. The conformations of 1,4-BD have been investigated using a combination of MP2 calculation, natural bond orbital (NBO) and AIM analysis, and matrix-isolation infrared spectroscopy by the same group in 2008.<sup>55</sup> They found that the intramolecular hydrogen bonded conformers contributes 46% in the equilibrium conformation at room temperature. In 2009, Ma et al. carried out IR spectroscopic study and DFT calculation on 1,2-EG, 1,2-PD, 2,3-BD and 1,2-BD in solution.<sup>56</sup> In solution they found that the red shift was of the order of  $40 \text{ cm}^{-1}$  in the vicinal diols and that is due to IHB.

For the past 20 years, extensive quantum-chemical calculations have been carried out for the conformational analysis and characterization of the hydrogen bond between two vicinal hydroxyl groups in EG.<sup>57-65</sup> Electron density topological analysis has shown a bond critical point (BCP) and atomic bond path to be absent which implies that no IHB is present in 1,2-EG.<sup>66,67</sup> Furthermore, quantum diffusion Monte Carlo (QDMC) simulations corroborated the absence of IHB in 1,2-EG.<sup>68</sup>

## **1.6 Scope and motivation of this thesis work**

From the above introduction it is clear that PAHs are important in atmospheric chemistry and astrophysics and, thus, it is important to identify and distinguish them in the gas phase at

## *Chapter 1: An Introduction to PAHs, Diols and Infrared Spectroscopy*

---

low concentrations by using a suitable spectroscopic technique. Also suitable vibrational analysis method is required for the unambiguous assignment of the observed infrared bands which may eventually lead to the identification of UIR bands from the interstellar space and identification PAHs in the earth atmosphere. Therefore, my motivation of this work is twofold: (i) to record the gas phase IR absorption spectra of some atmospherically and astronomically important PAHs namely 1, 5-, 1, 6-, and 2, 6-dimethyl naphthalenes (DMNs); 2, 4-, 2, 6-, 2, 7-, and 2,8-dimethyl quinolines (DMQs); and 1, 9-, 2, 4-, and 3, 9-dimethyl phenanthrenes (DMPs) and (ii) unambiguously assign the vibrational bands in the observed spectra. However, the second part of the work is tricky since various theoretical methods of calculation of vibrational spectra are available. I have used scaled harmonic and anharmonic frequencies as well as scaled force fields to fit the experimental spectra. The error limits of each of these assignment methods have also been analyzed.

In another related objective, I have investigated the IR spectra of diols namely 1,2-EG and 1,4-BD in the gas phase and performed DFT calculation in order to look for intramolecular hydrogen bonding in them. These are biologically and industrially important molecules and exist in a mixture of conformers as discussed in section 1.1.3. The most abundant conformer of diols is the *gauche* conformer which is thought to be stabilized by IHB. The existence of IHB in 1,2-EG is still controversial although many papers have been written on it. My hope in this work is to throw some light on this problem.

## **1.7 References**

- [1] (a) Sonnefeld, W. J.; Zoller, W. H.; May, W. E. *Anal. Chem.* **1983**, *55*, 275 (b) Blermann, H. W.; Leod, H. M.; Atkinson, R.; Winer, A. M.; Pitts, J. N. *Environ. Sci. Technol.* **1985**, *19*, 244.
- [2] <http://www.thegoodscentcompany.com/data/rw1161171.html>
- [3] Wild, S. R.; Jones, K. C. *Environ. Pollut.* **1995**, *88*, 91.
- [4] Baumard, P.; Budzinski, H.; Garrigues, P.; Dizer, H.; Hansen, P. D. *Marine Environ. Res.* **1999**, *47*, 17.
- [5] (a) Allamandola, L. J.; Sandford, S. A.; Wopenka, B. *Science* **1987**, *237*, 56 (b) Sagan, C.; Khare, B. N.; Thompson, W. R.; Mc Donald, G. D.; Wing, M. R.; Bada, J. L.; Vo-Dinh, T.; Arakawa, E. T. *Astrophys. J.* **1993**, *414*, 399 (c) Clemett, S. J.; Maechling, C. R.; Zare, R. N.; Swan, P. D.; Walker, R. M. *Science* **1993**, *262*, 721.
- [6] Smith, K. R. *Biofuels, Air Pollution and Health-a Global Review*. Plenum Press, New York, **1987**.
- [7] World Health organization (WHO), **2002**. *World Health Report 2002: Reducing Risks, Promoting Life*.
- [8] (a) Rogge, W. F.; Hildemann, L. M.; Mazurek, M. A.; Cass, G. R.; Simoneit, B. R. T. *Environ. Sci. Technol.* **1993**, *27*, 636 (b) Miguel, A. H.; Kirchstetter, T. W.; Harley, R. B.; Hering, R. A. *Environ. Sci. Technol.* **1998**, *32*, 450 (c) Marr, L. C.; Kirchstetter, T. W.; Harley, R. A.; Miguel, A. H.; Hering, S. V.; Hammond, S. K. *Environ. Sci. Technol.* **1999**, *33*, 3091 (d) Ravindra, K.; Wauters, E.; Taygi, S. K.; Mor, S.; Grieken, V. R. *Environ. Monitor. Asses.* **2006**, *115*, 405.

**Chapter 1: An Introduction to PAHs, Diols and Infrared Spectroscopy**

---

- [9] (a) Yang, H. H.; Lee, W. J.; Chen, S. J.; Lai, S. O. *J. Hazard. Materials* **1998**, *60*, 159 (b) Pisupati, S. V.; Wasco, R. S.; Scaroni, A. W. *J. Hazard. Materials* **2000**, *74*, 91 (c) Yang, H. H.; Jung, R. C.; Wang, Y. F.; Hsieh, L. T. *Atmos. Environ* **2005**, *39*, 3305 (d) Ciaparra, D.; Aries, E.; Booth, M.; Anderson, D. R.; Almeida, S. M. A.; Harrad, S. *Atmos. Environ.* **2009**, *43*, 2070.
- [10] (a) Jenkins, B. M.; Jones, A. D.; Turn, S. Q.; Williams, R. B. *Environ. Sci. Technol.* **1996**, *30*, 2462 (b) Fang, M.; Zheng, M.; Wang, F.; To, K. L.; Jaafar, A. B.; Tong, S. L. *Atmos. Environ.* **1999**, *33*, 783 (c) Godoi, A. F. L.; Ravindra, K.; Godoi, R. H. M.; Andrade, S. J.; Santiago-Silva, M.; Van Vaeck, L.; Van Grieken, R. *J. Chromatog. A* **2004**, *1027*, 49.
- [11] Allamandola, L. J.; Tielens, A. G. M.; Barker, J. R. *Astrophys. J. Supplemen. Ser.* **1989**, *71*, 733.
- [12] Hirao, K.; Shinohara, Y.; Tsuda, H.; Fukushima, S.; Takahashi, M.; Ito N. *Cancer Res.* **1976**, *36*, 329.
- [13] Murata, Y.; Denda, A.; Murayama, H.; Konishi, Y. *Fund. Appl. Toxicol.* **1993**, *21*, 44.
- [14] Kaden, D. A.; Hites, R. A.; Thilly, W. G. *Cancer Res.* **1979**, *39*, 4152.
- [15] Royer, R. E.; Mitchell, C. E.; Hanson, R. L.; Dutcher, J. S.; Bechtold, W. E. *Environ. Res.* **1983**, *31*, 460.
- [16] Birkholz, D. A.; Coutts, R. T.; Hrudey, S. E.; Danell, R. W. Lockhart, W. L. *Water Res.* **1990**, *24*, 67.
- [17] (a) Plakogiannis, F. M. *J. Med. Chem.* **1971**, *14*, 430 (b) Temple, C.; Rose, J. D.; Montgomery, J. A. *J. Med. Chem.* **1974**, *17*, 615 (c) Thomas, J.; Berkoff C. E.; Flagg W. B.; Gallo J. J.; Haff, R. F.; Pinto C. A. *J. Med. Chem.* **1975**, *18*, 245 (d) Shamsuddin, Z. A.;

*Chapter 1: An Introduction to PAHs, Diols and Infrared Spectroscopy*

---

- Rahimtula, A. D. *Drug. Metab. Dispos.* **1986**, *14*, 724 (e) Kilanowicz, A.; Sapota, A.; Czerski, B. *Toxicol. Lett.* **2002**, *134*, 227.
- [18] Schmeltz, I.; Tosk, J.; Hoffmann, D. *Anal. Chem.* **1976**, *48*, 645.
- [19] Ming-Li Yu; Hites, Ronald, A. *Anal. Chem.* **1981**, *53*, 951.
- [20] Later, D. W.; Lee, M. L.; Bartle, K. D.; Kong, R. C.; Vassilaros, D. L. *Anal. Chem.* **1981**, *53*, 1612.
- [21] Khalilli, N. R.; Schefft, P. A.; Holsen, T. M. *Atmos. Environ.* **1995**, *29*, 533.
- [22] Correa, S. M.; Arbilla, G. *Atmos. Environ.* **2006**, *40*, 6821.
- [23] Abrantes, R.; Assunção, J. V.; Pesquero, C. R.; Bruns, R. E.; Nobrega, R. P. *Atmos. Environ.* **2009**, *43*, 648.
- [24] Dmitrikov, V. P.; Fedorov, Yu. V. *Chromatogr.* **1984**, *18*, 28.
- [25] Zamperlini, G. C. M.; Silva, M. R. S.; Vilegas, W. *Chromatogr.* **1997**, *46*, 655.
- [26] Wise, S. A.; Chesler, S. N.; Hertz, H. S.; Hipert, L. R.; May, W. E. *Anal. Chem.* **1977**, *49*, 2306.
- [27] Lee, M. L.; Vassilaros, D. L. *Anal. Chem.* **1979**, *51*, 768.
- [28] Novotny, M.; Kump, R.; Merli, F.; Todd, L. J. *Anal. Chem.* **1980**, *52*, 401.
- [29] Bates, M.; Bruno, P.; Caputi, M.; Caselli, M.; Gennaro, G.; Tutino, M. *Atmos. Environ.* **2008**, *42*, 6144.
- [30] Porter, D. J.; Mayer, P. M.; Fingas, M. *Energy & Fuels* **2004**, *18*, 987.
- [31] Stockton, A. M.; Chiesl, T. N.; Scherer, J. R.; Mathies, R. A. *Anal. Chem.* **2009**, *81*, 790.
- [32] Wornat, M. J.; Sarofim, A. F.; Longwell, J. P. *Energy & Fuel* **1987**, *1*, 431.



*Chapter 1: An Introduction to PAHs, Diols and Infrared Spectroscopy*

---

- [33] (a) Gurka, D. F.; Hiatt, M.; Titus, R. *Anal. Chem.* **1984**, *56*, 1102 (b) Gurka, D. F.; Pyle, S. M. *Environ. Sci. Technol.* **1988**, *22*, 963 (c) Gurka, D. F.; Farnham, I.; Potter, B. B.; Pyle, S.; Titus, R.; Duncan, W. *Anal. Chem.* **1989**, *61*, 1584.
- [34] Jonsdottir, S. O.; Klein, R. A. *Fluid Phase Equilib.* **1997**, *132*, 117.
- [35] Patel, R. N.; Banerjee, A.; Pendri, Y. R.; Liang, J.; Mueller, R. *Tetrahedron: Asymmetry* **2006**, *17*, 175.
- [36] Wang, X.; Wang, L.; Tang, H. Li. X.; Chang, F. –C. *J. Appl. Polym. Sci.* **2000**, *77*, 184.
- [37] (a) Szarek, W. A.; Hay, G. W.; Sood, R. K.; Trouton, K.; Fortier, S. *Can. J. Chem.* **1998**, *66*, 1600 (b) Bako, I.; Grosz, T.; Palinkas, G.; Bellissent, M. C. *J. Chem. Phys.* **2003**, *118*, 3215.
- [38] (a) Tratteberg, M.; Hedberg, K. *J. Am. Chem. Soc.* **1994**, *116*, 1382 (b) Kazerouni, M. R.; Hedberg, L.; Hedberg, K. *J. Am. Chem. Soc.* **1997**, *119*, 8324.
- [39] (a) Marstokk, K. -M.; Mollendal, H. *J. Mol. Struct. (THEOCHEM)* **1974**, *22*, 301 (b) Christen, D.; Coudert, L. H.; Suenram, R. D.; Lovas, F. J. *J. Mol. Spectros.* **1995**, *172*, 57 (c) Christen, D.; Coudert, L. H.; Larsson, J. A.; Cremer, D. *J. Mol. Spectros.* **2001**, *185*, 205 (d) Muller, H. S. P.; Christen, D. *J. Mol. Spectros.* **2004**, *228*, 298.
- [40] (a) Nakao, Y.; Sugeta, H.; Kyogoku, Y. *Spectrochim. Acta.* **1986**, *42A*, 251 (b) Gallwey, F. B.; Hawkes, J. E.; Haycock, P.; Lewis, D. *J. Chem. Soc., Perkin Trans* **1990**, *2*, 1979 (c) Petterson, K. A.; Stein, R. S.; Drake, M. D.; Roberts, J. D. *Magn. Reson. Chem.* **2005**, *43*, 225.
- [41] (a) Buckley, P.; Giguere, P. A. *Canad. J. Chem.* **1967**, *45*, 397 (b) Fishman, E.; Chen, T. L. *Spectrochim. Acta* **1969**, *25A*, 1231.
- [42] Chopra, D.; Row, T. N. G.; Arunan, E.; Klein, R. A. *J. Mol. Struct.* **2010**, *964*, 126.

**Chapter 1: An Introduction to PAHs, Diols and Infrared Spectroscopy**

---

- [43] Steiner, T. *Angew. Chem., Int. Ed.* **2002**, *41*, 48.
- [44] Morse, P. M. *Phys. Rev.* **1929**, *34*, 57.
- [45] Kaplan, I. G. *Handbook of Molecular Physics and Quantum Chemistry*, Wiley, **2003**, p-207.
- [46] (a) Szczepanski, J.; Roser, D.; Personette, W.; Eyring, M.; Pellow, R.; Vala, M. *J. Phys. Chem.* **1992**, *96*, 7876 (b) Szczepanski, J.; Chapo, C.; Vala, M. *Chem. Phys. Lett.* **1993**, *205*, 434 (c) Vala, M.; Szczepanski, J.; Pauzat, F.; Parisel, O.; Talbi, D.; Ellinger, Y. *J. Phys. Chem.* **1994**, *98*, 9187 (d) Hudgins, D. M.; Sandford, S. A.; Allamandola, L. J. *J. Phys. Chem.* **1994**, *98*, 4243 (e) Hudgins, D. M.; Allamandola, L. J.; *J. Phys. Chem.* **1995**, *99*, 8987 (f) Hudgins, D. M.; Allamandola, L. J. *J. Phys. Chem.* **1995**, *99*, 3033 (g) Bauschlicher, C. W.; Langhoff, S. R.; Sandford, S. A. *J. Phys. Chem. A* **1997**, *101*, 2414 (h) Hudgins, D. M.; Allamandola, L. J. *J. Phys. Chem. A* **1997**, *101*, 3472 (i) Hudgins, D. M.; Sandford, S. A. *J. Phys. Chem. A* **1998**, *102*, 329 (j) Hudgins, D. M.; Sandford; S. A. *J. Phys. Chem. A* **1998**, *102*, 344 (k) Hudgins, D. M.; Sandford, S. A. *J. Phys. Chem. A* **1998**, *102*, 353 (l) Hudgins, D.M.; Bauschlicher, Jr., C. W.; Allamandola, L. J.; Fetzer, J. C. *J. Phys. Chem. A* **2000**, *104*, 3655.
- [47] Joblin, C.; d'Hendecourt, L.; Leger, A.; Defourneau, D. *Astron. Astrophys.* **1994**, *281*, 923.
- [48] Joblin, C.; Boissel, P.; d'Hendecourt, L.; Leger, A.; Defourneau, D. *Astron. Astrophys.* **1995**, *299*, 835.
- [49] (a) Cane, E.; Miani, A.; Palmieri, P.; Tarroni, R.; Trombetti, A. *J. Chem. Phys.* **1997**, *106*, 9004 (b) Cane, E.; Miani, A.; Palmieri, P.; Tarroni, R.; Trombetti, A. *Spectrochim. Acta. A* **1997**, *53*, 1839.

*Chapter 1: An Introduction to PAHs, Diols and Infrared Spectroscopy*

---

- [50] Pirali, O.; Vervloet, M.; Mulas, G.; Mallocci, G.; Joblin, C. *Phys. Chem. Chem. Phys.* **2009**, *11*, 3443.
- [51] (a) Langhoff, S. R. *J. Phys. Chem.* **1996**, *100*, 2819 (b) Martin, J. M. L.; El-Yazal, J.; Francois, J. P. *J. Phys. Chem.* **1996**, *100*, 15358 (c) Bauschlicher, Jr., C. W.; Langhoff, S. R.; Sandford, S. A.; Hudgins, D. M. *J. Phys. Chem. A* **1997**, *101*, 2414 (d) Cane, E.; Miani, A.; Trombetti, A. *J. Phys. Chem. A* **2007**, *111*, 8218.
- [52] Das, P.; Arunan, E.; Das, P. K. *Vibr. Spectrosc.* **2008**, *47*, 1.
- [53] (a) McKean, D. C. *J. Phys. Chem. A* **2003**, *107*, 6538 (b) McKean, D. C.; Craig, N. C.; Law, M. M. *J. Phys. Chem. A* **2008**, *112*, 6760.
- [54] Jesus, A. J. L.; Rosado, M. T. S.; Leitao, M. L. P.; Redinha, J. S. *J. Phys. Chem. A* **2003**, *107*, 3891.
- [55] Jesus, A. J. L.; Rosado, M. T. S.; Reva, I.; Fausto, R.; Eusebio, M. E.; Redinha, J. S. *J. Phys. Chem. A* **2008**, *112*, 4669.
- [56] Ma, X.; Wang, J. *J. Phys. Chem. A* **2009**, *113*, 6079.
- [57] Nagy, P. I.; Dunn III, W. J.; Alagona, G.; Ghio, C. *J. Am. Chem. Soc.* **1991**, *113*, 6719.
- [58] Cramer, C. J.; Truhlar, D. *J. Am. Chem. Soc.* **1994**, *116*, 3892.
- [59] Oie, T.; Topol, I. A.; Burt, S. K. *J. Phys. Chem.* **1994**, *98*, 1121.
- [60] Csonka, G. I.; Csizmadia, I. G. *Chem. Phys. Lett.* **1995**, *243*, 419.
- [61] Klein, R. A. *J. Comput. Chem.* **2002**, *24*, 1120.
- [62] Trindle, C.; Crum, P.; Douglass, K. *J. Phys. Chem. A* **2003**, *107*, 6236.
- [63] Mandado, M.; Grana, A. M.; Mosquera, R. A. *Phys. Chem. Chem. Phys.* **2004**, *6*, 4391.
- [64] Klein, R. A. *Chem. Phys. Lett.* **2006**, *429*, 633.

*Chapter 1: An Introduction to PAHs, Diols and Infrared Spectroscopy*

---

- [65] Jesus, A. J. L.; Rosado, M. T. S.; Reva, I.; Fausto, R.; Eusebio, M. E.; Redinha, J. S. *J. Phys. Chem. A* **2006**, *110*, 9934.
- [66] Klein, R. A. *J. Comp. Chem.* **2002**, *23*, 585.
- [67] Klein, R. A. *J. Am. Chem. Soc.* **2002**, *124*, 13931.
- [68] Crittenden, D. L.; Thompson, K. C.; Jordan, M. J. T. *J. Phys. Chem. A* **2005**, *109*, 2971.

# **Chapter-2**

**Methods: Experimental and Theoretical**

## **2.1 Introduction**

This chapter describes the experimental set-ups and computational methods which were used for the IR spectroscopic studies of PAHs, methyl-PAHs and diols. The FT-IR spectroscopic technique has been used to record IR absorption spectra of PAHs and diols in the gas phase. DFT calculations with valence polarized basis sets have been carried out to obtain the harmonic and anharmonic frequencies and their intensities calculations. In addition to this, I have carried out scaled quantum mechanical (SQM) force field calculations for the unambiguous assignments of the observed bands. The observed spectra can be used for the identification of gaseous PAHs and methylated derivatives of PAHs which are present in the atmosphere at low concentrations. On the other hand, the gas phase IR spectra of diols can be used for the characterization of the nature of hydrogen bonding in diols. In both the cases a variable path-length long-path gas cell was coupled with a FT-IR spectrometer to record the IR spectra at low concentration.

## **2.2 Experimental technique**

### **2.2.1 Principle of FT-IR spectrometry: Michelson interferometer**

The design of interferometers used for IR spectroscopy is based on a two-beam interferometer which was originally designed by Michelson in 1891.<sup>1, 2</sup> The Michelson interferometer is a device that can divide a beam of radiation into two paths and then recombine the two beams after a path difference has been introduced. A condition thereby created under which interference between the beams can occur. The variation of intensity of the beam emerging from the interferometer is measured as a function of the path difference obtained.

The simplest form of Michelson interferometer, interferogram and spectrum (for monochromatic light source) is shown in Figure 2.1. Here a constructive interference will occur only when the distance between the movable mirror and the fixed mirror,  $\delta$  also called retardation, is an integral multiple of  $\lambda$ , whereas a destructive interference will take place when  $\delta$  is an integral multiple of  $\lambda/2$ .

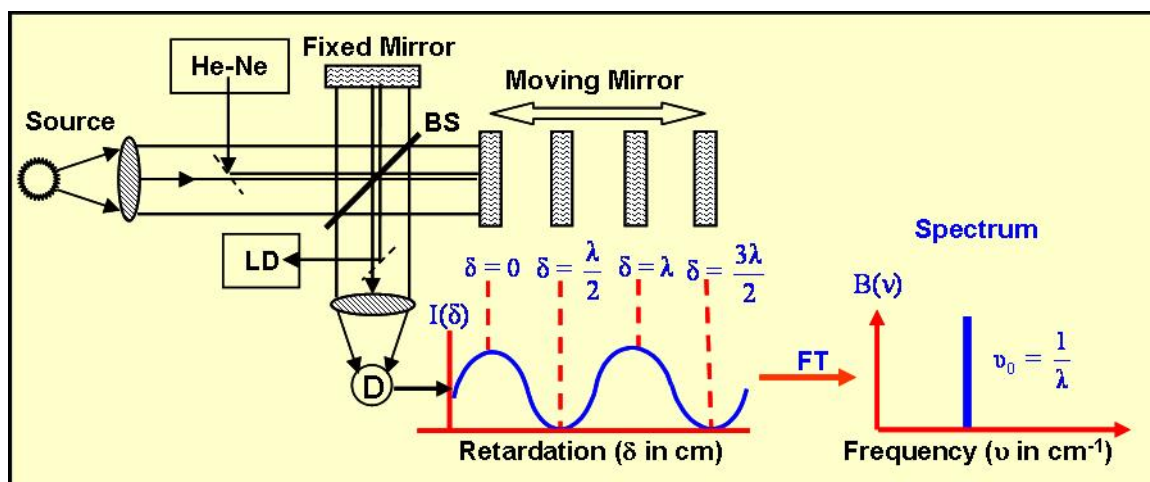


Figure 2.1. Optical diagram of a Michelson interferometer with the He-Ne laser running co-axial, Interferogram and Spectrum for a single frequency light source. The Interferometer consists of four major components: a fixed mirror, a moving mirror, BS: beamsplitter, D: Detector. LD: He-Ne laser detector.

To obtain an interferogram,  $I(\delta)$ , the detector signal is digitized and recorded as a function of retardation. The interferogram intensity of polychromatic source is mathematically described as:

$$I(\delta) = \int_{-\infty}^{+\infty} B(\nu) \cos(2\pi\nu\delta) d\nu \text{ ----- (2.1)}$$

where  $B(\nu)$  is the spectral intensity at wave number  $\nu$  (in  $\text{cm}^{-1}$ ).

Fourier transformation (FT) of  $I(\delta)$  gives the single-beam IR spectrum expressed as:

$$B(\nu) = \int_{-\infty}^{+\infty} I(\delta) \cos(2\pi\nu\delta) d\delta \text{ -----(2.2)}$$

The movable mirror moves continuously in case of continuous scan mode.

### 2.2.2 Continuous-Scan Interferometry

The continuous-scan is preferably used for the routine static or relatively slow kinetic measurements that require time resolution not faster than 20 ms. In the continuous-scan FT-IR spectrometer, the moving mirror moves continuously at a constant velocity,  $V(\text{cm s}^{-1})$ , and the optical path difference at time  $t(\text{s})$  is given by  $\delta = 2Vt(\text{cm})$ .

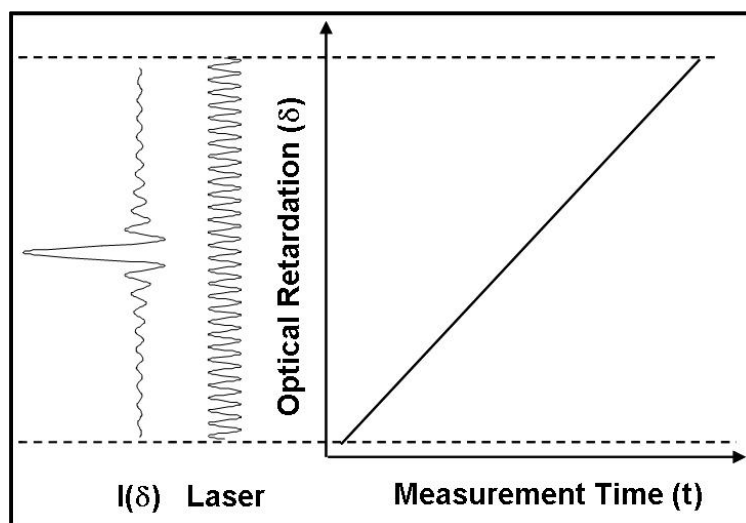


Figure 2.2. Schematic of data collection in continuous-scan interferometer.

The interferogram data points are digitized at the zero crossings of the He-Ne laser signal as shown in Figure 2.2. The use of laser signal ensures that  $I(\delta)$  is measured at precisely equal intervals of mirror positions and provides an internal wavelength calibration for every scan.



---

Because of continuous movement of the mirror, the interferogram  $I(\delta)$  changes as a function of time. The Fourier frequency ( $f_F$  in Hz) of IR light at wave number  $\nu$  is given by:

$$f_F = 2V\nu \text{ --- --- --- --- --- (2.3)}$$

where  $V$  is the mirror velocity in  $\text{cm s}^{-1}$ . The slow velocities are chosen for thermal detectors; such as deuterated triglycine sulfate (DTGS). The fast velocities are chosen for fast quantum detectors, such as a mercury cadmium telluride (MCT) or indium antimonide (InSb) detector, for routine or kinetic measurements.

### 2.2.3 Variable Path-length Long Path Gas Cell

In chapter 1, it has been discussed that PAHs and methyl-PAHs have insufficient vapor pressures at room temperature.<sup>3</sup> So, it is difficult to obtain sufficient amount of these compounds in the gas phase for the IR spectroscopic study with a normal gas cell having an optical path length  $\sim 10$  cm. Kurtz used a stainless steel cell to get the IR spectrum of coronene at elevated temperatures.<sup>4</sup> Later Joblin and coworkers recorded the IR spectra of neutral PAHs in the gas phase using an oven of  $7.0 \text{ cm}^3$  which made from nickel-chromium alloy and fitted with IR transparent diamond windows.<sup>5,6</sup> I have used multi-pass gas cell of 7.2 and 8.0 meters. Figure 2.3 shows the variable path-length long-path gas cell<sup>7</sup> which made according to the “white cell” principle.<sup>8</sup> The cell contains three internal gold-coated mirrors. Out of these, two are immovable and one is movable. Two potassium chloride (KCl)/zinc selenide (ZnSe) windows of 2.5/1.9 cm diameter, respectively, have been used for the entrance and exit of IR radiation into the cell. In addition, there are two plane transfer mirrors. These mirrors guide the

IR light into the cell and then to the detector. The cell can be evacuated by a mechanical pump and the sample holder is connected through a valve to the cell.

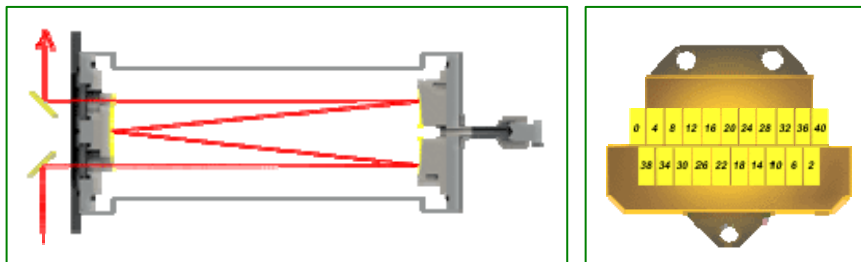


Figure 2.3. Schematic diagram of typical “white cell” and field mirror.

The beam comes through one window (left) and reflects back and forth between the field mirror (left) on the input side and the objective mirror (right) on the other end of the gas cell. After each 4 passes, the beam migrates across the top of the field mirror on the input side until it misses that mirror and exits through the exit window. The field mirror on the left shows the migration of 48 and 40 passes of the IR beam in the gas cell of 7.2 and 8.0 meter, respectively. The IR beam comes in at the position marked 0 and exits at the position marked 40 for the 7.2 meter gas cell (see Figure 2.3). The field mirror has the corners cut out to allow the IR beam to enter and exit the gas cell. These multi-pass gas cells were coupled with a FT-IR spectrometer through homemade aluminum or commercially available cell holders as shown in the subsequent sections.

## 2.3 Experimental set-up

### 2.3.1 Set-up for PAHs and diols

The schematic experimental set-up for the gas phase FT-IR spectroscopic studies of PAHs and diols are shown in Figure 2.4. In this figure, I have shown how a multi-pass cell of

7.2 meter has been coupled with the FT-IR spectrometer, the sample-tube, the vacuum pump, and the pressure gauge. The commercially available variable long path-length cell (Model 7.2-V, REFLEX Analytical Corporation, USA) were coupled with the FT-IR spectrometer (Nexus-870, Thermo Nicolet / Vertex-70, Bruker Optics) by a homemade aluminum cell holder.

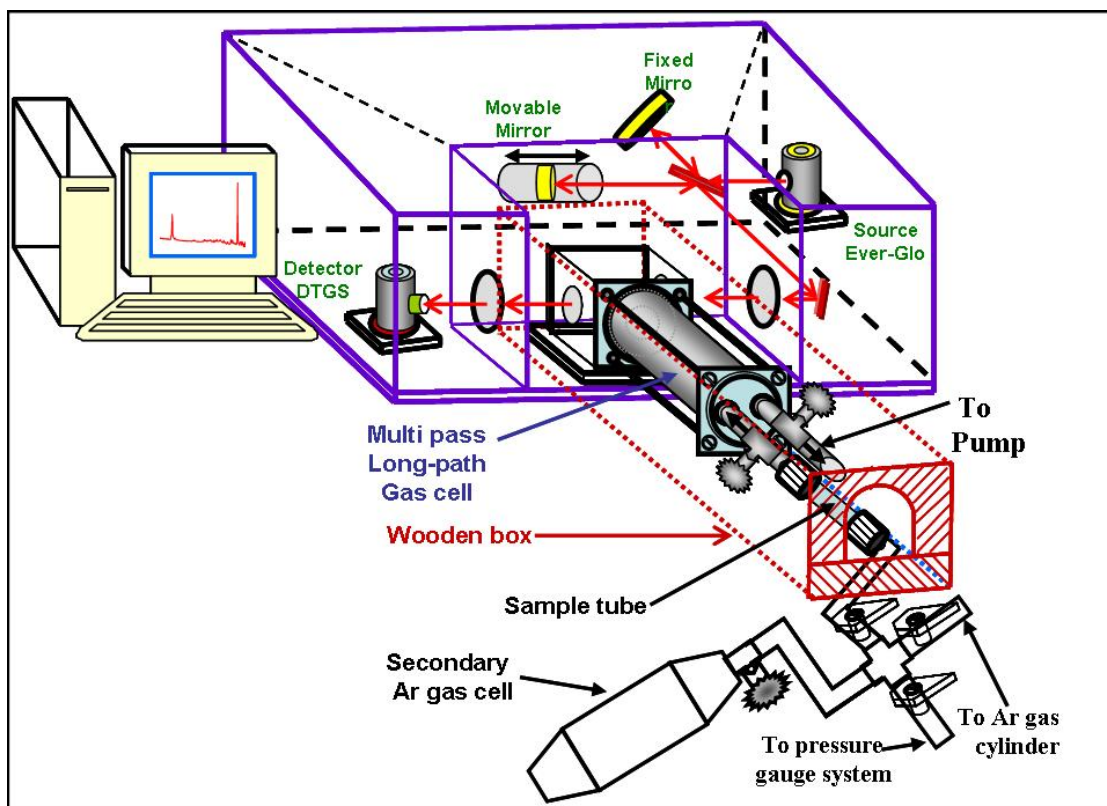
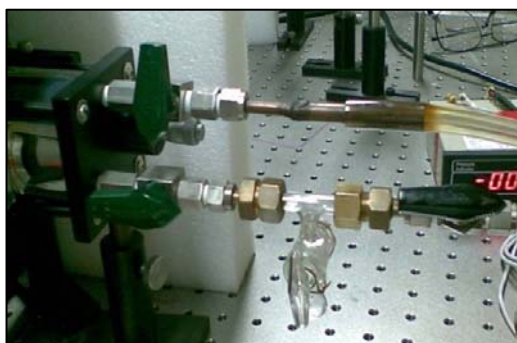


Figure 2.4. Schematic representation of the FT-IR spectrometer coupled with a multi-pass long-path gas cell of 7.2 meter.

The variable path-length cell body is a cylinder of borosilicate glass of length 15 cm, with an inside diameter of 6 cm. It has an optical path adjustable from 0.6 to 7.2 meter in increments of 0.6 meter. This cell is connected to two valves; one side is connected to the sample tube made of pyrex glass and the other side is connected to the vacuum pump. The sample tube was then connected to a four-ways valve system with the help of a homemade

brass coupler and a viton O-ring, which, in turn, is attached with the secondary gas cylinder, the primary Ar gas cylinder and the pressure gauge system (PRM-300MX, IRA). The cell is evacuated by a rotary pump (RV-8, Boc Edward). The cell body and the sample tube were wrapped with a heating tape (Thermolyne Heating Tape, Aldrich) and the temperature was maintained with the help of a temperature controller (DIGITHERM-2000MCX, IRA) fitted with a feedback heat sensor. The multi-pass gas cell along with the sample tube has been kept inside a wooden box covered with a heat-insulating silicon sheet. It maintains the uniformity of temperature of the gas cell along with the sample tube, and also protects the spectrometer from high temperature.

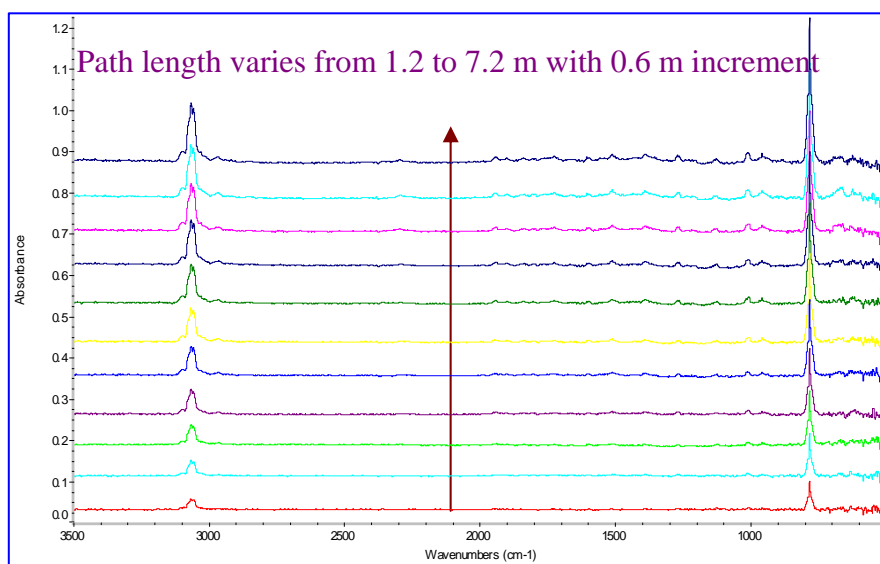


**Figure 2.5. A small bulb for liquid samples is connected to the gas cell and the four-ways valve arrangement.**

In case of liquid samples, the sample tube was replaced by a small glass bulb of volume 2 ml which is isolated by a valve as shown in Figure 2.5. This set-up has been used to record the IR spectra of compounds which are having vapor pressures up to  $10^{-4}$  mmHg at room temperature.

### 2.3.2 Standardization of multi-pass gas cell of 7.2 meter path-length coupled with Nexus-870 (Thermonicolet, US) spectrometer

The variable multi-pass gas cell was first standardized with naphthalene. For the standardization, solid naphthalene (~10 mg) was taken in the sample tube which was kept isolated from the cell and the four-ways valve arrangement. The gas cell, along with the sample tube, was then evacuated up to ~ 0 mmHg. The vacuum single-beam spectrum was then recorded with a spectral resolution of 4 cm<sup>-1</sup> and averaging over 64 scans, which is the reference spectrum.



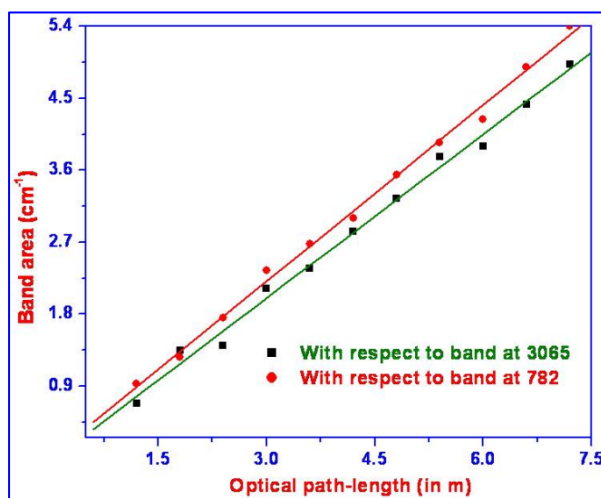
**Figure 2.6. Gas phase IR absorption spectra of naphthalene as a function of path length.**

After recording the reference spectrum, ultrahigh pure Ar (carrier) gas was allowed to pass through the sample tube to carry naphthalene inside the gas cell. The total pressure of Ar and naphthalene was maintained at 20 mmHg. The spectra of naphthalene were recorded at optical path lengths (OPL) of 1.2, 1.8, 2.4, 3.0, 3.6, 4.2, 4.8, 5.4, 6.0, 6.6, and 7.2 meter at room temperature (25 °C) after normalization with respect to the reference spectrum. The observed

spectra are presented in Figure 2.6. The observed band areas (in  $\text{cm}^{-1}$ ) for the strong bands at 3065 and 782  $\text{cm}^{-1}$ , were measured by OMNIC software provided by Thermo Nicolet.<sup>9</sup> The optical path lengths and band areas with respect to the strong band are listed in Table 2.1.

**Table 2.1: Optical path-length (OPL, in m) and integrated band area (in  $\text{cm}^{-1}$ )**

OPL (m)	Band area at 3065 $\text{cm}^{-1}$	Band area at 782 $\text{cm}^{-1}$
1.2	0.681	0.928
1.8	1.343	1.263
2.4	1.402	1.753
3.0	2.117	2.35
3.6	2.375	2.683
4.2	2.834	3.002
4.8	3.244	3.548
5.4	3.773	3.950
6.0	3.898	4.235
6.6	4.422	4.893
7.2	4.924	5.406

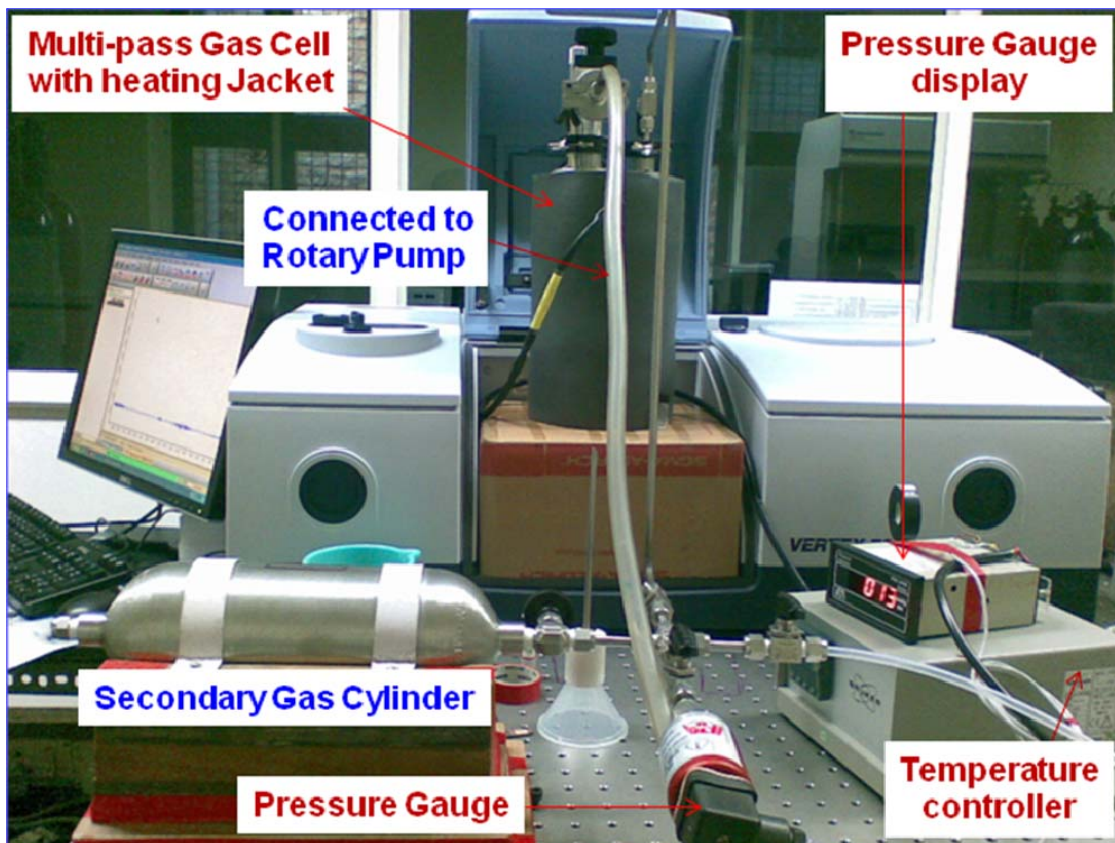


**Figure 2.7. Observed band area (in  $\text{cm}^{-1}$ ) vs optical path length (in m) for naphthalene.**

The optical path length (in m) vs band area (in  $\text{cm}^{-1}$ ) is plotted in Figure 2.7. From this figure it was found that the observed band area follows a linear relationship with the optical path-length. It helps us to set the optical path-length for different compounds having different vapor pressure at a particular temperature.

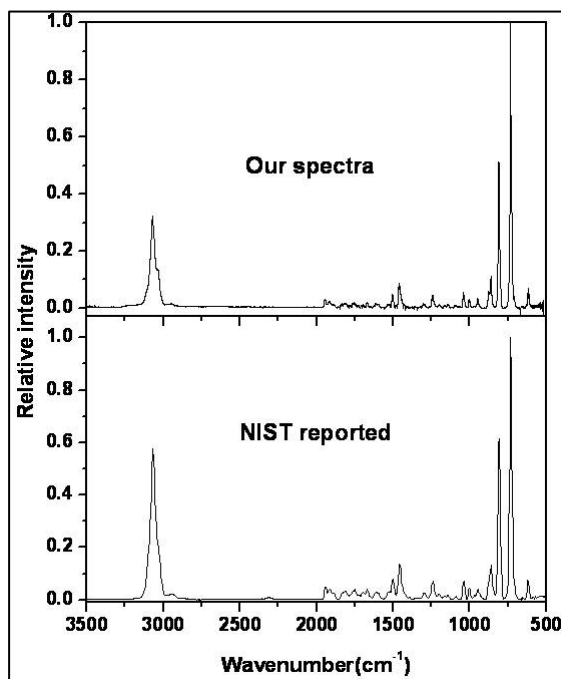
### 2.3.3 Standardization of the multi-pass gas cell of 8.0 meter coupled with Vertex-70 (Bruker Optics, Germany) spectrometer

Another experimental set-up has been employed to record the IR spectra of compounds having a vapor pressure of  $\sim 10^{-5}$  mmHg at room temperature, where we have used a 8.0 meter path-length white cell (136G/3TQ, Bruker Optics) equipped with a heating jacket.



*Figure 2.8. Photograph of the FT-IR spectrometer (Vertex-70) coupled with a multi-pass long-path gas cell of 8.0 meter.*

The cell was coupled with the FT-IR spectrometer (Vertex-70, Bruker Optics) as shown in Figure 2.8. The gas cell is made of borosilicate glass tube of (23 cm x 11 cm) and equipped with ZnSe windows. The cell was placed vertically inside the sample chamber of the spectrometer and aligned with the help of an external He-Ne laser before use. The rotary pump and Ar-line were connected to the cell through ball valves. Phenanthrene (90%, Fluka) was used as a standard compound for the optimization of our set-up and purified by vacuum distillation method before use. Compound was thermally vaporized at 100 °C and the reported spectrum was reproduced (see Figure 2.9).



**Figure 2.9. Our and NIST reported gas phase IR spectra of phenanthrene.**

The total pressure of Ar gas containing phenanthrene in the cell was maintained at 30 mmHg. The mid-IR spectra (4000 - 400  $\text{cm}^{-1}$ ) were collected using a liquid nitrogen cooled MCT detector and KBr beam splitter combination. The spectrometer was continuously purged with



N<sub>2</sub> gas (UHP grade). The spectra were recorded at 0.5 cm<sup>-1</sup> resolution with averaging over 2048 scans. Total time required for this number of scans is about one hour. DMPs have low infrared absorbance (OD<sub>max</sub>= 0.03) and small amounts of H<sub>2</sub>O vapor present inside the cell give rise to infrared absorption bands that overlap with those of DMPs. We have collected the spectra of Ar at the same pressure without DMP separately and subtracted the same from the sample spectra in order to get H<sub>2</sub>O band free spectra of the DMPs. Therefore, the suitable H<sub>2</sub>O spectrum was recorded and subtracted from the sample spectra in order to get clear spectra of phenanthrene. This set-up has been used for the gas phase IR spectroscopic study of dimethylphenanthrenes (DMPs).

## 2.4 Theoretical methods

### 2.4.1 Harmonic and anharmonic frequency calculations

The potential energy for a polyatomic molecule can be expanded in a Taylor series,<sup>10</sup>

$$V = \frac{1}{2} \sum_i \omega_i q_i^2 + \frac{1}{6} \sum_{ijk} \phi_{ijk} q_i q_j q_k + \frac{1}{24} \sum \phi_{ijkl} q_i q_j q_k q_l + \dots, \quad (2.4)$$

where  $\omega_i$ s are the harmonic frequencies (in cm<sup>-1</sup>),  $q_i$ s the normal coordinates, and  $\phi_{ijk}$  and  $\phi_{ijkl}$  the third and fourth order force constants of the molecules, respectively. Further  $\phi_{ijk}$  and  $\phi_{ijkl}$  are given by

$$\phi_{ijk} = \frac{\partial^3 E^{el}}{\partial q_i \partial q_j \partial q_k} \text{ and } \phi_{ijkl} = \frac{\partial^4 E^{el}}{\partial q_i \partial q_j \partial q_k \partial q_l} \quad (2.5)$$

where  $E^{el}$  is the electronic plus the nuclear repulsion energy term in the BO approximation.

The total vibrational energy including anharmonicity is then

$$E = \sum_i \omega_i \left( \nu_i + \frac{d_i}{2} \right) + \sum_{i \leq j} x_{ij} \left( \nu_i + \frac{d_i}{2} \right) \left( \nu_j + \frac{d_j}{2} \right) + \sum_{i \leq j} l_i l_j g_{ij} \quad (2.6)$$

where  $\omega_i$  and  $d_i$  are, respectively, the harmonic frequencies and the degeneracy of the  $i$ -th mode;  $\nu_i$ , the vibrational and  $l_i$ , the nuclear vibrational angular-momentum quantum numbers, and  $x_{ij}$  and  $g_{ij}$  the anharmonic constants, which are related to the third and fourth order force fields as shown in details in Ref.<sup>11</sup>

In this thesis, the optimized geometry, harmonic and anharmonic frequency calculations were carried out at the DFT/B3LYP level of theory and polarized-basis sets such as 6-31G\*, 6-311G\*\* and 6-311++G\*\* were used depending on the size of the molecules and time taken to finish a single point calculation. All the calculations have been carried out using G98, G03 and G09 computational codes in an IBM RS/6000, IBM Cluster P720 (IBL-64) and Tesla Cluster (EM64L) computers, respectively.

#### **2.4.2 Scaled quantum mechanical (SQM) force field calculation**

The characterization of the observed infrared spectra requires correct identification of the fundamental and non-fundamental vibrational modes. The electronic structure calculations derive harmonic frequencies by diagonalizing the matrix of the second derivative of energy with respect to the nuclear coordinates. But for accuracy we need anharmonic force constants which include the cubic and quartic force constants. Another way to resolve this problem is to consider only the harmonic frequencies and make corrections for errors by means of some scaling procedure.<sup>12, 13</sup>

Most accepted scaling procedure is Pulay's scaled quantum mechanical (SQM) method where force constants were scaled rather frequencies. Therefore, I have carried out scaled force field calculation in order to get calculated frequencies closer to experimental frequencies and potential energy distributions (PEDs) of the normal modes in terms of the local

coordinates of the molecule using a modified UMAT program<sup>14</sup> in the QCPE package.<sup>15</sup> The QCPE consists of four FORTRAN programs which have been designed to solve Wilson's GF matrix for a complete vibrational analysis. This method requires the definition of a basis set which is employed to construct the normal coordinates. The UMAT program allows for the definition of unsymmetrized or symmetrized basis sets, referred to as internal and symmetry coordinates, respectively. These are related to Cartesian coordinates via the B and U Matrices through the following relationships:

$$R = BX \text{ ----- (2.7)}$$

$$S = UR = UBX = B^{Sym} X \text{ ----- (2.8)}$$

where  $R$ ,  $S$  and  $X$  represent the column vectors of the internal, symmetry and Cartesian coordinates, respectively. The inverse Kinetic Energy Matrices,  $G$  and  $G^{Sym}$  defined by the B or  $B^{Sym}$  as

$$G = BM^{-1}B^t \text{ ----- (2.9)}$$

$$G^{Sym} = (B^{Sym})M^{-1}(B^{Sym})^t = UBM^{-1}B^tU^t \text{ ----- (2.10)}$$

where the superscript "t" indicates "transpose" and the  $M^{-1}$  is a diagonal matrix which contains the inverses of the masses of the atoms.<sup>16</sup> Using the  $G$  or  $G^{Sym}$  matrix, in conjunction with the appropriate Potential Energy ( $F$  or  $F^{Sym}$ ) matrix, the vibrational secular equation has been formulated in either an unsymmetrized or a symmetrized fashion:

$$GFL = L\Lambda \text{ ----- (2.11)}$$

$$G^{Sym}F^{Sym}L^{Sym} = L^{Sym}\Lambda \text{ ----- (2.12)}$$

Where  $\Lambda$  is the frequency matrix ( $\lambda_i=4\pi^2\nu_i^2$ ) and L is the eigenvector matrix describing the normal modes. Usually  $F$  is varied and  $\Lambda$  is calculated until it matches with the experimental frequencies. We modify  $\Lambda$  with small correction  $\Delta\Lambda$  given by  $\Delta\Lambda = (\Lambda_{\text{expt.}} - \Lambda)(\text{iter} - 1)/N_{\text{iter}}$  where  $N_{\text{iter}}$  is the total number of iterations. In our fitting I have used  $N_{\text{iter}}=100$ . The details can be found in Ref.<sup>17</sup>

In order to do this analysis, the following steps were followed: First, the internal coordinates were defined for PAHs. Then a set of nonredundant local coordinates were constructed as recommended by Pulay.<sup>12, 13</sup> Force constants in Cartesian coordinates obtained from Gaussian outputs were transformed in terms of nonredundant local coordinates.<sup>18</sup> Finally scaled force constants were obtained by fitting calculated frequencies to the observed frequencies by means of a least square fitting procedure using an algorithm developed by Chakraborty et al.<sup>14</sup> We have done this analysis with the experimental band origin frequencies. The fitting algorithm requires all the experimental frequencies; however, experimentally it was not possible to resolve all the fundamentals in the PAHs studied here. The fitting algorithm requires all the experimental frequencies to obtain a good fit. Therefore, we guessed some of the fundamental frequencies that are not seen in the recorded spectra. The guessed frequencies are chosen to be close to the scaled harmonic frequencies (C-H stretching and non C-H stretching frequencies were multiplied by factors, 0.9588 and 0.9733, respectively) which give minimum RMS errors. Then the PEDs were obtained using fitted force constants using FTRY-ATOM-RMSA-INTY program in the QCPE package.

### **2.4.3 Error analysis**

An error analysis was done in terms of mean deviation,  $\delta$  (in  $\text{cm}^{-1}$ ), between the observed and calculated (harmonic, anharmonic and force field fitted) frequencies using

$$\delta = \frac{\sum_{i=1}^n |v_i^{\text{cal.}} - v_i^{\text{exp.}}|}{n} \quad \text{--- (2.13)}$$

where  $v^{\text{cal.}}$  &  $v^{\text{exp.}}$  are calculated and observed frequencies, respectively, and  $n$  is the total number of fundamentals assigned in the recorded spectra.

## 2.5 IR band intensity calculation

### 2.5.1 Intensity

The quantity of interest in the intensity calculation is the integrated absorption coefficient  $A$  (in  $\text{km mol}^{-1}$ ) which can be determined theoretically using the following equation<sup>19</sup>

$$A_i = 42.254 \left| \frac{\partial \mu}{\partial Q_i} \right|^2 \quad \text{--- (2.14)}$$

where  $\partial \mu / \partial Q_i$  are the dipole moment derivatives in  $\text{D}(\text{\AA} \text{ amu}^{1/2})$  evaluated via analytical derivatives computed at the DFT/B3LYP level of theory.

On the other hand, absolute intensity (in  $\text{cm}^{-2} \text{ atm}^{-1}$ ) can be obtained experimentally by using the following expression given by Galabov et al.<sup>20</sup>

$$A_i = \frac{2.303 \int \log(I_o / I)_i d\nu_i}{P_i l} \quad \text{--- (2.15)}$$

where  $l$  (in cm) is the optical path length and  $P_i$ s are the vapor pressures. In our experiment, it is not possible to get the vapor pressure of PAHs or dimethyl-PAHs by conventional pressure gauge system since they are seeded on Ar gas. Therefore, we estimated the vapor pressures

$(P_i)$  under all the bands with the help of the observed band areas and their corresponding calculated intensities by using the same equation (see the next section). The average pressure obtained from all the bands were then calculated using  $P = \sum_{i=1}^n \frac{P_i}{n}$ , where  $n$  is the total number of observed bands and was used to calculate the observed band intensities (in  $\text{cm}^{-2} \text{atm}^{-1}$ ). In order to get the experimental intensities in  $\text{km mol}^{-1}$ , the values in  $\text{cm}^{-2} \text{atm}^{-1}$  were multiplied by factor of 82.056 (T/K).<sup>21</sup>

### 2.5.2 Vapor pressure calculation

In section 2.5.1, it has been discussed that the vapor pressure is a necessary parameter for the absolute intensity calculation. The vapor pressures at experimental temperatures under all the observed bands were calculated with the help of the following equation which is obtained by rearranging 2.15

$$P_i(\text{atm}) = 2.303 \times 82.056 \times T(K) \times 10^{-5} \tau_i / A_i l \text{ --- (2.16)}$$

where  $\tau_i = \int \log I_0 / I d\nu$  are the integrated band areas ( $\text{cm}^{-1}$ ) obtained experimentally and  $A_i$  are the infrared band intensities (in  $\text{km mol}^{-1}$ ) obtained from DFT calculations. The average value over all the partial pressures is considered as vapor pressure of the PAHs.

### 2.6 Simulated spectra

From the Gaussian output results we could predict the spectra of PAHs and diols. Simulated spectra were produced with the calculated frequencies and their intensities using FORTRAN code, where each frequency-intensity pair was modeled as a Gaussian function,  $f(\nu)$ , centered at the calculated frequency.<sup>22</sup>

$$f(\nu) = \tau \exp\{-(\nu - \nu_o)^2 / 2\sigma^2\} \text{ --- (2.17)}$$

Here,  $\tau$  is the intensities in  $\text{km mol}^{-1}$ ,  $\nu$  is the energy in units of  $\text{cm}^{-1}$ , and  $\sigma$  is the FWHM.

## 2.7 References

- [1] Michelson, A. A. *Philos. Mag.* **1981**, 31, 245.
- [2] *Hand book of Vibrational spectroscopy* by Smith, G. D.; Palmer, R. A. **2002**, 1, 625.
- [3] Sonnefeld, W. J.; Zoller, W.H.; May, W. E. *Anal. Chem.* **1983**, 55, 275.
- [4] Kurtz, J. *Astron. Astrophys.* **1992**, 255, L1.
- [5] Joblin, C.; d'Hendecourt, L.; Léger, A.; Défourneau, D. *Astron. Astrophys.* **1944**, 281, 923.
- [6] Joblin, C.; Boissel, P.; Léger, A.; d'Hendecourt, L.; Défourneau, D. *Astron. Astrophys.* **1995**, 299, 835.
- [7] [http://www.ftir.com/html/long\\_path\\_gas\\_cell.html](http://www.ftir.com/html/long_path_gas_cell.html)
- [8] Herriott, D. R.; Schulte, H. J. *Appl. Optics.* **1965**, 4, 883.
- [9] ONIC Software in "870 User's Guide, Nexus, Thermonicolet".
- [10] Miani, A.; Cane, E.; Palmieri, P.; Trombetti, A.; Handy, N. C. *J. Chem. Phys.* **2000**, 112, 248.
- [11] Papousek, D.; Aliev, M. R. *Molecular Vibrational/Rotational Spectra* (Academia, Parague, **1982**).
- [12] Pulay, P.; Fogarasi, G.; Pongor, G.; Boggs, J. E.; Vargha, A. *J. Am. Chem. Soc.* **1983**, 105, 7037.
- [13] Sellers, H.; Pulay, P.; Boggs, J. E. *J. Am. Chem. Soc.* **1985**, 107, 6487.
- [14] Chakraborty, D.; Ambashta, R.; Monogaran, S. *J. Phys. Chem.* **1996**, 100, 13963.
- [15] UMAT, McIntosh D.F.; Peterson, M. R. *General Vibrational Analysis System, QCPE 576*. Indiana University, Bloomington, IN 47405.



- [16] Wilson, Jr., E. B; Decius, J. C.; Cross, P. C. *Molecular Vibrations: The Theory of Infrared and Raman Vibrational Spectra*, Dover Publications, Inc., New York, **1980**.
- [17] Manogaran, S.; Chakraborty, D. *J. Mol. Struct. (THEOCHEM)* **1998**, *432*, 139.
- [18] Raghubanshi, D.; Maheshwary, S.; Manogaran, S. *J. Mol. Struct. (THEOCHEM)* **2001**, *574*, 245.
- [19] Stoppa, P.; Charmet, P. A.; Tasinato, N.; Giorgianni, S.; Gambi, A. *J. Phys. Chem. A* **2009**, *113*, 1497.
- [20] Galabov, B. S.; Dudev, T. *Vibrational Intensities*. In: J. R. Durig (Ed.), *Vibrational Spectra and Structure*, Vol-22, Elsevier, Amsterdam, **1996**.
- [21] Pugh, L. A.; Rao, K. N. *Infrared Intensities from Infrared Spectra*. In: K. Narahari Rao (Ed.), *Molecular spectroscopy: Modern Research, Volume II*, **1976**.
- [22] Levine, I. N. *Molecular Spectroscopy*, John Willey & Sons, **1975**.

# **Chapter-3**

## **Infrared Spectroscopic Studies of Dimethylnaphthalenes (DMNs) in the Gas Phase**

### **3.1 Introduction**

In chapter 1, I have discussed that the naphthalene and alkylated naphthalenes are semi-volatile polycyclic aromatic hydrocarbons (PAHs) present in the atmosphere in the gas and particle phases.<sup>1</sup> Diesel fuel contains alkyl-PAHs including methyl naphthalenes (MNs) and dimethylnaphthalenes (DMNs).<sup>2, 3</sup> In urban areas emission from diesel-fueled vehicles puts these compounds in the atmosphere.<sup>4, 5</sup> The alkylated PAHs have also been identified in individual interplanetary dust particles (IDPs).<sup>6</sup> The toxicity, carcinogenicity and mutagenicity of DMNs are different, and thus, it is important to identify and distinguish them at low concentrations.<sup>7-9</sup>

In this chapter, I report the infrared spectra at 0.5 cm<sup>-1</sup> resolution of three dimethylnaphthalenes (DMNs), namely 1,5-DMN, 1,6-DMN, and 2,6-DMN in the gas phase at an elevated temperature recorded with the help of a variable path-length cell. I have carried out DFT calculations to assign the experimentally observed spectral lines. The calculations have been performed at B3LYP level of theory with 6-31G\* as basis set to determine the harmonic frequencies and intensities of the DMNs. The motivation to do this work is to identify and distinguish DMNs by IR spectroscopy.

### **3.2 Materials and Methods**

#### **3.2.1 Materials**

DMNs used in this investigation are 1,6-dimethylnaphthalene (98.0%, Fluka), 1,5-dimethylnaphthalene (98.0%, Aldrich Chem. Co.), and 2, 6-dimethylnaphthalene (99.8%, Oekanal) which were obtained commercially. Some physical properties of DMNs are listed in Table 3.1.

**Table 3.1: Physical properties of DMNs**

Name of DMNs	m.p/b.p (°C)	P(in mmHg at 25 °C) <sup>est</sup>
1,5-DMN (Solid)	82.0	$1.17 \times 10^{-2}$
1,6-DMN (Liquid)	-17.0/263.0	$1.41 \times 10^{-2}$
2,6-DMN (Solid)	109.4	$1.66 \times 10^{-2}$

<sup>est</sup>Estimated vapor pressure taken from Ref.<sup>10</sup>

### 3.2.2 Experimental method

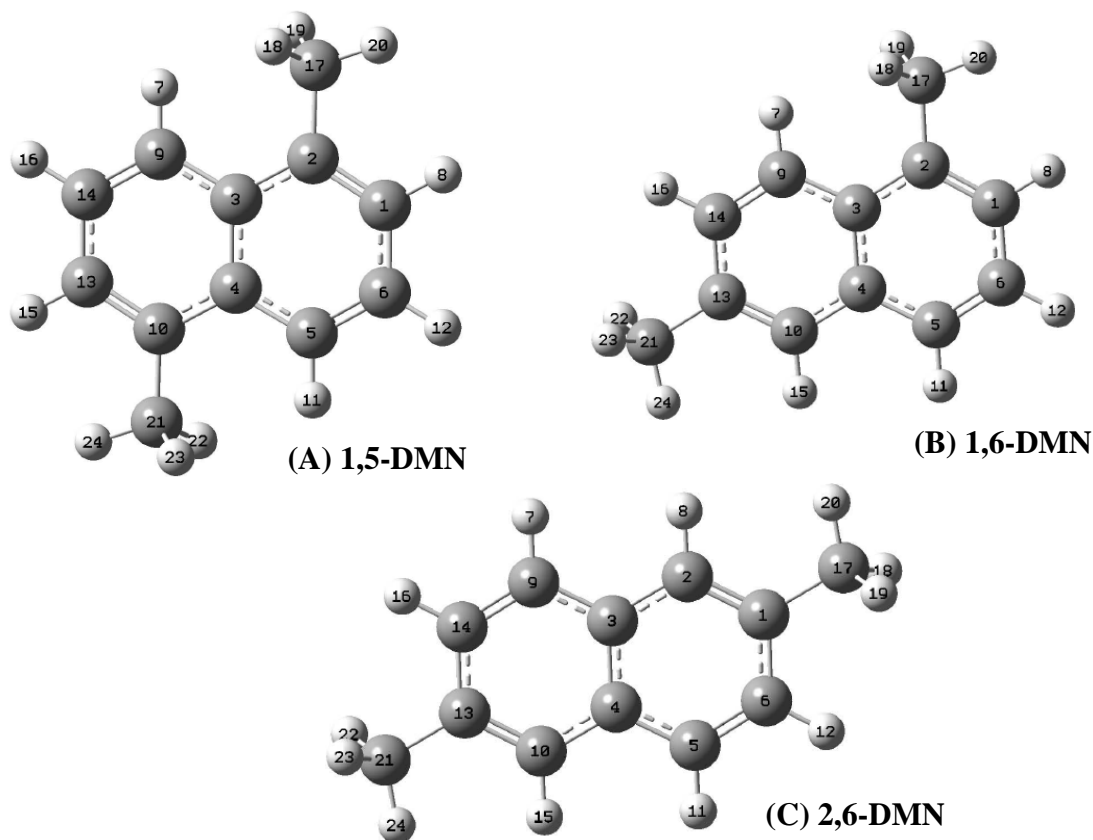
The experimental set-up, which has been used in this study, was discussed in section 2.3.1 of chapter 2. Since the compounds have low vapor pressure at RT (see Table 3.1), ultra high purity (99.999%) argon was used as a carrier gas to get the samples inside the cell. In this study, the optical path length was fixed at 6 meter. The sample DMN vapor mixed with Ar was introduced into the long path-length cell. Including the sample holder, the cell was heated and maintained at 90 °C. The DMNs were subjected to a repeated freeze/pump thaw procedure before use. The total pressure of argon gas containing DMNs in the cell was maintained at ~25 mmHg. Mid-infrared spectra (4000 – 400)  $\text{cm}^{-1}$  of DMNs were collected using a Deuterated Triglycine Sulphate (DTGS) detector/KBr beam splitter combination at 0.5  $\text{cm}^{-1}$  resolution with averaging over 2048 scans.

### 3.2.3 Theoretical calculation

Theoretical calculations were carried out using density functional theory (DFT) to determine the harmonic frequencies and intensities of 1,6-DMN, 1,5-DMN, and 2,6-DMN. The geometry optimization was carried out with standard polarization basis set 6-31G\* at the B3LYP (Becke 1993; Lee, Yang, & Parr 1988) level of theory using Gaussian 98 codes<sup>11</sup> in an

IBM RS/6000 computers. The frequencies and intensities were determined at the fully optimized  $C_1$  geometry (Figure 3.1). It was reported by Langhoff et al.<sup>12</sup> that many of the methyl PAHs is found to be of lower symmetry ( $C_1$ ) due to slight rotation of the methyl group, although the true point group of the molecule is  $C_s$ . In B3LYP calculations on DMNs, I found at least one imaginary frequency at the  $C_s$  optimized structure which is not realistic and thus  $C_1$  symmetry was chosen for calculation. The calculated frequencies were scaled by a factor of 0.9588 for the C-H stretch and 0.9733 for other vibrational modes to compare with experiment.<sup>13</sup>

**Figure 3.1. Optimized structure of (A) 1,5-DMN, (B) 1,6-DMN, and (C) 2,6-DMN at B3LYP/6-31G\* level.**



### 3.2.4 Vapor pressure and absolute intensity calculation

Observed band intensities were calculated with the help of measured band area and DFT calculated intensities as described in section 2.5 of chapter 2. The vapor pressure is a necessary parameter for the intensity calculation. For DMNs, the vapor pressures at 90 °C under all observed band were calculated with the help of equation 2.16 and result has been presented in Table 3.2. Estimated partial pressure found to be  $3.294 \times 10^{-5}$  atm for 1,5-DMN;  $5.590 \times 10^{-5}$  atm for 1,6-DMN; and  $2.743 \times 10^{-5}$  atm for 2,6-DMN at 90 °C.

**Table 3.2: Calculated intensity (A, km mol<sup>-1</sup>), observed band area ( $\tau$ , cm<sup>-1</sup>) and estimated vapor pressure (P, atm) for individual observed bands at 90 °C of DMNs.**

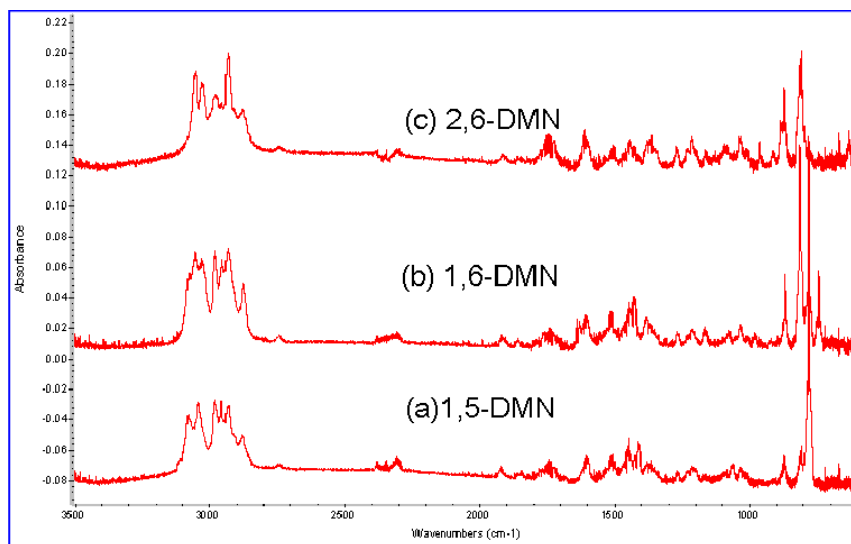
No	1,5-DMN			1,6-DMN			2,6-DMN		
	A	$\tau$	P $\times 10^{-5}$	A	$\tau$	P $\times 10^{-5}$	A	$\tau$	P $\times 10^{-5}$
1	0.34		--	0.51		--	1.16		--
2	0.00		--	0.47		--	0.00		--
3	0.00		--	0.11		--	0.04		--
4	2.27		--	0.69		--	0.39		--
5	0.00		--	0.61		--	0.00		--
6	0.44		--	1.71		--	0.88		--
7	3.76		--	0.22		--	0.00		--
8	0.00		--	0.05		--	2.91		--
9	0.00		--	3.04		--	0.00		--
10	0.00		--	0.13		--	0.00		--
11	0.00		--	0.89		--	2.31		--
12	1.23		--	2.61		--	5.94		--
13	0.00		--	2.15		--	0.00		--
14	5.30		--	0.39		--	0.00		--
15	0.89		--	1.03		--	1.21		--
16	0.00		--	0.66		--	3.40		--
17	0.00		--	1.03		--	1.35		--
18	0.00		--	0.64		--	0.00		--
19	2.48		--	5.93	0.49	9.446	0.00		--
20	66.58	1.77	3.039	14.14	0.66	5.336	0.00		--
21	0.00		--	31.45	1.39	5.052	31.33	0.80	2.919
22	0.00		--	0.68		--	0.00		--
23	<b>1.39</b>	0.17	11.100	<b>6.73</b>		--	22.41	0.55	2.806
24	<b>0.36</b>		--	<b>2.80</b>	0.44	5.277	0.00		--
25	0.00		--	0.41		--	<b>0.98</b>		--
26	1.11	0.18	18.538	0.17		--	<b>0.94</b>	0.06	3.571
27	0.00		--	0.91		--	0.00		-

**Table 3.2: (Continued) calculated intensity (A, km mol<sup>-1</sup>), observed band area (in cm<sup>-1</sup>) and estimated vapor pressure (P, atm) for individual observed bands at 90 °C of DMNs.**

No	1,5-DMN			1,6-DMN			2,6-DMN		
	A	$\tau$	$P \times 10^{-5}$	A	$\tau$	$P \times 10^{-5}$	A	$\tau$	$P \times 10^{-5}$
28	0.00		--	2.71		--	0.00		--
29	2.20		--	5.66	0.09	1.817	0.00		--
30	0.00		--	<b>5.39</b>		--	13.82	0.04	0.331
31	4.12	0.07	1.942	<b>1.09</b>	0.13	2.290	<b>8.56</b>	0.20	2.667
32	6.49	0.12	2.113	0.85			<b>0.01</b>		
33	0.00		--	2.64	0.12	5.196	1.83	0.10	6.247
34	0.00		--	0.56		--	0.00		--
35	1.19		--	1.00		--	3.95		--
36	0.00		--	2.59	0.13	5.730	0.00		--
37	2.76		--	1.71	0.14	9.357	1.02		--
38	0.00		--	0.30			0.00		--
39	2.43	0.06	2.823	3.18	0.14	5.033	5.22	0.32	7.008
		0.05	--			--	1.69	0.12	--
40	0.92		--	1.45		--	0.00		--
41	0.00		--	2.03		--	5.58	0.36	--
42	0.00		--	2.14			1.38		7.375
43	0.48	0.18	--	<b>0.77</b>	0.52	47.9	0.01		--
44	17.25		1.193	<b>0.47</b>		--	0.00		--
45	0.00		--	9.57	0.29	3.463	7.38		--
46	0.00	0.16	--	2.90		--	3.47	0.18	--
47	6.13		2.984	4.16			11.15		5.93
48	6.60		--	7.79	0.18	2.641	0.00		--
49	18.53		--	4.28		--	0.00		--
50	0.00	0.09	--	4.32		--	11.66	0.14	--
51	8.57		1.200	9.85	0.37	4.294	0.00		1.372
52	0.00	0.37	--	1.35		--	25.93	0.48	--
53	12.97		3.261	11.07	0.28	2.891	0.00		2.116
54	0.00	0.19	--	8.73	0.2	2.619		0.51	--
		0.07	--		0.45	--		0.04	--
		0.08	--		0.08	--		0.05	--
		0.04	--		0.19	--			--
			--		0.1	--	<b>81.85</b>		--
55	<b>58.53</b>	0.26	--	<b>35.41</b>		--	<b>4.79</b>	0.17	
56	<b>1.66</b>		0.493	<b>35.11</b>	0.55	0.864	17.05		0.224
57	12.25	0.19	--	9.81		--	27.68	0.44	--
58	29.00		0.526	23.10	0.55	1.910	<b>16.32</b>		1.817
59	<b>18.16</b>	0.09	--	<b>16.61</b>		--	<b>16.48</b>	0.01	--
60	<b>19.24</b>		0.270	<b>18.91</b>	0.11	0.353	21.39	0.15	0.034
61	25.83	0.32	--	16.86	0.56	3.797	0.00		0.802
62	0.00		1.41	<b>14.64</b>		--	33.06	0.21	--
63	0.16	0.44	--	<b>0.76</b>	0.38	2.820	0.00		0.726
64	49.13		1.023	30.16		--	62.53	0.38	--
65	<b>41.41</b>	0.29	--	37.47	0.22	0.671	0.00		0.695
66	<b>0.03</b>		0.799	15.71	0.18	1.309			

### 3.3 Results and Discussion

The gas phase IR spectra of the three DMNs are shown in Figure 3.2 and the experimental and theoretical infrared frequencies and intensities are listed in Tables 3.3 – 3.5. Absolute intensities are listed first while relative intensities are shown in parentheses. The relative intensities are given with respect to the strongest band seen in the range  $780 - 815 \text{ cm}^{-1}$ . The bands observed at  $783.3$ ,  $812.8$  and  $808.5 \text{ cm}^{-1}$  in 1,5-, 1,6-, and 2,6-DMN, respectively, correlate with the calculated fundamentals at  $786.5$ ,  $812.4$ , and  $811.6 \text{ cm}^{-1}$  and are assigned to a aromatic C-H out-of-plane bending mode of the DMNs. To compare the experimental, calculated and reported<sup>14</sup> spectra, I have displayed all DMN spectra separately in Figures 3.3 – 3.5. No IR spectrum for 1,6-DMN has been reported and, therefore, only observed and calculated spectra have been displayed in Figure 3.4.

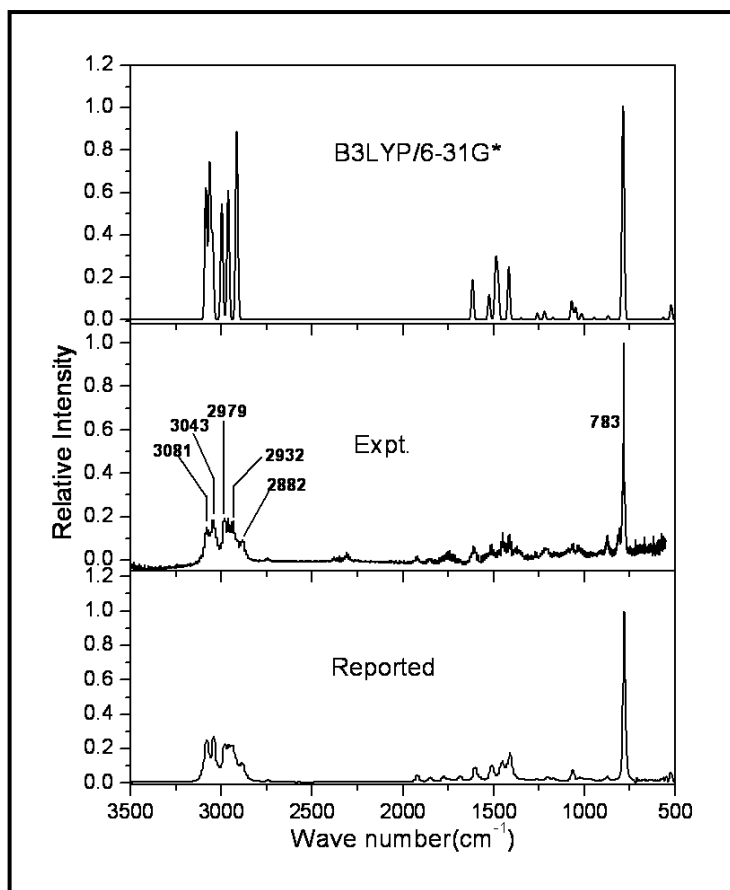


**Figure 3.2.** IR absorption spectra for (a) 1,5-DMN; (b) 1,6-DMN; and (c) 2,6-DMN at  $0.5 \text{ cm}^{-1}$  resolution.

Apart from the intense aromatic C-H out-of-plane bending mode mentioned above, many other low frequency aromatic C-H out-of-plane bending modes with lower intensities have been

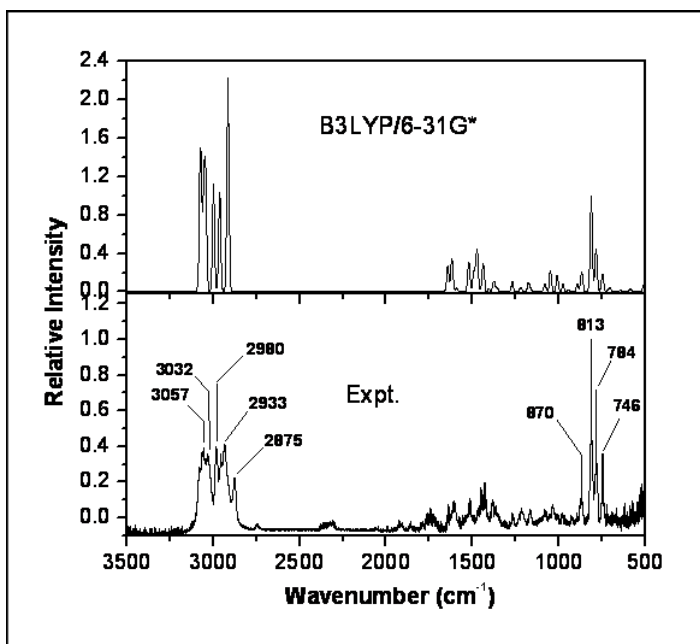


recorded and assigned in the spectra. Bands observed at 807.5 and 872.2  $\text{cm}^{-1}$  in 1,5-DMN; 746.2, 784.1, and 870.2  $\text{cm}^{-1}$  in 1,6-DMN; and 873.6 and 914.2  $\text{cm}^{-1}$  in 2,6-DMN are assigned to aromatic C-H out-of-plane bending vibrations by comparing with the respective calculated bands at 869.6 and 945.8  $\text{cm}^{-1}$  in 1,5-DMN; 747.3, 784.5, and 893.1  $\text{cm}^{-1}$  in 1,6-DMN; and 874.7 and 940.4  $\text{cm}^{-1}$  in 2,6-DMN. The next low intensity band appears at 1034.7  $\text{cm}^{-1}$  in 1,5-DMN, 1038.1  $\text{cm}^{-1}$  in 1,6-DMN, and at 1037.9  $\text{cm}^{-1}$  in 2,6-DMN.



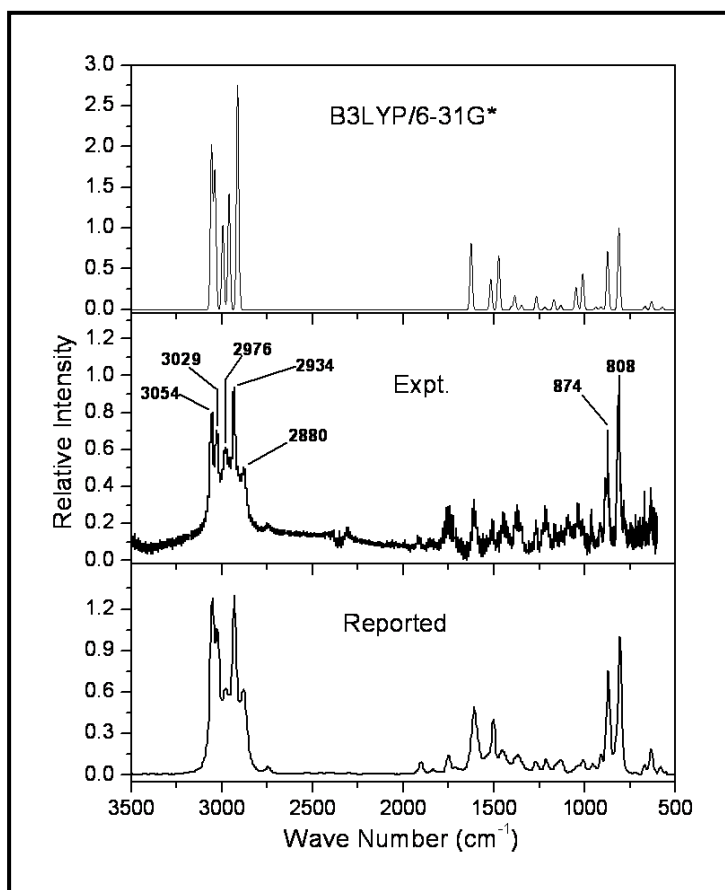
**Figure 3.3. Comparison of experimental, theoretical and NIST reported<sup>14</sup> IR reported spectra of 1,5-DMN. In the calculated spectrum, the FWHM is assumed to be 15  $\text{cm}^{-1}$ . Prominent peaks are labeled in the observed spectrum. Weak bands such as  $\text{Me}(\text{C-H})_{\text{asym. str.}}$  at 2956.9  $\text{cm}^{-1}$ , etc. are not labeled in the observed spectrum.**

This band has been assigned to a methyl C-H out-of-plane bending mode appearing at 1047.2/1048.5  $\text{cm}^{-1}$  in 1,5-DMN, 1048.2/1048.4  $\text{cm}^{-1}$  in 1,6-DMN, and 1047.6/1048.3  $\text{cm}^{-1}$  in 2,6-DMN in calculation. A methyl C-H in-plane bending vibration of low intensity is seen in 1,6-DMN at 981.9  $\text{cm}^{-1}$ . In 2,6-DMN the same band appears at 961.4  $\text{cm}^{-1}$ . The methyl C-H in-plane bending vibration is not observed in 1,5-DMN. A weak band at 1062.6  $\text{cm}^{-1}$  corresponding to the aromatic ring deformation mode is seen only in 1,5-DMN which match with the calculated band at 1069.7  $\text{cm}^{-1}$ . The aromatic C-H in-plane bending as well as ring deformation occurs at a slightly higher frequency. For 1,5-DMN it is observed at 1217.3  $\text{cm}^{-1}$ , for 1,6-DMN at 1217.5  $\text{cm}^{-1}$  and for 2,6-DMN at 1216.4  $\text{cm}^{-1}$ . The calculated positions are 1258.6, 1220.4, and 1267.7  $\text{cm}^{-1}$ , respectively.



**Figure 3.4.** Comparison of experimental and calculated IR spectra of 1,6-DMN. In the calculated spectrum the FWHM is assumed to be 15  $\text{cm}^{-1}$ . Prominent peaks are labeled in the observed spectrum. Weak bands such as  $\text{Me}(\text{C-H})_{\text{asym. str.}}$  at 2953.8  $\text{cm}^{-1}$ , Aromatic C-H stretch at 3078.0  $\text{cm}^{-1}$ , etc. are not labeled in the observed spectrum.

For the first and last compounds a band at  $1264.0\text{ cm}^{-1}$  and a band at  $1273.0\text{ cm}^{-1}$ , respectively, have been observed which do not correspond to any harmonic bands in the respective calculated spectrum. They have been tentatively assigned to either a combination or a difference band. For example, the  $1264.0\text{ cm}^{-1}$  band in 1,5-DMN may be a difference band arising from the two strong fundamentals ( $2882.4 - 1606.1\text{ cm}^{-1}$ ) while the  $1273.0\text{ cm}^{-1}$  band in 2,6-DMN may be a difference band from ( $2880.0 - 1612.9\text{ cm}^{-1}$ ).



**Figure 3.5. Comparison of experimental, theoretical and NIST reported<sup>14</sup> IR spectra of 2,6-DMN. In the calculated spectrum the FWHM is assumed to be  $15\text{ cm}^{-1}$ . Prominent peaks are labeled in the observed spectrum. Very weak band such as  $\text{Me}(\text{C-H})_{\text{asym. str.}}$  at  $2955.2\text{ cm}^{-1}$ , etc. are not labeled in the observed spectrum.**

Another weak aromatic C-H in-plane bending occurs at  $1413.9\text{ cm}^{-1}$  in 1,5-DMN,  $1426.5\text{ cm}^{-1}$  in 1,6-DMN, and  $1365.0\text{ cm}^{-1}$  in 2,6-DMN which correspond to the calculated bands at  $1416.2$ ,  $1437.9$ , and  $1386.1\text{ cm}^{-1}$ , respectively. In addition, in 1,6-DMN and 2,6-DMN a low intensity band, respectively, at  $1076.0$  and  $1093.1\text{ cm}^{-1}$  have been assigned to aromatic C-H in-plane bending vibration. The next identifiable band in the spectra occurs at  $1448.9\text{ cm}^{-1}$  in 1,5-DMN,  $1450.0\text{ cm}^{-1}$  in 1,6-DMN, and at  $1450.1\text{ cm}^{-1}$  in 2,6-DMN. This band corresponds to the calculated bands in the respective compounds at  $1474.0/1474.1$ ,  $1473.5/1474.1$ , and  $1472.6/1472.7\text{ cm}^{-1}$  belonging to the methyl C-H out-of-plane twisting. The next set of weak bands appears at  $1510.9$  and  $1606.1\text{ cm}^{-1}$  in 1,5-DMN;  $1513.6$ ,  $1605.8$ , and  $1638.6\text{ cm}^{-1}$  in 1,6-DMN; and at  $1510.9$  and  $1612.9\text{ cm}^{-1}$  in 2,6-DMN. These bands have been identified as the aromatic C-C stretching vibrations from the calculations.

The next groups of 3 - 4 bands in the spectra of the DMNs do not correspond to any band positions in the calculated spectra and, thus, have been generally identified as combination or difference bands. In 1,5-DMN, the observed band at  $1745.3\text{ cm}^{-1}$  matches with a difference band of  $(2956.9 - 1217.3)\text{ cm}^{-1}$  consisting of two fundamentals and that at  $1848.6\text{ cm}^{-1}$  is due to a combination of two bands  $(1062.6 + 807.5)\text{ cm}^{-1}$ . Similarly, a combination band at  $1922.2\text{ cm}^{-1}$  of fundamental frequencies  $(1062.6 + 872.2)\text{ cm}^{-1}$  has been identified. The observed band at  $2744.6\text{ cm}^{-1}$  in 1,5-DMN may be assigned as a difference band originating from the combination of fundamental frequencies  $(2931.8 - 1217.3 + 1034.7)\text{ cm}^{-1}$ . The bands observed at  $1741.0$ ,  $1858.9$ ,  $1922.4$ , and  $2746.6\text{ cm}^{-1}$  in 1,6-DMN do not correspond to any calculated band. The band observed at  $1741.0\text{ cm}^{-1}$  could be a difference band of two fundamental frequencies  $(2953.8 - 1217.5)\text{ cm}^{-1}$  whereas the weak  $1858.9\text{ cm}^{-1}$  band may originate from a coupled vibration of aromatic C-H in plane bending vibration at  $1076.0\text{ cm}^{-1}$  and aromatic C-H

out-of-plane bending vibration at  $812.8\text{ cm}^{-1}$ , while the band observed at  $1922.4\text{ cm}^{-1}$  is a combination band of frequencies ( $1076.0 + 870.2\text{ cm}^{-1}$ ).

**Table 3.3: Calculated and experimental infrared frequencies (in  $\text{cm}^{-1}$ ) and intensities (in  $\text{km mol}^{-1}$ ) for 1,5-DMN.**

No	Theoretical		Experimental		NIST Data <sup>b</sup>		Mode of Vibrations
	Freq. <sup>a</sup>	Int. (Rel. Int.)	Freq.	Int. (Rel. Int.)	Freq.(Rel. Int.) <sup>c</sup>		
1	93.89	0.34 (0.005)					
2	162.66	0.00 (0.000)					
3	182.99	0.00 (0.000)					
4	190.28	2.27 (0.034)					
5	202.17	0.00 (0.000)					
6	253.25	0.44 (0.006)					
7	263.59	3.76 (0.056)					
8	323.01	0.00 (0.000)					
9	453.84	0.00 (0.000)					
10	455.30	0.00 (0.000)					
11	469.75	0.00 (0.000)					
12	479.88	1.23 (0.018)					
13	504.95	0.00 (0.000)					
14	521.55	5.30(0.079)					
15	567.17	0.89 (0.013)					
16	626.00	0.00 (0.000)					
17	628.42	0.00 (0.000)					
18	730.99	0.00 (0.000)					
19	777.75	2.48 (0.037)					
20	786.50	66.58 (1.000)	783.3	61.42(1.000)	781.9	(1.000)	$\alpha_{\text{Ar(C-H)}}$
21	802.06	0.00 (0.000)					
22	842.89	0.00 (0.000)					
23	869.65	1.39 (0.020)	807.5	5.89(0.096)			$\alpha_{\text{Ar(C-H)}}$
24	877.85	0.36 (0.005)					
25	889.48	0.00 (0.000)					
26	945.88	1.11 (0.016)	872.2	6.24(0.101)	873.9	(0.042)	$\alpha_{\text{Ar(C-H)}}$
27	947.32	0.00 (0.000)					
28	985.96	0.00 (0.000)					
29	1015.13	2.20(0.033)					
30	1047.22	0.00(0.000)					
31	1048.50	4.12(0.061)	1034.7	2.42(0.039)			$\beta_{\text{Me(C-H)}}$
32	1069.71	6.49(0.097)	1062.6	4.16(0.067)	1064.1	(0.075)	$\gamma_{\text{Ar-ring}}$
33	1100.39	0.00(0.000)					
34	1135.14	0.00(0.000)					
35	1174.00	1.19(0.017)					
36	1174.16	0.00(0.000)					
37	1218.38	2.76(0.041)					
38	1233.35	0.00(0.000)					
39	1258.63	2.43(0.036)	1217.3	2.08(0.033)			$\delta_{\text{Ar(C-H)}} + \gamma_{\text{Ar-ring}}$
			1264.0	1.73(0.028)			
40	1348.38	0.92(0.013)					

**Table 3.3: (Continued) calculated and experimental infrared frequencies (cm<sup>-1</sup>) and intensities in km mol<sup>-1</sup> for 1,5-DMN.**

No	Theoretical		Experimental		NIST Data <sup>b</sup>		Mode of Vibrations
	Freq. <sup>a</sup>	Int. (Rel. Int.)	Freq.	Int. (Rel. Int.)	Freq.(Rel. Int.) <sup>c</sup>		
41	1362.95	0.00(0.000)					
42	1403.11	0.00(0.000)					
43	1404.75	0.48(0.007)					
44	1416.24	17.25(0.259)	1413.9	6.24(0.101)	1410.2	(0.173)	$\delta_{\text{Ar(C-H)}}$
45	1416.69	0.00(0.000)					
46	1472.51	0.00(0.000)					
47	1474.06	6.13(0.092)	1448.9	5.55(0.090)	1451.0	(0.068)	$\tau_{\text{Me(C-H)}}$
48	1474.19	6.60(0.099)					
49	1486.78	18.53 (0.278)					
50	1494.33	0.00(0.000)					
51	1524.04	8.57(0.128)	1510.9	3.12(0.050)	1510.7	(0.116)	$\nu_{\text{Ar(C-C)}}$
52	1598.43	0.00(0.000)					
53	1615.03	12.97(0.194)	1606.1	12.83(0.209)	1600.5	(0.146)	$\nu_{\text{Ar(C-C)}}$
54	1629.94	0.00(0.000)					
					1681.8	(0.040)	
			1745.3	6.59(0.107)	1774.1	(0.034)	
			1848.6	2.42(0.039)	1848.8	(0.044)	
			1922.2	2.77(0.045)	1920.0	(0.608)	
			2744.6	1.38(0.022)			
55	2913.59	58.53(0.879)					
56	2913.92	1.66(0.024)	2882.4	9.02(0.146)	2882.6	(0.043)	$\chi_{\text{Me(C-H) Sym}}$
57	2961.12	12.25(0.183)					
58	2961.25	29.00(0.435)	2931.8	6.59(0.107)	2938.6	(0.055)	$\chi_{\text{Me(C-H) Asym}}$
59	2995.98	18.16(0.272)					
60	2997.18	19.24(0.288)	2956.9	3.12(0.050)	2957.9	(0.012)	$\chi_{\text{Me(C-H) Asym}}$
61	3045.84	25.83(0.387)					
62	3046.36	0.00(0.000)	2979.4	11.10(0.180)	2977.2	(0.085)	$\Pi_{\text{Ar(C-H)}}$
63	3062.31	0.16(0.002)					
64	3062.45	49.13(0.737)	3043.2	15.26(0.248)	3041.3	(0.175)	$\Pi_{\text{Ar(C-H)}}$
65	3083.33	41.41(0.621)					
66	3083.79	0.03(0.000)	3081.0	10.06(0.163)	3079.9	(0.252)	$\Pi_{\text{Ar(C-H)}}$

<sup>a</sup>The B3LYP/6-31G\* frequencies are scaled by 0.9588 for C-H stretching and 0.9733 for other modes.<sup>13</sup>

<sup>b</sup>adapted from Ref.<sup>14</sup>

<sup>c</sup>In case of the NIST reported spectra, only relative intensities are given in parentheses.

$\alpha_{\text{Ar(C-H)}}$ = Aromatic C-H out-of-plane,  $\beta_{\text{Me(C-H)}}$ = Methyl C-H out-of-plane bending,  $\gamma_{\text{Ar-ring}}$ = Aromatic ring deformation,  $\delta_{\text{Ar(C-H)}}$ = Aromatic C-H in-plane bending,  $\tau_{\text{Me(C-H)}}$ = Methyl C-H out-

of-plane twist,  $\nu_{\text{Ar(C-C)}}$ = Aromatic (C-C) stretching,  $\chi_{\text{Me(C-H)Sym}}$ = Methyl C-H symmetric stretching,  $\chi_{\text{Me(C-H)Asym}}$ = Methyl C-H asymmetric stretching,  $\Pi_{\text{Ar(C-H)}}$ = Aromatic C-H stretching.

**Table 3.4: Calculated and experimental infrared frequencies (in  $\text{cm}^{-1}$ ) and intensities (in  $\text{km mol}^{-1}$ ) for 1,6-DMN.**

No	Theoretical		Experimental		Mode of Vibrations
	Freq. <sup>a</sup>	Int. (Rel.Int.)	Freq.	Int. (Rel.Int.)	
1	88.72	0.51(0.016)			
2	107.00	0.47(0.014)			
3	148.54	0.11(0.003)			
4	189.46	0.69(0.022)			
5	233.38	0.61(0.019)			
6	247.55	1.71(0.054)			
7	285.04	0.22(0.007)			
8	328.34	0.05(0.001)			
9	426.34	3.04(0.096)			
10	452.48	0.13(0.004)			
11	463.72	0.89(0.028)			
12	494.88	2.61(0.083)			
13	509.77	2.15(0.068)			
14	561.05	0.39(0.012)			
15	584.63	1.03(0.032)			
16	642.55	0.66(0.021)			
17	703.38	1.03(0.033)			
18	710.37	0.64(0.020)			
19	747.33	5.93(0.188)	746.2	10.02(0.352)	$\alpha_{\text{Ar(C-H)}}$
20	784.54	14.14(0.449)	784.1	13.49(0.474)	$\alpha_{\text{Ar(C-H)}}$
21	812.42	31.45(1.000)	812.8	28.42(1.000)	$\alpha_{\text{Ar(C-H)}}$
22	823.60	0.68(0.021)			
23	867.99	6.73(0.214)			
24	893.11	2.80(0.089)	870.2	8.99(0.316)	$\alpha_{\text{Ar(C-H)}}$
25	921.59	0.41(0.013)			
26	939.58	0.17(0.005)			
27	946.68	0.91(0.028)			
28	976.12	2.71(0.086)			
29	1009.17	5.66(0.179)	981.9	1.84(0.064)	$\sigma_{\text{Me(C-H)}}$
30	1048.29	5.39(0.171)			
31	1048.44	1.09(0.034)	1038.1	2.65(0.093)	$\beta_{\text{Me(C-H)}}$
32	1051.11	0.85(0.027)			
33	1080.50	2.64(0.084)	1076.0	2.45(0.086)	$\delta_{\text{Ar(C-H)}}$
34	1162.61	0.56(0.018)			
35	1167.46	1.00(0.032)			
36	1176.66	2.59(0.082)	1167.3	2.65(0.093)	$\delta_{\text{Ar(C-H)}}^+ \gamma_{\text{Ar-ring}}$
37	1220.44	1.71(0.054)	1217.5	2.86(0.101)	$\delta_{\text{Ar(C-H)}}^+ \gamma_{\text{Ar-ring}}$
38	1248.59	0.30(0.009)			
39	1268.85	3.18(0.101)	1269.7	2.86(0.101)	$\delta_{\text{Ar(C-H)}}^+ \gamma_{\text{Ar-ring}}$
40	1357.95	1.45(0.046)			

**Table 3.4: (Continued) calculated and experimental infrared frequencies (in  $\text{cm}^{-1}$ ) and intensities (in  $\text{km mol}^{-1}$ ) for 1,6-DMN.**

No	Theoretical		Experimental		Mode of Vibrations
	Freq. <sup>a</sup>	Int. (Rel.Int.)	Freq.	Int. (Rel.Int.)	
41	1373.18	2.03(0.064)			
42	1378.15	2.14(0.068)			
43	1404.22	0.77(0.024)	1380.4	10.63(0.374)	$\sigma_{\text{Me(C-H)}}$
44	1405.16	0.47(0.015)			
45	1437.97	9.57(0.304)	1426.5	5.93(0.208)	$\delta_{\text{Ar(C-H)}}$
46	1467.29	2.90(0.092)			
47	1473.55	4.16(0.132)			
48	1474.13	7.79(0.247)	1450.0	3.68(0.129)	$\tau_{\text{Me(C-H)}}$
49	1485.63	4.28(0.136)			
50	1494.07	4.32(0.137)			
51	1520.97	9.85(0.313)	1513.6	7.56(0.266)	$\nu_{\text{Ar(C-C)}}$
52	1590.91	1.35(0.043)			
53	1618.56	11.07(0.352)	1605.8	5.72(0.201)	$\nu_{\text{Ar(C-C)}}$
54	1642.67	8.73(0.277)	1638.6	4.08(0.143)	$\nu_{\text{Ar(C-C)}}$
			1741.0	9.2(0.323)	
			1858.9	1.63(0.057)	
			1922.4	3.88(0.136)	
			2746.6	2.04(0.072)	
55	2913.63	35.41(1.126)			
56	2914.28	35.11(1.116)	2874.8	11.24(0.395)	$\chi_{\text{Me(C-H) Sym}}$
57	2960.69	9.81(0.312)			
58	2961.83	23.10(0.734)	2933.3	11.24(0.395)	$\chi_{\text{Me(C-H) Asym}}$
59	2997.16	16.61(0.528)			
60	2997.86	18.91(0.601)	2953.8	2.24(0.079)	$\chi_{\text{Me(C-H) Asym}}$
61	3040.66	16.86(0.536)	2980.5	11.45(0.402)	$\Pi_{\text{Ar(C-H)}}$
62	3044.43	14.64(0.465)			
63	3045.16	0.76(0.024)	3031.8	7.77(0.273)	$\Pi_{\text{Ar(C-H)}}$
64	3052.60	30.16(0.958)			
65	3070.49	37.47(1.191)	3056.8	4.49(0.158)	$\Pi_{\text{Ar(C-H)}}$
66	3077.56	15.71(0.499)	3078.0	3.68(0.129)	$\Pi_{\text{Ar(C-H)}}$

<sup>a</sup>The B3LYP/6-31G\* frequencies are scaled by 0.9588 for C-H stretching and 0.9733 for other modes.<sup>13</sup>

$\alpha_{\text{Ar(C-H)}}$ =Aromatic C-H out-of-plane bending,  $\sigma_{\text{Me(C-H)}}$ = Methyl C-H in-plane bending,  $\beta_{\text{Me(C-H)}}$ = Methyl C-H out-of-plane bending,  $\gamma_{\text{Ar-ring}}$ = Aromatic ring deformation,  $\delta_{\text{Ar(C-H)}}$ = Aromatic C-H in-plane bending,  $\tau_{\text{Me(C-H)}}$ = Methyl C-H out-of-plane twist,  $\nu_{\text{Ar(C-C)}}$ = Aromatic (C-C) stretching,  $\chi_{\text{Me(C-H) Sym}}$ = Methyl C-H symmetric stretching,  $\chi_{\text{Me(C-H) Asym}}$ = Methyl C-H asymmetric stretching,  $\Pi_{\text{Ar(C-H)}}$ = Aromatic C-H stretching.



**Table 3.5: Calculated and experimental infrared frequencies (in  $\text{cm}^{-1}$ ) and intensities (in  $\text{km mol}^{-1}$ ) for 2,6-DMN.**

No	Theoretical		Experimental		NIST Data <sup>b</sup>		Mode of Vibrations
	Freq. <sup>a</sup>	Int. (Rel. Int.)	Freq.	Int. (Rel. Int.)	Freq.(Rel. Int.) <sup>c</sup>		
1	76.86	1.16(0.037)					
2	87.45	0.00(0.000)					
3	95.69	0.04(0.001)					
4	180.07	0.39(0.012)					
5	201.25	0.00(0.000)					
6	215.90	0.88(0.028)					
7	313.50	0.00(0.000)					
8	333.87	2.91(0.093)					
9	395.74	0.00(0.000)					
10	402.16	0.00(0.000)					
11	429.88	2.31(0.074)					
12	482.68	5.94(0.189)					
13	521.53	0.00(0.000)					
14	525.00	0.00(0.000)					
15	574.59	1.21(0.038)					
16	632.80	3.40(0.108)					
17	668.29	1.35(0.043)					
18	747.20	0.00(0.000)					
19	757.53	0.00(0.000)					
20	789.89	0.00(0.000)					
21	811.61	31.33(1.000)	808.5	33.33(1.000)	807.3	(1.00)	$\alpha_{\text{Ar(C-H)}}$
22	820.21	0.00(0.000)					
23	874.72	22.41(0.715)	873.6	22.91(0.687)	870.7	(0.61)	$\alpha_{\text{Ar(C-H)}}$
24	884.62	0.00(0.000)					
25	911.05	0.98(0.031)					
26	940.49	0.94(0.030)	914.2	2.50(0.075)			$\alpha_{\text{Ar(C-H)}}$
27	941.29	0.00(0.000)					
28	957.44	0.00(0.000)					
29	1004.40	0.00(0.000)					
30	1012.35	13.82(0.441)	961.4	1.66(0.049)			$\sigma_{\text{Me(C-H)}}$
31	1047.62	8.56(0.273)	1037.9	8.33(0.249)			$\beta_{\text{Me(C-H)}}$
32	1048.39	0.01(0.000)					
33	1132.27	1.83(0.058)	1093.1	4.16(0.124)			$\delta_{\text{Ar(C-H)}}$
34	1151.69	0.00(0.000)					
35	1170.53	3.95(0.126)					
36	1179.34	0.00(0.000)					
37	1220.40	1.02(0.032)					
38	1258.61	0.00(0.000)					
39	1267.74	5.22(0.166)	1216.4 1273.0	13.33(0.399) 5.00(0.150)			$\delta_{\text{Ar(C-H)}}^+ \gamma_{\text{Ar-ring}}$
40	1348.64	1.69(0.054)					
41	1383.14	0.00(0.000)					
42	1386.19	5.58(0.178)	1365.0	15.00(0.450)			$\delta_{\text{Ar(C-H)}}$
43	1405.15	1.38(0.044)					

**Table 3.5: (Continued) calculated and experimental infrared frequencies (in  $\text{cm}^{-1}$ ) and intensities (in  $\text{km mol}^{-1}$ ) for 2,6-DMN.**

No	Theoretical		Experimental		NIST Data <sup>b</sup>		Mode of Vibrations
	Freq. <sup>a</sup>	Int. (Rel. Int.)	Freq.	Int. (Rel. Int.)	Freq.(Rel. Int.) <sup>c</sup>		
44	1405.60	0.01(0.000)					
45	1412.03	0.00(0.000)					
46	1472.61	7.38(0.235)					
47	1472.76	3.47(0.110)	1450.1	7.50(0.225)	1449.9	(0.113)	$\tau_{\text{Me(C-H)}}$
48	1476.34	11.15(0.356)					
49	1485.87	0.00(0.000)					
50	1495.08	0.00(0.000)					
51	1518.62	11.66(0.372)	1510.9	5.83(0.175)	1504.7	(0.194)	$\nu_{\text{Ar(C-C)}}$
52	1582.20	0.00(0.000)					
53	1627.21	25.93(0.827)	1612.9	20.00(0.600)	1611.3	(0.714)	$\nu_{\text{Ar(C-C)}}$
54	1648.64	0.00(0.000)					
			1741.8	21.25(0.637)	1745.3	(0.125)	
			1908.1	1.66(0.049)	1906.0	(0.109)	
			2744.5	2.08(0.062)			
55	2913.68	81.85(2.612)					
56	2914.04	4.79(0.153)	2880.0	7.08(0.212)	2879.4	(0.312)	$\chi_{\text{Me(C-H) Sym}}$
57	2961.26	17.05(0.544)					
58	2961.40	27.68(0.883)	2933.9	18.33(0.549)	2931.2	(0.727)	$\chi_{\text{Me(C-H) Asym}}$
59	2995.19	16.32(0.521)					
60	2996.49	16.48(0.526)	2955.2	0.42(0.012)			$\chi_{\text{Me(C-H) Asym}}$
61	3037.89	21.39(0.682)	2976.5	6.25(0.187)	2978.8	(0.059)	$\Pi_{\text{Ar(C-H)}}$
62	3038.20	0.00(0.000)					
63	3040.93	33.06(1.055)	3028.9	8.75(0.262)	3027.8	(0.185)	$\Pi_{\text{Ar(C-H)}}$
64	3041.16	0.00(0.000)					
65	3058.03	62.53(1.996)	3054.5	15.83(0.474)	3053.7	(0.589)	$\Pi_{\text{Ar(C-H)}}$
66	3058.98	0.00(0.000)					

<sup>a</sup>The B3LYP/6-31G\* frequencies are scaled by 0.9588 for C-H stretching and 0.9733 for other modes.<sup>13</sup>

<sup>b</sup>adapted from Ref.<sup>14</sup>

<sup>c</sup> In case of the NIST reported spectrum, only relative intensities are given in parentheses.  $\alpha_{\text{Ar(C-H)}}$ = Aromatic C-H out-of-plane bending,  $\sigma_{\text{Me(C-H)}}$ = Methyl C-H In-plane bending,  $\beta_{\text{Me(C-H)}}$ = Methyl C-H out-of-plane bending,  $\gamma_{\text{Ar-ring}}$ = Aromatic ring deformation,  $\delta_{\text{Ar(C-H)}}$ = Aromatic C-H in-plane bending,  $\tau_{\text{Me(C-H)}}$ = Methyl C-H out-of-plane twist,  $\nu_{\text{Ar(C-C)}}$ = Aromatic (C-C) stretching,  $\chi_{\text{Me(C-H) Sym}}$ = Methyl C-H symmetric stretching,  $\chi_{\text{Me(C-H) Asym}}$ = Methyl C-H asymmetric stretching,  $\Pi_{\text{Ar(C-H)}}$ = Aromatic C-H stretching.

The observed band at  $2746.6\text{ cm}^{-1}$  may be assigned to a difference band of fundamental frequencies  $(2933.3 - 1217.5 + 1038.1)\text{ cm}^{-1}$ . In 2,6-DMN, the observed bands at  $1741.8$ ,  $1908.1$  and  $2744.5\text{ cm}^{-1}$  do not match with any band in the calculated spectrum. The band at  $1741.8\text{ cm}^{-1}$  is likely to be a difference band of the fundamental frequencies  $(2955.2 - 1216.4)\text{ cm}^{-1}$ . In general, the difference and combination bands are less intense than the fundamental bands.<sup>15</sup> The band observed at  $1908.1\text{ cm}^{-1}$  may be a combination band of frequencies  $(1093.1 + 808.5)\text{ cm}^{-1}$ . There is a medium intensity band observed at  $2744.5\text{ cm}^{-1}$  which is a difference band of three frequencies  $(2933.9 - 1216.4 + 1037.9)\text{ cm}^{-1}$ .

The next sets of bands observed in the DMNs are at high frequencies ( $2870 - 3090\text{ cm}^{-1}$ ), forms a broad envelope with several peaks and are of moderate intensities. The first three bands in this group are at  $2882.4$ ,  $2931.8$ , and  $2956.9\text{ cm}^{-1}$  in 1,5-DMN;  $2874.8$ ,  $2933.3$ , and  $2953.8\text{ cm}^{-1}$  in 1,6-DMN; and  $2880.0$ ,  $2933.9$ , and  $2955.2\text{ cm}^{-1}$  in 2,6-DMN; which from comparison with calculations have been identified as the methyl C-H symmetric and asymmetric stretching fundamentals. However, the calculated bands at these frequencies are doubly degenerate for each mode due to the presence of two methyl groups in the molecules. At our experimental resolution, these degeneracies cannot be lifted. The next 3 - 4 bands are also of moderate intensities and appear at  $2979.4$ ,  $3043.2$ , and  $3081.0\text{ cm}^{-1}$  in 1,5-DMN;  $2980.5$ ,  $3031.8$ ,  $3056.8$ , and  $3078.0\text{ cm}^{-1}$  in 1,6-DMN; and  $2976.5$ ,  $3028.9$ , and  $3054.5\text{ cm}^{-1}$  in 2,6-DMN. These bands correspond to 3 pairs of doublets in calculation as shown in Tables 3.3 - 3.5 and are assigned to aromatic C-H stretching modes. In 1,6-DMN the last doublet appears as the doublet in the observed spectrum and is clearly resolved.

Error analysis has done by means of mean deviation as discussed in section 2.4.3. Table 3.6 lists the mean deviations between two types of scaled harmonic frequencies and observed

fundamentals for DMNs. From this table it is clear that (i) the extent of anharmonicity of aromatic and methyl C-H stretching modes is more compared to non C-H stretching modes and (ii) altogether, the deviation is more than 20  $\text{cm}^{-1}$  irrespective of different types of vibrations of DMNs. It clearly indicates that the two scaling factors (one for the aromatic C-H stretches and another for all other modes) calculated by Bauschlicher et al.<sup>13</sup> for the non-substituted PAHs is less suitable for the scaling of the harmonic frequencies of substituted PAHs like methyl-PAHs at the B3LYP/6-31G\* level of theory.

**Table 3.6: Mean deviation,  $\delta$  (in  $\text{cm}^{-1}$ ) between scaled harmonic and experimental frequencies (in  $\text{cm}^{-1}$ ) for different modes of vibration in DMNs.**

Mode of vibration	1,5-DMN	1,6-DMN	2,6-DMN
Non C-H str	25.2	12.4	23.2
Aromatic and methyl C-H str	31.6	28.4	29.9

By comparing the DMN and MN spectra, it has been found that there is only one strong band in the reported spectrum of 1-MN due to the aromatic C-H stretching vibration above 3000.0  $\text{cm}^{-1}$  while there are two or more moderate intensity bands in the observed spectrum of the DMNs in that region. In Table 3.7, I have listed four characteristic bands of the DMNs which may help in their identification in an unknown mixture. The aromatic C-H out-of-plane bending vibration is the strongest in intensity among all the bands in DMNs and is easy to identify around 800.0  $\text{cm}^{-1}$ . The DMNs are distinguishable from the position of this band which appears with a clear separation in different DMNs. Methyl C-H symmetric and asymmetric stretching set of three bands is the next set of bands which are distinct in all the

DMNs. They appear clearly resolved at the high frequency end of the IR spectrum around  $2900.0\text{ cm}^{-1}$  with moderate intensities and can be easily marked.

**Table 3.7: Comparison of observed aromatic(C-H) out-of-plane bending and methyl C-H symmetric<sup>a</sup> and asymmetric stretching<sup>b</sup> vibrations in DMNs.**

Mode of vibration	1,5-DMN		1,6-DMN		2,6-DMN	
Aromatic C-H out-of-plane	783.2	(1.000)	812.8	(1.000)	808.5	(1.000)
Methyl C-H stretching	2882.4 <sup>a</sup>	(0.146)	2874.8 <sup>a</sup>	(0.395)	2880.0 <sup>a</sup>	(0.212)
	2931.8 <sup>b</sup>	(0.107)	2933.3 <sup>b</sup>	(0.395)	2933.9 <sup>b</sup>	(0.549)
	2956.9 <sup>b</sup>	(0.050)	2953.8 <sup>b</sup>	(0.079)	2955.2 <sup>b</sup>	(0.012)

*The band positions are given in  $\text{cm}^{-1}$  and the relative intensities in parentheses.*

### 3.4 Conclusion

In this chapter, I have reported the gas phase IR spectra of 1, 5-DMN, 1, 6-DMN, and 2, 6-DMN and assigned their vibrational modes using harmonic DFT calculation. In general experimental spectra are in good agreement with calculated spectra. However, deviations between calculated and observed frequencies are more than  $20\text{ cm}^{-1}$  which is less reliable for the quantitative analysis of experimental spectra. From the experimentally observed spectra it is possible to distinguish the DMNs based on the intensity and position of the aromatic C-H out-of-plane bending and methyl C-H symmetric and asymmetric stretching vibrations which are well resolved in frequency among various DMNs. These spectra at  $0.5\text{ cm}^{-1}$  resolution have many more features over the previously reported low resolution spectra of the DMNs. Further

studies with isotope substitution along with anharmonic analysis of the data are necessary to fully assign the vibrations of these differently substituted DMNs.

### 3.5 References

- [1] Wania, F.; Mackay, D. *Environ. Sci. Technol.* **1996**, *30*, 390A.
- [2] Williams, P. T.; Bartle, K. D.; Andrews, G. E. *Fuel* **1986**, *65*, 1150.
- [3] Bundt, J.; Herbel, W.; Steinhart, H.; Franke, S.; Francke, W. *High Resolut. Chromatogr.* **1991**, *14*, 91.
- [4] Nelson, P. F. *Fuel* **1989**, *68*, 283.
- [5] Zielinska, B.; Sagebiel, J. C.; Harshfield, G.; Gertler, A. W.; Pierson, W. R. *Atmos. Environ.* **1996**, *30*, 2269.
- [6] Clemett, S. J.; Maechling, C. R.; Zare, R. N.; Swan, P. D.; Walker, R. M. *Science* **1993**, *262*, 721.
- [7] Horton, A. W.; Denman, D. T.; Trosset, R. P. *Cancer Res.* **1957**, *17*, 758.
- [8] Rossi, S. S.; Neff, J. M. *Mar. Pollut. Bull.* **1978**, *9*, 220.
- [9] Shamsuddin, Z. A.; Rahimtula, A. D. *Drug Metab. Dispos.* **1988**, *14*, 724.
- [10] Christidis, P. D.; Harris, B. C.; McDonald, T. J.; Reese, E.; Autenrieth, R. L. *Chemosphere* **2003**, *52*, 869.
- [11] Eileen Frisch, M.J. Frisch, GAUSSIAN 98 User's Reference, Gaussian, Inc., Pittsburgh, PA, **1999**.
- [12] Langhoff, S. R.; Bauschlicher, C. W.; Hudgins, D. M.; Sandford, S. A.; Allamandola, L. J. *J. Phys. Chem. A* **1998**, *102*, 1632.
- [13] Bauschlicher, C. W.; Langhoff, S. R. *Spectrochim. Acta Part A* **1997**, *53*, 1225.
- [14] <http://webbook.nist.gov/chemistry>.
- [15] Herzberg, G. *Infrared and Raman Spectra of Polyatomic Molecules*, D. Van Nostrand Company, Inc., New York, **1946**.

# **Chapter-4**

## **Infrared Spectra of Dimethylquinolines (DMQs) in the Gas Phase: Experiment and Theory**



## **4.1 Introduction**

Methylated quinolines belong to a class of polycyclic aromatic hydrocarbons (PAHs) present in ambient air, in lake and marine sediments, in coal-tar, and in coker gas oil.<sup>1 - 4</sup> Synthetic fuel contains methylated quinolines, including methyl quinolines (MQs) and dimethylquinolines (DMQs).<sup>5</sup> MQs and DMQs have been found in ground water adjacent to an underground coal gasification site and in low-Btu coal gasifier tar.<sup>6-7</sup> They have also been identified in petroleum and petroleum substitutes.<sup>8 - 11</sup> In section 1.1.2 of chapter 1, I have discussed that many of these compounds have been reported to be mutagenic, toxic, and carcinogenic, they also act as tumor initiating agent.<sup>12 - 14</sup>

A few experimental techniques have been employed for the identification and detection of PAHs including alkylquinolines in the gas phase (see section 1.2, chapter 1). The infrared spectra of MQs are available in the NIST - IR spectral library.<sup>15</sup> Ozel et al. have carried out DFT calculation for the assignment of the vibrational bands of MQs.<sup>16</sup> Infrared spectra of 2,8-DMQ and trimethylquinolines (TMQs) have been recorded in CS<sub>2</sub> solution.<sup>17</sup>

In this chapter, I present the IR absorption spectra of DMQs in the gas phase which were recorded at low pressures using a heated multi-pass long-path gas cell. I have carried out DFT calculations to calculate harmonic and anharmonic frequencies and their intensities. Then SQM force field vibrational analysis have done to get fitted frequencies closer to the experimental frequencies and potential energy distributions (PEDs) of normal modes in terms of nonredundant local coordinates using a modified version of the UMAT program in the QCPE package.

## 4.2 Experimental: Materials and Methods

### 4.2.1 Materials

DMQs used in this investigation were obtained commercially and used as received. They are 2,4-dimethylquinoline (98.0%, Chiron AS), 2,6-dimethylquinoline (98.0%, Aldrich Inc), 2,7-dimethylquinoline (99.0%, Aldrich Inc) and 2,8-dimethylquinoline (99.9%, Chiron AS). Some physical properties of the DMQs are listed in Table 4.1. Ultra high purity (99.999%) argon was used in these experiments as a carrier gas.

**Table 4.1: Physical properties of DMQs**

Name	State at 25 °C	m.p/b.p (in °C)	P(in mmHg) <sup>a</sup> at 25 °C
2,4-DMQ	Liquid (98.0%)	b.p = 265	$1.64 \times 10^{-2}$
2,6-DMQ	Solid-powder (98.0%)	m.p = 58	$1.42 \times 10^{-2}$
2,7-DMQ	Solid -powder (99.0%)	m.p = 61	$1.82 \times 10^{-2}$
2,8-DMQ	Liquid (99.9%)	b.p = 255	$2.63 \times 10^{-2}$

<sup>a</sup>Since experimental vapor pressures are not available, calculated values are given<sup>18</sup> in column

4.

### 4.2.2 Methods

Infrared spectra of polycyclic aromatic compound (PAHs) have been reported mostly in Ar/He matrix because of their low vapor pressures at room temperature. I have used a multi-pass long-path gas cell to record the gas phase IR spectra of DMQs. The details of the experimental set-up have been discussed in section 2.2.4.1 of chapter 2. The FT-IR spectrometer, Vertex-70 (Bruker Optic), equipped with the liquid N<sub>2</sub> cooled HgCdTe (LN - MCT) detector/KBr beam splitter was used in this study. The optical path-length of gas cell was fixed at 6 meter. Temperature of the cell and sample tube was maintained at 80 °C with

the help of a temperature controller fitted with a feedback heat sensor. The total pressure of argon gas in the cell containing DMQs was maintained at ~30 mmHg. The spectral band areas  $\int \log(I_0/I) dv$  (in  $\text{cm}^{-1}$ ) were calculated with the help of OPUS software provided by Bruker Optics.

The observed IR band intensities were calculated with the help of equation 2.15. Vapor pressure was calculated in similar fashion as was done for DMNs in chapter 3. The estimated vapor pressure found to be  $1.47 \times 10^{-5}$ ,  $1.23 \times 10^{-5}$ ,  $2.01 \times 10^{-5}$ , and  $2.52 \times 10^{-5}$  atm at 80 °C for 2,4-, 2,6-, 2,7-, and 2,8-DMQ, respectively. The detail of the intensity calculation was discussed in section 2.5 of chapter 2.

### **4.3 Theoretical calculation**

#### **4.3.1 Harmonic and anharmonic calculation**

DFT calculations were carried out to determine the harmonic and anharmonic frequencies of the vibrational modes and their intensities for the DMQs. The geometry optimization was carried out with standard polarization basis set 6-31G\* at the B3LYP (Becke 1993; Lee, Yang, & Parr 1988) level of theory using Gaussian 03 codes<sup>19</sup> in an IBM Cluster P720 (IBL-64) computers. The frequencies and intensities were determined at the fully optimized  $C_s$  geometry of the DMQs (see Figure 4.1).

#### **4.3.2 Force field calculation**

In section 2.4.2 of chapter 2, I have discussed that SQM vibrational analysis is the alternative way to resolve the discrepancy between observed fundamentals and calculated harmonic frequencies by means of some scaling procedure. Therefore, I have carried out SQM

force field calculation which was described in section 2.4.2 of chapter 2. Cartesian Force constants matrix obtained from DFT calculations were transformed to the nonredundant local coordinate matrix of the DMQs using modified version of UMAT program in the QCPE package.<sup>20</sup> All the 63 nonredundant internal coordinates of the DMQs are shown in Table 4.2. The symbolic force constant matrix, unscaled and scaled force constants in term of nonredundant local coordinates can be found in supporting information of Ref.<sup>21</sup> For completeness, the same has been shown for one representative molecule 2,4-DMQ in the Appendix at the end of the thesis.

An error analysis have been done in terms of mean deviation,  $\delta$  (in  $\text{cm}^{-1}$ ), between the observed and calculated (harmonic, anharmonic and fitted) frequencies using equation 2.13. The mean deviations between the calculated (harmonic, anharmonic and force field fitted) and observed frequencies for three different types of vibrations in DMQs are listed in Table 4.3. From this table it is clear that the aromatic and methyl C-H stretching frequencies deviate more than non-C-H stretching vibrations vis-a-vis the calculated harmonic and anharmonic frequencies. It also indicates that the extent of anharmonicity is not the same for the different modes of vibrations. Overall, the force field fitted frequencies are closest to the observed frequencies. This gives us more confidence in unambiguous and correct assignments of the observed bands although for non C-H vibrations, the differences between the calculated anharmonic frequencies and observed frequencies are less significant.

Figure 4.1. Optimized B3LYP/6-31G\* structure and internal coordinates of (a) 2,4-DMQ, (b) 2,6-DMQ, (c) 2,7-DMQ, and (d) 2,8-DMQ.

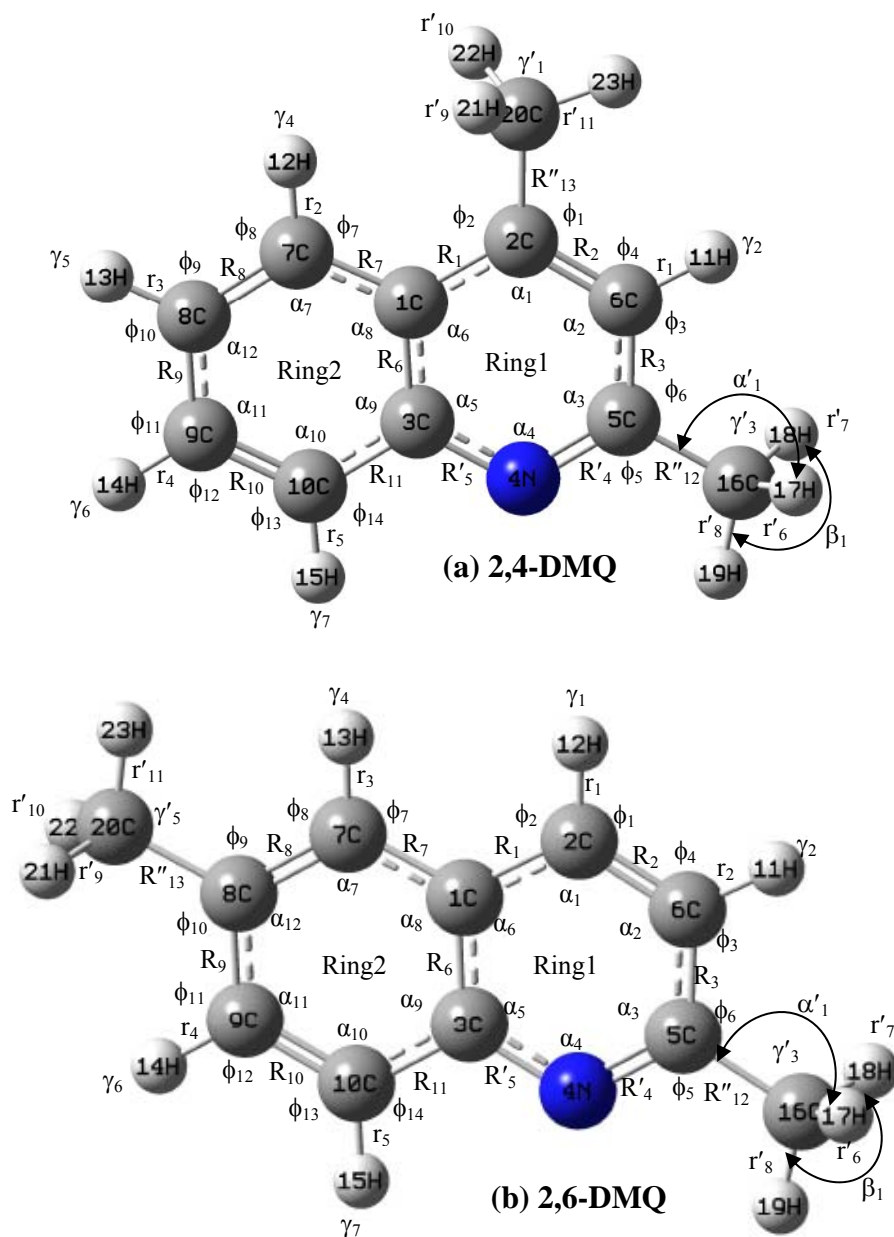
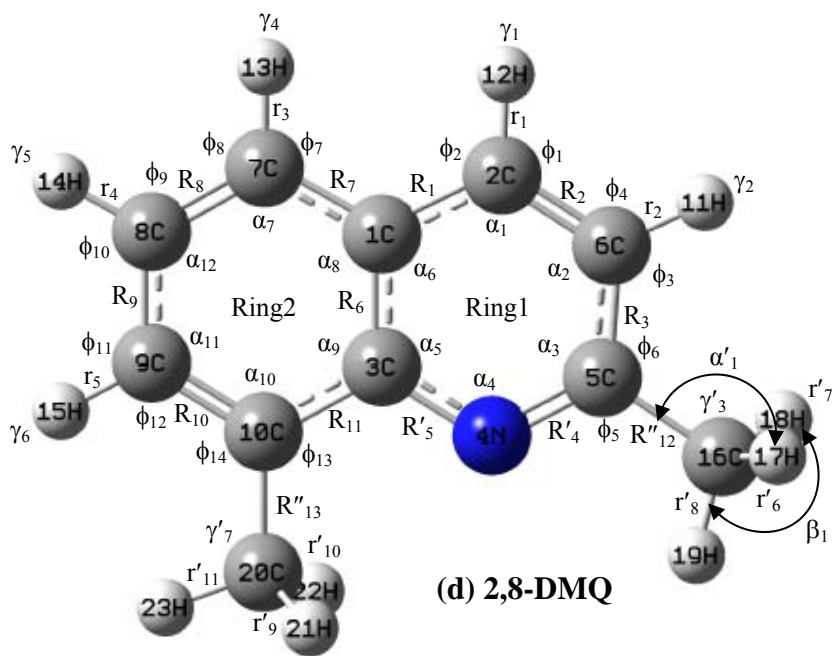
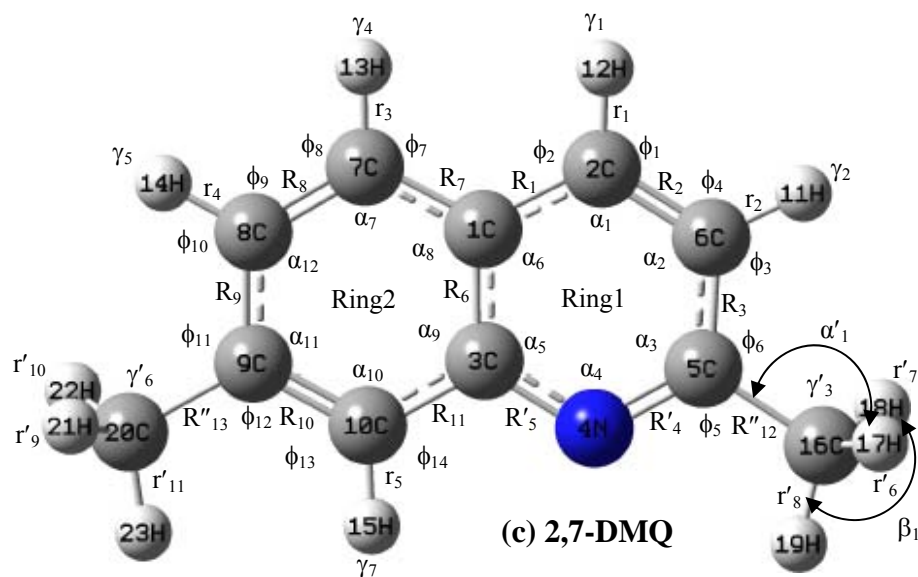


Figure 4.1. (Continued)



Twist coordinates,  $\tau$ 's numbering are the same as defined for  $R$  (the C-C bond coordinates).  $\alpha_1'$  is one of the C-C-H angle coordinate of the  $\text{CH}_3$  groups. The other C-C-H angle coordinates,  $\alpha_2'$ ,  $\alpha_3'$ , etc. are defined similarly.  $\beta_1$  is one of the H-C-H angle coordinate of  $\text{CH}_3$  groups. The other H-C-H angle coordinates,  $\beta_2$ ,  $\beta_3$ , etc. are defined similarly.

Table 4.2: Nonredundant local coordinates of the DMQs studied in this thesis.

Compound	Nonredundant local coordinates
<b>2,4-DMQ</b>  <b>See Fig 4.1 (a)</b> <b>for the internal-</b> <b>coordinates</b>	$S_{1-3, 6-11} = R(\text{Ar, C-C stretch}) (R_i)$ ; $S_{4,5} = R(\text{Ar, C-N stretch}) (R'_i)$ $S_{12, 14} = R(\text{Ar-CH}_3, \text{C-C stretch}) (R''_i)$ $S_{13, 15-18} = r(\text{Ar, C-H stretch}) (r_i)$ ; $S_{19-24} = r(\text{CH}_3, \text{C-H stretch}) (r'_i)$ $S_{25, 27} = (\phi_1-\phi_2); (\phi_5-\phi_6)$ (C-CH <sub>3</sub> def.)( $\beta'_i$ ) $S_{26, 28-31} = (\phi_3-\phi_4); (\phi_7-\phi_8) \dots$ (Ar, C-H def.)( $\beta_i$ ) $S_{32, 35} = 6^{-1/2}(\alpha_1 - \alpha_2 + \alpha_3 - \alpha_4 + \alpha_5 - \alpha_6)$ (ring def.)( $\delta_1, \delta_4$ ) $S_{33, 36} = 12^{-1/2}(2\alpha_1 - \alpha_2 - \alpha_3 + 2\alpha_4 - \alpha_5 - \alpha_6)$ (ring def.)( $\delta_2, \delta_5$ ) $S_{34, 37} = 1/2(\alpha_2 - \alpha_3 + \alpha_5 - \alpha_6)$ (ring def.)( $\delta_3, \delta_6$ ) $S_{38, 43} = 6^{-1/2}(\alpha'_1 + \alpha'_2 + \alpha'_3 - \beta_1 - \beta_2 - \beta_3)$ (CH <sub>3</sub> sym. def.) ( $\delta_a$ ) $S_{39, 44} = 6^{-1/2}(2\alpha'_1 - \alpha'_2 - \alpha'_3)$ (CH <sub>3</sub> antisym. def.) ( $\delta_s$ ) $S_{40, 45} = 2^{-1/2}(\alpha'_2 - \alpha'_3)$ (CH <sub>3</sub> antisym. def.) ( $\delta_s$ ) $S_{41, 46} = 6^{-1/2}(2\beta_1 - \beta_2 - \beta_3)$ (CH <sub>3</sub> rock) $\rho(\text{CH}_3)$ $S_{42, 47} = 2^{-1/2}(\beta_2 - \beta_3)$ (CH <sub>3</sub> rock) $\rho(\text{CH}_3)$ $S_{48, 50} = \gamma(\text{Ar-CH}_3, \text{C-C wag}) \gamma_i$ $S_{49, 51-54} = \gamma(\text{Ar, C-H wag}) \gamma'_i$ $S_{55, 58} = 6^{-1/2}(\tau_1 - \tau_2 + \tau_3 - \tau_4 + \tau_5 - \tau_6)$ (ring torsion)( $\tau_1, \tau_4$ ) $S_{56, 59} = 1/2(\tau_1 - \tau_3 + \tau_4 - \tau_6)$ (ring torsion)( $\tau_2, \tau_5$ ) $S_{57, 60} = 12^{-1/2}(-\tau_1 + 2\tau_2 - \tau_3 - \tau_4 + 2\tau_5 - \tau_6)$ (ring torsion)( $\tau_3, \tau_6$ ) $S_{61} = 2^{-1/2}(\tau_{2-1-3-10} - \tau_{7-1-3-4})$ ( $\tau_{\text{ring}}$ ) $S_{62, 63} = \tau_{5-16}; \tau_{2-20}$ (C-CH <sub>3</sub> twist) ( $\tau''_i$ )
<b>2,6-DMQ</b>  <b>See Fig 4.1 (b)</b> <b>for the internal-</b> <b>coordinates</b>	$S_{1-3, 6-11} = R(\text{Ar, C-C stretch}) (R_i)$ ; $S_{4,5} = R(\text{Ar, C-N stretch}) (R'_i)$ $S_{14, 16} = R(\text{Ar-CH}_3, \text{C-C stretch}) (R''_i)$ $S_{12, 13, 15, 17, 18} = r(\text{Ar, C-H stretch}) (r_i)$ ; $S_{19-24} = r(\text{CH}_3, \text{C-H stretch}) (r'_i)$ $S_{25, 26, 28, 30, 31} = (\phi_1-\phi_2) \dots; (\phi_7-\phi_8); (\phi_{11}-\phi_{12}) \dots$ (C-H def.)( $\beta_i$ ) $S_{27, 29} = (\phi_5-\phi_6); (\phi_9-\phi_{10})$ (C-CH <sub>3</sub> def.)( $\beta'_i$ ) $S_{32, 35} = 6^{-1/2}(\alpha_1 - \alpha_2 + \alpha_3 - \alpha_4 + \alpha_5 - \alpha_6)$ (ring def.)( $\delta_1, \delta_4$ ) $S_{33, 36} = 12^{-1/2}(2\alpha_1 - \alpha_2 - \alpha_3 + 2\alpha_4 - \alpha_5 - \alpha_6)$ (ring def.)( $\delta_2, \delta_5$ ) $S_{34, 37} = 1/2(\alpha_2 - \alpha_3 + \alpha_5 - \alpha_6)$ (ring def.)( $\delta_3, \delta_6$ ) $S_{38, 43} = 6^{-1/2}(\alpha'_1 + \alpha'_2 + \alpha'_3 - \beta_1 - \beta_2 - \beta_3)$ (CH <sub>3</sub> sym. def.) ( $\delta_a$ ) $S_{39, 44} = 6^{-1/2}(2\alpha'_1 - \alpha'_2 - \alpha'_3)$ (CH <sub>3</sub> antisym. def.) ( $\delta_s$ ) $S_{40, 45} = 2^{-1/2}(\alpha'_2 - \alpha'_3)$ (CH <sub>3</sub> antisym. def.) ( $\delta_s$ ) $S_{41, 46} = 6^{-1/2}(2\beta_1 - \beta_2 - \beta_3)$ (CH <sub>3</sub> rock) $\rho(\text{CH}_3)$ $S_{42, 47} = 2^{-1/2}(\beta_2 - \beta_3)$ (CH <sub>3</sub> rock) $\rho(\text{CH}_3)$ $S_{48, 49, 51, 53, 54} = \gamma(\text{Ar, C-H wag}) \gamma_i$ $S_{50, 52} = \gamma(\text{Ar-CH}_3, \text{C-C wag}) \gamma'_i$ $S_{55, 58} = 6^{-1/2}(\tau_1 - \tau_2 + \tau_3 - \tau_4 + \tau_5 - \tau_6)$ (ring torsion)( $\tau_1, \tau_4$ ) $S_{56, 59} = 1/2(\tau_1 - \tau_3 + \tau_4 - \tau_6)$ (ring torsion)( $\tau_2, \tau_5$ ) $S_{57, 60} = 12^{-1/2}(-\tau_1 + 2\tau_2 - \tau_3 - \tau_4 + 2\tau_5 - \tau_6)$ (ring torsion)( $\tau_3, \tau_6$ ) $S_{61} = 2^{-1/2}(\tau_{2-1-3-10} - \tau_{7-1-3-4})$ ( $\tau_{\text{ring}}$ ) $S_{62, 63} = \tau_{5-16}; \tau_{8-20}$ (C-CH <sub>3</sub> twist) ( $\tau''_i$ )

Table 4.2: (Continued) nonredundant local coordinates of the DMQs studied in this thesis.

Compound	Nonredundant local coordinates
<b>2,7-DMQ</b>  <b>See Fig 4.1 (c)</b> <b>for the internal-</b> <b>coordinates</b>	$S_{1-3, 6-11} = R(\text{Ar, C-C stretch}) (R_i)$ ; $S_{4,5} = R(\text{Ar, C-N stretch}) (R'_i)$ $S_{14, 17} = R(\text{Ar-CH}_3, \text{C-C stretch}) (R''_i)$ $S_{12, 13, 15, 16, 18} = r(\text{Ar, C-H stretch}) (r_i)$ ; $S_{19-24} = r(\text{CH}_3, \text{C-H stretch}) (r'_i)$ $S_{25, 26, 28, 29, 31} = (\phi_1-\phi_2)\dots; (\phi_7-\phi_8)\dots (\phi_{13}-\phi_{14}) (\text{C-H def.})(\beta_i)$ $S_{27, 30} = (\phi_5-\phi_6); (\phi_{11}-\phi_{12}) (\text{C-CH}_3 \text{ def.})(\beta'_i)$ $S_{32, 35} = 6^{-1/2}(\alpha_1 - \alpha_2 + \alpha_3 - \alpha_4 + \alpha_5 - \alpha_6) (\text{ring def.})(\delta_1, \delta_4)$ $S_{33, 36} = 12^{-1/2}(2\alpha_1 - \alpha_2 - \alpha_3 + 2\alpha_4 - \alpha_5 - \alpha_6) (\text{ring def.})(\delta_2, \delta_5)$ $S_{34, 37} = 1/2(\alpha_2 - \alpha_3 + \alpha_5 - \alpha_6) (\text{ring def.})(\delta_3, \delta_6)$ $S_{38, 43} = 6^{-1/2}(\alpha'_1 + \alpha'_2 + \alpha'_3 - \beta_1 - \beta_2 - \beta_3) (\text{CH}_3 \text{ sym. def.}) (\delta_a)$ $S_{39, 44} = 6^{-1/2}(2\alpha_1 - \alpha_2 - \alpha_3) (\text{CH}_3 \text{ antisym. def.}) (\delta_s)$ $S_{40, 45} = 2^{-1/2}(\alpha'_2 - \alpha'_3) (\text{CH}_3 \text{ antisym. def.}) (\delta_s)$ $S_{41, 46} = 6^{-1/2}(2\beta_1 - \beta_2 - \beta_3) (\text{CH}_3 \text{ rock}) \rho(\text{CH}_3)$ $S_{42, 47} = 2^{-1/2}(\beta_2 - \beta_3) (\text{CH}_3 \text{ rock}) \rho(\text{CH}_3)$ $S_{48, 49, 51, 52, 54} = \gamma(\text{Ar, C-H wag}) \gamma_i$ $S_{50, 53} = \gamma(\text{Ar-CH}_3, \text{C-C wag}) \gamma'_i$ $S_{55, 58} = 6^{-1/2}(\tau_1 - \tau_2 + \tau_3 - \tau_4 + \tau_5 - \tau_6) (\text{ring torsion})(\tau_1, \tau_4)$ $S_{56, 59} = 1/2(\tau_1 - \tau_3 + \tau_4 - \tau_6) (\text{ring torsion})(\tau_2, \tau_5)$ $S_{57, 60} = 12^{-1/2}(-\tau_1 + 2\tau_2 - \tau_3 - \tau_4 + 2\tau_5 - \tau_6) (\text{ring torsion})(\tau_3, \tau_6)$ $S_{61} = 2^{-1/2}(\tau_{2-1-3-10} - \tau_{7-1-3-4}) (\tau_{\text{ring}})$ $S_{62, 63} = \tau_{5-16}; \tau_{9-20} (\text{C-CH}_3 \text{ twist}) (\tau''_i)$
<b>2,8-DMQ</b>  <b>See Fig 4.1 (d)</b> <b>for the internal-</b> <b>coordinates</b>	$S_{1-3, 6-11} = R(\text{Ar, C-C stretch}) (R_i)$ ; $S_{4, 5} = R(\text{Ar, C-N stretch}) (R'_i)$ $S_{14, 18} = R(\text{Ar-CH}_3, \text{C-C stretch}) (R''_i)$ $S_{12, 13, 15-17} = r(\text{Ar, C-H stretch}) (r_i)$ ; $S_{19-24} = r(\text{CH}_3, \text{C-H stretch}) (r'_i)$ $S_{25, 26, 28-30} = (\phi_1-\phi_2)\dots; (\phi_7-\phi_8)\dots (\text{C-H def.})(\beta_i)$ $S_{27, 31} = (\phi_5-\phi_6); (\phi_{13}-\phi_{14}) (\text{C-CH}_3 \text{ def.})(\beta'_i)$ $S_{32, 35} = 6^{-1/2}(\alpha_1 - \alpha_2 + \alpha_3 - \alpha_4 + \alpha_5 - \alpha_6) (\text{ring def.})(\delta_1, \delta_4)$ $S_{33, 36} = 12^{-1/2}(2\alpha_1 - \alpha_2 - \alpha_3 + 2\alpha_4 - \alpha_5 - \alpha_6) (\text{ring def.})(\delta_2, \delta_5)$ $S_{34, 37} = 1/2(\alpha_2 - \alpha_3 + \alpha_5 - \alpha_6) (\text{ring def.})(\delta_3, \delta_6)$ $S_{38, 43} = 6^{-1/2}(\alpha'_1 + \alpha'_2 + \alpha'_3 - \beta_1 - \beta_2 - \beta_3) (\text{CH}_3 \text{ sym. def.}) (\delta_a)$ $S_{39, 44} = 6^{-1/2}(2\alpha'_1 - \alpha'_2 - \alpha'_3) (\text{CH}_3 \text{ antisym. def.}) (\delta_s)$ $S_{40, 45} = 2^{-1/2}(\alpha'_2 - \alpha'_3) (\text{CH}_3 \text{ antisym. def.}) (\delta_s)$ $S_{41, 46} = 6^{-1/2}(2\beta_1 - \beta_2 - \beta_3) (\text{CH}_3 \text{ rock}) \rho(\text{CH}_3)$ $S_{42, 47} = 2^{-1/2}(\beta_2 - \beta_3) (\text{CH}_3 \text{ rock}) \rho(\text{CH}_3)$ $S_{48, 49, 51-53} = \gamma(\text{Ar, C-H wag}) \gamma_i$ $S_{50, 54} = \gamma(\text{Ar-CH}_3, \text{C-C wag}) \gamma'_i$ $S_{55, 58} = 6^{-1/2}(\tau_1 - \tau_2 + \tau_3 - \tau_4 + \tau_5 - \tau_6) (\text{ring torsion})(\tau_1, \tau_4)$ $S_{56, 59} = 1/2(\tau_1 - \tau_3 + \tau_4 - \tau_6) (\text{ring torsion})(\tau_2, \tau_5)$ $S_{57, 60} = 12^{-1/2}(-\tau_1 + 2\tau_2 - \tau_3 - \tau_4 + 2\tau_5 - \tau_6) (\text{ring torsion})(\tau_3, \tau_6)$ $S_{61} = 2^{-1/2}(\tau_{2-1-3-10} - \tau_{7-1-3-4}) (\tau_{\text{ring}})$ $S_{62, 63} = \tau_{5-16}; \tau_{10-20} (\text{C-CH}_3 \text{ twist}) (\tau''_i)$



**Table 4.3: Mean deviation,  $\delta$  (in  $\text{cm}^{-1}$ ) between the calculated (harmonic, anharmonic and force field fitted) and observed frequencies for different modes of vibration in the DMQs.**

$\delta$ /Mode of vibration	Harmonic				Anharmonic				Force Field Fitted			
	(a)	(b)	(c)	(d)	(a)	(b)	(c)	(d)	(a)	(b)	(c)	(d)
Aromatic C-H str	166.9	139.4	165.6	167.9	26.2	7.6	40.8	25.4	0.16	0.15	0.36	0.36
Methyl C-H str	176.9	176.2	176.6	186.8	41.1	49.1	48.7	57.4	3.1	1.7	2.5	8.3
Non-C-H str	31.7	31.0	32.6	31.1	14.6	12.9	11.1	9.8	1.7	1.8	2.6	1.5

*(a), (b), (c), and (d) represents the 2,4-, 2,6-, 2,7-, and 2,8-DMQ, respectively.*

#### 4.4 Results and discussion

The gas phase IR spectra of the DMQs are shown in Figure 4.2. The experimental and theoretical infrared frequencies, intensities and potential energy distributions (PEDs) of vibrational modes of the DMQs are listed in Tables 4.4 – 4.7. Observed non-fundamental and corresponding calculated non-fundamental anharmonic bands are listed in Table 4.8. To compare the experimental and calculated spectra, we have displayed spectra of all the four DMQs separately in Figure 4.3. For the calculated spectra, force field fitted frequencies were used and FWHM of each band was assumed to be  $15 \text{ cm}^{-1}$  (see section 2.5 in chapter 2). Each DMQ molecule has 23 atoms; and thus 63 normal modes which belong to the irreducible representation  $41A' + 22A''$  under the  $C_s$  point group. The observed spectra have been divided in three distinct regions: (A) aromatic and methyl C-H stretching region, (B) non C-H stretching region including aromatic C-C/C-N, aromatic-methyl C-C stretch, C-H in-plane and

out-of-plane, methyl C-H symmetric and asymmetric deformations, etc. and (C) non-fundamental vibration region: combination and overtone bands. Initially, fundamental bands are tentatively assigned using calculated anharmonic frequencies. The assignment is then confirmed by fitted frequencies obtained by scaled force field calculations since some of the observed frequencies, particularly aromatic and methyl C-H stretching frequencies differ by as much as  $50\text{ cm}^{-1}$  from the calculated anharmonic frequencies. The fitting by the force field method is extremely good and RMS errors (in  $\text{cm}^{-1}$ ) with 100 iterations remain within a few wavenumbers,  $3\text{ cm}^{-1}$ . Details of the assignment have been discussed in the subsequent sections.

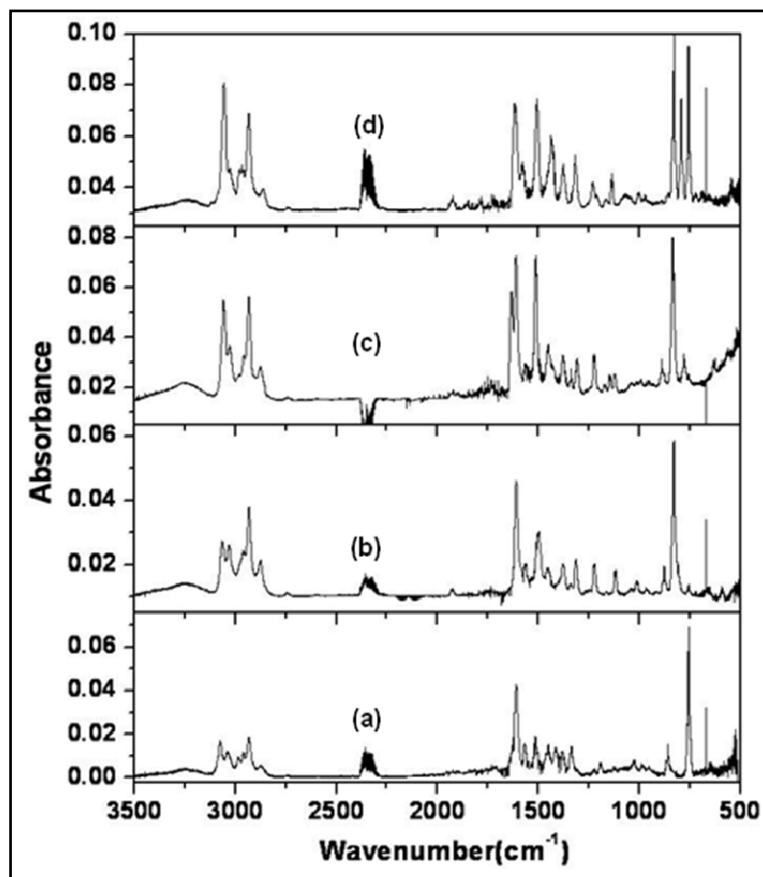


Figure 4.2. Experimental gas phase IR absorption spectra of (a) 2,4-DMQ, (b) 2,6-DMQ, (c) 2,7-DMQ, and (d) 2,8-DMQ at  $0.5\text{ cm}^{-1}$  resolution.

#### 4.4.1 C-H stretching Vibrations:

The aromatic C-H stretching region in the experimental spectra is always more complex than that predicted by DFT due to the occurrence of Fermi resonances and the presence overtone and combination modes.<sup>22</sup> However, we could assign the bands observed in this region with the help of PEDs. Groups of two to three bands in the spectral range of (2980 – 3070)  $\text{cm}^{-1}$  are assigned to aromatic C-H stretching vibrations. Bands observed at 3075.8, 3039.2, and 2984.9  $\text{cm}^{-1}$  in 2,4-DMQ; 3066.1 and 3032.9  $\text{cm}^{-1}$  in 2,6-DMQ; 3059.3, 3028.2, and 2987.7  $\text{cm}^{-1}$  in 2,7-DMQ and 3056.8, 3027.3, and 2978.9  $\text{cm}^{-1}$  in 2,8-DMQ correspond to the calculated anharmonic fundamental bands at 3079.4, 3052.2, and 3046.9  $\text{cm}^{-1}$  in 2,4-DMQ; 3057.3 and 3026.4  $\text{cm}^{-1}$  in 2,6-DMQ; 3064.1, 3053.5, and 3020.0  $\text{cm}^{-1}$  in 2,7-DMQ; 3069.3, 3049.4, and 3020.6  $\text{cm}^{-1}$  in 2,8-DMQ, respectively. On the other hand, their respective fitted frequencies are 3076.3, 3039.2, and 2984.9  $\text{cm}^{-1}$  in 2,4-DMQ; 3066.0 and 3032.7  $\text{cm}^{-1}$  in 2,6-DMQ; 3059.3, 3028.2, and 2988.8  $\text{cm}^{-1}$  in 2,7-DMQ; 3056.8, 3027.3, and 2980.0  $\text{cm}^{-1}$  in 2,8-DMQ. The force field fitted frequencies match very well with the observed bands which add evidence to our assignment.

The next three bands observed in the spectral range of 2860 – 2970  $\text{cm}^{-1}$  are assigned to antisymmetric and symmetric C-H stretching vibrations of methyl groups. The interpretation of the methyl C-H stretching regions of the vibrational spectra of methylated compounds is normally hindered by a Fermi resonance which occurs between the methyl C-H symmetric stretch and an overtone involving two quanta of a methyl deformation mode.<sup>23</sup> For large aromatic hydrocarbons such as the DMQs, it is difficult to ascertain the presence or absence of such resonances in the methyl C-H stretching region, however, the closeness of our fitted frequencies to the observed ones provides the basis of our assignment. Bands observed at

2961.0 and 2933.5  $\text{cm}^{-1}$  in 2,4-DMQ; 2959.9 and 2933.3  $\text{cm}^{-1}$  in 2,6-DMQ; 2958.6 and 2934.4  $\text{cm}^{-1}$  in 2,7-DMQ; 2966.3 and 2934.7  $\text{cm}^{-1}$  in 2,8-DMQ are assigned to asymmetric stretching vibrations of the methyl C-H by comparing with the force field fitted frequencies at 2959.7 and 2930.4  $\text{cm}^{-1}$  in 2,4-DMQ; 2959.3 and 2931.9  $\text{cm}^{-1}$  in 2,6-DMQ; 2957.7 and 2932.6  $\text{cm}^{-1}$  in 2,7-DMQ; 2963.5 and 2925.5  $\text{cm}^{-1}$  in 2,8-DMQ, respectively. Their corresponding anharmonic frequencies at 3007.3 and 2955.8  $\text{cm}^{-1}$  in 2,4-DMQ; 3013.1 and 2944.0  $\text{cm}^{-1}$  in 2,6-DMQ; 3007.2 and 2945.1  $\text{cm}^{-1}$  in 2,7-DMQ; 3007.3 and 2958.1  $\text{cm}^{-1}$  in 2,8-DMQ which deviate by  $\sim 30 \text{ cm}^{-1}$ . The symmetric methyl C-H stretching band of moderate intensity appears at 2873.8  $\text{cm}^{-1}$  in 2,4-DMQ, 2876.0  $\text{cm}^{-1}$  in 2,6-DMQ, 2875.8  $\text{cm}^{-1}$  in 2,7-DMQ, and 2863.1  $\text{cm}^{-1}$  in 2,8-DMQ. This band can be correlated with the calculated anharmonic frequencies at 2928.5  $\text{cm}^{-1}$  in 2,4-DMQ, 2959.6  $\text{cm}^{-1}$  in 2,6-DMQ, 2962.8  $\text{cm}^{-1}$  in 2,7-DMQ, and 2971.4  $\text{cm}^{-1}$  in 2,8-DMQ, respectively. DFT calculated asymmetric and symmetric anharmonic frequencies are generally overestimated, whereas the force field fitted frequencies are quite close to the observed frequencies as seen from Tables 4.4 – 4.7. It is also found that the absolute intensities of the C-H stretching bands do not match well with the calculated band intensities perhaps partially due to the occurrence of Fermi resonances in the region.

#### **4.4.2 Non C-H stretching Vibrations:**

Except aromatic C-H out-of-plane bending vibrations, most of the non C-H stretching vibrations belong to the irreducible representation,  $A'$ . A highly intense band observed at 1609.7  $\text{cm}^{-1}$  in 2,4-DMQ, at 1610.3  $\text{cm}^{-1}$  in 2,6-DMQ, at 1612.5  $\text{cm}^{-1}$  in 2,7-DMQ and at 1615.1  $\text{cm}^{-1}$  in 2,8-DMQ is assigned to the aromatic C-C stretching vibration.

Table 4.4: Calculated harmonic, anharmonic frequencies (in  $cm^{-1}$ ) and intensities (in km/mol) at  $B3LYP/6-31G^*$ , observed frequencies (in  $cm^{-1}$ ) and intensities (in km/mol), fitted frequencies (in  $cm^{-1}$ ) and PED of 2, 4 –  $DMQ$ .

Sym	B3LYP/6-31G*			Observed		Force field	
	No	Harm.	Int.	Anharm.	Freq.	Int.	Fitted PED
$A'$							
1	3218.3	14.954	3079.4	3075.8	16.327	3076.3	$r_2$ ( 48) + $r_5$ ( 47)
2	3210.0	27.665	3072.2	(3075.0)		3074.5	$r_2$ ( 50) + $r_5$ ( 47)
3	3197.5	14.608	3052.2	3039.2	8.577	3039.2	$r_4$ ( 92)
4	3185.1	1.440	3046.9	2984.9	3.009	2984.9	$r_3$ ( 96)
5	3180.9	19.449	3041.6	(2984.0)		2984.0	$r_1$ ( 98)
6	3157.6	8.121	3007.3	2961.0	2.106	2959.7	$r'_7$ ( 77) + $r'_6$ ( 23)
7	3131.4	16.314	2985.1	(2960.0)		2958.8	$r'_9$ ( 80) + $r'_8$ ( 18)
8	3044.8	17.224	2928.5	2873.8	5.643	2878.8	$r'_8$ ( 81) + $r'_9$ ( 18)
9	3044.1	25.493	2942.6	(2873.0)		2877.2	$r'_6$ ( 77) + $r'_7$ ( 23)
10	1672.5	4.589	1633.2	(1627.0)		1626.2	$R_8$ ( 26) + $R_{10}$ ( 18) + $R_{11}$ ( 11)
11	1661.7	76.208	1619.5	1609.7	73.664	1610.9	$R_2$ ( 36)
12	1617.6	23.918	1577.2	1566.9	14.371	1568.2	$R'_4$ ( 23) + $R_9$ ( 13) + $R_{10}$ ( 13)
13	1561.7	19.393	1525.8	1512.8	18.510	1513.0	$R_9$ ( 17)
14	1529.7	10.823	1472.0	(1488.0)		1489.1	$\delta_s CH_3(2)$ ( 67)
15	1514.7	9.856	1498.1	(1474.0)		1470.2	$\delta_s CH_3(1)$ ( 16) + $\delta_s CH_3(2)$ ( 14) + $\beta_4$ ( 10)
16	1499.6	3.227	1464.6	(1449.0)		1450.8	$\delta_s CH_3(1)$ ( 58)
17	1457.7	20.604	1423.8	1413.8	11.136	1412.6	$\beta_2$ ( 18)
18	1440.1	0.491	1433.7	(1401.0)		1401.1	$\rho CH_3(1)$ ( 86)
19	1431.2	5.113	1422.1	1380.1	8.201	1381.3	$\delta_5$ ( 63) + $R''_{12}$ ( 17)
20	1411.0	2.956	1375.5	(1373.0)		1371.4	$R_6$ ( 30) + $R'_5$ ( 14)
21	1386.6	3.509	1358.5	(1349.0)		1347.5	$R'_4$ ( 12) + $R_{10}$ ( 12) + $R_2$ ( 10)
22	1370.0	16.948	1341.7	1336.9	12.415	1332.1	$R_3$ ( 18) + $R'_5$ ( 12)
23	1300.0	0.247	1279.6	(1265.0)		1263.3	$\beta_6$ ( 17) + $\beta_2$ ( 15) + $R_{11}$ ( 13) + $\beta_5$ ( 11)
24	1268.5	1.101	1246.6	1223.3	2.106	1226.6	$R_7$ ( 23) + $R'_5$ ( 15) + $R_1$ ( 13) + $r'_{11}$ ( 12)
25	1223.6	6.944	1202.0	1192.9	4.966	1192.1	$r'_{11}$ ( 34) + $R''_{12}$ ( 14)
26	1192.8	0.750	1177.9	(1160.0)		1161.0	$\beta'_3$ ( 39) + $\beta_2$ ( 16) + $R_8$ ( 11)
27	1157.6	1.904	1142.4	1121.2	2.332	1122.9	$\beta_4$ ( 30) + $\beta_5$ ( 22) + $R_{10}$ ( 12)
28	1093.0	0.707	1078.3	(1063.0)		1063.2	$\delta_2$ ( 16) + $R''_{13}$ ( 14) + $\delta_a CH_3(2)$ ( 14) + $R_{11}$ ( 12)
29	1053.6	4.610	1035.0	(1025.0)		1025.6	$R_9$ ( 38) + $R_{10}$ ( 12)
30	1042.4	2.048	1028.2	1024.0	3.837	1021.0	$\delta_a CH_3(1)$ ( 24) + $\delta_a CH_3(2)$ ( 14) + $R_9$ ( 12)
31	1003.3	6.645	989.2	982.5	2.558	980.4	$\delta_2$ ( 21) + $\delta_a CH_3(2)$ ( 17) + $R''_{13}$ ( 16) + $R''_{12}$ ( 11)
32	977.3	1.703	966.0	951.2	1.655	953.2	$R_3$ ( 29) + $\beta_6$ ( 18) + $\delta_1$ ( 10)
33	877.3	4.283	863.9	( 853.0)		855.3	$\delta_2$ ( 33)
34	758.3	2.064	750.0	( 738.0)		737.4	$R_1$ ( 15) + $R_7$ ( 15) + $\delta_1$ ( 12) + $\delta_3$ ( 11) + $R_6$ ( 11) + $\beta_6$ ( 11)
35	657.9	4.115	650.4	645.8	3.837	645.3	$\delta_3$ ( 44) + $\beta_6$ ( 12)
36	546.9	1.913	540.5	531.0	1.882	531.2	$\beta_7$ ( 27) + $\delta_4$ ( 16) + $R''_{13}$ ( 11) + $\delta_1$ ( 10)

Table 4.4:(Continued) Calculated harmonic, anharmonic frequencies (in  $cm^{-1}$ ) and intensities (in km/mol) at  $B3LYP/6-31G^*$ , observed frequencies (in  $cm^{-1}$ ) and intensities (in km/mol), fitted frequencies (in  $cm^{-1}$ ) and PED of 2,4 – DMQ.

Sym	B3LYP/6-31G*			Observed		Force field	
	No	Harm.	Int.	Anharm.	Freq.	Int.	Fitted PED
	37	533.0	1.397	529.4	( 518.0)		518.7 $\delta_3$ ( 25)+ $\delta_4$ ( 19)
	38	501.6	2.765	500.9	( 488.0)		487.9 $\delta_1$ (24)+ $r'_{10}$ (21)+ $\beta'_1$ (20)
	39	452.7	2.050	449.6	( 440.7)		439.8 $\beta_7$ ( 30)+ $\delta_1$ ( 29) + $\delta_4$ ( 13)
	40	280.6	0.932	285.1	( 273.0)		273.1 $r'_{10}$ ( 43)+ $\beta'_1$ ( 37)
	41	266.9	1.142	267.2	( 259.0)		259.0 $\beta'_1$ (30)+ $\delta_4$ (25)+ $r'_{10}$ (15)
$A''$							
	42	3097.2	15.845	2955.8	2933.5	15.500	2930.4 $r'_6$ (100)
	43	3094.4	18.237	2947.2	(2933.0)		2928.9 $r'_8$ (100)
	44	1513.7	3.042	1508.6	(1473.3)		1472.6 $\delta_s CH_3$ (1) ( 92)
	45	1512.2	10.639	1504.7	1450.7	11.813	1450.3 $\delta_s CH_3$ (2) ( 92)
	46	1076.8	1.079	1053.0	(1048.0)		1052.3 $\delta_6$ ( 55) + $\delta_a CH_3$ (1) ( 19)
	47	1069.0	3.989	1049.2	(1040.0)		1044.1 $\rho CH_3$ (1) ( 48)+ $\delta_a CH_3$ (2) ( 17) + $\rho CH_3$ (2) ( 10)
	48	996.2	0.136	982.2	( 969.0)		968.6 $\gamma_5$ ( 35)+ $\gamma_4$ ( 24)+ $\gamma'_3$ ( 15) + $\tau_2$ ( 12)
	49	961.4	1.579	953.1	( 950.0)		949.2 $\gamma_2$ ( 34)+ $\gamma'_3$ ( 30)+ $\gamma_5$ ( 25)
	50	895.2	2.926	877.2	( 871.0)		872.0 $\rho CH_3$ (2) ( 23)+ $\gamma_2$ ( 22)+ $\gamma_4$ ( 15)+ $\gamma'_3$ ( 10)
	51	882.7	8.855	866.7	857.1	9.932	856.4 $\rho CH_3$ (2) ( 59)
	52	799.9	0.986	791.3	( 778.0)		780.6 $\tau_2$ ( 38)+ $\gamma_6$ ( 35)
	53	778.8	47.456	766.0	755.7	63.256	756.2 $\gamma'_3$ ( 29)+ $\gamma_4$ ( 23)+ $\gamma_2$ ( 22) + $\gamma_5$ ( 12)
	54	664.9	0.130	656.4	( 647.0)		645.2 $\tau_2$ ( 33)+ $\gamma_6$ ( 25)+ $\gamma'_1$ ( 18)
	55	573.3	0.124	568.1	( 558.0)		556.4 $\rho CH_3$ (2) ( 26)+ $\tau_1$ ( 17) + $\tau_5$ ( 17)+ $\gamma_7$ ( 11)
	56	533.5	0.100	526.3	( 519.0)		519.7 $\tau_4$ ( 21)+ $\gamma'_1$ ( 14) + $\tau_2$ ( 13) + $\tau_6$ ( 11)
	57	434.7	2.376	429.5	( 427.0)		427.2 $\tau_3$ ( 32)+ $\tau_4$ ( 25) + $\rho CH_3$ (2) ( 13)
	58	309.9	0.848	304.6	( 301.0)		300.7 $\tau_4$ ( 42)+ $\gamma'_1$ ( 11)
	59	206.6	0.493	207.8	( 201.0)		200.9 $\tau_1$ ( 39)+ $\tau_{ring}$ ( 19) + $\rho CH_3$ (2) ( 12)
	60	163.0	0.070	186.5	( 158.0)		158.0 $\tau_{ring}$ ( 67)+ $\tau_1$ ( 14)
	61	153.9	2.721	153.6	( 149.0)		149.0 $\tau_5$ ( 29)+ $\rho CH_3$ (2) ( 19) + $\tau_3$ ( 17)
	62	114.3	0.191	103.9	( 111.0)		111.1 $\gamma_7$ ( 49) + $\tau_4$ ( 15) + $\tau_3$ ( 11)
	63	81.0	0.624	49.8	( 78.0)		78.0 $\tau_6$ ( 72)

Since the fitting algorithm required all the experimental frequencies, the numbers in parenthesis are introduced as good guesses for 2,4 – DMQ and do not have any other significance. RMS error is 1.9720 for the fitting of experimental frequencies.

Table 4.5: Calculated harmonic, anharmonic frequencies (in  $cm^{-1}$ ) and intensities (in km/mol) at  $B3LYP/6-31G^*$ , observed frequencies (in  $cm^{-1}$ ) and intensities (in km/mol), fitted frequencies (in  $cm^{-1}$ ) and PED of 2, 6 –  $DMQ$ .

Sym	B3LYP/6-31G*			Observed		Force field	
	No	Harm.	Int.	Anharm.	Freq.	Int.	Fitted PED
$A'$							
1	3215.0	9.908	3073.9	(3066.0)		3066.3	$r_2$ ( 46) + $r_5$ ( 46)
2	3199.7	23.718	3057.3	3066.1	16.737	3066.0	$r_5$ ( 47) + $r_2$ ( 46)
3	3178.7	12.350	3024.2	(3033.0)		3033.4	$r_4$ ( 34) + $r_1$ ( 32) + $r_3$ ( 27)
4	3178.2	15.913	3026.4	3032.9	10.258	3032.7	$r_4$ ( 56) + $r_1$ ( 32)
5	3169.8	16.336	3008.7	(3030.0)		3029.8	$r_3$ ( 67) + $r_1$ ( 28)
6	3158.9	8.269	3013.1	2959.9	4.409	2959.3	$r'_7$ ( 76) + $r'_6$ ( 24)
7	3126.1	15.737	2980.7	(2959.0)		2958.2	$r'_9$ ( 81) + $r'_8$ ( 19)
8	3044.4	23.522	2959.6	2876.0	13.497	2879.3	$r'_8$ ( 81) + $r'_9$ ( 18)
9	3041.1	40.044	2982.6	(2876.0)		2877.9	$r'_6$ ( 76) + $r'_7$ ( 24)
10	1685.0	2.275	1648.0	(1640.0)		1639.9	$R_8$ (23) + $R_{10}$ (20) + $\delta_4$ (11)
11	1661.8	63.725	1624.8	1610.3	62.269	1609.1	$R_2$ ( 36)
12	1614.0	13.368	1571.9	1565.5	8.098	1568.6	$R'_4$ ( 18) + $R_6$ ( 12) + $R_1$ ( 11) + $R_{10}$ ( 11)
13	1552.0	29.518	1516.4	1498.6	33.024	1503.7	$\delta_s CH_3$ (2) (16) + $R_9$ (13)
14	1537.8	0.596	1502.0	(1496.0)		1493.5	$R_{11}$ ( 13) + $\delta_s CH_3$ (2) ( 12)
15	1514.5	14.448	1511.4	(1474.0)		1473.1	$\delta_s CH_3$ (2) ( 53) + $r'_{11}$ ( 10)
16	1506.5	8.419	1499.0	1453.1	8.278	1453.3	$\delta_s CH_3$ (1) ( 75)
17	1445.2	0.275	1427.4	(1406.0)		1406.1	$\rho CH_3$ (1) ( 88)
18	1440.9	4.430	1411.5	(1402.4)		1398.7	$R_{10}$ ( 17) + $R_7$ ( 14) + $\beta_2$ ( 13) + $\delta_5$ ( 10)
19	1431.1	2.951	1415.5	(1392.0)		1392.7	$\delta_5$ ( 76)
20	1413.4	3.843	1380.5	1378.6	14.037	1381.4	$R_6$ ( 27) + $R_8$ ( 13)
21	1394.9	10.995	1358.8	1340.0	1.709	1341.7	$R'_4$ ( 26) + $R_2$ ( 20)
22	1349.3	11.198	1326.3	1313.1	13.587	1311.2	$R'_5$ ( 28) + $\beta_4$ ( 14) + $\delta_2$ ( 13)
23	1295.6	1.855	1279.0	1266.8	0.899	1265.4	$\beta_6$ ( 23) + $\beta_2$ ( 19) + $\beta'_5$ ( 13)
24	1260.7	5.395	1235.6	1223.0	12.507	1221.7	$R'_5$ ( 15) + $R_7$ ( 14) + $R''_{12}$ ( 14)
25	1252.5	5.537	1223.7	(1219.1)		1217.4	$R''_{13}$ (14) + $\delta_2$ (13) + $R_{11}$ (12) + $r'_{11}$ ( 11) + $R_9$ ( 11)
26	1201.8	1.263	1182.7	1162.0	0.899	1162.8	$r'_{10}$ ( 22) + $\beta_2$ ( 17) + $R''_{13}$ ( 16) + $R_1$ ( 13)
27	1174.7	0.602	1157.7	(1143.0)		1143.9	$\beta'_5$ ( 28) + $\beta_4$ ( 17) + $R_{10}$ ( 12) $r'_{11}$ ( 12)
28	1151.2	6.650	1136.8	1118.2	8.998	1118.6	$r'_{11}$ ( 17) + $r'_{10}$ ( 12) + $R'_5$ ( 11)
29	1040.3	15.703	1022.0	1013.1	4.859	1013.1	$\delta_a CH_3$ (2) ( 30) + $\delta_a CH_3$ (1) ( 14)
30	1030.6	2.056	1016.1	(1003.0)		1002.9	$\delta_a CH_3$ (1) ( 28) + $\delta_a CH_3$ (2) ( 19)
31	976.3	1.277	962.0	( 950.0)		948.9	$\beta_6$ ( 21) + $\delta_2$ ( 19) + $R_3$ ( 13)
32	935.6	0.795	922.9	( 910.0)		908.4	$R_3$ ( 16) + $R_9$ ( 14)
33	842.5	3.581	829.6	( 820.0)		824.0	$\beta_6$ ( 20) + $\delta_2$ ( 15) + $R_6$ ( 11)
34	765.4	0.285	754.1	755.0	1.709	744.1	$R_6$ ( 20) + $\delta_3$ ( 15) + $\beta_7$ ( 10)
35	678.0	1.062	670.0	( 659.0)		663.9	$\beta_7$ ( 26) + $\delta_3$ ( 25)
36	599.3	4.151	593.4	592.4	4.139	589.4	$\beta_7$ ( 30) + $\delta_3$ ( 20) + $R''_{12}$ ( 10)
37	545.5	0.120	540.4	( 530.0)		530.2	$\delta_1$ ( 38) + $\delta_4$ ( 20)

Table 4.5:(Continued) Calculated harmonic, anharmonic frequencies (in  $cm^{-1}$ ) and intensities (in km/mol) at  $B3LYP/6-31G^*$ , observed frequencies (in  $cm^{-1}$ ) and intensities (in km/mol), fitted frequencies (in  $cm^{-1}$ ) and PED of 2,6 – DMQ.

Sym	B3LYP/6-31G*			Observed		Force field	
	No	Harm.	Int.	Anharm.	Freq.	Int.	Fitted PED
	38	457.8	6.570	456.9	( 445.0)		444.9 $\delta_4$ ( 26)+ $\beta_1$ ( 25)+ $\beta_3'$ ( 13) + $\delta_1$ ( 11)
	39	419.2	0.184	416.2	( 408.0)		408.9 $\delta_3$ ( 16)+ $\delta_1$ ( 14) + $\delta_4$ ( 14)+ $\beta_7$ ( 11)
	40	328.7	0.259	330.3	( 319.0)		318.8 $\beta_3'$ ( 37)+ $\beta_1$ ( 32)
	41	226.9	1.338	226.7	( 220.0)		220.1 $\beta_3'$ ( 29)+ $\beta_1$ ( 26)
A''							
	42	3094.6	19.309	2944.0	2933.3	27.265	2931.9 $r_6'$ (100)
	43	3091.5	20.426	2946.2	(2933.0)		2927.3 $r_8'$ (100)
	44	1514.2	5.39	1514.4	(1473.8)		1473.8 $\delta_s CH_3(1)$ ( 93)
	45	1513.8	6.609	1521.2	(1473.0)		1473.0 $\delta_s CH_3(2)$ ( 92)
	46	1077.9	3.969	1050.9	(1049.0)		1049.0 $\rho CH_3(1)$ ( 52)+ $\delta_a CH_3(2)$ ( 18)
	47	1069.9	3.886	1045.5	1042.0	1.079	1042.6 $\delta_6$ ( 55)+ $\delta_a CH_3(1)$ ( 19) + $\gamma_1$ ( 12)
	48	987.9	1.514	973.3	968.2	2.159	967.9 $\rho CH_3(2)$ ( 59)+ $\rho CH_3(2)$ ( 28)
	49	983.5	0.100	965.9	( 957.0)		957.1 $\gamma_5'$ ( 47)+ $\gamma_4$ ( 39)
	50	902.6	7.831	887.9	877.9	8.458	877.7 $\gamma_2$ ( 65)+ $\tau_2$ ( 12)
	51	853.4	39.968	838.7	830.3	65.418	830.2 $\gamma_4$ ( 30)+ $\gamma_5'$ ( 28)+ $\gamma_6$ ( 11) + $\rho CH_3(2)$ ( 10)
	52	830.4	2.229	818.1	( 808.0)		808.6 $\rho CH_3(2)$ ( 34)+ $\rho CH_3(2)$ ( 27) + $\gamma_2$ ( 14)
	53	789.3	0.065	778.1	( 768.0)		768.1 $\gamma_6$ ( 34)+ $\tau_2$ ( 28)+ $\gamma_4$ ( 11)
	54	668.4	0.727	658.2	( 650.0)		649.9 $\tau_2$ ( 33)+ $\gamma_6$ ( 21)+ $\gamma_1$ ( 17)
	55	551.0	1.014	542.6	( 536.0)		535.4 $\gamma_3'$ ( 26)+ $\tau_4$ ( 23)+ $\gamma_1$ ( 17) + $\gamma_7$ ( 14)
	56	501.8	0.462	490.9	( 488.0)		488.3 $\tau_5$ ( 35)+ $\tau_3$ ( 27) + $\tau_1$ ( 20)
	57	410.5	1.894	404.1	( 399.0)		399.0 $\tau_3$ ( 44)+ $\tau_1$ ( 31)
	58	348.1	3.157	339.1	( 338.0)		337.8 $\gamma_1$ ( 23)+ $\gamma_3'$ ( 23)+ $\tau_2$ ( 11)
	59	211.1	0.815	200.0	( 205.0)		205.2 $\tau_4$ ( 30)+ $\gamma_3'$ ( 15)+ $\gamma_1$ ( 15)
	60	173.6	1.947	171.4	( 169.0)		169.0 $\tau_1$ ( 26)+ $\gamma_7$ ( 16)+ $\tau_5$ (15)+ $\tau_4$ (12)+ $\tau_3$ (12)
	61	101.0	0.010	56.8	( 98.0)		98.1 $\tau_{ring}$ ( 59)+ $\gamma_7$ ( 11)
	62	89.3	0.330	58.2	( 86.9)		86.7 $\tau_{ring}$ ( 29)+ $\tau_6$ ( 23)
	63	75.6	0.828	60.7	( 73.6)		73.7 $\tau_6$ ( 58)

Since the fitting algorithm required all the experimental frequencies, the numbers in parenthesis are introduced as good guesses for 2,6 – DMQ and do not have any other significance. RMS error is 1.6618 for the fitting of experimental frequencies.



Table 4.6: Calculated harmonic, anharmonic frequencies (in  $cm^{-1}$ ) and intensities (in km/mol) at  $B3LYP/6-31G^*$ , observed frequencies (in  $cm^{-1}$ ) and intensities (in km/mol), fitted frequencies (in  $cm^{-1}$ ) and PED of 2,7 - DMQ.

Sym	B3LYP/6-31G*			Observed		Force field	
	No	Harm.	Int.	Anharm.	Freq.	Int.	Fitted PED
$A'$							
1	3203.3	5.150	3064.1	3059.3	33.825	3059.3	$r_5$ ( 93)
2	3200.5	25.686	3054.6	(3059.0)		3059.0	$r_2$ ( 91)
3	3190.2	33.904	3053.5	3028.2	7.572	3028.2	$r_4$ ( 94)
4	3178.6	6.619	3020.0	2987.7	0.829	2988.8	$r_1$ ( 49)+ $r_3$ ( 47)
5	3172.0	4.946	3025.8	(2987.0)		2985.9	$r_1$ ( 49)+ $r_3$ ( 47)
6	3159.3	8.184	3007.2	2958.6	1.989	2957.7	$r'_7$ ( 74)+ $r'_6$ ( 25)
7	3130.7	15.511	2981.8	(2958.0)		2956.6	$r'_9$ ( 78)+ $r'_8$ ( 21)
8	3044.5	22.728	2962.8	2875.8	9.175	2880.0	$r'_8$ ( 79)+ $r'_9$ ( 21)
9	3041.0	37.099	2976.1	(2875.0)		2877.6	$r'_6$ ( 74)+ $r'_7$ ( 25)
10	1683.7	37.525	1644.9	1633.0	22.716	1633.8	$R_{10}$ ( 21)+ $R_8$ ( 15)+ $R_{11}$ ( 11) + $\delta_4$ ( 11)
11	1663.7	55.653	1625.8	1612.5	33.991	1612.9	$R_2$ ( 34)
12	1611.3	11.888	1574.2	1563.6	11.275	1563.3	$R'_4$ ( 16)+ $R_{10}$ ( 15)+ $R_6$ ( 12)
13	1562.0	41.169	1525.9	1513.5	44.216	1518.4	$R_9$ ( 18)+ $R_7$ ( 11)+ $\beta'_3$ ( 11)
14	1528.3	2.965	1464.9	(1487.0)		1486.8	$\delta_s CH_3(2)$ ( 61)
15	1509.9	10.262	1494.3	(1469.0)		1469.4	$\delta_s CH_3(1)$ ( 66)+ $\delta_s CH_3(2)$ ( 16)
16	1497.9	10.566	1469.4	1450.6	13.375	1454.0	$\beta_2$ ( 19)+ $r'_{11}$ ( 15)+ $r'_{10}$ ( 14) + $R_8$ ( 11)
17	1460.8	5.779	1430.7	1425.4	1.602	1422.8	$R_{11}$ ( 13)+ $\delta_s CH_3(1)$ ( 12)+ $R'_5$ ( 11)
18	1441.2	0.284	1434.5	(1402.0)		1402.1	$\rho CH_3(1)$ ( 89)
19	1429.1	3.010	1419.6	(1390.0)		1390.1	$\delta_5$ ( 89)
20	1413.7	7.207	1380.3	1380.1	11.551	1378.0	$R_6$ ( 30)+ $R_8$ ( 12)+ $R_{11}$ ( 10)
21	1394.3	7.627	1363.4	1340.6	2.708	1343.5	$R'_4$ ( 24)+ $R_2$ ( 16)
22	1341.5	9.909	1318.8	1308.7	11.993	1310.5	$R'_5$ ( 19)+ $\delta_2$ ( 14)
23	1291.0	0.493	1265.6	(1256.6)		1253.8	$\beta_2$ ( 26)+ $\beta_5$ ( 17)+ $\beta'_6$ ( 17)
24	1254.7	12.347	1230.2	1222.6	16.083	1218.6	$R''_{12}$ ( 16)+ $R_7$ ( 13)+ $R_3$ ( 13)
25	1247.1	0.375	1221.3	(1213.0)		1210.7	$R_1$ ( 21)+ $r'_{10}$ ( 17)+ $R_{11}$ ( 13)
26	1201.7	3.384	1177.9	1172.2	2.542	1170.2	$R''_{13}$ ( 27)+ $\beta_5$ ( 25)
27	1183.5	4.870	1172.9	1145.8	4.366	1145.6	$\beta'_3$ ( 28)+ $\beta_2$ ( 18)+ $R_8$ ( 16)+ $r'_{11}$ ( 10)
28	1153.6	2.837	1134.2	1121.8	5.029	1120.6	$r'_{11}$ ( 26)+ $\beta'_3$ ( 14)
29	1055.9	1.447	1038.0	1014.6	0.497	1024.1	$\delta_a CH_3(2)$ ( 21)+ $\delta_a CH_3(1)$ ( 16)
30	1018.5	16.659	1006.1	993.4	1.602	987.6	$\delta_a CH_3(2)$ ( 28)+ $\delta_a CH_3(1)$ ( 22)
31	969.0	2.740	956.9	952.7	1.823	949.7	$\delta_2$ ( 28)+ $\beta'_6$ ( 19)+ $R_9$ ( 14)
32	956.9	1.827	941.4	929.8	0.552	930.8	$R_3$ ( 24)+ $\delta_a CH_3(1)$ ( 14)+ $\beta'_6$ ( 13)
33	789.9	2.027	779.7	( 768.0)		768.1	$R_6$ ( 32)+ $R_1$ ( 13)+ $R_7$ ( 11)
34	782.9	1.276	768.7	( 762.0)		762.5	$R''_{12}$ ( 18)+ $R''_{13}$ ( 17)+ $\delta_2$ ( 17) + $\beta'_6$ ( 15)
35	689.2	0.901	681.4	( 670.0)		670.7	$R''_{12}$ ( 14)+ $\beta'_6$ ( 14)+ $\delta_2$ ( 12) + $\delta_3$ ( 10)
36	643.2	3.884	636.5	( 629.6)		629.2	$\beta_7$ ( 47)+ $\delta_3$ ( 36)
37	482.0	0.266	479.8	( 469.0)		469.2	$\delta_1$ ( 52)+ $\delta_4$ ( 11)

Table 4.6:(Continued) Calculated harmonic, anharmonic frequencies (in  $cm^{-1}$ ) and intensities (in km/mol) at  $B3LYP/6-31G^*$ , observed frequencies (in  $cm^{-1}$ ) and intensities (in km/mol), fitted frequencies (in  $cm^{-1}$ ) and PED of 2,7 – DMQ.

Sym	B3LYP/6-31G*			Observed		Force field	
	No	Harm.	Int.	Anharm.	Freq.	Int.	Fitted PED
38	464.1	1.301	462.2	( 451.0)		451.3	$\delta_4$ ( 30)+ $\beta_1$ ( 18)+ $\beta_7$ ( 15)
39	436.2	1.655	433.3	( 424.0)		424.0	$\delta_4$ ( 25)+ $\delta_3$ ( 17)
40	332.9	2.589	338.6	( 324.0)		323.9	$\beta_4$ ( 38)+ $\beta_1$ ( 32)
41	222.5	1.211	224.6	( 216.0)		216.5	$\beta_4$ ( 30)+ $\beta_1$ ( 27)
$A''$							
42	3094.8	19.158	2945.1	2934.4	27.303	2932.6	$r'_6$ (100)
43	3091.0	20.452	2945.1	(2934.0)		2930.3	$r'_8$ (100)
44	1513.9	7.285	1504.0	(1473.0)		1473.1	$\delta_s CH_3$ (1) ( 93)
45	1513.0	4.978	1512.9	(1472.0)		1472.1	$\delta_s CH_3$ (2) ( 93)
46	1076.9	5.034	1052.1	1041.5	1.658	1041.0	$\rho CH_3$ (1) ( 50)+ $\delta_a CH_3$ (2) ( 17)
47	1069.3	3.100	1046.8	(1040.0)		1038.6	$\delta_6$ ( 53)+ $\delta_a CH_3$ (1) ( 18) + $\gamma_1$ ( 12)
48	987.1	1.198	972.2	968.1	0.276	968.5	$\rho CH_3$ (2) ( 60)+ $\rho CH_3$ (2) ( 26)
49	963.6	0.214	959.3	( 937.0)		937.1	$\gamma'_3$ ( 44)+ $\gamma_2$ ( 42)
50	919.2	6.222	893.6	888.9	8.511	889.4	$\gamma_5$ ( 71)+ $\tau_2$ ( 12)
51	860.0	36.431	845.5	835.6	56.266	835.8	$\rho CH_3$ (2) (32)+ $\rho CH_3$ (2) (15) + $\gamma_2$ (14)+ $\gamma'_3$ ( 13)
52	803.7	2.470	790.4	( 782.0)		782.0	$\gamma'_3$ (30)+ $\gamma_2$ (26)+ $\rho CH_3$ (2) (12) + $\rho CH_3$ (2) ( 11)
53	796.4	4.847	790.1	780.0	8.788	777.0	$\gamma'_6$ (45)+ $\tau_2$ (ring1) (23) + $\rho CH_3$ (2) (15)
54	665.5	0.830	660.2	( 647.0)		648.0	$\tau_2$ ( 37)+ $\gamma'_6$ ( 18)+ $\gamma_1$ ( 15) + $\gamma_4$ ( 10)
55	574.6	2.968	569.9	562.7	1.879	559.3	$\tau_4$ ( 20)+ $\gamma_4$ ( 19) + $\gamma_1$ ( 15)+ $\tau_1$ ( 10)
56	492.2	2.575	483.5	( 479.0)		478.2	$\tau_3$ ( 28)+ $\tau_5$ ( 27) + $\tau_1$ ( 14)
57	420.5	1.112	415.1	( 409.0)		408.9	$\tau_3$ ( 36)+ $\tau_1$ ( 25)
58	295.4	1.193	291.5	( 287.0)		287.5	$\gamma_1$ ( 21)+ $\tau_4$ ( 17)+ $\tau_3$ ( 15)+ $\gamma'_6$ ( 10)
59	270.6	0.078	269.8	( 263.4)		263.4	$\tau_1$ (29)+ $\gamma_4$ (19)
60	123.7	0.001	120.0	( 120.0)		120.1	$\gamma_7$ ( 45)+ $\tau_4$ ( 33)
61	119.4	2.413	116.5	( 116.0)		116.2	$\tau_5$ ( 26)+ $\tau_3$ ( 18) + $\gamma_5$ ( 12)
62	87.3	0.221	15.8	( 84.9)		84.8	$\tau$ (ring) ( 68)+ $\tau_6$ ( 11)
63	79.4	1.176	-1.0	( 77.0)		77.0	$\tau_6$ ( 64)

Since the fitting algorithm required all the experimental frequencies, the numbers in parenthesis are introduced as good for 2,7 – DMQ and do not have any other significance. RMS error is 2.1157 for the fitting of experimental frequencies.

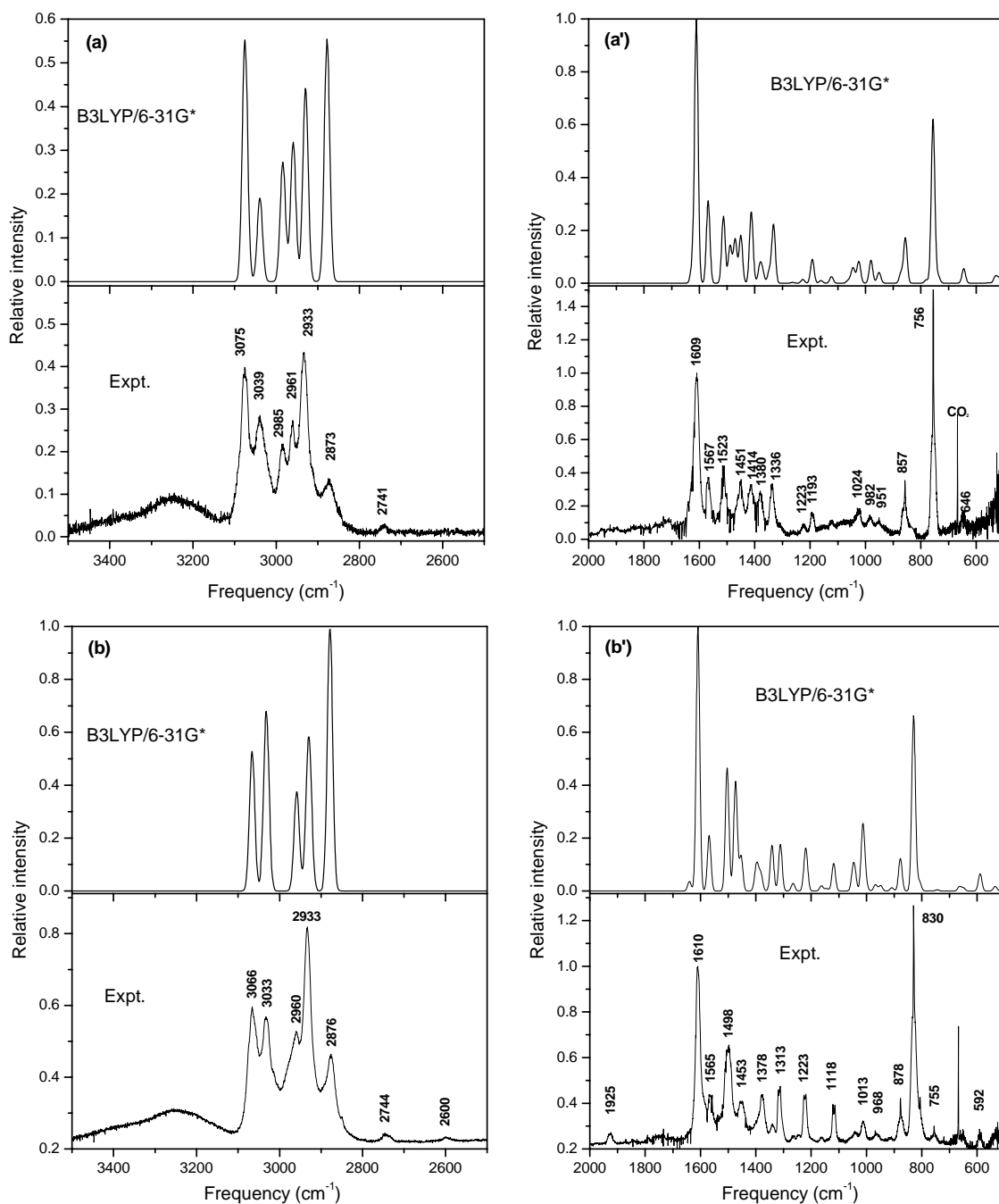
Table 4.7: Calculated harmonic, anharmonic frequencies (in  $cm^{-1}$ ) and intensities (in km/mol) at  $B3LYP/6-31G^*$ , observed frequencies (in  $cm^{-1}$ ) and intensities (in km/mol), fitted frequencies (in  $cm^{-1}$ ) and PED of 2, 8 - DMQ.

Sym	B3LYP/6-31G*			Observed		Force field	
	No	Harm.	Int.	Anharm.	Freq.	Int.	Fitted PED
$A'$							
1	3203.8	31.229	3069.3	3056.8	33.585	3056.8	$r_2$ ( 96)
2	3200.5	27.074	3055.8	(3056.0)		3056.0	$r_4$ ( 89)
3	3184.0	26.451	3049.4	3027.3	1.909	3027.3	$r_5$ ( 90)
4	3179.1	4.992	3020.6	2978.9	2.343	2980.0	$r_1$ ( 49)+ $r_3$ ( 49)
5	3176.5	1.497	3021.4	(2978.0)		2976.8	$r_1$ ( 49)+ $r_3$ ( 49)
6	3156.8	8.124	3007.3	2966.3	0.998	2963.5	$r'_7$ ( 78)+ $r'_6$ ( 18)
7	3129.3	20.645	2980.9	(2966.0)		2963.0	$r'_9$ ( 79)+ $r'_8$ ( 17)
8	3055.0	26.142	2971.4	2863.1	4.642	2876.5	$r'_8$ ( 82)+ $r'_9$ ( 17)
9	3044.4	24.186	2967.7	(2863.0)		2874.5	$r'_6$ ( 81)+ $r'_7$ ( 18)
10	1671.6	17.805	1631.4	(1626.0)		1626.4	$R_{10}$ ( 19)+ $R_7$ ( 13)+ $R_2$ ( 11)
11	1662.3	39.932	1623.8	1615.1	34.149	1615.8	$R_2$ ( 27)+ $R_8$ ( 16)
12	1625.6	11.462	1583.4	1578.2	6.335	1579.3	$R'_4$ ( 16)+ $R_8$ ( 12)+ $R_9$ ( 12) + $R_6$ ( 10)
13	1553.6	37.373	1516.6	1506.4	32.631	1504.4	$\beta'_3$ ( 13)+ $R_3$ ( 11) + $R_9$ (10) $\delta_s CH_3(2)$ ( 10)
14	1529.9	1.326	1493.2	(1489.0)		1489.7	$\delta_s CH_3(2)$ ( 58)
15	1517.8	1.023	1486.9	(1477.0)		1474.5	$\delta_s CH_3(1)$ ( 15)+ $R'_4$ ( 14)+ $\delta_s CH_3(2)$ ( 13)+ $R_{11}$ ( 10)
16	1490.5	22.922	1454.8	1434.3	27.510	1434.8	$\delta_s CH_3(1)$ ( 62)
17	1477.2	11.949	1445.6	(1430.0)		1430.8	$r'_{10}$ (13) + $\beta_2$ (12)+ $\beta'_3$ ( 11) + $R_7$ (10)
18	1444.4	0.657	1432.5	(1405.0)		1405.0	$\rho CH_3(1)$ ( 87)
19	1430.9	2.578	1417.4	1378.1	11.455	1377.9	$\delta_5$ ( 84)
20	1408.7	4.682	1372.5	(1371.0)		1371.9	$R_6$ ( 33)
21	1377.3	7.638	1345.1	(1340.0)		1339.6	$R_2$ ( 14)+ $R'_4$ ( 13)+ $R_{10}$ ( 12)
22	1353.8	10.832	1326.3	1318.7	13.321	1317.5	$R'_5$ ( 25)+ $\delta_2$ ( 18)
23	1290.3	0.338	1263.1	(1255.0)		1256.1	$\beta_4$ ( 26)+ $\beta_6$ ( 12)+ $R_{11}$ ( 11) $\beta_2$ ( 10)
24	1261.4	5.952	1233.5	1231.5	4.382	1234.0	$R''_{12}$ ( 21)+ $r'_{10}$ ( 16)+ $\delta_2$ ( 11)
25	1250.2	5.628	1226.2	1207.0	0.911	1213.5	$R_1$ ( 18)+ $R_7$ ( 18)+ $R'_5$ ( 14) + $\beta'_3$ ( 12)
26	1197.9	1.932	1183.0	1164.0	1.562	1161.5	$\beta'_3$ ( 32)+ $\beta_2$ ( 19)
27	1173.6	3.832	1155.2	1135.3	5.207	1133.7	$r'_{11}$ ( 33)+ $r'_{10}$ ( 23)+ $R_2$ ( 12)
28	1113.1	1.794	1092.3	(1083.0)		1081.4	$R_9$ ( 13)+ $\beta_4$ ( 13)+ $\delta_a CH_3(2)$ ( 13) + $\beta_6$ ( 12)
29	1095.0	3.601	1073.5	1066.9	7.246	1068.4	$R_9$ ( 22)+ $\beta_6$ ( 14)+ $\beta_2$ ( 12) $R_8$ ( 11)+ $R'_{13}$ ( 11)
30	1030.4	11.371	1008.6	1002.5	2.386	1003.2	$\delta_a CH_3(1)$ ( 40)+ $\delta_6$ ( 13)
31	999.6	2.432	978.2	970.0	0.477	972.4	$\delta_a CH_3(2)$ ( 31)+ $\delta_2$ ( 11)
32	922.4	0.213	906.4	( 897.0)		894.7	$R_3$ ( 25)+ $\delta_1$ ( 14)
33	870.2	4.122	854.3	858.1	0.998	858.2	$\delta_2$ ( 34)
34	730.2	2.969	720.2	721.0	1.518	718.3	$\delta_4$ ( 18)+ $\beta_6$ ( 14)+ $R_7$ ( 11)
35	703.1	0.699	692.9	687.6	1.518	689.9	$\beta'_7$ ( 37)+ $\beta_6$ ( 11)

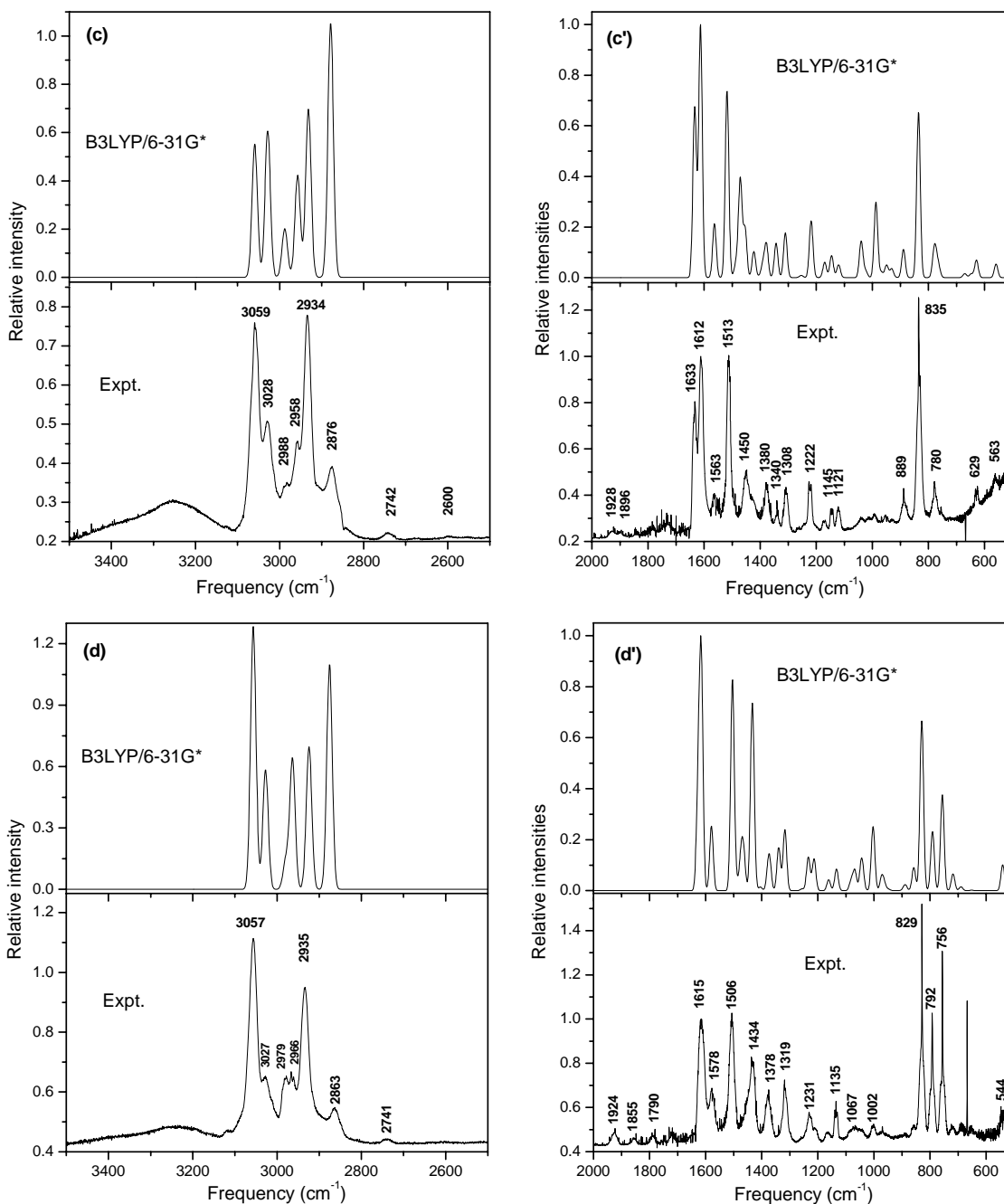
Table 4.7:(Continued) Calculated harmonic, anharmonic frequencies (in  $cm^{-1}$ ) and intensities (in km/mol) at  $B3LYP/6-31G^*$ , observed frequencies (in  $cm^{-1}$ ) and intensities (in km/mol), fitted frequencies (in  $cm^{-1}$ ) and PED of 2, 8 –  $DMQ$ .

Sym	B3LYP/6-31G*			Observed		Force field	
	No	Harm.	Int.	Anharm.	Freq.	Int.	Fitted PED
36	553.2	4.581	546.3	544.2	3.514	541.2	$\delta_3$ (31)+ $\beta_7'$ ( 29)+ $R''$ 13 (10)
37	535.7	0.195	528.6	( 512.0)		515.1	$\delta_1$ ( 28)+ $\delta_3$ ( 22) + $\delta_4$ ( 16)
38	490.5	1.453	485.1	( 477.0)		477.4	$\delta_1$ ( 39)+ $\beta_1$ ( 19)+ $\beta_5$ ( 13)
39	440.2	0.803	435.3	( 428.0)		426.6	$\delta_1$ ( 41)+ $\delta_3$ ( 18)
40	346.7	3.800	341.3	( 337.0)		337.4	$\beta_1$ ( 43)+ $\beta_5$ ( 33)
41	221.2	0.672	215.4	( 215.0)		214.6	$\beta_1$ (28)+ $\beta_5$ (28)+ $\delta_4$ (18)
$A''$							
42	3112.9	13.690	2958.1	2934.7	23.952	2925.5	$r_6'$ (100)
43	3094.8	18.313	2949.5	(2934.0)		2923.1	$r_8'$ (100)
44	1513.8	5.458	1512.2	(1473.0)		1473.1	$\delta_s CH_3$ (1) ( 93)
45	1504.4	5.865	1474.7	(1464.0)		1464.3	$\delta_s CH_3$ (2) ( 93)
46	1079.4	4.245	1053.5	(1050.0)		1045.2	$\rho CH_3$ (1) (39)+ $\delta_a CH_3$ (2) (13) + $\delta_6$ ( 12)
47	1069.1	2.024	1043.9	(1040.0)		1040.1	$\delta_6$ ( 42)+ $\delta_a CH_3$ (1) ( 14) + $\rho CH_3$ (1) ( 12)
48	989.4	1.126	970.5	( 963.0)		963.0	$\rho CH_3$ (2) ( 56)+ $\rho CH_3$ (2) ( 28)
49	974.0	0.259	962.4	( 948.0)		947.8	$\gamma_3'$ ( 49)+ $\gamma_4$ ( 23)+ $\gamma_2$ ( 13)
50	913.1	0.950	896.3	( 888.0)		888.2	$\gamma_4$ ( 47)+ $\gamma_2$ ( 37)
51	853.8	30.146	835.6	829.3	27.207	829.7	$\rho CH_3$ (2) ( 27)+ $\tau_2$ ( 20) + $\rho CH_3$ (2) ( 18)
52	813.6	10.504	802.5	792.3	16.662	791.4	$\gamma_6$ ( 32)+ $\tau_2$ ( 30) + $\rho CH_3$ (2) ( 16)
53	779.8	17.015	762.9	756.2	19.569	756.4	$\gamma_2$ ( 39)+ $\gamma_3'$ ( 34)
54	670.3	0.092	659.7	( 652.0)		651.9	$\gamma_6$ (29)+ $\tau_2$ (24)+ $\gamma_1$ (19)
55	564.4	0.002	555.3	( 549.0)		549.3	$\tau_3$ ( 29)+ $\tau_2$ (ring2) ( 21) + $\tau_2$ ( 13)
56	520.1	0.631	511.4	( 506.0)		505.4	$\tau_4$ (23)+ $\gamma_7'$ (20)+ $\gamma_1$ (18) + $\gamma_5$ ( 14)
57	424.1	0.035	417.2	( 412.0)		412.0	$\tau_1$ ( 48)+ $\gamma_5$ ( 12) + $\tau_3$ ( 12)
58	311.3	0.003	306.0	( 302.0)		302.4	$\tau_4$ (32)+ $\gamma_1$ (21)+ $\gamma_5$ (11) + $\gamma_6$ ( 10)
59	212.2	0.974	203.4	( 206.0)		206.0	$\tau_3$ ( 48)
60	168.4	5.545	163.9	( 163.0)		163.0	$\tau_5$ ( 33)+ $\tau_1$ ( 24) + $\gamma_5$ ( 13)
61	136.5	0.090	27.7	( 132.0)		132.0	$\tau_{ring}$ ( 81)
62	101.4	0.074	106.7	( 98.0)		98.0	$\gamma_7'$ ( 39)+ $\tau_4$ ( 17) + $\tau_3$ ( 16)
63	74.7	0.426	211.0	( 72.0)		72.0	$\tau_6$ ( 72)

Since the fitting algorithm required all the experimental frequencies, the numbers in parenthesis are introduced as good guesses for 2, 8 –  $DMQ$  and do not have any other significance. RMS error is 3.3118 for the fitting of experimental frequencies.



**Figure 4.3.** Comparison of observed and calculated IR spectra of (a, a') 2,4-DMQ and (b, b') 2,6-DMQ. In the calculated spectrum, FWHM assumed to be 15 cm<sup>-1</sup>. Prominent peaks are labeled in the observed spectrum.



**Figure 4.3. (Continued) Comparison of observed and calculated IR spectra of (c, c') 2,7-DMQ and (d, d') 2,8-DMQ. In the calculated spectrum, FWHM assumed to be 15 cm<sup>-1</sup>. Prominent peaks are labeled in the observed spectrum.**

The corresponding force field fitted frequency is  $1610.9\text{ cm}^{-1}$  in 2,4-DMQ,  $1609.1\text{ cm}^{-1}$  in 2,6-DMQ,  $1612.9\text{ cm}^{-1}$  in 2,7-DMQ, and  $1615.8\text{ cm}^{-1}$  in 2,8-DMQ. The relative intensity of this band in DMQs is more intense compared to that in dimethylnaphthalenes (DMNs).<sup>24</sup> The larger intensity result from a large change in dipole moment as the ring is stretched. In 2,7-DMQ one extra band observed at  $1632.2\text{ cm}^{-1}$  which is not clearly resolved from the adjacent band at  $1612.5\text{ cm}^{-1}$ . This band is not observed for the rest of the isomers of DMQ. In the calculated spectra of 2,8-DMQ, this band is moderately intense however in the experimental spectra it is not observed. Perhaps this band is masked by the adjacent band found at  $1615.1\text{ cm}^{-1}$ . A low intensity band observed at  $1566.9\text{ cm}^{-1}$  in 2,4-DMQ, at  $1565.5\text{ cm}^{-1}$  in 2,6-DMQ, at  $1563.6\text{ cm}^{-1}$  in 2,7-DMQ, and at  $1578.2\text{ cm}^{-1}$  in 2,8-DMQ is assigned as a mixture of local coordinate vibration of aromatic C-N stretching (R') and aromatic C-C stretching (R) by comparing with the force field fitted frequency calculated at  $1568.2\text{ cm}^{-1}$  in 2,4-DMQ,  $1568.6\text{ cm}^{-1}$  in 2,6-DMQ,  $1563.3\text{ cm}^{-1}$  in 2,7-DMQ, and  $1579.3\text{ cm}^{-1}$  in 2,8-DMQ, respectively. A moderately intense band observed at  $1512.8$ ,  $1498.6$ ,  $1513.5$ , and  $1506\text{ cm}^{-1}$  for 2,4-, 2,6-, 2,7- and 2,8-DMQ, respectively, is unique for different isomers of DMQ. The agreement between the calculated anharmonic frequencies and observed frequencies is satisfactory for these non C-H stretching vibrations.

A band observed at  $1450.7\text{ cm}^{-1}$  in 2,4-DMQ and  $1453.1\text{ cm}^{-1}$  in 2,6-DMQ is of low intensity whereas the same band observed at  $1450.6\text{ cm}^{-1}$  in 2,7-DMQ and  $1434.3\text{ cm}^{-1}$  in 2,8-DMQ is of moderate intensity. This band is correlated with the calculated anharmonic frequency at  $1504.7\text{ cm}^{-1}$  in 2,4-DMQ,  $1499.0\text{ cm}^{-1}$  in 2,7-DMQ,  $1469.4\text{ cm}^{-1}$  in 2,7-DMQ, and  $1454.8\text{ cm}^{-1}$  in 2,8-DMQ, respectively, which is responsible for methyl C-H antisymmetric deformation ( $\delta_s$ ). In 2,4-DMQ this band can also be correlated with the fundamental

anharmonic band at  $1464.4\text{ cm}^{-1}$  instead of that at  $1504.7\text{ cm}^{-1}$  since its corresponding fitted frequency and the nature of vibration is the same. In such a case assignment is confirmed with the help of the intensity. A band observed at  $1413.8\text{ cm}^{-1}$  in 2,4-DMQ corresponds to the force field fitted frequency at  $1412.6\text{ cm}^{-1}$  which is responsible for aromatic C-H in-plane bending ( $\beta$ ) vibration. A pair of aromatic C-C stretching/aromatic ring deformation bands found at  $1380.1$  and  $1336.9\text{ cm}^{-1}$  in 2,4-DMQ; at  $1376.8$  and  $1313.1\text{ cm}^{-1}$  in 2,6-DMQ; at  $1380.1$  and  $1308.7\text{ cm}^{-1}$  in 2,7-DMQ; at  $1378.1$  and  $1318.7\text{ cm}^{-1}$  in 2,8-DMQ correspond to the DFT calculated anharmonic frequencies at  $1422.1$  and  $1341.7\text{ cm}^{-1}$  in 2,4-DMQ; at  $1380.5$  and  $1326.3\text{ cm}^{-1}$  in 2,6-DMQ; at  $1380.3$  and  $1318.8\text{ cm}^{-1}$  in 2,7-DMQ; at  $1417.4$  and  $1326.3\text{ cm}^{-1}$  in 2,8-DMQ, respectively. In this region the agreement between observed and calculated anharmonic frequencies are not very good for 2,4-DMQ and 2,8-DMQ. They deviate by more than  $10\text{ cm}^{-1}$ , however, the force field fitted frequencies are quite close and calculated at  $1381.3$  and  $1332.1\text{ cm}^{-1}$  in 2,4-DMQ; at  $1381.4$  and  $1311.2\text{ cm}^{-1}$  in 2,6-DMQ; at  $1378.0$  and  $1310.5\text{ cm}^{-1}$  in 2,7-DMQ; at  $1377.9$  and  $1317.5\text{ cm}^{-1}$ , respectively.

A band observed at  $1223.3\text{ cm}^{-1}$  in 2,4-DMQ, at  $1223.0\text{ cm}^{-1}$  in 2,6-DMQ, at  $1222.6\text{ cm}^{-1}$  in 2,7-DMQ, and at  $1231.5\text{ cm}^{-1}$  in 2,8-DMQ match well with the calculated fundamental anharmonic band at  $1246.6\text{ cm}^{-1}$  in 2,4-DMQ,  $1223.7/1235.6\text{ cm}^{-1}$  in 2,6-DMQ,  $1230.2\text{ cm}^{-1}$  in 2,7-DMQ, and  $1233.5\text{ cm}^{-1}$  in 2,8-DMQ. In 2,4-DMQ this band is assigned to a mixture of local coordinate vibration of aromatic C-C stretch (R) and aromatic C-N stretch (R'); whereas for other three isomers it is assigned to a mixture of local coordinate vibration of aromatic-methyl C-C stretch (R'') and aromatic C-C stretch (R) as obtained from PEDs. A low intensity aromatic C-C/C-N stretching vibration appears at  $1207.0\text{ cm}^{-1}$  in 2,8-DMQ which is close to the calculated anharmonic band at  $1226.2\text{ cm}^{-1}$  and with the force field fitted frequency at



1213.5  $\text{cm}^{-1}$ . This band is not observed in other three isomers. In 2,7-DMQ two extra bands observed at 1172.2 and 1145.8  $\text{cm}^{-1}$  are assigned to aromatic-methyl C-C stretching ( $R''$ ) and aromatic C-H in-plane bending ( $\beta$ ) vibrations with the help of force field fitted frequencies at 1170.2 and 1145.6  $\text{cm}^{-1}$ , respectively. A band observed at 1121.2, 1118.2, 1121.8, and 1135.3  $\text{cm}^{-1}$  for 2,4-, 2,6-, 2,7-, and 2,8-DMQ, respectively, is assigned to aromatic C-H in-plane bending vibrations ( $\beta$ ) by comparing with the calculated anharmonic bands at 1142.4, 1136.8, 1134.2, and 1155.2  $\text{cm}^{-1}$  which differ by  $\sim 20 \text{ cm}^{-1}$  from their respective observed frequencies.

In 2,8-DMQ, one moderately intense band observed at 1066.9  $\text{cm}^{-1}$  is identified as a mixture of local coordinate vibration of aromatic C-H in-plane bending ( $\beta$ ), aromatic C-C stretching ( $R$ ) and aromatic-methyl C-C stretching ( $R''$ ) by correlating with the DFT calculated anharmonic frequency at 1073.5  $\text{cm}^{-1}$ . A low intensity band observed at 1024.3  $\text{cm}^{-1}$  in 2,4-DMQ is assigned to a mixture of local-coordinate vibration of aromatic C-C stretching ( $R$ ) and methyl C-H symmetric deformation ( $\delta_a$ ) by comparing with the calculated anharmonic band at 1028.2  $\text{cm}^{-1}$ . Next one set of band observed at 1013.1, 1014.6, and 1002.5  $\text{cm}^{-1}$  for 2,6-, 2,7- and 2,8-DMQ, respectively, is assigned to the methyl C-H symmetric deformation ( $\delta_a$ ). This band is correlated with the calculated anharmonic band at 1022.0, 1038.0, and 1008.6  $\text{cm}^{-1}$  in 2,6-, 2,7-, and 2,8-DMQ, respectively. In 2,4- and 2,8-DMQ one extra band observed at 982.5 and 970.0  $\text{cm}^{-1}$ , respectively, correspond to the DFT calculated anharmonic band at 989.2 and 978.2  $\text{cm}^{-1}$ . This band is assigned as a mixture of local coordinate vibration of aromatic ring deformation ( $\delta$ ) and methyl C-H symmetric deformation ( $\delta_a$ ).

The next groups of two to three intense bands in the recorded spectra at 857.1 and 755.7  $\text{cm}^{-1}$  in 2,4-DMQ; at 877.9 and 830.3  $\text{cm}^{-1}$  in 2,6-DMQ; at 888.9, 835.6, and 780.0  $\text{cm}^{-1}$  in 2,7-DMQ; at 829.3, 792.3, and 756.2  $\text{cm}^{-1}$  in 2,8-DMQ are assigned to aromatic C-H out-of-plane

bending vibrations ( $\gamma$ ) by comparing with the anharmonic frequencies calculated at 866.7 and 766.0  $\text{cm}^{-1}$  in 2,4-DMQ; 887.9 and 838.7  $\text{cm}^{-1}$  in 2,6-DMQ; 893.6, 845.5, and 790.4  $\text{cm}^{-1}$  in 2,7-DMQ; 835.6, 802.5, and 762.9  $\text{cm}^{-1}$  in 2,8-DMQ, respectively. In the lower frequency region bands observed at 645.8 and 531.0  $\text{cm}^{-1}$  in 2,4-DMQ; at 755.0 and 592.4  $\text{cm}^{-1}$  in 2,6-DMQ; at 562.7  $\text{cm}^{-1}$  in 2,7-DMQ; at 721.0, 687.6, and 544.2  $\text{cm}^{-1}$  in 2,8-DMQ are assigned to aromatic ring deformation ( $\delta$ ) vibrations. Their corresponding anharmonic frequencies are 650.4 and 540.5  $\text{cm}^{-1}$  in 2,4-DMQ; 754.1 and 593.4  $\text{cm}^{-1}$  in 2,6-DMQ; 569.9  $\text{cm}^{-1}$  in 2,7-DMQ; 720.2, 692.9, and 546.3  $\text{cm}^{-1}$  in 2,8-DMQ, respectively.

#### **4.4.3 Non-fundamental bands**

In DMQs a few weak bands are seen in the spectral range of (2800 - 1780)  $\text{cm}^{-1}$  which do not correspond to any calculated fundamentals. They are identified as non-fundamental (combination/overtone) bands (see Table 4.8). I have assigned these bands with the help of calculated force field fitted frequencies. There are many possibilities for the assignment of the observed non-fundamental bands with the calculated ones, and we have assigned them by correlating with those whose corresponding fundamental bands are intense. The band observed at 2741.2  $\text{cm}^{-1}$  in 2,4-DMQ, at 2744.0  $\text{cm}^{-1}$  in 2,6-DMQ, at 2743.9  $\text{cm}^{-1}$  in 2,7-DMQ, and at 2741.0  $\text{cm}^{-1}$  in 2,8-DMQ is assigned to the first overtone band of  $\nu_{19}$  in 2,4- and 2,8-DMQ and to the first overtone of  $\nu_{20}$  in 2,6- and 2,7-DMQ by comparing with the force field fitted band at 2762.2  $\text{cm}^{-1}$  in 2,4-DMQ, at 2762.8  $\text{cm}^{-1}$  in 2,6-DMQ, at 2756.0  $\text{cm}^{-1}$  in 2,7-DMQ, and at 2755.8  $\text{cm}^{-1}$  in 2,8-DMQ. The low intensity band observed at 2600.0  $\text{cm}^{-1}$  in 2,6-DMQ and at 2599.8  $\text{cm}^{-1}$  in 2,7-DMQ is compared with the force field fitted frequencies at 2622.4/2603.1 and 2621.0/2596.6  $\text{cm}^{-1}$ , respectively. It could be a first overtone of  $\nu_{22}$  or a combination of the

fundamentals,  $\nu_{24}$  and  $\nu_{20}$ . A non-fundamental band observed at  $1925.0\text{ cm}^{-1}$  in 2,6-DMQ,  $1928.9\text{ cm}^{-1}$  in 2,7-DMQ and  $1923.9\text{ cm}^{-1}$  in 2,8-DMQ corresponds to the non-fundamental band at  $1948.8\text{ cm}^{-1}$  in 2,6-DMQ, at  $1956.4\text{ cm}^{-1}$  in 2,7-DMQ, and at  $1963.4\text{ cm}^{-1}$  in 2,8-DMQ, respectively, which is a combination of  $\nu_{51}$  and  $\nu_{27}$  in 2,8-DMQ, and  $\nu_{51} + \nu_{28}$  in 2,6-, and 2,7-DMQs. Combination bands are not seen in the 2,4-DMQ spectrum perhaps due to lower absorbances of the fundamentals compared to the other dimethylquinolines.

**Table 4.8: Observed and calculated fitted and anharmonic non-fundamental bands in DMQs. All frequencies are in  $\text{cm}^{-1}$ .**

Compound	Observed Non-fundamental bands		Force Field Fitted		Anharmonic Non-fundamental Bands	
	Freq.	Int.	Overtone	Combination	Overtone	Combination
2,4-DMQ	2741.2	1.053	2762.6( $2\nu_{19}$ )		2817.1	
2,6-DMQ	2744.0	1.709	2762.8( $2\nu_{20}$ )		2757.5	
	2600.0	0.539	2622.4( $2\nu_{22}$ )	2603.1( $\nu_{24}+\nu_{20}$ )	2649.0	2616.6
	1925.0	3.149		1948.8( $\nu_{51}+\nu_{28}$ )		1955.5
2,7-DMQ	2743.9	1.713	2756.0( $2\nu_{20}$ )		2756.5	
	2599.8	0.386	2621.0( $2\nu_{22}$ )	2596.6( $\nu_{24}+\nu_{20}$ )	2631.4	2609.0
	1928.9	1.602		1956.4( $\nu_{51}+\nu_{28}$ )		1980.0
	1896.0	0.663		1897.6( $\nu_{53}+\nu_{28}$ )		1924.1
2,8-DMQ	2741.0	0.968	2755.8( $2\nu_{19}$ )		2805.1	
	1923.9	4.313		1963.4( $\nu_{51}+\nu_{27}$ )		1991.8
	1855.8	1.628		1859.8( $\nu_{52}+\nu_{29}$ )		1879.0
	1789.7	2.205		1824.8( $\nu_{53}+\nu_{29}$ )		1874.9

*In parentheses frequency,  $\nu_i$  refers to the  $i$ -th fundamental vibration. For description see Tables 4.4 - 4.7.*

One band observed at  $1896.0\text{ cm}^{-1}$  in 2,7-DMQ corresponds to the calculated band at  $1897.6\text{ cm}^{-1}$  which is a combination band of fundamental vibrations,  $\nu_{53}$  and  $\nu_{28}$ . In 2,8-DMQ two non-fundamental bands observed at  $1855.8$  and  $1789.7\text{ cm}^{-1}$  can be correlated with the non-fundamental bands at  $1859.8$  and  $1824.8\text{ cm}^{-1}$  which are assigned to a combination band of  $(\nu_{52} + \nu_{29})$  and  $(\nu_{53} + \nu_{29})$ , respectively. It is worth noting that the assignment of the non-fundamental modes may be done as well by comparison with calculated anharmonic frequencies in the region. However, the mismatch between the observed and calculated anharmonic frequencies is much more than that found between the observed and force field fitted frequencies. For comparison, we have included the corresponding calculated anharmonic frequencies in Table 4.8 for all the nonfundamental modes.

In 2,4-, 2,6-, and 2,7-DMQs the comparison of the observed and calculated spectra indicates that the intense vibrations in the experimental spectra are also intense in the theoretical spectra except for bands that are present in the lower frequency region which are generally intense in the observed spectra compared to those in the calculated spectra.

## **4.5 Conclusion**

In this chapter, I have reported the gas phase IR spectra of 2,4-, 2,6-, 2,7-, and 2,8-DMQ recorded at low concentrations and assigned their vibrational spectra using force field fitted frequencies and their PEDs of normal modes and DFT calculated anharmonic frequencies. The anharmonic frequencies match well with the observed frequencies at lower frequency region. Unambiguously, I have assigned the aromatic C-H and methyl C-H stretching bands with the help of force field fitted frequencies. The error in fitting is within  $3\text{ cm}^{-1}$  between the observed fundamental vibrations and the force field fitted frequencies. PEDs help identify the type of

vibrations in terms of the activity in the local coordinate motion. For nonfundamental vibrations such as combinations or overtones, however, the error in fitting is higher than  $3\text{ cm}^{-1}$  but still better than that found between the calculated anharmonic and observed frequencies.

#### 4.6 References

- [1] Adams, J.; Atlas, E. L.; Giam, C. S. *Anal. Chem.* **1982**, *54*, 1515.
- [2] Onuska, F. I.; Terry, K. A. *J. High Res. Chromatog.* **1989**, *12*, 362.
- [3] Dmitrikov, V. P.; Fedorov, Y. V.; Nabivach, V. M. *Chromatographia* **1984**, *18*, 28.
- [4] Schmitter, J. M.; Ignatiadis, I.; Dorbon, M.; Arpino, P.; Guiochon, G.; Toulhoat, H. Huc, A. *Fuel* **1984**, *63*, 557.
- [5] Later, D. W.; Lee, M. L.; Bartle, K. D.; Kong, R. C.; Vassilaros, D. L. *Anal. Chem.* **1981**, *53*, 1612.
- [6] Stuermer, D. H.; Ng, D. J.; Morris, C. J. *Environ. Sci. Technol.* **1982**, *16*, 582.
- [7] Royer, R. E.; Mitchell, C. E.; Hanson, R. L.; Dutcher, J. S.; Bechtold, W. E. *Environ. Res.* **1983**, *31*, 460.
- [8] Qian, K.; Edwards, K. E.; Diehl, J. H.; Green, L. A. *Energy & Fuel* **2004**, *18*, 1784.
- [9] Guerin, M. R.; Rubin, I. B.; Rao, T. K.; Clark, B. R.; Epler, J. L. *Fuel* **1981**, *60*, 282.
- [10] Drushel, H. V.; Sommers, A. L. *Anal. Chem.* **1966**, *38*, 10.
- [11] Drushel, H. V.; Sommers, A. L. *Anal. Chem.* **1966**, *38*, 19.
- [12] Kaden, D. A.; Hites, R. A.; Thilly, W. G. *Cancer Res.* **1979**, *39*, 4152.
- [13] Birkholz, D. A.; Coutts, R. T.; Hruday, S. E.; Danell, R. W.; Lockhart, W. L. *Wat. Res.* **1990**, *24*, 67.
- [14] Lavoie, E. J.; Shigematsu, A.; Adams E. A.; Rigotty, J.; Hoffmann, D. *Cancer Lett.* **1984**, *22*, 269.
- [15] NIST Chemistry WeBook, IR database, <http://www.webbook.nist.gov/chemistry/>
- [16] Ozel, A. E.; Kecel, S.; Akyuz, S. *Vibr. Spectrosc.* **2006**, *42*, 325.
- [17] Karr, C. B.; Estep, P. A.; Papa, A. J. *J. Am. Chem.* **1959**, *81*, 152.

- [18] Calculated using Advanced Chemistry Development (ACD/Labs) software.
- [19] M. J. Frisch, G. W. Trucks, H. B. Schlegel, G. E. Scuseria, M. A. Robb, J. R. Cheeseman, J. A. Montgomery, Jr., T. Vreven, K. N. Kudin, J. C. Burant, J. M. Millam, S. S. Iyengar, J. Tomasi, V. Barone, B. Mennucci, M. Cossi, G. Scalmani, N. Rega, G. A. Petersson, H. Nakatsuji, M. Hada, M. Ehara, K. Toyota, R. Fukuda, J. Hasegawa, M. Ishida, T. Nakajima, Y. Honda, O. Kitao, H. Nakai, M. Klene, X. Li, J. E. Knox, H. P. Hratchian, J. B. Cross, C. Adamo, J. Jaramillo, R. Gomperts, R. E. Stratmann, O. Yazyev, A. J. Austin, R. Cammi, C. Pomelli, J. W. Ochterski, P. Y. Ayala, K. Morokuma, G. A. Voth, P. Salvador, J. J. Dannenberg, V. G. Zakrzewski, S. Dapprich, A. D. Daniels, M. C. Strain, O. Farkas, D. K. Malick, A. D. Rabuck, K. Raghavachari, J. B. Foresman, J. V. Ortiz, Q. Cui, A. G. Baboul, S. Clifford, J. Cioslowski, B. B. Stefanov, G. Liu, A. Liashenko, P. Piskorz, I. Komaromi, R. L. Martin, D. J. Fox, T. Keith, M. A. Al-Laham, C. Y. Peng, A. Nanayakkara, M. Challacombe, P. M. W. Gill, B. Johnson, W. Chen, M. W. Wong, C. Gonzalez, and J. A. Pople, Gaussian 03, Revision D.01, Gaussian, Inc Pittsburg, PA, **2003**.
- [20] UMAT, McIntosh D.F.; Peterson M. R.; General Vibrational Analysis System, QCPE 576. Indiana University, Bloomington, IN 47405.
- [21] Das, P.; Manogaran, S.; Arunan, E.; Das, P. K. *J. Phys. Chem. A* **2010**, *114*, 8351.
- [22] (a) Daunt, S. J.; Shurvell, H. F. *Spectrochim. Acta*, **1976**, *32A*, 1545 (b) Reddy, K. V.; Heller, D. F.; Berry, M. J. *J. Chem. Phys.* **1982**, *76*, 2814.
- [23] (a) McKean, D. C. *Spectrochim. Acta* **1973**, *29A*, 1559 (b) Gellini, C.; Moroni, L.; Muniz-Miranda, M. *J. Phys. Chem. A* **2002**, *106*, 10999.
- [24] Das, P.; Arunan, E.; Das, P. K. *Vibr. Spectrosc.* **2008**, *47*, 1.

# **Chapter-5**

**An Experimental and Theoretical investigation of  
Infrared spectra of Dimethylphenanthrenes (DMPs)  
in the Gas Phase**



## **5.1 Introduction**

In chapter 3 and 4, I have investigated the gas phase IR spectra of dimethyl polycyclic aromatic compounds having two fused benzene/nitrogen substituted benzene rings in the gas phase.<sup>1</sup> By combining IR spectroscopy and theory, I have assigned the fundamental and non-fundamental bands in the observed spectra. Here, I continue with tricyclicaromatic compounds namely dimethylphenanthrenes (DMPs) and report their IR spectra. They are present in interplanetary dust particles (IDPs), meteorites individual, diesel fuels, and sugar cane soot.<sup>2-6</sup> The residential wood combustion and motor vehicle exhaust emissions contribute to monomethylphenanthrene (MMPs) and DMPs to the lower atmosphere.<sup>7-11</sup> The isomer of DMPs have different biological activities, e.g., 4,10-DMP acts as a tumor initiating agent and 9,10-DMP is mutagenic whereas 1,4-DMP exhibits both the activities.<sup>12</sup> Another interesting feature of these molecules is that they are known to be the reasons behind unidentified infrared bands (UIR) in the interstellar medium (ISM).<sup>13</sup> Therefore, it is necessary to find accurate frequencies and intensities for DMPs and to identify different isomers of DMP in the gas phase.

In section 1.2 of chapter 1, I have discussed that a few experimental techniques employed for the analysis and identification of PAHs including DMPs.<sup>2, 10</sup> Pakdel et al. used FTNMR and FT-IR technique for the analysis of aromatic fractions of pyrolysis oil containing DMPs along with other methylated PAHs.<sup>14</sup> In 1997, Cane et al. recorded the gas phase IR spectra of anthracene and phenanthrene with the help of a multi-pass gas cell of 4.2 meter.<sup>15</sup> There is no literature report on the infrared spectroscopy of DMPs in the gas phase.

In this chapter, I report the mid-IR spectra of DMPs at low concentrations using a long-path gas cell and assign the observed vibrational frequencies unambiguously using scaled force field calculation at the B3LYP/6-311G\*\* level of theory as discussed in chapter 2.

## 5.2 Experimental section

### 5.2.1 Materials

DMPs chosen in this study are 1, 9-dimethylphenanthrene (Chiron, 99.1 %), 2,4-dimethylphenanthrene (Chiron, 99.9 %), and 3,6-dimethylphenanthrene (Chiron, 99.9 % purity) and they were used as received.

**Table 5.1: Some physical properties of phenanthrene and DMPs.**

Compound	State at 25 °C	m.p (in °C)	P (at 25 °C in mmHg)
Phenanthrene	Solid powder	100	<sup>a</sup> $1.25 \times 10^{-4}$
1,9-DMP	Solid powder	88	<sup>b</sup> $2.89 \times 10^{-5}$
2,4-DMP	Solid powder	80	<sup>b</sup> $2.60 \times 10^{-5}$
3,9-DMP	Solid powder	62	<sup>b</sup> $2.49 \times 10^{-5}$

<sup>a</sup> *Experimentally measured value.*<sup>16</sup>

<sup>b</sup> *Since experimental vapor pressures are not available, calculated values found through SciFinder search are given.*<sup>17</sup>

### 5.2.2 Methods

Experimental set-up employed for this study has been discussed in section 2.3.3 of chapter 2. DMPs have very low vapor pressures ( $\sim 10^{-5}$  mmHg) at room temperature [see Table 5.1]. I have thermally vaporized the DMPs by placing them inside a gas cell at 110 °C. During the vaporization, UHP Ar gas was introduced through a ball valve to seed the DMPs. The total pressure of Ar gas containing DMPs in the cell was maintained at 30 mmHg. For this study optical path length was fixed at 7.2 meter. The mid-IR spectra (4000 - 400  $\text{cm}^{-1}$ ) were collected using a liquid nitrogen cooled mercury cadmium telluride or HgCdTe (MCT) detector and KBr beam splitter combination. The spectra were recorded at 0.5  $\text{cm}^{-1}$  spectral

resolution with averaging over 2048 scans. The suitable H<sub>2</sub>O spectrum was recorded and subtracted from sample spectra in order to get clear spectra of DMPs. The integrated band area  $\int \log(I_0/I) dv$  (in cm<sup>-1</sup>) for each band was obtained with the help of OPUS software provided by Bruker. Levenberg Marquardt algorithm is used in the OPUS software to calculate single component band area in the region of overlapping bands particularly in the C-H stretching region.

Intensity of observed was calculated for DMPs using experimental band area and DFT calculated intensity. The detail of the intensity calculation was discussed in section 2.5 of chapter 2. The estimated vapor pressures found to be  $1.069 \times 10^{-5}$ ,  $0.913 \times 10^{-5}$ , and  $0.533 \times 10^{-5}$  atm at 110 °C for 1,9-, 2,4-, and 3,9-DMP, respectively, when B3LYP/6-311G\*\* calculated intensities were considered in the vapor pressure calculation under all the bands.

### **5.3 Theoretical calculations**

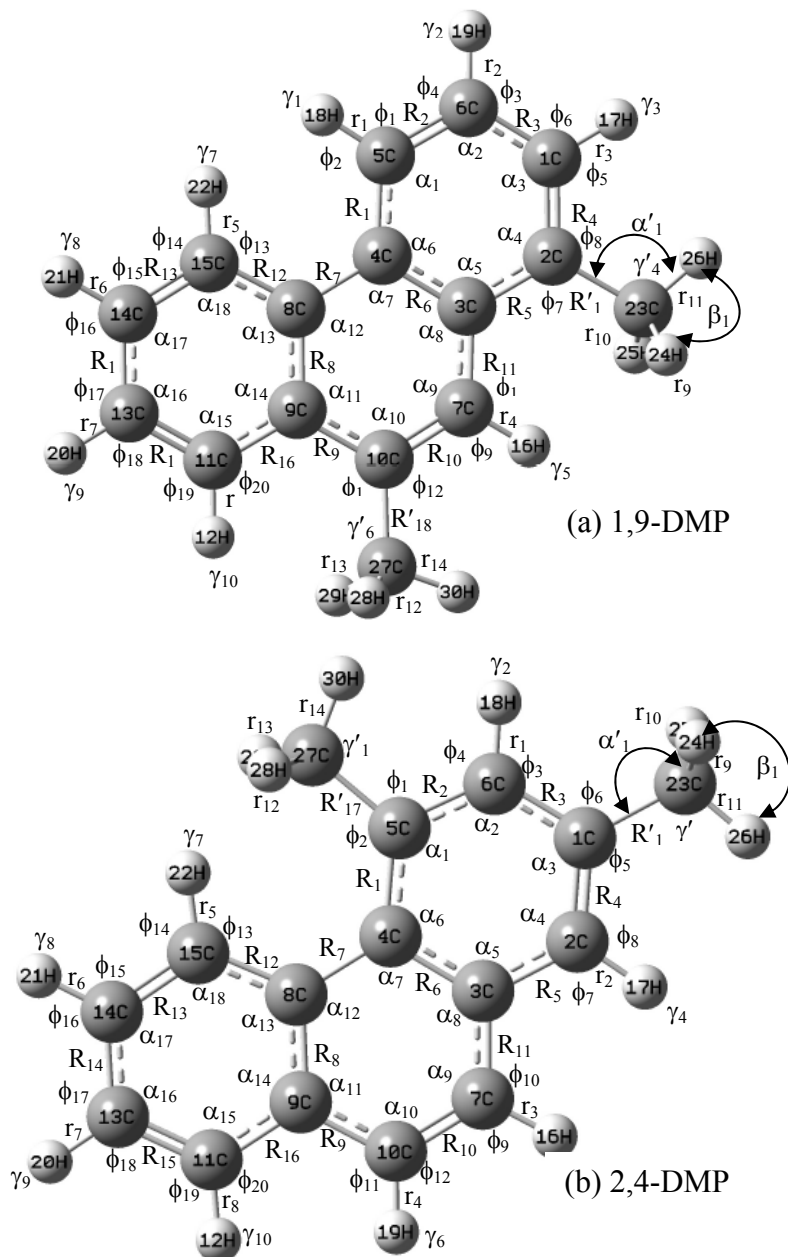
I followed the approach which was applied to DMQs (see section 4.3 of chapter 3). At first the molecular geometry of DMPs were optimized at C<sub>s</sub> point group with the B3LYP/6-31G\* and B3LYP/6-311G\*\* levels of theory using the Gaussian 09 program.<sup>18</sup> At the computed equilibrium geometry, the harmonic and anharmonic frequencies and their intensities were calculated in a Tesla Cluster (EM64L) system. For 2,4-DMP, I found one imaginary frequency due to the interaction between an aromatic C-H bond and the methyl group present in the adjacent ring. For the quantitative fitting of observed bands with calculated spectra, I have performed scaled quantum mechanical force field calculation as described in section 2.4.2 of chapter 2. The internal coordinates were defined for DMPs as shown in Figure 5.1. Then the set of nonredundant local coordinates were constructed (see

---

Table 5.2). The symbolic force constant matrix, unscaled and scaled force constants in term of nonredundant local coordinates was calculated for DMPs in a similar manner as was done for DMQs (data not shown).

Calculations were carried out with 6-311G\*\* and 6-31G\* basis sets and mean deviation between calculated (harmonic, anharmonic and scaled force field fitted) and observed frequencies were evaluated using equation 2.13. Table 5.3 lists the mean deviation between calculated and observed frequencies for three different types of vibration. It is clear that (i) the extent of anharmonicity is different for different types of vibration, (ii) fundamental anharmonic frequencies obtained with 6-31G\* basis set differ by  $\sim 10 \text{ cm}^{-1}$  from that with 6-311G\*\* whereas for the non-fundamental frequencies the difference is more significant and (iii) the force field fitted frequencies obtained by the SQM method are more reliable in the C-H stretching region irrespective of the basis sets. It should be noted that the SQM approach relies on minimizing the fitting error and it can be applied with confidence to the methylated polycyclic compounds.

Figure 5.1. Optimized B3LYP/6-311G\*\* structure and internal coordinates of (a) 1,9-DMP (b) 2,4-DMP and (c) 3,9-DMP.



Twist coordinates,  $\tau$ 's numbering are the same as defined for R (the C-C bond coordinates).  $\alpha_1'$  and  $\beta_1$  is one of the C-C-H and H-C-H angle coordinate of the CH<sub>3</sub> groups, respectively. The other C-C-H and H-C-H angle coordinates,  $\alpha_2'$ ,  $\alpha_3'$ , etc. and  $\beta_2$ ,  $\beta_3$ , etc., respectively, are defined similarly.

Figure 5.1. (Continued)

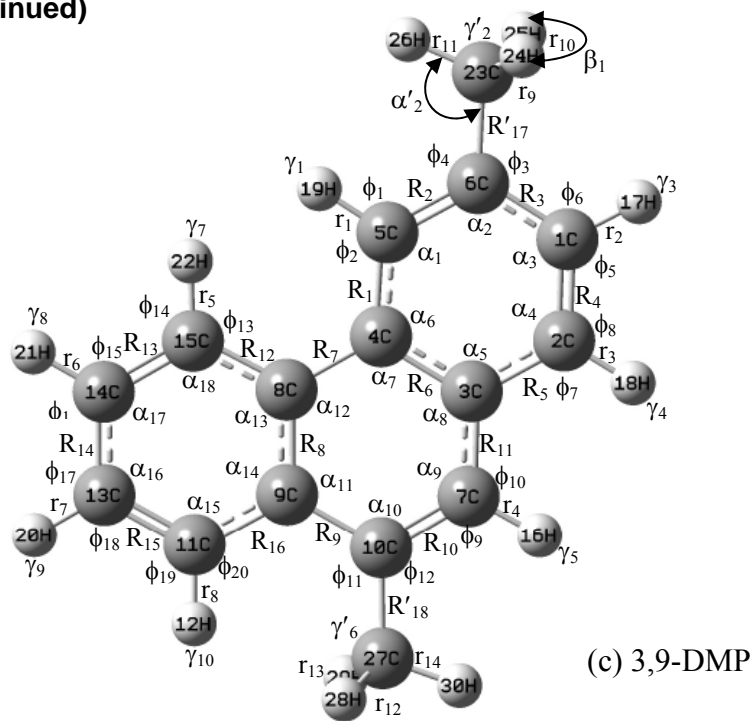


Table 5.2: Nonredundant local coordinates of DMPs used in this thesis.

Compound	Nonredundant local coordinates
<b>1,9-DMP</b> See Fig 5.1 (a) for the internal- coordinates	In-plane $S_{1-16} = R$ (Ar, C-C stretch) ( $R_i$ ) ; $S_{20, 22} = R$ (Ar-CH <sub>3</sub> , C-C stretch) ( $R'_i$ ) $S_{17-19, 21, 23-26} = r$ (Ar, C-H stretch) ( $r_i$ ) ; $S_{27-32} = r$ (CH <sub>3</sub> , C-H stretch) ( $r'_i$ ) $S_{33-35, 37, 39-42} = 2^{-1/2}(\phi_3 - \phi_4); (\phi_7 - \phi_8) \dots$ (Ar, C-H def.)( $\beta_i$ ) $S_{36, 38} = 2^{-1/2}(\phi_1 - \phi_2); (\phi_5 - \phi_6)$ (C-CH <sub>3</sub> def.)( $\beta'_i$ ) $S_{43, 46, 49} = 6^{-1/2}(\alpha_1 - \alpha_2 + \alpha_3 - \alpha_4 + \alpha_5 - \alpha_6)$ (ring def.)( $\delta_1, \delta_4, \delta_7$ ) $S_{44, 47, 50} = 3^{-1/2}(2\alpha_1 - \alpha_2 - \alpha_3 + 2\alpha_4 - \alpha_5 - \alpha_6)$ (ring def.)( $\delta_2, \delta_5, \delta_8$ ) $S_{45, 48, 51} = 1/2(\alpha_2 + \alpha_3 - \alpha_5 - \alpha_6)$ (ring def.) ( $\delta_3, \delta_6, \delta_9$ ) Out-of-plane $S_{52, 57} = 6^{-1/2}(\alpha'_1 + \alpha'_2 + \alpha'_3 - \beta_1 - \beta_2 - \beta_3)$ (CH <sub>3</sub> sym. def.) ( $\delta_a$ ) $S_{53, 58} = 6^{-1/2}(2\alpha'_1 - \alpha'_2 - \alpha'_3)$ (CH <sub>3</sub> antisym. def.) ( $\delta_s$ ) $S_{54, 59} = 2^{-1/2}(\alpha'_2 - \alpha'_3)$ (CH <sub>3</sub> antisym. def.) ( $\delta_s$ ) $S_{55, 60} = 6^{-1/2}(2\beta_1 - \beta_2 - \beta_3)$ (CH <sub>3</sub> rock) $\rho$ (CH <sub>3</sub> ) $S_{56, 61} = 2^{-1/2}(\beta_2 - \beta_3)$ (CH <sub>3</sub> rock) $\rho$ (CH <sub>3</sub> ) $S_{62, 64, 65, 68-71} = \gamma$ (Ar, C-H wag) $\gamma_i$ ; $S_{65, 67} = \gamma$ (Ar-CH <sub>3</sub> , C-C wag) $\gamma'_i$ $S_{72, 75, 78} = 6^{-1/2}(\tau_1 - \tau_2 + \tau_3 - \tau_4 + \tau_5 - \tau_6)$ (ring torsion)( $\tau_1, \tau_4, \tau_7$ ) $S_{73, 76, 79} = 1/2(\tau_1 - \tau_3 + \tau_4 - \tau_6)$ (ring torsion) ( $\tau_2, \tau_5, \tau_8$ ) $S_{74, 77, 80} = 12^{-1/2}(-\tau_1 + 2\tau_2 - \tau_3 - \tau_4 + 2\tau_5 - \tau_6)$ (ring torsion) ( $\tau_3, \tau_6, \tau_9$ ) $S_{81} = 2^{-1/2}(\tau_{5-4-3-7} - \tau_{8-4-3-2})$ ( $\tau_{ring}$ ); $S_{82} = 2^{-1/2}(\tau_{4-8-9-11} - \tau_{15-8-9-10})$ ( $\tau_{ring}$ ) $S_{83, 84} = \tau_{2-23}; \tau_{10-17}$ (C-CH <sub>3</sub> twist) ( $\tau''_i$ )

Table 5.2: Continued.....

Compound	Nonredundant local coordinates
<p><b>2,4-DMP</b> See Fig 5.2 (b) for the internal- coordinates</p>	<p>In-plane  <math>S_{1-16} = R(\text{Ar, C-C stretch}) (R_i)</math> ; <math>S_{17, 19} = R(\text{Ar-CH}_3, \text{C-C stretch}) (R'_i)</math>  <math>S_{18, 22-26} = r(\text{Ar, C-H stretch}) (r_i)</math> ; <math>S_{27-32} = r(\text{CH}_3, \text{C-H stretch}) (r'_i)</math>  <math>S_{33, 35} = 2^{-1/2}(\phi_1-\phi_2)</math>; <math>(\phi_5-\phi_6)</math> (C-CH<sub>3</sub> def.)(<math>\beta'_i</math>)  <math>S_{34, 36-42} = 2^{-1/2}(\phi_3-\phi_4)</math>; <math>(\phi_7-\phi_8)</math>... (Ar, C-H def.)(<math>\beta_i</math>)  <math>S_{43, 46, 49} = 6^{-1/2}(\alpha_1 - \alpha_2 + \alpha_3 - \alpha_4 + \alpha_5 - \alpha_6)</math> (ring def.)(<math>\delta_1, \delta_4, \delta_7</math>)  <math>S_{44, 47, 50} = 3^{-1/2}(2\alpha_1 - \alpha_2 - \alpha_3 + 2\alpha_4 - \alpha_5 - \alpha_6)</math> (ring def.)(<math>\delta_2, \delta_5, \delta_8</math>)  <math>S_{45, 48, 51} = 1/2(\alpha_2 + \alpha_3 - \alpha_5 - \alpha_6)</math> (ring def.) (<math>\delta_3, \delta_6, \delta_9</math>)  Out-of-plane  <math>S_{52, 57} = 6^{-1/2}(\alpha'_1 + \alpha'_2 + \alpha'_3 - \beta_1 - \beta_2 - \beta_3)</math> (CH<sub>3</sub> sym. def.) (<math>\delta_a</math>)  <math>S_{53, 58} = 6^{-1/2}(2\alpha'_1 - \alpha'_2 - \alpha'_3)</math> (CH<sub>3</sub> antisym. def.) (<math>\delta_s</math>)  <math>S_{54, 59} = 2^{-1/2}(\alpha'_2 - \alpha'_3)</math> (CH<sub>3</sub> antisym. def.) (<math>\delta_s</math>)  <math>S_{55, 60} = 6^{-1/2}(2\beta_1 - \beta_2 - \beta_3)</math> (CH<sub>3</sub> rock) <math>\rho(\text{CH}_3)</math>  <math>S_{56, 61} = 2^{-1/2}(\beta_2 - \beta_3)</math> (CH<sub>3</sub> rock) <math>\rho(\text{CH}_3)</math>  <math>S_{62, 64} = \gamma(\text{Ar-CH}_3, \text{C-C wag}) \gamma'_i</math> ; <math>S_{63, 65-71} = \gamma(\text{Ar, C-H wag}) \gamma_i</math>  <math>S_{72, 75, 78} = 6^{-1/2}(\tau_1 - \tau_2 + \tau_3 - \tau_4 + \tau_5 - \tau_6)</math> (ring torsion)(<math>\tau_1, \tau_4, \tau_7</math>)  <math>S_{73, 76, 79} = 1/2(\tau_1 - \tau_3 + \tau_4 - \tau_6)</math> (ring torsion) (<math>\tau_2, \tau_5, \tau_8</math>)  <math>S_{74, 77, 80} = 12^{-1/2}(-\tau_1 + 2\tau_2 - \tau_3 - \tau_4 + 2\tau_5 - \tau_6)</math> (ring torsion) (<math>\tau_3, \tau_6, \tau_9</math>)  <math>S_{81} = 2^{-1/2}(\tau_{5-4-3-7} - \tau_{8-4-3-2})</math> (<math>\tau_{\text{ring}}</math>); <math>S_{82} = 2^{-1/2}(\tau_{4-8-9-11} - \tau_{15-8-9-10})</math> (<math>\tau_{\text{ring}}</math>)  <math>S_{83, 84} = \tau_{1-23}</math>; <math>\tau_{5-27}</math> (C-CH<sub>3</sub> twist) (<math>\tau''_i</math>)</p>
<p><b>3,9-DMP</b> See Fig 5.2 (c) for the internal- coordinates</p>	<p>In-plane  <math>S_{1-16} = R(\text{Ar, C-C stretch}) (R_i)</math> ; <math>S_{18, 22} = R(\text{Ar-CH}_3, \text{C-C stretch}) (R'_i)</math>  <math>S_{17, 19-21, 23-26} = r(\text{Ar, C-H stretch}) (r_i)</math> ; <math>S_{27-32} = r(\text{CH}_3, \text{C-H stretch}) (r'_i)</math>  <math>S_{33, 35-37, 39-42} = 2^{-1/2}(\phi_3-\phi_4)</math>; <math>(\phi_7-\phi_8)</math>... (Ar, C-H def.)(<math>\beta_i</math>)  <math>S_{34, 38} = 2^{-1/2}(\phi_1-\phi_2)</math>; <math>(\phi_5-\phi_6)</math> (C-CH<sub>3</sub> def.)(<math>\beta'_i</math>)  <math>S_{43, 46, 49} = 6^{-1/2}(\alpha_1 - \alpha_2 + \alpha_3 - \alpha_4 + \alpha_5 - \alpha_6)</math> (ring def.)(<math>\delta_1, \delta_4, \delta_7</math>)  <math>S_{44, 47, 50} = 3^{-1/2}(2\alpha_1 - \alpha_2 - \alpha_3 + 2\alpha_4 - \alpha_5 - \alpha_6)</math> (ring def.)(<math>\delta_2, \delta_5, \delta_8</math>)  <math>S_{45, 48, 51} = 1/2(\alpha_2 + \alpha_3 - \alpha_5 - \alpha_6)</math> (ring def.) (<math>\delta_3, \delta_6, \delta_9</math>)  Out-of-plane  <math>S_{52, 57} = 6^{-1/2}(\alpha'_1 + \alpha'_2 + \alpha'_3 - \beta_1 - \beta_2 - \beta_3)</math> (CH<sub>3</sub> sym. def.) (<math>\delta_a</math>)  <math>S_{53, 58} = 6^{-1/2}(2\alpha'_1 - \alpha'_2 - \alpha'_3)</math> (CH<sub>3</sub> antisym. def.) (<math>\delta_s</math>)  <math>S_{54, 59} = 2^{-1/2}(\alpha'_2 - \alpha'_3)</math> (CH<sub>3</sub> antisym. def.) (<math>\delta_s</math>)  <math>S_{55, 60} = 6^{-1/2}(2\beta_1 - \beta_2 - \beta_3)</math> (CH<sub>3</sub> rock) <math>\rho(\text{CH}_3)</math>  <math>S_{56, 61} = 2^{-1/2}(\beta_2 - \beta_3)</math> (CH<sub>3</sub> rock) <math>\rho(\text{CH}_3)</math>  <math>S_{62, 64-66, 69-71} = \gamma(\text{Ar, C-H wag}) \gamma_i</math> ; <math>S_{63, 68} = \gamma(\text{Ar-CH}_3, \text{C-C wag}) \gamma'_i</math>  <math>S_{72, 75, 78} = 6^{-1/2}(\tau_1 - \tau_2 + \tau_3 - \tau_4 + \tau_5 - \tau_6)</math> (ring torsion)(<math>\tau_1, \tau_4, \tau_7</math>)  <math>S_{73, 76, 79} = 1/2(\tau_1 - \tau_3 + \tau_4 - \tau_6)</math> (ring torsion) (<math>\tau_2, \tau_5, \tau_8</math>)  <math>S_{74, 77, 80} = 12^{-1/2}(-\tau_1 + 2\tau_2 - \tau_3 - \tau_4 + 2\tau_5 - \tau_6)</math> (ring torsion) (<math>\tau_3, \tau_6, \tau_9</math>)  <math>S_{81} = 2^{-1/2}(\tau_{5-4-3-7} - \tau_{8-4-3-2})</math> (<math>\tau_{\text{ring}}</math>); <math>S_{82} = 2^{-1/2}(\tau_{4-8-9-11} - \tau_{15-8-9-10})</math> (<math>\tau_{\text{ring}}</math>)  <math>S_{83, 84} = \tau_{6-23}</math>; <math>\tau_{10-27}</math> (C-CH<sub>3</sub> twist) (<math>\tau''_i</math>)</p>

**Table 5.3: Mean deviation,  $\delta$  (in  $\text{cm}^{-1}$ ), between the calculated (harmonic, anharmonic and force field fitted) and observed band position of DMPs.**

$\delta$ Mode of Vibration	Basis set	Harmonic			Anharmonic			Fitted		
		(a)	(b)	(c)	(a)	(b)	(c)	(a)	(b)	(c)
AromaticC- H str	6-31G*	181.5	149.4	178.9	43.6	19.0	41.6	0.1	0.8	0.2
	6-311G**	161.6	125.5	161.6	36.8	20.0	36.8	<0.1	0.7	<0.1
Methyl C-H str	6-31G*	181.3	161.3	180.0	34.5	13.8	61.0	7.6	0.7	6.5
	6-311G**	160.2	140.4	160.2	23.5	13.8	23.5	6.4	1.0	6.4
Non-C-H str	6-31G*	35.3	33.7	30.6	14.3	15.9	15.5	1.3	1.7	1.5
	6-311G**	24.1	23.7	24.1	8.6	8.0	8.6	0.8	1.7	0.8
Non- Fundam.	6-31G*				84.8	97.6	170.2			
	6-311G**				48.8	79.5	67.3	57.1	71.9	60.9

**(a), (b) and (c) represent the 1,9-, 2,4- and 3,9-DMP, respectively.**

## 5.4 Results and discussion

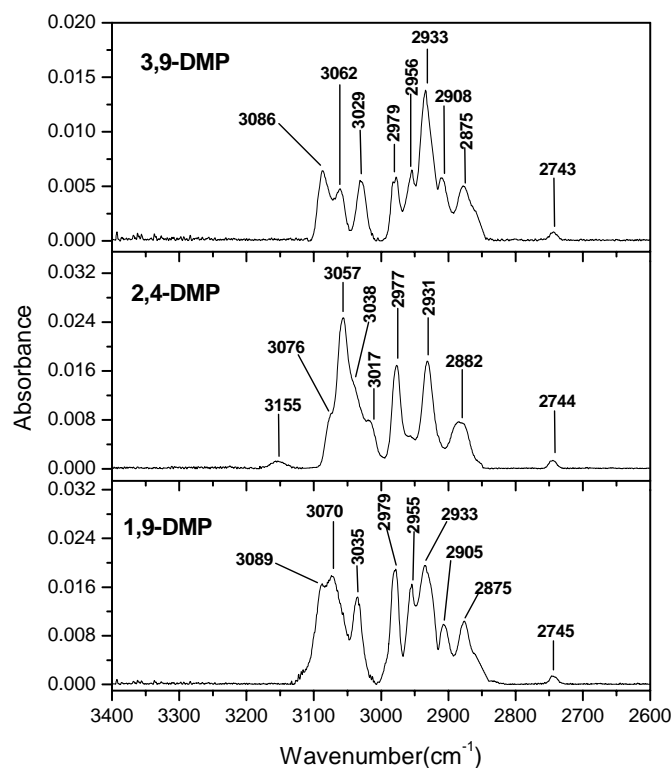
The gas phase IR absorption spectra of DMPs are shown in Figures 5.2 – 5.4. The DMP molecule in  $C_s$  symmetry has 84 normal modes which belong to the irreducible representation  $55A' + 29A''$ . The recorded band-origin frequencies and their intensities, calculated (harmonic, anharmonic and force field fitted) frequencies of DMPs with 6-311G\*\* and 6-31G\* basis sets are presented in Tables 5.4 (a - c) and 5.5 (a - c), respectively. A few observed non-fundamental and corresponding calculated anharmonic and force field fitted frequencies are listed in Table 5.6. Observed bands are assigned with the help of scaled force field fitted frequencies and PEDs at the B3LYP/6-311G\*\* level of theory. From Tables 5.4 (a - c) and 5.5 (a - c) it is clear that the description of PEDs of normal modes remains the same for the 6-31G\* and 6-311G\*\* basis sets, although, percent contribution of coordinates to PEDs change by a small extent. The observed spectra of DMPs can be divided into five distinct regions: (1)



aromatic C-H and methyl C-H stretching, (2) aromatic C-C stretching (3) methyl C-H symmetric and asymmetric and aromatic in-plane ring deformation, (4) aromatic C-H out-of-plane and aromatic out-of-plane ring deformation, and (5) non-fundamental modes: overtone and combination. Details of the assignment have been discussed region wise in the following section.

#### 5.4.1 Spectral region of 2800 – 3200 $\text{cm}^{-1}$

Two types of bands appear in this region. They are aromatic C-H and methyl C-H stretching vibrations. The assignment of the observed bands in this region is always difficult because of the presence of Fermi resonances.<sup>1b, 19</sup>



**Figure 5.2. Expanded gas phase IR absorption spectra of 1,9-, 2,4-, and 3,9 - DMPs from 2600 to 3400  $\text{cm}^{-1}$  at 0.5  $\text{cm}^{-1}$  resolution.**

In the aromatic C-H stretching region, this occurs due to interaction of a fundamental mode with an overtone or a combination of lower frequency modes. On the other hand in the methyl C-H stretching region, Fermi resonance occurs between the methyl C-H symmetric stretch and an overtone involving two quanta of a methyl deformation mode. Therefore, an assignment of the observed bands in this region with the help of force fitted frequencies and their PEDs is tentative. We have tried to use intensity criteria to resolve this but it is not straightforward.

A group of five bands observed at 3089.1, 3069.7, 3035.3, 2979.6, and 2955.2  $\text{cm}^{-1}$  in 1,9-DMP; 3155.1, 3076.5, 3057.2, 3038.0, and 3017.1  $\text{cm}^{-1}$  in 2,4-DMP; 3085.7, 3062.5, 3029.1, 2978.9, and 2956.3  $\text{cm}^{-1}$  in 3,9-DMP match well with the scaled force field frequencies at 3089.1, 3069.8, 3035.3, 2979.8, and 2955.2  $\text{cm}^{-1}$  in 1,9- DMP; 3155.1, 30765.2, 3057.7, 3039.3, and 3018.1  $\text{cm}^{-1}$  in 2,4-DMP; 3085.8, 3062.5, 3030.6, 2978.9, and 2957.0  $\text{cm}^{-1}$  in 3,9-DMP, respectively. Their respective anharmonic frequencies deviate by 40 and 25  $\text{cm}^{-1}$  with 6-31G\* and 6-311G\*\* basis sets, respectively. These bands are assigned to aromatic C-H stretching vibration.

A groups of three bands of methyl C-H stretching vibration is seen in the experimental spectra of DMPs. Bands at 2933.5 and 2905.0  $\text{cm}^{-1}$  in 1,9-DMP; 2976.7 and 2930.8  $\text{cm}^{-1}$  in 2,4-DMP; 2933.5 and 2908.2  $\text{cm}^{-1}$  in 3,9-DMP correspond to the force field fitted frequencies at 2936.1 and 2912.4  $\text{cm}^{-1}$  in 1,9-DMP; 2976.3 and 2930.6  $\text{cm}^{-1}$  in 2,4-DMP; 2936.0 and 2914.1  $\text{cm}^{-1}$  in 3,9-DMP, respectively. These bands are assigned to the asymmetric C-H stretching vibrations of methyl group. The symmetric C-H stretching band observed at a lower frequency region such as 2875.3, 2882.3, and 2875.0  $\text{cm}^{-1}$  for 1,9-, 2,4-, and 3,9-DMP, respectively, is correlated with the fitted frequency at

Table 5.4(a): Calculated harmonic, anharmonic frequencies (in  $cm^{-1}$ ) and intensities (in  $km/mol$ ) at  $B3LYP/6-311G^{**}$ , observed frequencies (in  $cm^{-1}$ ) and intensities (in  $km/mol$ ), fitted frequencies (in  $cm^{-1}$ ) and PEDs of 1,9 – DMP.

Sym	B3LYP/6-311G <sup>**</sup>			Observed		Force field	
	No	Harm.	Int.	Anharm.	Freq.	Int.	Fitted PED
$A'$							
$\nu_1$	3210.7	23.82	3069.7	3089.1	14.454	3089.1	$r_5$ ( 70)+ $r_1$ ( 28)
$\nu_2$	3198.3	23.42	3064.8	3069.7	31.830	3069.8	$r_1$ ( 54)+ $r_8$ ( 25)+ $r_5$ ( 19)
$\nu_3$	3194.1	0.78	3069.0	(3069.0)		3069.0	$r_8$ ( 73)+ $r_1$ ( 17)
$\nu_4$	3184.7	12.70	3043.7	3035.3	11.215	3035.3	$r_4$ ( 99)
$\nu_5$	3179.1	14.98	3053.9	2979.6	14.454	2979.8	$r_2$ ( 43)+ $r_6$ ( 43)
$\nu_6$	3175.1	33.10	3034.2	(2979.0)		2979.4	$r_2$ ( 43)+ $r_6$ ( 43)
$\nu_7$	3164.2	2.11	3033.1	2955.2	8.293	2955.2	$r_7$ ( 81)+ $r_6$ ( 43)
$\nu_8$	3157.9	11.45	3036.8	(2955.0)		2954.9	$r_3$ ( 79)+ $r_2$ ( 11)
$\nu_9$	3105.4	17.77	2971.9	2933.5	34.121	2936.1	$r'12$ ( 77)+ $r'11$ ( 21)
$\nu_{10}$	3104.5	22.23	2961.5	(2933.0)		2935.6	$r'10$ ( 76)+ $r'9$ ( 20)
$\nu_{11}$	3021.1	32.70	2895.4	2875.3	14.533	2866.0	$r'11$ ( 65)+ $r'12$ ( 17)+ $r'9$ ( 14)
$\nu_{12}$	3019.5	34.69	2903.5	(2875.0)		2865.6	$r'9$ ( 65)+ $r'10$ ( 16)+ $r'11$ ( 14)
$\nu_{13}$	1659.8	9.84	1620.0	1626.5	9.952	1626.9	$R_{10}$ ( 36)
$\nu_{14}$	1651.4	1.34	1613.6	(1619.0)		1619.6	$R_{15}$ ( 21)+ $R_{13}$ ( 16)+ $\delta_7$ ( 11)
$\nu_{15}$	1642.4	7.32	1605.3	1604.6	7.819	1604.9	$R_4$ ( 25)+ $R_2$ ( 14)+ $R_1$ ( 12)
$\nu_{16}$	1614.5	1.72	1578.5	1584.5		1583.0	$R_2$ ( 13)+ $R_3$ ( 13)+ $R_6$ ( 11)
$\nu_{17}$	1567.1	4.28	1533.4	(1536.2)		1535.5	$R_{14}$ ( 21)
$\nu_{18}$	1523.9	10.68	1491.6	1495.4	3.791	1495.3	$R_9$ ( 14)
$\nu_{19}$	1507.7	11.54	1459.7	1471.2		1473.9	$\delta_s(1)$ ( 40)+ $\delta_s(2)$ ( 21)
$\nu_{20}$	1497.9	4.44	1459.7	(1469.0)		1465.8	$\delta_s(1)$ ( 33)+ $\delta_s(2)$ ( 14)
$\nu_{21}$	1487.9	16.63	1458.1	1456.0	25.433	1455.7	$\delta_s(2)$ ( 34)
$\nu_{22}$	1475.2	0.14	1445.0	(1446.0)		1445.8	$\beta_5$ ( 17)+ $R_{10}$ ( 11)+ $R_{15}$ ( 10)
$\nu_{23}$	1440.8	11.59	1414.8	1412.4	6.713	1413.5	$\beta_8$ ( 15)+ $R_{11}$ ( 11)
$\nu_{24}$	1419.1	5.78	1379.8	1389.5	5.213	1390.6	$\delta_8$ ( 36)+ $\rho(1)$ ( 33)
$\nu_{25}$	1427.0	0.16	1373.5	(1389.0)		1388.2	$\delta_8$ ( 44)+ $\rho(1)$ ( 44)
$\nu_{26}$	1405.6	0.33	1374.9	(1378.0)		1377.9	$R_9$ ( 16)+ $\beta_3$ ( 11)
$\nu_{27}$	1374.1	0.27	1344.9	(1347.0)		1347.9	$R_6$ ( 16)+ $R_7$ ( 14)+ $R_2$ ( 11)
$\nu_{28}$	1362.4	0.59	1332.7	(1336.0)		1337.0	$R_8$ ( 19)
$\nu_{29}$	1319.6	2.33	1293.7	1296.1	1.263	1295.2	$R_7$ ( 15)+ $\beta_9$ ( 14)+ $R_{11}$ ( 12)
$\nu_{30}$	1299.9	1.33	1281.3	1273.2	0.868	1274.6	$\delta_2$ (19)+ $\beta_1$ (14)+ $\beta_5$ (13)+ $\beta_8$ (11)
$\nu_{31}$	1271.5	2.22	1253.9	1249.5	3.712	1247.7	$R_{16}$ ( 14)+ $\beta_3$ ( 14)+ $\beta_8$ ( 13)
$\nu_{32}$	1253.1	3.98	1233.5	(1228.0)		1228.1	$\beta_3$ (23)+ $R'_{17}$ (15)+ $\beta_1$ (15)+ $R_5$ (15)
$\nu_{33}$	1236.0	2.55	1217.3	1213.0	0.789	1213.4	$R_1$ ( 18)+ $R_{11}$ ( 16)
$\nu_{34}$	1203.1	0.54	1192.8	(1179.0)		1179.4	$r'14$ ( 31)+ $r'13$ ( 12)
$\nu_{35}$	1191.2	0.46	1185.4	(1168.0)		1168.6	$\beta_7$ ( 26)+ $\beta'_6$ ( 22)+ $\beta_8$ ( 11)+ $\beta_5$ ( 10)
$\nu_{36}$	1173.4	1.57	1160.9	1152.7	0.631	1151.7	$R_{15}$ ( 4)+ $\beta_7$ (13)+ $\beta'_6$ (11)+ $\delta_2$ (10)
$\nu_{37}$	1110.8	3.96	1097.5	1089.9	2.290	1089.9	$R_3$ ( 35)+ $\beta_1$ ( 16)
$\nu_{38}$	1089.3	0.15	1070.5	(1068.0)		1068.5	$\delta_a(2)$ ( 11)
$\nu_{39}$	1082.7	0.14	1063.4	(1061.0)		1061.6	$\delta_5$ ( 41)
$\nu_{40}$	1058.6	7.41	1040.0	1036.4	7.108	1036.5	$R_{14}$ ( 42)
$\nu_{41}$	1018.6	0.85	989.8	( 998.0)		998.7	$\delta_a(1)$ (19)+ $\beta_9$ (16)+ $\delta_a(2)$ (13)
$\nu_{42}$	1012.4	4.98	985.4	995.3	2.843	993.6	$\delta_a(1)$ (22)+ $\delta_a(2)$ (18)+ $\delta_5$ (13)
$\nu_{43}$	891.3	2.22	879.2	( 874.0)		873.5	$\delta_5$ ( 16)+ $\delta_4$ ( 11)+ $R'_{17}$ ( 11)
$\nu_{44}$	867.9	0.31	854.0	( 851.0)		851.0	$\beta_9$ ( 31)

Table 5.4(a): (Continued) Calculated harmonic, anharmonic frequencies (in  $cm^{-1}$ ) and intensities (in  $km/mol$ ) at  $B3LYP/6-311G^{**}$ , observed frequencies (in  $cm^{-1}$ ) and intensities (in  $km/mol$ ), fitted frequencies (in  $cm^{-1}$ ) and PED of 1,9 - DMP.

Sym	B3LYP/6-311G**			Observed		Force field	
	No	Harm.	Int.	Anharm.	Freq.	Int.	Fitted PED
$\nu_{45}$	778.9	0.19		767.5	( 763.0)	763.3	$\delta_7$ ( 26)+ $\delta_5$ ( 12)+ $R_9$ ( 12)
$\nu_{46}$	710.7	3.66		702.2		697.8	$\delta_6$ ( 22)+ $\delta_1$ ( 15)+ $\delta_2$ ( 13)
$\nu_{47}$	635.7	0.54		630.7	( 623.0)	623.5	$\delta_6$ ( 35)+ $\delta_1$ ( 22)+ $\delta_2$ ( 14)
$\nu_{48}$	574.2	0.58		569.8	( 563.0)	562.7	$\delta_7$ ( 25)+ $\beta'_4$ ( 22)+ $\delta_1$ ( 20)
$\nu_{49}$	552.4	5.63		548.4		539.6	$\beta_{10}$ ( 37)+ $R'_{17}$ ( 12)+ $\delta_3$ ( 11)
$\nu_{50}$	513.8	1.71		508.0	( 503.0)	502.8	$\delta_4$ ( 23)+ $\beta_{10}$ ( 16)+ $\delta_7$ ( 11)
$\nu_{51}$	447.2	0.82		443.6	( 438.0)	437.9	$\delta_4$ ( 29)+ $\beta_2$ ( 25)+ $\delta_3$ ( 14)
$\nu_{52}$	425.7	0.21		423.1	( 417.0)	417.0	$\delta_3$ ( 38)+ $\beta_{10}$ ( 12)
$\nu_{53}$	334.0	0.57		330.6	( 327.0)	327.7	$\beta_2$ ( 28)+ $\beta'_4$ ( 19)
$\nu_{54}$	282.4	0.24		281.1	( 277.0)	277.0	$\beta'_4$ ( 47)+ $\delta_7$ ( 18)
$\nu_{55}$	221.7	0.43		223.3	( 217.0)	217.1	$\delta_1$ ( 24)+ $\beta_2$ ( 22)
$A''$							
$\nu_{56}$	3067.9	21.34		2917.2	2905.0	2912.4	$r'_9$ ( 81) + $r'_{11}$ ( 18)
$\nu_{57}$	3065.2	18.34		2919.7	(2905.0)	2912.1	$r'_{11}$ ( 82) + $r'_9$ ( 18)
$\nu_{58}$	1490.3	5.47		1432.3	(1461.0)	1460.9	$\delta_s(1)$ ( 90)
$\nu_{59}$	1487.2	9.70		1442.7	(1458.0)	1457.9	$\delta_s(2)$ ( 90)
$\nu_{60}$	1063.8	0.99		1034.2	(1043.0)	1043.5	$\rho(1)$ ( 51)+ $\delta_a(2)$ ( 18)
$\nu_{61}$	1061.9	1.94		1030.9	(1041.0)	1042.3	$\delta_9$ ( 50)+ $\delta_a(1)$ ( 18)
$\nu_{62}$	990.7	0.00		987.1	( 971.0)	970.7	$\gamma_7$ ( 38)+ $\gamma_8$ ( 28)+ $\gamma'_6$ ( 18)
$\nu_{63}$	972.7	0.49		977.8	( 954.0)	954.1	$\rho(2)$ ( 48)+ $\gamma_1$ ( 16)+ $\rho(2)$ ( 15)
$\nu_{64}$	954.0	0.58		957.9	( 935.0)	934.6	$\gamma'_6$ ( 33)+ $\gamma_5$ ( 26)+ $\gamma_8$ ( 19)
$\nu_{65}$	902.1	4.12		911.3	( 884.0)	883.8	$\gamma_1$ ( 42)+ $\rho(2)$ ( 31)+ $\gamma_3$ ( 11)
$\nu_{66}$	890.5	11.95		882.4	871.4	871.5	$\gamma_3$ ( 66)
$\nu_{67}$	873.0	0.26		886.4	( 856.0)	856.9	$\gamma_5$ (26)+ $\gamma_8$ (18)+ $\tau_2$ (13)+ $\gamma_7$ (11)
$\nu_{68}$	815.9	5.82		846.3	803.5	801.9	$\gamma_9$ ( 26)+ $\tau_2$ ( 22)+ $\tau_5$ ( 10)
$\nu_{69}$	768.5	41.94		767.3	748.3	749.0	$\gamma'_6$ (30)+ $\gamma_5$ (19)+ $\gamma_7$ (16)+ $\gamma_8$ (12)
$\nu_{70}$	761.5	49.77		764.0	746.0	746.7	$\rho(2)$ ( 31)+ $\rho(2)$ ( 25)+ $\tau_5$ ( 13)+ $\tau_2$ ( 11)
$\nu_{71}$	744.2	0.23		745.9	( 729.0)	729.3	$\gamma_9$ ( 36)+ $\tau_5$ ( 30)
$\nu_{72}$	610.7	0.13		619.5	( 598.0)	598.2	$\tau_5$ ( 28)+ $\tau_2$ ( 17)+ $\gamma'_4$ ( 14)
$\nu_{73}$	578.5	1.32		577.0	( 567.0)	565.2	$\tau_8$ ( 17)+ $\gamma_2$ ( 14)+ $\tau_9$ ( 11)
$\nu_{74}$	538.5	0.55		538.6	( 528.0)	527.8	$\tau_1$ ( 29)+ $\gamma_9$ ( 14)
$\nu_{75}$	482.9	0.12		476.8	( 473.0)	472.9	$\tau_7$ (23)+ $\gamma_2$ (17)+ $\gamma_{10}$ (13)+ $\tau_3$ (11)
$\nu_{76}$	420.9	4.21		414.8	( 412.0)	411.9	$\tau_6$ ( 54)
$\nu_{77}$	328.6	0.95		322.3	( 322.0)	322.1	$\gamma_2$ ( 16)+ $\gamma'_4$ ( 16)+ $\tau_8$ ( 16)+ $\tau_1$ ( 12)+ $\tau_7$ ( 11)
$\nu_{78}$	245.6	0.64		243.5	( 240.0)	240.2	$\gamma_{10}$ ( 27)+ $\tau_6$ ( 23)+ $\tau_9$ ( 11)
$\nu_{79}$	212.0	0.07		195.7	( 207.0)	207.0	$\tau_{ring}$ ( 64)
$\nu_{80}$	192.3	0.00		163.3	( 188.0)	187.9	$\tau_{ring}$ ( 38)+ $\tau_1$ ( 17)+ $\tau_{ring}$ ( 15)
$\nu_{81}$	183.7	1.33		167.8	( 180.0)	180.0	$\tau_{ring}$ ( 44)+ $\gamma_2$ ( 16)+ $\tau_1$ ( 10)
$\nu_{82}$	140.6	2.71		146.5	( 137.0)	137.0	$\gamma'_4$ ( 20)+ $\tau_9$ ( 16)+ $\tau_8$ ( 14)+ $\tau_7$ ( 14)
$\nu_{83}$	93.2	0.39		98.7	( 91.0)	91.1	$\tau_3$ ( 39)+ $\tau_7$ ( 23)+ $\tau_8$ ( 11)
$\nu_{84}$	59.1	0.03		71.5	( 57.0)	57.0	$\tau_4$ (33)+ $\tau_3$ (13)+ $\gamma_{10}$ (12)+ $\tau_1$ (12)

Since the fitting algorithm required all the experimental frequencies, the numbers in parenthesis are introduced as good guesses for 1,9 - DMP and do not have any other significance. RMS error is 1.9880 for the fitting of experimental frequencies.

Table 5.4(b): Calculated harmonic, anharmonic frequencies (in  $cm^{-1}$ ) and intensities (in  $km/mol$ ) at  $B3LYP/6-311G^{**}$ , observed frequencies (in  $cm^{-1}$ ) and intensities (in  $km/mol$ ), fitted frequencies (in  $cm^{-1}$ ) and PED of 2,4-DMP.

Sym	B3LYP/6-311G <sup>**</sup>			Observed		Force field	
	No	Harm.	Int.	Anharm.	Freq.	Int.	Fitted PED
$A'$							
$\nu_1$	3309.7	3.69	3159.7	3155.1	2.350	3155.1	$r_5$ (98)
$\nu_2$	3185.9	33.46	3048.3	3076.5	2.644	3075.2	$r_7$ (70)+ $r_6$ (25)
$\nu_3$	3176.8	36.94	3030.4	3057.2	41.917	3057.7	$r_4$ (47)+ $r_3$ (23)+ $r_6$ (21)
$\nu_4$	3168.2	13.30	3032.5	(3057.0)		3056.7	$r_6$ (52)+ $r_7$ (17)+ $r_4$ (16)+ $r_3$ (10)
$\nu_5$	3159.5	7.58	3011.1	3038.0	17.237	3039.3	$r_8$ (50)+ $r_3$ (32)
$\nu_6$	3156.9	7.63	3018.9	(3038.0)		3036.3	$r_8$ (38)+ $r_3$ (32)+ $r_4$ (25)
$\nu_7$	3154.1	4.46	3007.9	3017.1	6.072	3018.1	$r_2$ (50)+ $r_1$ (48)
$\nu_8$	3151.1	26.29	3002.8	(3017.0)		3016.1	$r_1$ (50)+ $r_2$ (48)
$\nu_9$	3103.6	18.24	2963.4	2976.7	20.273	2976.3	$r'_{10}$ (87)+ $r'_9$ (12)
$\nu_{10}$	3102.5	22.85	2957.8	(2976.0)		2976.0	$r'_{12}$ (89)
$\nu_{11}$	3026.6	21.74	2862.3	2882.3	18.902	2884.9	$r'_9$ (88)+ $r'_{10}$ (11)
$\nu_{12}$	3021.8	43.87	2905.4	(2882.0)		2883.6	$r'_{11}$ (91)
$\nu_{13}$	1668.3	0.72	1632.3	(1636.0)		1635.0	$R_{10}$ (36)+ $R_4$ (13)
$\nu_{14}$	1659.9	24.46	1618.4	1621.4	28.206	1624.0	$R_4$ (15)+ $R_2$ (12)+ $R_5$ (12)
$\nu_{15}$	1648.2	8.53	1614.8	1609.1		1609.9	$R_{15}$ (20)+ $R_{13}$ (17)+ $R_{16}$ (11) + $\delta_7$ (11)
$\nu_{16}$	1604.7	2.56	1563.3	(1573.0)		1570.8	$R_{14}$ (14)+ $R_3$ (10)
$\nu_{17}$	1562.7	1.45	1521.6	(1532.0)		1531.1	$R_{14}$ (15)+ $R_3$ (12)
$\nu_{18}$	1527.8	3.25	1492.6	(1498.0)		1495.7	$R_9$ (17)
$\nu_{19}$	1518.7	18.47	1407.0	1470.9	40.742	1471.5	$\delta_s$ (2) (66)
$\nu_{20}$	1492.6	13.15	1468.8	1457.4		1460.2	$\delta_s$ (1) (36)+ $\beta_5$ (11)
$\nu_{21}$	1484.9	13.46	1450.0	1456.0		1454.4	$\delta_s$ (1) (28)+ $\beta_5$ (11)
$\nu_{22}$	1458.1	2.28	1428.5	1431.8	1.567	1429.6	$\beta_7$ (15)+ $\beta_6$ (11)
$\nu_{23}$	1430.0	0.10	1399.1	(1402.0)		1399.0	$R_5$ (14)+ $r'_{14}$ (12)+ $\beta_2$ (12)
$\nu_{24}$	1425.3	0.39	1391.5	(1390.0)		1389.0	$R_2$ (11)
$\nu_{25}$	1419.9	2.08	1361.9	1384.4	2.644	1384.4	$\rho$ (1) (76)
$\nu_{26}$	1414.3	0.17	1403.3	(1380.0)		1380.2	$\delta_8$ (79)
$\nu_{27}$	1361.4	1.28	1326.3	(1335.0)		1331.7	$R_8$ (21)+ $R_{13}$ (14)+ $R_{15}$ (14)+ $R_{16}$ (12)
$\nu_{28}$	1356.9	4.85	1321.3	1324.7	1.371	1321.1	$R_6$ (21)+ $R_2$ (12)
$\nu_{29}$	1325.0	2.35	1294.8	1300.0	1.469	1298.6	$R_7$ (12)+ $\beta_5$ (12)+ $\beta_9$ (10)
$\nu_{30}$	1298.2	1.81	1268.4	1270.6	0.976	1271.7	$r'_{14}$ (27)+ $R_7$ (17)
$\nu_{31}$	1275.1	0.86	1251.3	(1250.0)		1250.1	$R_1$ (11)+ $\beta_8$ (10)
$\nu_{32}$	1242.8	3.26	1213.2	1217.4	2.546	1218.2	$\beta_6$ (13)+ $\beta_5$ (12)
$\nu_{33}$	1227.6	0.09	1204.1	(1203.0)		1203.9	$R_9$ (20)+ $R_{12}$ (17)+ $\beta_7$ (11)
$\nu_{34}$	1208.1	1.37	1186.5	(1184.0)		1185.0	$\beta_2$ (25)+ $\beta'_3$ (13)+ $r'_{14}$ (11)
$\nu_{35}$	1191.7	2.41	1168.8	1170.6	2.056	1169.8	$\beta_6$ (19)
$\nu_{36}$	1176.4	1.33	1166.3	1148.6	0.391	1150.3	$\beta_4$ (19)+ $\beta'_3$ (15)+ $\beta_8$ (11)
$\nu_{37}$	1148.7	0.66	1128.6	(1126.0)		1126.7	$\beta_7$ (18)+ $\delta_5$ (12)+ $R_{15}$ (10)
$\nu_{38}$	1077.3	5.00	1057.7	1053.2	3.525	1053.9	$R_{14}$ (47)+ $R_{15}$ (11)
$\nu_{39}$	1057.0	0.54	1015.8	(1036.0)		1032.1	$\delta_a$ (2) (39)+ $\rho$ (1) (12)
$\nu_{40}$	1040.5	3.53	1026.2	(1020.0)		1019.6	$\delta_a$ (1) (38)+ $\delta_9$ (12)
$\nu_{41}$	1010.2	3.40	995.1	996.4	4.896	995.1	$\beta_9$ (32)+ $\delta_5$ (24)
$\nu_{42}$	983.7	1.32	968.9	968.8	0.587	967.1	$R'_{18}$ (23)+ $R'_{17}$ (17)+ $\delta_5$ (12)
$\nu_{43}$	979.6	2.27	955.5	944.9	0.489	952.2	$\delta_a$ (2) (12)+ $\delta_1$ (11)+ $R_6$ (11)+ $R_{11}$ (10)

Table 5.4(b): (Continued) Calculated harmonic, anharmonic frequencies (in  $cm^{-1}$ ) and intensities (in  $km/mol$ ) at  $B3LYP/6-311G^{**}$ , observed frequencies (in  $cm^{-1}$ ) and intensities (in  $km/mol$ ), fitted frequencies (in  $cm^{-1}$ ) and PED of 2, 4 – DMP.

Sym	B3LYP/6-311G**			Observed		Force field	
	No	Harm.	Int.	Anharm.	Freq.	Int.	Fitted PED
$\nu_{44}$	857.9	1.78	846.6	( 841.0)		843.7	$\delta_5 ( 19)+ \delta_3 ( 11)+ R_8 ( 11)+ \delta_7 ( 11)$
$\nu_{45}$	773.4	0.92	765.4	( 758.0)		757.0	$\delta_2 ( 27)+ \delta_7 ( 14)+ \delta_4 ( 12)$
$\nu_{46}$	698.2	2.94	687.4	688.7	3.623	688.1	$\delta_6 ( 44)+ R_8 ( 11)$
$\nu_{47}$	589.7	0.45	585.3	( 578.0)		579.1	$R'_{18} ( 17)+ \beta_9 ( 15)+ \delta_1 ( 12)+ \delta_6 ( 12)$
$\nu_{48}$	568.9	0.73	562.7	( 557.0)		557.7	$\delta_6 ( 20)+ \delta_3 ( 16)+ \delta_4 ( 11)+ \delta_7 ( 11)$
$\nu_{49}$	557.3	0.61	551.5	( 546.0)		546.3	$\beta_{10} ( 39)+ R'_{17} ( 13)$
$\nu_{50}$	529.1	2.61	520.6	( 518.0)		517.2	$\delta_1 ( 27)+ r'_{13} ( 18)+ \beta_{10} ( 12)$
$\nu_{51}$	504.9	0.39	503.0	( 495.0)		493.7	$\delta_7 ( 30)+ \delta_1 ( 22)+ \delta_3 ( 13)$
$\nu_{52}$	392.0	0.47	388.1	( 384.0)		383.8	$\delta_4 ( 45)$
$\nu_{53}$	327.6	0.72	315.2	( 321.0)		321.2	$r'_{13} ( 47)+ \delta_3 ( 18)$
$\nu_{54}$	303.8	0.00	300.8	( 298.0)		297.8	$\beta'_1 ( 38)+ \delta_1 ( 16)$
$\nu_{55}$	214.8	0.81	211.8	( 210.0)		210.4	$\beta'_1 ( 34)+ \delta_4 ( 11)$
$A''$							
$\nu_{56}$	3081.0	15.52	2939.1	2930.8	30.458	2930.6	$r'_{11} ( 100)$
$\nu_{57}$	3069.6	19.95	2918.1	(2930.0)		2927.7	$r'_9 ( 100)$
$\nu_{58}$	1501.8	7.02	1460.3	(1469.0)		1468.7	$\delta_s(2) ( 94)$
$\nu_{59}$	1486.6	7.30	1468.5	(1456.0)		1456.2	$\delta_s(1) ( 92)$
$\nu_{60}$	1061.8	3.94	1045.3	1038.5	2.938	1042.7	$\rho(1) ( 50)+ \delta_a(2) ( 18)+$ $\rho(2) ( 10)$
$\nu_{61}$	1060.3	0.83	1023.2	(1038.0)		1035.9	$\delta_9 ( 52)+ \delta_a(1) ( 18)$
$\nu_{62}$	992.4	0.04	978.0	( 973.0)		974.4	$\gamma_7 ( 30)+ \gamma_6 ( 28)+ \gamma_8 ( 14)+ \tau_5 ( 10)$
$\nu_{63}$	979.8	0.00	972.9	( 960.0)		959.1	$\gamma_4 ( 40)+ \gamma'_3 ( 39)$
$\nu_{64}$	955.5	1.21	958.6	( 937.0)		936.5	$\gamma_8 ( 30)+ \gamma_5 ( 26)+ \gamma_7 ( 15)+ \gamma_6 ( 15)$
$\nu_{65}$	903.0	6.90	895.6	885.3	4.505	885.3	$\rho(2) ( 53)+ \gamma_2 ( 30)$
$\nu_{66}$	881.1	21.29	875.1	864.2	29.969	863.0	$\gamma_5 ( 15)+ \gamma_8 ( 15)+ \rho(2) ( 12)+ \gamma_2 ( 11)$
$\nu_{67}$	871.8	4.43	861.9	855.0		853.3	$\gamma_2 ( 25)+ \gamma_9 ( 17)+ \rho(2) ( 16)$
$\nu_{68}$	823.7	19.41	810.7	806.4	24.190	808.5	$\gamma'_3 ( 27)+ \gamma_2 ( 17)+ \gamma_4 ( 14)+ \tau_2 ( 10)$
$\nu_{69}$	806.9	2.02	807.7	( 791.0)		792.6	$\tau_2 ( 30)+ \gamma_9 ( 15)+ \gamma_4 ( 14)+ \tau_5 ( 13)$
$\nu_{70}$	757.0	40.94	746.9	742.7	47.598	741.4	$\gamma_7 ( 24)+ \gamma_6 ( 22)+ \gamma_5 ( 19)+ \gamma_8 ( 16)$
$\nu_{71}$	727.3	10.01	718.0	708.7	16.159	708.0	$\tau_5 ( 38)+ \gamma_9 ( 30)$
$\nu_{72}$	616.6	3.42	606.0	603.2	3.525	603.9	$\tau_5 ( 19)+ \tau_2 ( 16)+ \gamma_9 ( 10)$
$\nu_{73}$	583.7	0.05	576.7	( 572.0)		573.8	$\gamma'_1 ( 18)+ \gamma_{10} ( 17)+ \tau_8 ( 14)$
$\nu_{74}$	532.0	0.20	522.6	( 521.0)		521.0	$\tau_7 ( 26)+ \tau_5 ( 14)+ \gamma'_1 ( 12)+ \gamma_{10} ( 11)$
$\nu_{75}$	490.3	4.75	484.6	( 480.0)		482.8	$\rho(2) ( 24)+ \tau_1 ( 18)+ \tau_9 ( 16)+ \tau_6 ( 14)$
$\nu_{76}$	419.3	1.43	403.9	( 411.0)		411.1	$\tau_6 ( 46)+ \tau_3 ( 12)$
$\nu_{77}$	351.3	0.78	327.6	( 344.0)		344.6	$\tau_{ring} ( 39)+ \tau_7 ( 14)$
$\nu_{78}$	325.4	0.86	318.0	( 319.0)		318.0	$\tau_{ring} ( 37)+ \tau_6 ( 16)+ \gamma'_1 ( 10)$
$\nu_{79}$	229.3	1.71	222.2	( 224.0)		223.8	$\tau_1 ( 23)+ \tau_9 ( 15)+ \tau_6 ( 12)+ \tau_4 ( 12)$
$\nu_{80}$	187.3	3.77	170.6	( 183.0)		182.9	$\tau_1 ( 33)+ \rho(2) ( 12)+ \rho(2) ( 11)$
$\nu_{81}$	177.8	0.36	168.1	( 174.0)		174.8	$\tau_4 ( 14)+ \tau_7 ( 14)+ \gamma'_1 ( 11)+ \gamma_{10} ( 11)$
$\nu_{82}$	78.1	0.03	61.8	( 76.0)		76.2	$\tau_{ring} ( 36)+ \tau_3 ( 16)+ \tau_8 ( 11)+ \tau_7 ( 11)$
$\nu_{83}$	66.8	0.52	51.8	( 65.0)		64.7	$\tau_{ring} ( 37)+ \tau_3 ( 18)$
$\nu_{84}$	-16.1	0.00	-76.1	( 15.0)		nan	$\tau_{ring} ( 40)+ \tau_3 ( 12)+ \gamma_{10} ( 11)$

Since the fitting algorithm required all the experimental frequencies, the numbers in parenthesis are introduced as good guesses for 2, 4 – DMP and do not have any other significance. RMS error is 2.3804 for the fitting of experimental frequencies.

Table 5.4(c): Calculated harmonic, anharmonic frequencies (in  $cm^{-1}$ ) and intensities (in  $km/mol$ ) at  $B3LYP/6-311G^{**}$ , observed frequencies (in  $cm^{-1}$ ) and intensities (in  $km/mol$ ), fitted frequencies (in  $cm^{-1}$ ) and PED of 3,9 – DMP.

Sym	B3LYP/6-311G**			Observed		Force field	
	No	Harm.	Int.	Anharm.	Freq.	Int.	Fitted PED
$A'$							
$\nu_1$	3203.4	17.48	3063.6	3085.7	19.159	3085.8	$r_5$ ( 95)
$\nu_2$	3197.7	26.27	3061.2	3062.5	13.063	3062.5	$r_8$ ( 98)
$\nu_3$	3182.7	5.00	3048.0	3029.1	10.757	3030.6	$r_1$ ( 50)+ $r_6$ ( 48)
$\nu_4$	3176.6	12.81	3026.0	(3029.0)		3027.5	$r_1$ ( 47)+ $r_6$ ( 46)
$\nu_5$	3170.5	38.13	3039.4	2978.9	10.668	2978.9	$r_7$ ( 95)
$\nu_6$	3163.8	2.47	3032.2	(2978.0)		2978.1	$r_3$ ( 79)+ $r_2$ ( 20)
$\nu_7$	3153.2	20.31	3012.6	2956.3	5.660	2957.0	$r_4$ ( 49)+ $r_2$ ( 43)
$\nu_8$	3150.2	6.45	3004.5	(2956.0)		2955.2	$r_4$ ( 47)+ $r_2$ ( 36)+ $r_3$ ( 14)
$\nu_9$	3106.2	18.06	2960.1	2933.5	51.838	2936.0	$r'_{12}$ ( 76)+ $r'_{11}$ ( 22)
$\nu_{10}$	3102.2	16.61	2954.3	(2933.0)		2935.7	$r'_{10}$ ( 76)+ $r'_9$ ( 23)
$\nu_{11}$	3020.5	36.57	2974.6	2875.0	19.377	2867.0	$r'_{11}$ ( 64)+ $r'_{12}$ ( 18) + $r'_9$ ( 14)
$\nu_{12}$	3019.0	46.34	2908.1	(2875.0)		2866.8	$r'_9$ ( 62)+ $r'_{10}$ ( 19) + $r'_{11}$ ( 14)
$\nu_{13}$	1664.1	0.33	1624.1	(1632.0)		1632.8	$R_{10}$ ( 43)+ $\beta_3$ ( 10)
$\nu_{14}$	1659.2	17.17	1621.2	1620.8	24.167	1623.6	$R_4$ ( 19)+ $R_2$ ( 11)
$\nu_{15}$	1648.8	6.94	1610.1	1614.2		1614.6	$R_{13}$ ( 17)+ $R_{15}$ ( 17)
$\nu_{16}$	1605.2	0.48	1567.4	(1574.0)		1574.9	$R_6$ ( 12)+ $R_{14}$ ( 12)
$\nu_{17}$	1560.4	0.99	1525.0	(1530.0)		1528.9	$R_3$ ( 14)+ $R_{14}$ ( 12)
$\nu_{18}$	1539.7	20.01	1505.6	1508.8	20.030	1507.9	$\beta_7$ ( 11)
$\nu_{19}$	1505.0	1.76	1461.3	(1476.0)		1476.1	$\delta_s(2)$ ( 74)
$\nu_{20}$	1496.3	19.19	1469.8	1460.6	34.618	1460.8	$\delta_s(1)$ ( 61)
$\nu_{21}$	1481.6	6.57	1451.6	(1437.0)		1439.7	$\beta'_6$ ( 16)
$\nu_{22}$	1459.8	5.28	1427.6	(1431.0)		1427.9	$\beta_8$ ( 17)+ $\beta_5$ ( 11)
$\nu_{23}$	1444.9	1.23	1419.3	(1417.0)		1412.0	$R_1$ ( 16)+ $\delta_s(1)$ ( 13)
$\nu_{24}$	1418.2	6.18	1390.0	1388.3	12.410	1390.8	$\rho(1)$ ( 24)+ $R_9$ ( 17)+ $\beta_3$ ( 10)
$\nu_{25}$	1414.3	0.78	1408.2	(1387.0)		1387.1	$\delta_8$ ( 87)
$\nu_{26}$	1412.4	0.17	1380.5	(1385.0)		1384.1	$\rho(1)$ ( 63)
$\nu_{27}$	1381.2	1.16	1346.0	(1349.0)		1349.5	$R_6$ ( 20)+ $R_2$ ( 16)+ $R_4$ ( 15)
$\nu_{28}$	1355.2	1.38	1326.9	1327.6	0.870	1329.3	$R_8$ ( 25)+ $R_{13}$ ( 13)+ $R_{15}$ ( 11)+ $R_{16}$ ( 10)
$\nu_{29}$	1325.1	1.92	1302.4	1296.3	1.088	1296.6	$\beta_1$ ( 12)+ $\beta_9$ ( 12)+ $R_{11}$ ( 11)+ $\beta_2$ ( 10)
$\nu_{30}$	1310.7	0.07	1287.0	(1260.0)		1268.3	$\delta_2$ ( 18)+ $\beta_5$ ( 14)+ $\beta_8$ ( 11)
$\nu_{31}$	1269.3	1.66	1249.4	(1244.0)		1241.4	$\beta_3$ ( 16)+ $R_{16}$ ( 13)+ $\beta_8$ ( 13)
$\nu_{32}$	1243.9	1.80	1223.3	1215.2	0.653	1215.9	$R_1$ ( 15)
$\nu_{33}$	1230.9	0.95	1210.9	(1207.0)		1206.6	$\beta_3$ ( 23)+ $R_5$ ( 18)
$\nu_{34}$	1209.2	2.25	1183.8	1185.0	0.653	1184.9	$R'_{17}$ ( 18)+ $R_7$ ( 14)+ $r'_{13}$ ( 13)
$\nu_{35}$	1191.0	1.51	1170.5	1166.5	1.306	1167.0	$\beta_7$ ( 35)
$\nu_{36}$	1174.7	2.93	1159.2	1150.0	1.524	1146.2	$\beta'_6$ ( 21)+ $\beta_5$ ( 13)+ $\beta_2$ ( 13)+ $\beta_1$ ( 12)
$\nu_{37}$	1138.3	0.19	1121.6	(1116.0)		1117.2	$\beta'_6$ ( 12)
$\nu_{38}$	1087.5	0.14	1065.6	(1066.0)		1065.3	$\delta_a(2)$ ( 18)+ $\delta_5$ ( 16)+ $R'_{18}$ ( 12)
$\nu_{39}$	1062.4	6.33	1048.6	1040.4	9.797	1040.8	$R_{14}$ ( 42)+ $\delta_5$ ( 12)
$\nu_{40}$	1056.8	3.71	1043.4	(1036.0)		1034.7	$\beta_9$ ( 30)+ $\delta_5$ ( 15)
$\nu_{41}$	1015.9	8.23	1001.9	999.6	3.701	999.4	$\delta_a(2)$ ( 29)+ $\delta_5$ ( 14)+ $R'_{18}$ ( 12)
$\nu_{42}$	1001.4	1.00	988.7	( 982.0)		982.2	$\delta_a(1)$ ( 39)+ $\delta_9$ ( 13)+ $R_3$ ( 11)
$\nu_{43}$	909.8	2.25	898.4	( 892.0)		892.4	$\delta_1$ ( 14)+ $\delta_5$ ( 12)
$\nu_{44}$	842.9	0.02	832.5	( 826.0)		826.9	$\beta_9$ ( 16)+ $\delta_2$ ( 13)

Table 5.4(c): (Continued) Calculated harmonic, anharmonic frequencies (in  $cm^{-1}$ ) and intensities (in  $km/mol$ ) at  $B3LYP/6-311G^{**}$ , observed frequencies (in  $cm^{-1}$ ) and intensities (in  $km/mol$ ), fitted frequencies (in  $cm^{-1}$ ) and PED of 3,9 – DMP.

Sym	B3LYP/6-311G <sup>**</sup>			Observed		Force field	
	No	Harm.	Int.	Anharm.	Freq.	Int.	Fitted PED
$\nu_{45}$	764.9	0.69		755.4	( 750.0)		750.3 $\delta_7$ ( 23)+ $R_9$ ( 12)+ $\delta_2$ ( 11)
$\nu_{46}$	721.0	0.23		713.8	( 707.0)		706.9 $\beta_{10}$ ( 31)+ $\delta_6$ ( 17)
$\nu_{47}$	642.1	3.84		636.4	629.1	2.394	629.2 $\delta_6$ ( 43)+ $\beta_{10}$ ( 21)
$\nu_{48}$	607.7	1.64		605.2	( 596.0)		594.8 $\delta_2$ ( 21)+ $R'_{18}$ ( 11)+ $\beta_{10}$ ( 10)
$\nu_{49}$	545.2	0.59		543.1	( 534.0)		533.9 $\delta_1$ ( 25)+ $\delta_7$ ( 24)+ $\beta_4$ ( 23)
$\nu_{50}$	505.0	0.57		499.8	( 495.0)		494.1 $\delta_4$ ( 31)
$\nu_{51}$	437.7	1.32		433.0	( 429.0)		429.2 $\delta_3$ ( 40)+ $r'_{14}$ ( 19)+ $\delta_4$ ( 13)
$\nu_{52}$	398.2	0.23		392.2	( 390.0)		390.2 $\delta_4$ ( 23)+ $\beta_{10}$ ( 15)+ $R_7$ ( 13)
$\nu_{53}$	340.3	0.49		340.7	( 333.0)		333.1 $r'_{14}$ ( 39)+ $\delta_1$ ( 20)+ $\delta_3$ ( 11)
$\nu_{54}$	287.3	0.62		281.3	( 281.0)		281.0 $\beta_4$ ( 62)+ $\delta_7$ ( 10)
$\nu_{55}$	191.9	0.51		191.1	( 188.0)		187.9 $r'_{14}$ ( 32)+ $\delta_1$ ( 10)
$A''$							
$\nu_{56}$	3067.5	21.10		2916.8	2908.2	7.838	2914.1 $r'_9$ ( 99)
$\nu_{57}$	3064.7	20.18		2921.9	(2908.0)		2914.0 $r'_{11}$ ( 99)
$\nu_{58}$	1486.2	6.30		1466.8	1453.5		1453.2 $\delta_s(1)$ ( 92)
$\nu_{59}$	1486.0	7.97		1449.1	(1453.0)		1452.9 $\delta_s(2)$ ( 92)
$\nu_{60}$	1062.6	0.68		1037.4	(1042.0)		1042.7 $\rho(1)$ ( 53)+ $\delta_a(2)$ ( 19)
$\nu_{61}$	1060.7	3.98		1043.2	(1039.0)		1039.4 $\delta_9$ (49)+ $\delta_a(1)$ (17)+ $\rho(2)$ (10)
$\nu_{62}$	989.6	0.00		977.4	( 970.0)		970.6 $\gamma'_6$ ( 34)+ $\gamma_7$ ( 34)
$\nu_{63}$	969.4	0.92		963.8	948.7	0.870	948.7 $\gamma'_2$ ( 44)+ $\gamma_1$ ( 43)
$\nu_{64}$	954.0	0.94		954.4	( 935.0)		934.5 $\gamma_5$ ( 28)+ $\gamma_8$ ( 28)+ $\gamma_7$ ( 18)+ $\gamma'_6$ ( 16)
$\nu_{65}$	901.8	17.60		882.9	879.1	33.094	879.1 $\gamma_3$ ( 53)+ $\rho(2)$ ( 16)
$\nu_{66}$	882.5	7.59		887.7	871.7		871.4 $\rho(2)$ ( 53)+ $\gamma_3$ ( 20)
$\nu_{67}$	873.2	0.13		875.0	( 856.0)		855.8 $\gamma_8$ ( 26)+ $\gamma_5$ ( 25)+ $\tau_5$ ( 14)+ $\tau_2$ ( 13)
$\nu_{68}$	818.8	13.29		806.4	801.8	16.982	801.7 $\gamma'_2$ ( 39)+ $\gamma_1$ ( 33)
$\nu_{69}$	794.4	2.94		786.5	( 779.0)		780.4 $\tau_2$ ( 33)+ $\tau_5$ ( 22)+ $\gamma_9$ ( 13)+ $\gamma_7$ ( 10)
$\nu_{70}$	768.0	48.25		760.6	753.9	62.487	753.4 $\gamma'_6$ ( 27)+ $\gamma_5$ ( 15)+ $\gamma_8$ ( 15)+ $\gamma_7$ ( 13)
$\nu_{71}$	738.1	8.66		724.8	723.6	8.055	724.1 $\gamma_9$ ( 41)+ $\tau_5$ ( 28)
$\nu_{72}$	611.9	2.23		601.9	602.1	4.572	600.5 $\tau_5$ (23)+ $\tau_2$ (15)+ $\gamma_9$ (14)+ $\rho(2)$ (12)
$\nu_{73}$	586.2	6.66		579.7	573.6	6.749	573.6 $\gamma_4$ ( 22)+ $\tau_4$ ( 12)+ $\rho(2)$ ( 11)+ $\gamma_{10}$ ( 10)
$\nu_{74}$	521.9	3.37		510.0	( 511.0)		511.7 $\tau_1$ ( 19)+ $\tau_3$ ( 17)+ $\tau_8$ ( 16)+ $\tau_7$ ( 15)+ $\rho(2)$ ( 11)
$\nu_{75}$	444.4	2.62		436.6	( 435.0)		435.9 $\tau_1$ ( 21)+ $\gamma_{10}$ ( 20)+ $\tau_6$ ( 20)+ $\tau_8$ ( 11)
$\nu_{76}$	423.1	1.10		414.6	( 414.0)		413.9 $\tau_6$ ( 39)+ $\tau_9$ ( 12)
$\nu_{77}$	357.2	1.70		349.2	( 350.0)		350.0 $\rho(2)$ ( 21)+ $\gamma_4$ ( 18)+ $\tau_1$ ( 11)
$\nu_{78}$	245.9	0.38		236.4	( 241.0)		240.7 $\tau_6$ ( 26)+ $\gamma_{10}$ ( 22)+ $\tau_9$ ( 14)
$\nu_{79}$	220.1	0.25		175.2	( 215.0)		214.9 $\tau_{ring}$ ( 60)
$\nu_{80}$	193.0	0.01		159.8	( 189.0)		189.2 $\tau_{ring}$ ( 30)+ $\tau_1$ ( 13)+ $\tau_3$ ( 12)
$\nu_{81}$	135.5	2.60		129.4	( 132.0)		132.0 $\tau_7$ ( 20)+ $\gamma_4$ ( 16)+ $\tau_9$ ( 13)+ $\tau_8$ ( 10)+ $\tau_2$ ( 10)
$\nu_{82}$	96.4	0.18		79.9	( 94.0)		94.2 $\tau_4$ ( 26)+ $\tau_7$ ( 15)+ $\tau_3$ ( 13)+ $\tau_9$ ( 13)
$\nu_{83}$	79.2	0.26		-90.1	( 77.0)		77.0 $\tau_{ring}$ ( 69)
$\nu_{84}$	62.2	0.42		44.4	( 61.0)		60.7 $\tau_3$ ( 25)+ $\tau_4$ ( 12)+ $\tau_1$ ( 11)

Since the fitting algorithm required all the experimental frequencies, the numbers in parenthesis are introduced as good guesses for 3,9 – DMP and do not have any other significance. RMS error is 2.2038 for the fitting of experimental frequencies.



Table 5.5(a): Calculated harmonic, anharmonic frequencies (in  $cm^{-1}$ ) and intensities (in  $km/mol$ ) at  $B3LYP/6-31G^*$ , observed frequencies (in  $cm^{-1}$ ) and intensities (in  $km/mol$ ), fitted frequencies (in  $cm^{-1}$ ) and PEDs of 1,9 - DMP.

Sym Mode	B3LYP/6-31G*			Observed		Force field	
	Harm.	Int.	Anharm.	Freq.	Int.	Fitted	PED
$A'$							
$\nu_1$	3230.3	29.723	3092.1	3089.1	14.454	3088.9	$r_5$ ( 63) + $r_1$ ( 36)
$\nu_2$	3218.2	29.562	3085.1	3069.7	31.830	3070.0	$r_1$ ( 50) + $r_5$ ( 27) + $r_8$ ( 21)
$\nu_3$	3213.0	0.968	3080.4	(3069.0)		3068.9	$r_8$ ( 77) + $r_1$ ( 12)
$\nu_4$	3204.8	14.918	3052.1	3035.3	11.215	3035.3	$r_4$ ( 99)
$\nu_5$	3199.2	16.626	3066.3	2979.6	14.454	2979.7	$r_2$ ( 43) + $r_7$ ( 43)
$\nu_6$	3195.2	39.278	3046.2	(2979.0)		2979.5	$r_2$ ( 43) + $r_7$ ( 43)
$\nu_7$	3184.4	2.290	3051.6	2955.2	8.293	2955.2	$r_6$ ( 83) + $r_7$ ( 12)
$\nu_8$	3178.4	11.562	3050.0	(2955.0)		2954.9	$r_3$ ( 82) + $r_2$ ( 12)
$\nu_9$	3127.0	17.148	2990.1	2933.5	34.121	2936.7	$r'_{12}$ ( 77) + $r'_{11}$ ( 21)
$\nu_{10}$	3125.8	21.105	2983.7	(2933.0)		2936.1	$r'_{10}$ ( 76) + $r'_9$ ( 20)
$\nu_{11}$	3040.3	31.839	2904.4	2875.3	14.533	2864.3	$r'_{11}$ ( 65) + $r'_{12}$ ( 18) + $r'_9$ ( 13)
$\nu_{12}$	3038.5	34.593	2909.2	(2875.0)		2863.9	$r'_9$ ( 66) + $r'_{10}$ ( 17) + $r'_{11}$ ( 13)
$\nu_{13}$	1676.3	8.892	1638.9	1626.5	9.952	1624.8	$R_{13}$ ( 16) + $R_{16}$ ( 12) + $R_{15}$ ( 11)
$\nu_{14}$	1668.0	1.370	1625.0	1619.0		1620.1	$R_{10}$ ( 32) + $R_{15}$ ( 11)
$\nu_{15}$	1659.4	6.687	1620.1	1604.6	7.819	1606.8	$R_4$ ( 28) + $R_1$ ( 12) + $R_2$ ( 10)
$\nu_{16}$	1629.5	1.478	1591.5	1584.5		1582.9	$R_2$ ( 16) + $R_3$ ( 11)
$\nu_{17}$	1584.8	3.469	1551.8	(1536.2)		1538.3	$R_{14}$ ( 20)
$\nu_{18}$	1541.7	11.020	1510.4	1495.4	3.791	1495.3	$R_9$ ( 14)
$\nu_{19}$	1533.7	11.699	1481.9	(1471.2)		1473.3	$\delta_s(1)$ ( 47) + $\delta_s(2)$ ( 13)
$\nu_{20}$	1521.8	3.263	1486.0	(1469.0)		1465.5	$\delta_s(1)$ ( 27) + $\delta_s(2)$ ( 13) + $r'_{14}$ ( 11)
$\nu_{21}$	1504.4	12.089	1472.8	1456.0	25.433	1456.4	$\delta_s(2)$ ( 42)
$\nu_{22}$	1491.3	0.408	1461.6	(1446.0)		1445.0	$\beta_5$ ( 17) + $R_{10}$ ( 12)
$\nu_{23}$	1457.2	9.055	1431.2	1412.4	6.713	1413.7	$\beta_8$ ( 14) + $R_{11}$ ( 11)
$\nu_{24}$	1445.4	1.807	1424.3	1389.5	5.213	1391.1	$\delta_8$ ( 34) + $\rho(1)$ ( 32)
$\nu_{25}$	1443.8	1.683	1425.0	(1389.0)		1387.9	$\delta_8$ ( 44) + $\rho(1)$ ( 44)
$\nu_{26}$	1423.4	0.315	1396.9	(1378.0)		1377.8	$R_9$ ( 17) + $\rho(1)$ ( 10)
$\nu_{27}$	1390.0	0.122	1358.0	(1347.0)		1347.9	$R_6$ ( 19) + $R_2$ ( 15) + $R_4$ ( 14)
$\nu_{28}$	1379.7	0.654	1351.1	(1336.0)		1339.2	$R_8$ ( 24) + $R_{13}$ ( 12)
$\nu_{29}$	1330.7	1.473	1308.9	1296.1	1.263	1295.3	$R_7$ ( 18) + $\beta_9$ ( 14) + $R_{11}$ ( 11)
$\nu_{30}$	1307.8	1.231	1291.3	1273.2	0.868	1274.5	$\delta_2$ ( 19) + $\beta_5$ ( 14) + $\beta_1$ ( 14) + $\beta_8$ ( 13)
$\nu_{31}$	1284.9	2.543	1265.9	1249.5	3.712	1248.3	$R_{16}$ ( 12) + $\beta_8$ ( 11) + $\beta_3$ ( 10)
$\nu_{32}$	1266.7	3.597	1250.0	(1228.0)		1228.1	$\beta_3$ ( 28) + $R'_{17}$ ( 16) + $R_5$ ( 11)
$\nu_{33}$	1249.7	2.711	1227.5	1213.0	0.789	1213.9	$R_1$ ( 20) + $R_{11}$ ( 19)
$\nu_{34}$	1213.3	0.241	1197.0	(1179.0)		1179.6	$r'_{14}$ ( 28) + $\beta'_6$ ( 11)
$\nu_{35}$	1202.2	0.447	1192.2	(1168.0)		1168.3	$\beta_7$ ( 29) + $\beta'_6$ ( 20) + $\beta_8$ ( 11)
$\nu_{36}$	1181.4	1.242	1166.6	1152.7	0.631	1151.5	$R_{15}$ ( 14) + $\beta_7$ ( 13) + $\beta'_6$ ( 11) + $\delta_2$ ( 10)
$\nu_{37}$	1121.7	3.163	1107.7	1089.9	2.290	1089.4	$R_3$ ( 33) + $\beta_1$ ( 15) + $R_2$ ( 11)
$\nu_{38}$	1099.2	0.091	1085.7	(1068.0)		1067.8	$\delta_a(2)$ ( 12) + $R'_{18}$ ( 10)
$\nu_{39}$	1086.7	0.285	1067.3	(1061.0)		1061.6	$\delta_5$ ( 43)
$\nu_{40}$	1068.0	6.035	1050.1	1036.4	7.108	1036.1	$R_{14}$ ( 42)
$\nu_{41}$	1027.1	0.609	1001.8	( 998.0)		998.4	$\delta_a(2)$ ( 17) + $\delta_a(1)$ ( 16) + $\beta_9$ ( 16)
$\nu_{42}$	1022.3	4.103	998.6	995.3	2.843	993.7	$\delta_a(1)$ ( 25) + $\delta_a(2)$ ( 17) + $\delta_5$ ( 12)
$\nu_{43}$	894.0	1.905	882.2	( 874.0)		872.4	$\delta_5$ ( 17) + $R'_{17}$ ( 13) + $\delta_4$ ( 11)
$\nu_{44}$	869.6	0.239	859.9	( 851.0)		850.5	$\beta_9$ ( 33) + $R_6$ ( 10)

Table 5.5(a): (Continued) Calculated harmonic, anharmonic frequencies (in  $cm^{-1}$ ) and intensities (in  $km/mol$ ) at  $B3LYP/6-31G^*$ , observed frequencies (in  $cm^{-1}$ ) and intensities (in  $km/mol$ ), fitted frequencies (in  $cm^{-1}$ ) and PED of 1, 9 – DMP.

Sym	B3LYP/6-31G*			Observed		Force field	
	Mode	Harm.	Int.	Anharm.	Freq.	Int.	Fitted PED
$\nu_{45}$	780.9	0.115	770.4	( 763.0)		763.3	$\delta_7$ ( 27) + $\delta_5$ ( 12) + $R_9$ ( 12)
$\nu_{46}$	711.6	3.574	702.2	698.5	3.633	697.1	$\delta_6$ ( 23) + $\delta_1$ ( 15) + $\delta_2$ ( 13)
$\nu_{47}$	635.5	0.490	628.9	( 623.0)		623.8	$\delta_6$ ( 35) + $\delta_1$ ( 21) + $\delta_2$ ( 15)
$\nu_{48}$	573.8	0.429	568.8	( 563.0)		560.5	$\delta_7$ ( 25) + $\delta_1$ ( 21) + $\beta'_4$ ( 21)
$\nu_{49}$	553.1	6.038	547.2	539.5	1.816	540.4	$\beta_{10}$ ( 37) + $R'_{17}$ ( 11) + $\delta_3$ ( 11)
$\nu_{50}$	514.5	1.761	506.6	( 503.0)		502.4	$\delta_4$ ( 23) + $\beta_{10}$ ( 17) + $\delta_7$ ( 11)
$\nu_{51}$	447.6	0.824	443.1	( 438.0)		437.1	$\delta_4$ ( 28) + $\beta_2$ ( 25) + $\delta_3$ ( 16)
$\nu_{52}$	426.5	0.230	422.4	( 417.0)		416.6	$\delta_3$ ( 35) + $\beta_{10}$ ( 12) + $\delta_4$ ( 10)
$\nu_{53}$	335.4	0.479	326.8	( 327.0)		327.6	$\beta_2$ ( 27) + $\beta'_4$ ( 18)
$\nu_{54}$	284.0	0.198	278.2	( 277.0)		277.3	$\beta'_4$ ( 47) + $\delta_7$ ( 18)
$\nu_{55}$	223.2	0.372	220.3	( 217.0)		217.6	$\delta_1$ ( 24) + $\beta_2$ ( 21)
$A''$							
$\nu_{56}$	3090.6	21.375	2922.9	2905.0	3.554	2913.6	$r'_9$ ( 89) + $r'_{11}$ ( 11)
$\nu_{57}$	3087.6	18.954	2946.7	(2905.0)		2913.4	$r'_{11}$ ( 89) + $r'_9$ ( 11)
$\nu_{58}$	1517.6	4.201	1466.2	(1461.0)		1460.8	$\delta_s(1)$ ( 90)
$\nu_{59}$	1514.6	8.336	1474.1	(1458.0)		1457.8	$\delta_s(2)$ ( 90)
$\nu_{60}$	1079.7	1.658	1054.2	(1043.0)		1044.3	$\rho(1)$ ( 26) + $\delta_9$ ( 25)
$\nu_{61}$	1077.1	2.322	1048.4	(1041.0)		1043.7	$\delta_9$ ( 27) + $\rho(1)$ ( 27)
$\nu_{62}$	982.9	0.000	975.8	( 971.0)		966.4	$\gamma'_6$ ( 32) + $\gamma_7$ ( 29) + $\gamma_8$ ( 17)
$\nu_{63}$	962.9	0.948	962.7	( 954.0)		954.0	$\rho(2)$ ( 50) + $\gamma_1$ ( 24)
$\nu_{64}$	942.8	0.699	945.8	( 935.0)		933.4	$\gamma_8$ ( 38) + $\gamma'_6$ ( 29) + $\gamma_5$ ( 15)
$\nu_{65}$	902.3	8.634	898.5	( 884.0)		882.7	$\gamma_1$ ( 33) + $\rho(2)$ ( 23) + $\gamma_3$ ( 22)
$\nu_{66}$	892.5	5.600	893.4	871.4	17.692	871.8	$\gamma_3$ ( 60) + $\gamma_1$ ( 12)
$\nu_{67}$	876.2	0.041	868.2	( 856.0)		855.4	$\gamma_5$ ( 33) + $\gamma_7$ ( 13) + $\gamma_8$ ( 13) + $\tau_5$ ( 13) + $\tau_2$ ( 11)
$\nu_{68}$	819.6	5.433	809.2	803.5	9.952	802.6	$\gamma_9$ (23) + $\tau_2$ (21) + $\tau_5$ (13) + $\rho(2)$ (12)
$\nu_{69}$	772.6	38.966	764.4	748.3	105.602	754.8	$\gamma_7$ (23) + $\gamma'_6$ (21) + $\gamma_5$ (21) + $\gamma_8$ (14)
$\nu_{70}$	765.2	30.851	760.2	( 746.0)		747.8	$\rho(2)$ ( 33) + $\tau_5$ ( 21) + $\rho(2)$ ( 13) + $\tau_2$ ( 11)
$\nu_{71}$	745.3	0.224	737.5	( 729.0)		730.8	$\gamma_9$ ( 40) + $\tau_5$ ( 25)
$\nu_{72}$	611.3	0.000	602.3	( 598.0)		597.9	$\tau_5$ ( 25) + $\tau_2$ ( 17) + $\gamma'_4$ ( 12)
$\nu_{73}$	585.8	1.030	576.5	( 567.0)		562.5	$\tau_8$ ( 19), $\gamma_2$ ( 12) + $\tau_9$ ( 11) + $\tau_3$ ( 10)
$\nu_{74}$	540.9	0.210	531.4	( 528.0)		526.9	$\tau_1$ ( 28) + $\gamma_9$ ( 14)
$\nu_{75}$	486.0	0.056	477.0	( 473.0)		473.8	$\tau_7$ (24) + $\gamma_2$ (17) + $\gamma_{10}$ (13) + $\tau_3$ (11)
$\nu_{76}$	423.8	2.196	413.8	( 412.0)		412.0	$\tau_6$ ( 54) + $\gamma'_4$ ( 10)
$\nu_{77}$	332.5	0.486	323.5	( 322.0)		322.6	$\gamma_2$ ( 17) + $\gamma'_4$ ( 16) + $\tau_8$ ( 16) + $\tau_1$ ( 13) + $\tau_7$ ( 10)
$\nu_{78}$	249.7	0.342	240.2	( 240.0)		240.4	$\gamma_{10}$ ( 28) + $\tau_6$ ( 23) + $\tau_9$ ( 11)
$\nu_{79}$	219.0	0.004	185.9	( 207.0)		207.1	$\tau_{ring}$ ( 65)
$\nu_{80}$	197.2	0.007	138.0	( 188.0)		187.5	$\tau_1$ ( 26) + $\tau_{ring}$ ( 17) + $\tau_{ring}$ ( 15)
$\nu_{81}$	189.5	1.125	169.8	( 180.0)		180.1	$\tau_{ring}$ ( 69) + $\gamma_2$ ( 11)
$\nu_{82}$	142.8	1.688	135.7	( 137.0)		136.9	$\gamma'_4$ (19) + $\tau_9$ (16) + $\tau_8$ (14) + $\tau_7$ (13)
$\nu_{83}$	95.2	0.259	90.7	( 91.0)		91.3	$\tau_3$ ( 40) + $\tau_7$ ( 22) + $\tau_8$ ( 10)
$\nu_{84}$	60.7	0.025	58.7	( 57.0)		57.0	$\tau_4$ (34) + $\tau_3$ (13) + $\gamma_{10}$ (12) + $\tau_1$ (11)

Since the fitting algorithm required all the experimental frequencies, the numbers in parenthesis are introduced as good guesses for 1, 9 – DMP and do not have any other significance. RMS error is  $2.7233\text{ cm}^{-1}$  for the fitting of experimental frequencies.

Table 5.5(b): Calculated harmonic, anharmonic frequencies (in  $cm^{-1}$ ) and intensities (in  $km/mol$ ) at  $B3LYP/6-31G^*$ , observed frequencies (in  $cm^{-1}$ ) and intensities (in  $km/mol$ ), fitted frequencies (in  $cm^{-1}$ ) and PED of 2, 4 – *DMP*.

Sym Mode	B3LYP/6-31G*			Observed		Force field	
	Harm.	Int.	Anharm.	Freq.	Int.	Fitted	PED
$A'$							
$\nu_1$	3335.7	5.028	3182.1	3155.1	2.350	3155.1	$r_5$ ( 99)
$\nu_2$	3206.6	29.258	3075.8	3076.5	2.644	3075.2	$r_7$ ( 70) + $r_6$ ( 24)
$\nu_3$	3196.6	40.682	3050.9	3057.2	41.917	3057.8	$r_4$ ( 47) + $r_3$ ( 23) + $r_6$ ( 22)
$\nu_4$	3188.2	14.459	3056.1	(3057.0)		3056.7	$r_6$ ( 52) + $r_4$ ( 17) + $r_7$ ( 17) + $r_3$ ( 10)
$\nu_5$	3179.0	7.684	3030.3	3038.0	17.237	3039.3	$r_8$ ( 50) + $r_3$ ( 32)
$\nu_6$	3176.0	7.570	3033.7	(3038.0)		3036.3	$r_8$ ( 38) + $r_3$ ( 32) + $r_4$ ( 25)
$\nu_7$	3173.3	8.308	3017.8	3017.1	6.072	3018.0	$r_2$ ( 50) + $r_1$ ( 48)
$\nu_8$	3171.2	27.353	3024.4	(3017.0)		3016.2	$r_1$ ( 50) + $r_2$ ( 48)
$\nu_9$	3125.7	16.627	2981.9	2976.7	20.273	2976.5	$r'_{10}$ ( 86) + $r'_9$ ( 13)
$\nu_{10}$	3121.5	22.597	2979.8	(2976.0)		2976.1	$r'_{12}$ ( 89)
$\nu_{11}$	3045.3	22.030	2890.6	2882.3	18.902	2883.5	$r'_9$ ( 87) + $r'_{10}$ ( 12)
$\nu_{12}$	3041.3	45.565	2930.3	(2882.0)		2881.0	$r'_{11}$ ( 90)
$\nu_{13}$	1685.5	0.908	1647.3	(1636.0)		1635.2	$R_{10}$ ( 41)
$\nu_{14}$	1677.1	20.827	1635.4	1621.4	28.206	1622.7	$R_4$ ( 19) + $R_5$ ( 13) + $R_2$ ( 12) + $\delta_1$ ( 11)
$\nu_{15}$	1665.5	6.941	1627.8	(1609.1)		1610.0	$R_{15}$ ( 20) + $R_{13}$ ( 16) + $R_{16}$ ( 11) + $\delta_7$ ( 10)
$\nu_{16}$	1620.3	2.093	1584.0	(1573.0)		1571.4	$R_{14}$ ( 17)
$\nu_{17}$	1580.4	1.524	1549.8	(1532.0)		1532.3	$R_3$ ( 13) + $R_{14}$ ( 13)
$\nu_{18}$	1547.2	14.780	1498.5	(1498.0)		1495.3	$R_9$ ( 17)
$\nu_{19}$	1543.8	5.145	1495.7	1470.9	40.742	1471.4	$\delta_s(2)$ ( 68)
$\nu_{20}$	1515.9	9.749	1476.5	1457.4		1459.2	$\delta_s(1)$ ( 45)
$\nu_{21}$	1502.4	12.860	1466.8	(1456.0)		1454.2	$\delta_s(1)$ ( 20) + $\beta_5$ ( 13)
$\nu_{22}$	1473.5	1.954	1454.3	1431.8	1.567	1430.4	$\beta_7$ ( 14) + $\beta_6$ ( 11)
$\nu_{23}$	1450.7	0.111	1405.3	(1402.0)		1400.1	$R_5$ ( 14) + $r'_{14}$ ( 12) + $\beta_2$ ( 11)
$\nu_{24}$	1445.8	0.632	1411.9	(1390.0)		1389.7	$R_2$ ( 12) + $\beta_2$ ( 10)
$\nu_{25}$	1440.7	0.616	1407.7	1384.4	2.644	1384.4	$\rho(1)$ ( 70)
$\nu_{26}$	1440.0	0.305	1404.0	(1380.0)		1380.1	$\delta_8$ ( 81)
$\nu_{27}$	1379.4	0.648	1354.4	(1335.0)		1333.2	$R_8$ ( 20) + $R_{13}$ ( 14) + $R_{15}$ ( 14) + $R_{16}$ ( 12)
$\nu_{28}$	1373.9	4.981	1344.8	1324.7	1.371	1322.7	$R_6$ ( 19) + $R_2$ ( 12)
$\nu_{29}$	1334.4	1.922	1313.0	1300.0	1.469	1299.5	$R_7$ ( 13) + $\beta_5$ ( 12) + $\beta_9$ ( 11)
$\nu_{30}$	1310.9	1.519	1276.2	1270.6	0.976	1271.7	$r'_{14}$ ( 27) + $R_7$ ( 16)
$\nu_{31}$	1286.3	0.732	1269.8	(1250.0)		1250.5	$\beta_8$ ( 11)
$\nu_{32}$	1255.2	3.485	1230.3	1217.4	2.546	1217.6	$\beta_6$ ( 13) + $\beta_5$ ( 12)
$\nu_{33}$	1239.3	0.104	1221.4	(1203.0)		1203.9	$R_9$ ( 21) + $R_{12}$ ( 18) + $R_{16}$ ( 10)
$\nu_{34}$	1222.7	1.195	1198.2	(1184.0)		1184.2	$\beta_2$ ( 26) + $\beta'_3$ ( 12) + $R'_{18}$ ( 11) + $r'_{14}$ ( 11)
$\nu_{35}$	1202.9	2.464	1191.1	1170.6	2.056	1170.2	$\beta_6$ ( 22) + $\beta_7$ ( 10)
$\nu_{36}$	1189.5	1.094	1186.8	1148.6	0.391	1149.4	$\beta_4$ ( 24) + $\beta'_3$ ( 20)
$\nu_{37}$	1156.0	0.316	1144.3	(1126.0)		1126.8	$\beta_7$ ( 20) + $R_{15}$ ( 11) + $\delta_5$ ( 11)
$\nu_{38}$	1086.8	3.888	1070.1	1053.2	3.525	1053.6	$R_{14}$ ( 47) + $R_{15}$ ( 11)
$\nu_{39}$	1068.7	0.805	1025.2	(1036.0)		1031.6	$\delta_a(2)$ ( 39) + $\rho(1)$ ( 12)
$\nu_{40}$	1052.2	3.620	1031.9	(1020.0)		1020.1	$\delta_a(1)$ ( 37) + $\delta_9$ ( 12)
$\nu_{41}$	1010.9	3.449	998.9	996.4	4.896	994.6	$\beta_9$ ( 31) + $\delta_5$ ( 24)
$\nu_{42}$	989.3	1.954	972.3	968.8	0.587	967.5	$R'_{18}$ ( 22) + $R'_{17}$ ( 17) + $\delta_5$ ( 12)
$\nu_{43}$	987.6	0.510	963.6	944.9	0.489	951.1	$\delta_1$ ( 12) + $\delta_a(2)$ ( 12) + $R_6$ ( 11) + $R_{11}$ ( 10)

Table 5.5(b): (Continued) Calculated harmonic, anharmonic frequencies (in  $cm^{-1}$ ) and intensities (in  $km/mol$ ) at  $B3LYP/6-31G^*$ , observed frequencies (in  $cm^{-1}$ ) and intensities (in  $km/mol$ ), fitted frequencies (in  $cm^{-1}$ ) and PED of 2, 4 – DMP.

Sym	B3LYP/6-31G*			Observed		Force field	
Mode	Harm.	Int.	Anharm.	Freq.	Int.	Fitted	PED
$\nu_{44}$	859.9	1.554	853.5	( 841.0)		842.7	$\delta_5 ( 18) + R_8 ( 11) + \delta_7 ( 11) + \delta_3 ( 10)$
$\nu_{45}$	773.2	1.029	768.6	( 758.0)		757.4	$\delta_2 ( 27) + \delta_7 ( 14) + \delta_4 ( 12)$
$\nu_{46}$	669.4	3.068	691.3	688.7	3.623	688.2	$\delta_6 ( 45) + R_8 ( 11)$
$\nu_{47}$	590.6	0.293	585.0	( 578.0)		578.7	$R'_{18} ( 16) + \beta_9 ( 14) + \delta_1 ( 12) + \delta_6 ( 12)$
$\nu_{48}$	569.7	0.816	562.5	( 557.0)		557.8	$\delta_6 ( 19) + \delta_3 ( 15) + \delta_7 ( 12) +$
$\nu_{49}$	558.3	0.775	547.7	( 546.0)		546.3	$\beta_{10} ( 40) + R'_{17} ( 13)$
$\nu_{50}$	530.0	2.734	522.1	( 518.0)		517.3	$\delta_1 ( 27) + r'_{13} ( 19) + \beta_{10} ( 10)$
$\nu_{51}$	505.1	0.335	501.6	( 495.0)		493.8	$\delta_7 ( 30) + \delta_1 ( 23) + \delta_3 ( 13)$
$\nu_{52}$	391.8	0.454	388.5	( 384.0)		383.7	$\delta_4 ( 45)$
$\nu_{53}$	328.6	0.632	319.6	( 321.0)		321.2	$r'_{13} ( 46) + \delta_3 ( 19)$
$\nu_{54}$	304.3	0.009	307.3	( 298.0)		297.7	$\beta'_1 ( 36) + \delta_1 ( 16)$
$\nu_{55}$	215.3	0.687	218.9	( 210.0)		210.4	$\beta'_1 ( 35) + \delta_4 ( 11)$
$A''$							
$\nu_{56}$	3102.9	16.738	2958.9	2930.8	30.458	2931.7	$r'_{11} ( 100)$
$\nu_{57}$	3092.4	20.430	2941.7	( 2930.0)		2929.0	$r'_9 ( 100)$
$\nu_{58}$	1530.0	5.686	1407.1	( 1469.0)		1468.6	$\delta_s ( 2) ( 94)$
$\nu_{59}$	1513.8	5.931	1511.6	( 1456.0)		1456.2	$\delta_s ( 1) ( 92)$
$\nu_{60}$	1076.0	3.310	1053.9	1038.5	2.938	1044.5	$\rho ( 1) ( 51) + \delta_a ( 2) ( 19) + \rho ( 2) ( 11)$
$\nu_{61}$	1074.3	3.063	1029.9	( 1038.0)		1035.9	$\delta_9 ( 53) + \delta_a ( 1) ( 18)$
$\nu_{62}$	986.1	0.027	987.2	( 973.0)		971.2	$\gamma_6 ( 26) + \gamma_7 ( 25) + \gamma_8 ( 19)$
$\nu_{63}$	972.7	0.016	975.0	( 960.0)		956.6	$\gamma'_3 ( 46) + \gamma_4 ( 28)$
$\nu_{64}$	945.7	2.141	953.9	( 937.0)		934.5	$\gamma_8 ( 41) + \gamma_6 ( 27) + \gamma_5 ( 14)$
$\nu_{65}$	903.7	8.070	895.3	885.3	4.505	883.7	$\gamma_2 ( 43) + \rho ( 2) ( 39)$
$\nu_{66}$	885.6	16.731	875.3	864.2	29.969	863.3	$\rho ( 2) ( 22) + \gamma_5 ( 16)$
$\nu_{67}$	876.0	4.954	867.1	( 855.0)		855.1	$\rho ( 2) ( 21) + \gamma_2 ( 20) + \gamma_5 ( 13) + \gamma_9 ( 12)$
$\nu_{68}$	828.0	19.735	824.5	806.4	24.190	811.9	$\gamma_4 ( 26) + \gamma'_3 ( 25) + \gamma_2 ( 13)$
$\nu_{69}$	809.2	0.656	821.4	( 791.0)		795.5	$\tau_2 ( 33) + \tau_5 ( 19) + \gamma_9 ( 11) + \gamma_7 ( 10)$
$\nu_{70}$	761.7	29.636	756.4	742.7	47.598	744.6	$\gamma_5 ( 26) + \gamma_7 ( 21) + \gamma_6 ( 19) + \gamma_8 ( 12)$
$\nu_{71}$	726.6	4.632	738.2	708.7	16.159	708.4	$\tau_5 ( 36) + \gamma_9 ( 32)$
$\nu_{72}$	617.0	1.768	618.0	603.2	3.525	602.5	$\tau_2 ( 17) + \tau_5 ( 14) + \gamma_9 ( 13)$
$\nu_{73}$	588.2	0.167	586.5	( 572.0)		570.8	$\gamma'_1 ( 17) + \gamma_{10} ( 16) + \tau_8 ( 13) + \gamma_9 ( 11)$
$\nu_{74}$	533.3	0.166	528.2	( 521.0)		521.0	$\tau_7 ( 25) + \gamma'_1 ( 13) + \gamma_{10} ( 12) + \tau_5 ( 11)$
$\nu_{75}$	494.3	2.642	489.6	( 480.0)		483.2	$\rho ( 2) ( 25) + \tau_1 ( 17) + \tau_9 ( 15) + \tau_6 ( 14)$
$\nu_{76}$	422.5	0.540	409.4	( 411.0)		411.1	$\tau_6 ( 44) + \tau_3 ( 12)$
$\nu_{77}$	358.7	0.999	341.3	( 344.0)		344.6	$\tau_{ring} ( 43) + \tau_7 ( 13)$
$\nu_{78}$	331.4	0.460	337.1	( 319.0)		317.4	$\tau_{ring} ( 31) + \tau_6 ( 16) + \gamma'_1 ( 12) + \tau_8 ( 11)$
$\nu_{79}$	233.1	0.910	233.4	( 224.0)		224.9	$\tau_1 ( 22) + \tau_9 ( 15) + \tau_6 ( 12) + \tau_4 ( 12)$
$\nu_{80}$	189.5	2.366	187.5	( 183.0)		182.6	$\tau_1 ( 34) + \rho ( 2) ( 10)$
$\nu_{81}$	180.0	0.345	177.3	( 174.0)		174.9	$\gamma'_1 ( 15) + \tau_7 ( 14) + \tau_4 ( 13)$
$\nu_{82}$	79.4	0.007	64.4	( 76.0)		76.5	$\tau_{ring} ( 32) + \tau_3 ( 17) + \tau_8 ( 13) + \tau_7 ( 11)$
$\nu_{83}$	67.7	0.418	55.3	( 65.0)		64.5	$\tau_{ring} ( 40) + \tau_3 ( 16)$
$\nu_{84}$	-11.6	0.001	-95.5	( 15.0)		nan	$\tau_{ring} ( 41) + \tau_3 ( 12) + \gamma_{10} ( 11)$

Since the fitting algorithm required all the experimental frequencies, the numbers in parenthesis are introduced as good guesses for 2, 4 – DMP and do not have any other significance. RMS error is  $2.4226\text{ cm}^{-1}$  for the fitting of experimental frequencies.

Table 5.5(c): Calculated harmonic, anharmonic frequencies (in  $cm^{-1}$ ) and intensities (in  $km/mol$ ) at  $B3LYP/6-31G^*$ , observed frequencies (in  $cm^{-1}$ ) and intensities (in  $km/mol$ ), fitted frequencies (in  $cm^{-1}$ ) and PED of 3, 9 – DMP.

Sym Mode	B3LYP/6-31G*			Observed		Force field	
	Harm.	Int.	Anharm.	Freq.	Int.	Fitted	PED
$A'$							
$\nu_1$	3223.3	21.701	3077.0	3085.7	19.159	3085.7	$r_5$ ( 96)
$\nu_2$	3217.4	32.672	3081.7	3062.5	13.063	3062.5	$r_8$ ( 92)
$\nu_3$	3202.4	7.123	3058.7	3029.1	10.757	3029.4	$r_1$ ( 49) + $r_7$ ( 44)
$\nu_4$	3196.4	12.566	3045.9	(3029.0)		3028.7	$r_1$ ( 47) + $r_7$ ( 46)
$\nu_5$	3190.8	43.623	3059.5	2978.9	10.668	2978.9	$r_6$ ( 93)
$\nu_6$	3184.2	2.660	3041.5	(2978.0)		2978.1	$r_3$ ( 77) + $r_2$ ( 19)
$\nu_7$	3173.5	21.030	3026.2	2956.3	5.660	2957.0	$r_4$ ( 49) + $r_2$ ( 43)
$\nu_8$	3170.2	7.174	3026.9	(2956.0)		2955.2	$r_4$ ( 48) + $r_2$ ( 36) + $r_3$ ( 14)
$\nu_9$	3127.7	17.218	2982.7	2933.5	51.838	2936.5	$r'_{12}$ ( 75) + $r'_{11}$ ( 22)
$\nu_{10}$	3124.3	15.728	2976.8	(2933.0)		2936.2	$r'_{10}$ ( 75) + $r'_9$ ( 24)
$\nu_{11}$	3039.6	37.050	2991.6	2875.0	19.377	2865.5	$r'_{11}$ ( 65) + $r'_{12}$ ( 19) + $r'_9$ ( 12)
$\nu_{12}$	3038.0	46.760	2980.2	(2875.0)		2865.1	$r'_9$ ( 64) + $r'_{10}$ ( 20) + $r'_{11}$ ( 12)
$\nu_{13}$	1680.4	0.288	1642.0	(1632.0)		1632.1	$R_{10}$ ( 43) + $\beta_3$ ( 10)
$\nu_{14}$	1675.4	15.146	1635.6	1620.8	24.167	1623.5	$R_4$ ( 18)
$\nu_{15}$	1666.0	6.173	1625.3	(1614.2)		1615.2	$R_{15}$ ( 17) + $R_{13}$ ( 16)
$\nu_{16}$	1620.2	0.454	1580.9	(1574.0)		1574.2	$R_6$ ( 12) + $R_{14}$ ( 12)
$\nu_{17}$	1578.3	0.623	1538.8	(1530.0)		1531.3	$R_3$ ( 16) + $R_{14}$ ( 13)
$\nu_{18}$	1556.4	17.345	1521.6	1508.8	20.030	1509.1	$\beta_7$ ( 10)
$\nu_{19}$	1531.6	2.139	1469.4	(1476.0)		1475.9	$\delta_s(2)$ ( 77)
$\nu_{20}$	1522.8	15.292	1479.8	1460.6	34.618	1460.8	$\delta_s(1)$ ( 63)
$\nu_{21}$	1496.4	5.066	1466.9	(1437.0)		1440.8	$\beta'_6$ ( 17)
$\nu_{22}$	1477.1	4.294	1444.9	(1431.0)		1427.8	$\beta_8$ ( 18) + $\beta_5$ ( 11)
$\nu_{23}$	1461.0	1.702	1430.6	(1417.0)		1411.4	$R_1$ ( 17) + $\delta_s(1)$ ( 13)
$\nu_{24}$	1442.1	1.179	1431.7	1388.3	12.410	1391.8	$R_9$ ( 20) + $\rho(1)$ ( 14) + $\beta_3$ ( 12)
$\nu_{25}$	1441.7	2.979	1431.0	(1387.0)		1387.0	$\delta_8$ ( 86)
$\nu_{26}$	1432.3	2.922	1403.8	(1385.0)		1384.5	$\rho(1)$ ( 72)
$\nu_{27}$	1398.0	1.220	1363.8	(1349.0)		1350.7	$R_6$ ( 20) + $R_2$ ( 17) + $R_4$ ( 15)
$\nu_{28}$	1373.2	1.350	1345.5	1327.6	0.870	1330.1	$R_8$ (25) + $R_{13}$ (12) + $R_{16}$ (11) + $R_{15}$ (10)
$\nu_{29}$	1337.5	1.189	1315.1	1296.3	1.088	1297.6	$\beta_9$ ( 14) + $\beta_1$ ( 12) + $R_{11}$ ( 12)
$\nu_{30}$	1318.5	0.032	1297.4	(1260.0)		1266.2	$\delta_2$ ( 19) + $\beta_5$ ( 15) + $\beta_8$ ( 11)
$\nu_{31}$	1282.5	1.930	1264.0	(1244.0)		1241.4	$\beta_3$ ( 15) + $R_{16}$ ( 14) + $\beta_8$ ( 13)
$\nu_{32}$	1258.2	1.388	1234.8	1215.2	0.653	1216.3	$R_1$ ( 18) + $R_{11}$ ( 13)
$\nu_{33}$	1244.7	0.986	1226.3	(1207.0)		1205.8	$\beta_3$ ( 28) + $R_5$ ( 16)
$\nu_{34}$	1220.5	2.387	1196.5	1185.0	0.653	1186.0	$R'_{17}$ ( 19) + $R_7$ ( 13) + $r'_{13}$ ( 13)
$\nu_{35}$	1201.8	1.052	1185.5	1166.5	1.306	1166.2	$\beta_7$ ( 37) + $\beta'_6$ ( 11)
$\nu_{36}$	1185.2	2.603	1170.4	1150.0	1.524	1146.5	$\beta'_6$ (20) + $\beta_2$ (16) + $\beta_1$ (14) + $\beta_5$ (12)
$\nu_{37}$	1146.2	0.079	1129.3	(1116.0)		1116.8	$\beta'_6$ ( 12)
$\nu_{38}$	1097.0	0.180	1078.0	(1066.0)		1065.2	$\delta_5$ ( 19) + $\delta_a(2)$ ( 16) + $R'_{18}$ ( 14)
$\nu_{39}$	1071.5	4.170	1058.4	1040.4	9.797	1040.5	$R_{14}$ ( 41) + $\delta_5$ ( 14)
$\nu_{40}$	1061.7	5.500	1047.9	(1036.0)		1034.6	$\beta_9$ ( 29) + $\delta_5$ ( 13)
$\nu_{41}$	1025.1	6.228	1012.0	999.6	3.701	999.4	$\delta_a(2)$ (31) + $\delta_5$ (12) + $\rho(1)$ (10) + $R'_{18}$ (10)
$\nu_{42}$	1012.4	1.024	996.5	( 982.0)		981.6	$\delta_a(1)$ ( 38) + $\delta_9$ ( 12) + $R_3$ ( 11)
$\nu_{43}$	913.0	1.800	901.3	( 892.0)		891.6	$\delta_1$ ( 14) + $\delta_5$ ( 12)
$\nu_{44}$	845.2	0.028	835.5	( 826.0)		826.5	$\beta_9$ ( 16) + $\delta_2$ ( 13)

Table 5.5(c): (Continued) Calculated harmonic, anharmonic frequencies (in  $cm^{-1}$ ) and intensities (in  $km/mol$ ) at  $B3LYP/6-31G^*$ , observed frequencies (in  $cm^{-1}$ ) and intensities (in  $km/mol$ ), fitted frequencies (in  $cm^{-1}$ ) and PED of 3,9 – DMP.

Sym Mode	B3LYP/6-31G*			Observed		Force field	
	Harm.	Int.	Anharm.	Freq.	Int.	Fitted	PED
$\nu_{45}$	766.2	0.983	754.0	( 750.0)		749.6	$\delta_7$ ( 23) + $R_9$ ( 12) + $\delta_2$ ( 10)
$\nu_{46}$	722.3	0.245	714.3	( 707.0)		706.9	$\beta_{10}$ ( 33) + $\delta_6$ ( 16)
$\nu_{47}$	641.7	3.798	635.5	629.1	2.394	629.5	$\delta_6$ ( 44) + $\beta_{10}$ ( 19)
$\nu_{48}$	608.1	1.718	602.9	( 596.0)		595.6	$\delta_2$ ( 21) + $R'_{18}$ ( 11) + $\beta_{10}$ ( 10)
$\nu_{49}$	544.5	0.605	543.1	( 534.0)		533.4	$\delta_1$ ( 25) + $\delta_7$ ( 25) + $\beta_4$ ( 23)
$\nu_{50}$	505.6	0.560	499.1	( 495.0)		494.0	$\delta_4$ ( 31)
$\nu_{51}$	437.1	1.295	433.1	( 429.0)		429.1	$\delta_3$ ( 40) + $r'_{14}$ ( 18) + $\delta_4$ ( 13)
$\nu_{52}$	399.0	0.203	395.8	( 390.0)		389.8	$\delta_4$ ( 23) + $\beta_{10}$ ( 14) + $R_7$ ( 13)
$\nu_{53}$	340.6	0.475	343.6	( 333.0)		332.9	$r'_{14}$ ( 39) + $\delta_1$ ( 19) + $\delta_3$ ( 10)
$\nu_{54}$	288.6	0.501	286.8	( 281.0)		281.1	$\beta_4$ ( 62) + $\delta_7$ ( 10)
$\nu_{55}$	192.6	0.444	195.1	( 188.0)		188.2	$r'_{14}$ ( 33)
$A''$							
$\nu_{56}$	3089.5	21.865	2925.4	2908.2	7.838	2915.3	$r'_{11}$ ( 98)
$\nu_{57}$	3087.0	20.419	2927.8	(2908.0)		2915.1	$r'_9$ ( 98)
$\nu_{58}$	1513.5	4.711	1525.2	(1453.5)		1453.3	$\delta_s(1)$ ( 92)
$\nu_{59}$	1513.4	7.105	1529.0	(1453.0)		1452.9	$\delta_s(2)$ ( 93)
$\nu_{60}$	1078.4	1.352	1055.6	(1042.0)		1043.3	$\rho(1)$ ( 53) + $\delta_a(2)$ ( 19)
$\nu_{61}$	1074.9	4.802	1048.4	(1039.0)		1040.8	$\delta_9$ ( 50) + $\delta_a(1)$ ( 17) + $\rho(2)$ ( 10)
$\nu_{62}$	981.8	0.002	972.8	( 970.0)		969.6	$\gamma_7$ ( 33) + $\gamma'_6$ ( 30) + $\gamma_8$ ( 19)
$\nu_{63}$	962.4	0.972	960.1	948.7	0.879	946.3	$\gamma'_2$ ( 55) + $\gamma_1$ ( 30)
$\nu_{64}$	943.6	1.650	947.0	( 935.0)		933.5	$\gamma_8$ ( 37) + $\gamma'_6$ ( 30) + $\gamma_5$ ( 16)
$\nu_{65}$	904.9	15.499	895.1	879.1	33.094	879.2	$\rho(2)$ ( 36) + $\gamma_3$ ( 31)
$\nu_{66}$	883.3	7.322	880.6	( 871.7)		870.7	$\gamma_3$ ( 45) + $\rho(2)$ ( 34)
$\nu_{67}$	876.4	0.009	874.3	( 856.0)		856.8	$\gamma_5$ ( 32) + $\gamma_8$ ( 14) + $\tau_5$ ( 14) + $\tau_2$ ( 12) + $\gamma_7$ ( 12)
$\nu_{68}$	822.3	11.194	814.1	801.8	16.982	805.5	$\gamma_1$ ( 43) + $\gamma'_2$ ( 29)
$\nu_{69}$	796.7	4.090	787.1	( 779.0)		780.0	$\tau_2$ ( 30) + $\tau_5$ ( 23) + $\gamma_7$ ( 15) + $\gamma_9$ ( 14)
$\nu_{70}$	772.0	35.830	766.8	753.9	62.487	754.5	$\gamma'_6$ ( 25) + $\gamma_5$ ( 24) + $\gamma_8$ ( 11) + $\gamma_7$ ( 10)
$\nu_{70}$	738.0	5.947	735.5	723.6	8.055	725.5	$\gamma_9$ ( 44) + $\tau_5$ ( 26)
$\nu_{72}$	611.5	0.719	603.3	602.1	4.572	600.2	$\tau_5$ ( 23) + $\tau_2$ ( 15) + $\gamma_9$ ( 13) + $\rho(2)$ ( 12)
$\nu_{73}$	591.3	4.534	584.5	573.6	6.749	570.3	$\gamma_4$ ( 23) + $\tau_4$ ( 13) + $\gamma_{10}$ ( 11) + $\rho(2)$ ( 10)
$\nu_{74}$	526.8	1.569	517.4	( 511.0)		511.2	$\tau_3$ ( 18) + $\tau_7$ ( 18) + $\tau_1$ ( 15) + $\tau_8$ ( 14) + $\rho(2)$ ( 11)
$\nu_{75}$	448.1	1.043	442.0	( 435.0)		435.5	$\tau_6$ ( 23) + $\tau_1$ ( 21), $\gamma_{10}$ ( 18) + $\tau_8$ ( 13)
$\nu_{76}$	425.8	0.523	419.6	( 414.0)		413.8	$\tau_6$ ( 38) + $\tau_9$ ( 11) + $\gamma_4$ ( 10)
$\nu_{77}$	359.3	1.246	355.7	( 350.0)		349.2	$\rho(2)$ ( 23) + $\gamma_4$ ( 16) + $\tau_1$ ( 13)
$\nu_{78}$	249.1	0.255	241.9	( 241.0)		241.1	$\tau_6$ ( 24) + $\gamma_{10}$ ( 23) + $\tau_9$ ( 15)
$\nu_{79}$	226.0	0.246	185.3	( 215.0)		214.8	$\tau_{ring}$ ( 62)
$\nu_{80}$	197.1	0.007	173.3	( 189.0)		189.5	$\tau_{ring}$ ( 26) + $\tau_1$ ( 16) + $\tau_3$ ( 13)
$\nu_{81}$	137.6	1.599	138.8	( 132.0)		132.3	$\tau_7$ ( 19) + $\gamma_4$ ( 15) + $\tau_9$ ( 13) + $\tau_2$ ( 11)
$\nu_{82}$	98.5	0.104	92.9	( 94.0)		94.3	$\tau_4$ ( 26) + $\tau_9$ ( 15) + $\tau_7$ ( 13) + $\tau_3$ ( 12)
$\nu_{83}$	79.6	0.243	-44.6	( 77.0)		77.0	$\tau_{ring}$ ( 72)
$\nu_{84}$	63.8	0.323	62.6	( 61.0)		60.9	$\tau_3$ ( 25) + $\tau_4$ ( 13) + $\tau_1$ ( 12)

Since the fitting algorithm required all the experimental frequencies, the numbers in parenthesis are introduced as good guesses for 3,9 – DMP and do not have any other significance. RMS error is  $2.5541\text{ cm}^{-1}$  for the fitting of experimental frequencies.

2866.0, 2884.9, and 2867.0  $\text{cm}^{-1}$  in the three DMPs. This band is of low intensity in 1,9-DMP and of moderate intensity in the other two isomers. From tables it is clear that the anharmonic frequencies of the antisymmetric/symmetric methyl C-H vibrations are overestimated /underestimated in the DFT calculations by about 20 and 30  $\text{cm}^{-1}$  for 6-31G\* and 6-311G\*\* basis sets, respectively. It is also found that the absolute intensities of the C-H stretching bands do not match well with the calculated band intensities since the bands are not well resolved.

#### **5.4.2 Spectral region 1700 – 2800 $\text{cm}^{-1}$ : Non-fundamental bands**

A limited number of bands is observed in this region which do not correspond to any calculated fundamentals (see Table 5.6). Initially, non-fundamental bands are tentatively assigned using calculated anharmonic frequencies obtained at the B3LYP/6-311G\*\* level since the calculated frequencies at the B3LYP/6-31G\* level of theory deviate from the frequencies at the B3LYP/6-311G\*\* level by more than 100  $\text{cm}^{-1}$  in some instances (see Table 5.3). The assignment is then confirmed by force field fitted frequencies. There are many possibilities for the assignment of the observed non-fundamental bands with the calculated ones. However, we have assigned these bands by correlating with the fundamental bands that are intense.

The band observed at 1915.5  $\text{cm}^{-1}$  in 1,9-DMP, 1912.5  $\text{cm}^{-1}$  in 2,4-DMP and 1913.8  $\text{cm}^{-1}$  in 3,9-DMP can be correlated with the calculated anharmonic band at 1922.4  $\text{cm}^{-1}$  in 1,9-DMP, 1952.9  $\text{cm}^{-1}$  in 2,4-DMP, and 1931.5  $\text{cm}^{-1}$  in 3,9-DMP, respectively. Their respective scaled force field fitted frequencies are 1908.0, 1916.9, and 1919.9  $\text{cm}^{-1}$ . This band is assigned to a combination of ( $\nu_{66} + \nu_{40}$ ) for 1,9-DMP, ( $\nu_{66} + \nu_{38}$ ) for 2,4-DMP and ( $\nu_{65} + \nu_{39}$ ) for 3,9-DMP. The next band observed at 1944.8, 1943.1, and 1942.9  $\text{cm}^{-1}$  for 1,9-, 2,4- and 3,9-DMP,

respectively, is assigned as the first overtone of  $\nu_{40}$ ,  $\nu_{41}$  and  $\nu_{39}$  in 1,9-, 2,4- and 3,9-DMP, respectively.

**Table 5.6: Comparison of the observed, anharmonic and force field fitted non-fundamental frequencies (in  $\text{cm}^{-1}$ ).**

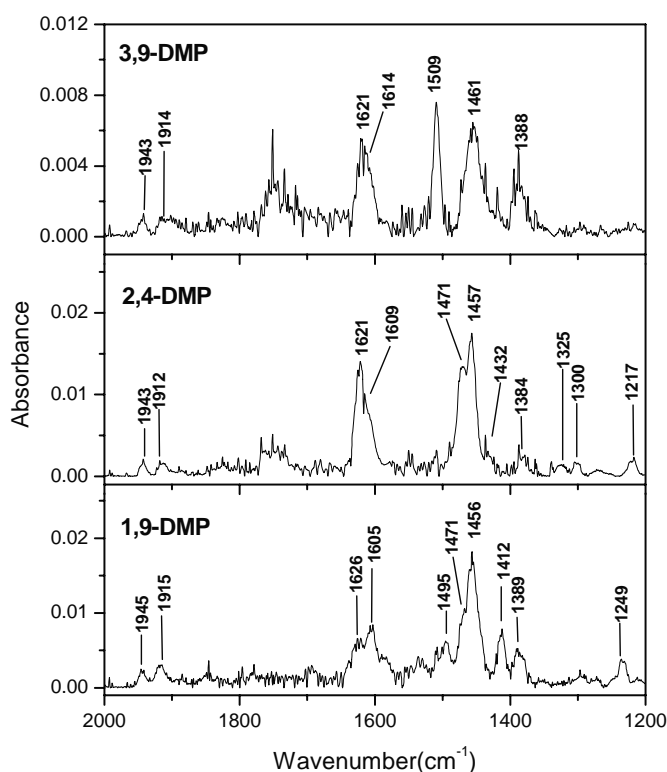
Compound	Observed		Anharmonic		Fitted	Assignment	
	Freq.	Int.	6-311G**	6-31G*	6-311G**	Overtone	Combination
1,9-DMP	1915.5	2.37	1922.4	1943.7	1908.0		$\nu_{66} + \nu_{40}$
	1944.8	1.18	2078.8	2099.4	2073.0	$2\nu_{40}$	
	2745.5	1.18	2751.0	2817.3	2781.2	$2\nu_{24}$	
2,4-DMP	1912.5	2.05	1952.9	1965.7	1916.9		$\nu_{66} + \nu_{38}$
	1943.1	1.66	1989.0	1997.3	1990.2	$2\nu_{41}$	
	2744.4	1.56	2896.6	2930.0	2908.8	$2\nu_{21}$	
3,9-DMP	1913.8	3.91	1931.5	2159.2	1919.9		$\nu_{65} + \nu_{39}$
	1942.9	2.61	2096.0	2115.3	2081.6	$2\nu_{39}$	
	2743.5	2.39	2774.7	2836.4	2781.6	$2\nu_{24}$	

*In the 5<sup>th</sup> column,  $\nu_i$  is the frequency of the  $i$ -th fundamental vibration. For description see Tables 5.4 and 5.5. All intensities are in  $\text{km mol}^{-1}$ .*

DFT calculated non-fundamental anharmonic band at 2078.8, 1989.0, and 2096.0  $\text{cm}^{-1}$  is correlated with the observed ones. This band can also be correlated with the force field fitted frequencies at 2073.0  $\text{cm}^{-1}$  in 1,9-DMP, 1990.2  $\text{cm}^{-1}$  in 2,4-DMP, and 2081.6  $\text{cm}^{-1}$  in 3,9-DMP. Another band found at 2745.5  $\text{cm}^{-1}$  in 1,9-DMP, 2744.4  $\text{cm}^{-1}$  in 2,4-DMP, and 2743.5  $\text{cm}^{-1}$  in 3,9-DMP corresponds to the calculated anharmonic band at 2751.0  $\text{cm}^{-1}$  in 1,9-DMP, 2896.6  $\text{cm}^{-1}$  in 2,4-DMP, and 2774.7  $\text{cm}^{-1}$  in 3,9-DMP which is also a first overtone of  $\nu_{24}$  for 1,9-



DMP,  $\nu_{21}$  for 2,4-DMP, and  $\nu_{24}$  for 3,9-DMP, respectively. Their respective force field fitted frequency is  $2781.2\text{ cm}^{-1}$  in 1,9-DMP,  $2908.8\text{ cm}^{-1}$  in 2,4-DMP and  $2781.6\text{ cm}^{-1}$  in 3,9-DMP. The deviation between observed non-fundamental frequencies and force field fitted frequencies calculated with 6-311G\*\* basis set is found to be  $63\text{ cm}^{-1}$  in the worse case. On the otherhand calculated anharmonic frequencies differ by  $65\text{ cm}^{-1}$  from the experimental frequencies (see Table 5.3). Therefore, it is clear that for the assignment of non-fundamental bands either scaled force fields or anharmonic calculation can be used.



**Figure 5.3.** Expanded gas phase IR spectra of 1,9-, 2,4- and 3,9 - DMPs from  $1200$  to  $2000\text{ cm}^{-1}$  at  $0.5\text{ cm}^{-1}$  resolution.

### 5.4.3 Spectral region $1200 - 1700\text{ cm}^{-1}$

Several bands have been identified in this region and they belong to  $A'$  irreducible representation. Assignment in the  $1400 - 1700\text{ cm}^{-1}$  region is difficult because of the presence

of H<sub>2</sub>O bands. However, we could assign a few bands in this region after subtracting the H<sub>2</sub>O spectrum. Bands observed at 1626.5 and 1604.6 cm<sup>-1</sup> in 1,9-DMP; 1621.4 and 1609.1 cm<sup>-1</sup> in 2,4-DMP; 1620.8 and 1614.2 cm<sup>-1</sup> in 3,9-DMP are assigned to aromatic C-C stretching vibrations. Their respective force field fitted frequencies are 1626.9 and 1604.9 cm<sup>-1</sup> in 1,9-DMP; 1624.0 and 1609.9 cm<sup>-1</sup> in 2,4-DMP; 1623.6 and 1614.6 cm<sup>-1</sup> in 3,9-DMP. These bands have low intensity in 1,9-DMP and moderate intensities in 2,4- and 3,9-DMP although they are not well resolved.

Another low intensity band found at 1495.4 cm<sup>-1</sup> in 1,9-DMP is correlated with the force field fitted frequency at 1495.3 cm<sup>-1</sup> whereas in 3,9-DMP, another moderate intensity band seen at 1508.8 cm<sup>-1</sup> corresponds to the force field fitted frequencies at 1507.9 cm<sup>-1</sup>. This band is assigned to aromatic C-C stretching vibration (R) in 1,9-DMP and aromatic C-H in-plane bending ( $\beta$ ) vibrations in 3,9-DMP. A pair of bands seen at 1471.2 and 1456.0 cm<sup>-1</sup> in 1,9-DMP; 1470.9 and 1457.4 cm<sup>-1</sup> in 2,4-DMP; 1460.6 and 1453.5 cm<sup>-1</sup> in 3,9-DMP have been assigned to methyl C-H asymmetric deformation vibrations ( $\delta_s$ ) by comparing with the force field fitted frequencies at 1473.9 and 1455.7 cm<sup>-1</sup> in 1,9-DMP; 1471.5 and 1460.2 cm<sup>-1</sup> in 2,4-DMP; 1460.8 and 1453.2 cm<sup>-1</sup> in 3,9-DMP, respectively. We could not measure individual band intensity in this region since bands are not well separated in the recorded spectra (see Figure 5.3). However, the total intensity of the observed bands is comparable with the sum of the calculated individual band intensity. In 2,4-DMP calculated anharmonic frequency corresponds to observed band at 1470.9 cm<sup>-1</sup> is underestimated by 60 cm<sup>-1</sup> with 6-311G\*\* basis set whereas it is overestimated by 25 cm<sup>-1</sup> with 6-31G\* basis set (see Tables 5.4b and 5.5b). A low intensity band observed at 1412.4 cm<sup>-1</sup> in 1,9-DMP and at 1384.4 cm<sup>-1</sup> in 2,4-DMP has been assigned to aromatic C-H in-plane bending vibration ( $\beta$ ) by comparing with

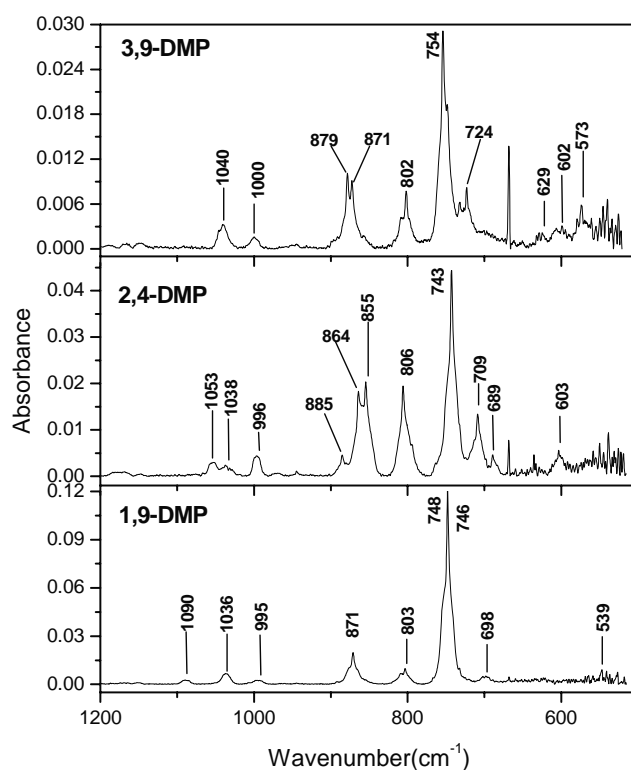
the scaled force field fitted frequencies at 1413.5 cm<sup>-1</sup> in 1,9-DMP and 1429.6 cm<sup>-1</sup> in 2,4-DMP, respectively. This band is not observed in 3,9-DMP, perhaps, it has been masked by the strong band at 1460.6 cm<sup>-1</sup>.

The next low intensity band observed at 1389.5, 1384.4, and 1388.3 cm<sup>-1</sup> for 1,9-DMP, 2,4-DMP and 3,9-DMP, respectively, corresponds to the force field fitted frequencies at 1390.6, 1384.4, and 1390.8 cm<sup>-1</sup> for 1,9-, 2,4-, and 3,9-DMP. This band is unique for different isomers of DMP and is assigned to a mixture of in-plane aromatic ring deformation ( $\delta$ ) and out-of-plane methyl rocking vibration ( $\rho$ ) in 1,9-DMP, out-of-plane methyl rocking vibration ( $\rho$ ) in 2,4-DMP and a mixture of out-of-plane methyl rocking ( $\rho$ ) and aromatic C-C stretching vibrations (R) in 3,9-DMP.

Another low intensity band observed at 1296.1cm<sup>-1</sup> in 1,9-DMP; 1300.0 cm<sup>-1</sup> in 2,4-DMP; 1296.0 cm<sup>-1</sup> in 3,9-DMP is correlated with the force field fitted frequencies at 1295.2 cm<sup>-1</sup> in 1,9-DMP, 1298.6 cm<sup>-1</sup> in 2,4-DMP, and 1296.6 cm<sup>-1</sup> in 3,9-DMP. This band is assigned to aromatic C-C stretching (R) vibration in 1,9- and 2,4-DMP and aromatic C-H in-plane bending ( $\beta$ ) vibration in 3,9-DMP. A low intensity band found at 1213.0, 1217.4, and 1215.2 cm<sup>-1</sup> for 1,9-, 2,4-, and 3,9-DMP, respectively, is assigned to aromatic C-C stretching vibration (R) in 1,9- and 3,9-DMP and aromatic C-H in-plane bending vibration ( $\beta$ ) in 2,4-DMP by comparing with the force field fitted frequency at 1213.4, 1218.2, and 1215.9 cm<sup>-1</sup> for 1,9-, 2,4-, and 3,9-DMP, respectively. The calculated anharmonic frequencies deviates by about 15 and 10 cm<sup>-1</sup> with the 6-31G\* and 6-311G\*\* basis sets, respectively (see Tables 5.4a and 5.5a). On the other hand, the force field fitted frequencies match well within 2 cm<sup>-1</sup> with the observed frequencies in this region.

5.4.4 Spectral region 500 – 1200  $\text{cm}^{-1}$ 

Bands observed in this region belong to both the  $A'$  and  $A''$  irreducible representations. The band observed at  $1185.0 \text{ cm}^{-1}$  in 3,9-DMP is assigned to a mixture of aromatic-methyl C-C stretching ( $R'$ ) and aromatic C-C stretching ( $R$ ) vibrations by comparing with the force field fitted frequency at  $1184.9 \text{ cm}^{-1}$  and DFT predicted anharmonic frequency at  $1183.8 \text{ cm}^{-1}$ . This band is of low intensity and is not observed in the rest of the isomers of DMP.



**Figure 5.4. Expanded gas phase IR spectra of 1,9-, 2,4- and 3,9 - DMPs from 500 to 1200  $\text{cm}^{-1}$  at 0.5  $\text{cm}^{-1}$  resolution.**

A low intensity band observed at  $1170.6 \text{ cm}^{-1}$  in 2,4-DMP and  $1166.5 \text{ cm}^{-1}$  in 3,9-DMP corresponds to aromatic C-H in-plane bending vibration ( $\beta$ ) by comparing with the scaled force fitted frequency at  $1169.8 \text{ cm}^{-1}$  in 2,4-DMP and  $1167.0 \text{ cm}^{-1}$  in 1,9-DMP, respectively.

The next band observed at  $1152.7\text{ cm}^{-1}$  in 1,9-DMP at  $1148.6\text{ cm}^{-1}$  in 2,4-DMP, and at  $1150.0\text{ cm}^{-1}$  in 3,9-DMP is of low intensity and corresponds to the force field fitted frequencies at  $1151.7\text{ cm}^{-1}$  in 1,9-DMP,  $1150.3\text{ cm}^{-1}$  in 2,4-DMP and  $1146.2\text{ cm}^{-1}$  in 3,9-DMP, respectively. It is assigned to the aromatic C-C stretching vibration (R) in 1,9-DMP, the aromatic C-H in-plane bending vibrations ( $\beta$ ) in 2,4-DMP and a mixture of aromatic methyl C-C stretching (R') and aromatic C-H in-plane-bending vibration ( $\beta$ ) in 3,9-DMP. Another weak band observed at  $1036.4\text{ cm}^{-1}$  in 1,9-DMP,  $1053.2\text{ cm}^{-1}$  in 2,4-DMP and  $1040.4\text{ cm}^{-1}$  in 3,9-DMP is correlated with the scaled force fitted frequency at  $1036.5\text{ cm}^{-1}$  in 1,9-DMP,  $1053.9\text{ cm}^{-1}$  in 2,4-DMP and  $1040.8\text{ cm}^{-1}$  in 3,9-DMP, respectively. This band is assigned as an aromatic C-C stretching vibration in 1,9- and 2,4-DMP and a mixture of aromatic C-C stretching (R) and aromatic ring deformation vibrations ( $\delta$ ) in 3,9-DMP.

The next one set of low intensity band observed at  $995.3$ ,  $996.4$  and  $999.6\text{ cm}^{-1}$  for 1,9-, 2,4- and 3,9-DMP, respectively, is assigned to methyl C-H symmetric deformation vibration ( $\delta_a$ ) for 1,9- and 3,9-DMP whereas in 2,4-DMP it is assigned to an aromatic C-H in-plane bending vibration ( $\beta$ ). The respective scaled force field fitted frequency is  $993.6$ ,  $995.1$  and  $999.4\text{ cm}^{-1}$  in 1,9-, 2,4- and 3,9-DMP. This band belongs to A' irreducible representation.

A band of low intensity observed at  $885.3\text{ cm}^{-1}$  in 2,4-DMP is assigned to a mixture of methyl rocking ( $\rho$ ) and aromatic C-H out-of-plane ( $\gamma$ ) vibration by comparing with the scaled force field fitted frequency at  $885.3\text{ cm}^{-1}$ . A moderately intense band observed at  $871.4\text{ cm}^{-1}$  in 1,9-DMP is assigned to aromatic C-H in-plane bending vibration ( $\beta$ ). On the other hand, in 2,4- and 3,9-DMP this band appears as a doublet, at  $864.2$  and  $855.0\text{ cm}^{-1}$  and  $879.1$  and  $871.7\text{ cm}^{-1}$ , respectively, due to a mixture of local coordinate vibrations of aromatic C-H out-of-plane ( $\gamma$ ) and methyl rocking ( $\rho$ ). A band observed at  $803.5\text{ cm}^{-1}$  in 1,9-DMP,  $806.4\text{ cm}^{-1}$  in

2,4-DMP and  $801.8\text{ cm}^{-1}$  in 3,9-DMP corresponds to the force field fitted frequencies at  $801.9\text{ cm}^{-1}$  in 1,9-DMP,  $808.5\text{ cm}^{-1}$  in 2,4-DMP and  $801.7\text{ cm}^{-1}$  for 3,9-DMP. This band is of moderate intensity and is assigned to the aromatic C-H out-of-plane bending vibration in 1,9-DMP and a mixture of local coordinate vibrations of aromatic-methyl C-C stretching ( $R$ ) and aromatic C-H out-plane-bending ( $\gamma$ ) in 2,4- and 3,9-DMP. A highly intense band observed at  $748.3/746.0\text{ cm}^{-1}$  in 1,9-DMP,  $742.7\text{ cm}^{-1}$  in 2,4-DMP and  $753.9\text{ cm}^{-1}$  in 3,9-DMP corresponds to the force field fitted band at  $749.0/746.7\text{ cm}^{-1}$  in 1,9-DMP,  $741.4\text{ cm}^{-1}$  in 2,4-DMP and  $753.4\text{ cm}^{-1}$  in 3,9-DMP, respectively, which is assigned to the aromatic C-H out-of-plane bending vibration ( $\gamma$ ). A band observed at  $708.7\text{ cm}^{-1}$  in 2,4-DMP and at  $723.6\text{ cm}^{-1}$  in 3,9-DMP is of low intensity and match well with the force field fitted frequency at  $708.0\text{ cm}^{-1}$  in 2,4-DMP and  $724.1\text{ cm}^{-1}$  in 3,9-DMP, respectively. This band is assigned to a mixture of local coordinate vibrations of torsion around C-C bond ( $\tau$ ) and an aromatic C-H out-of-plane bending ( $\gamma$ ).

Next a low intensity band observed at  $698.5\text{ cm}^{-1}$  in 1,9-DMP,  $688.7\text{ cm}^{-1}$  in 2,4-DMP, and  $629.1\text{ cm}^{-1}$  in 3,9-DMP is correlated with the force field fitted frequency at  $697.8\text{ cm}^{-1}$  in 1,9-DMP,  $688.1\text{ cm}^{-1}$  in 2,4-DMP, and  $629.2\text{ cm}^{-1}$  in 3,9-DMP, respectively. This band is assigned to in-plane aromatic ring deformation vibration ( $\delta$ ). A band observed in the lower frequency region such as  $603.2\text{ cm}^{-1}$  in 2,4-DMP and  $602.1\text{ cm}^{-1}$  in 3,9-DMP is assigned to a mixture of torsion around C-C bond ( $\tau$ ) and aromatic C-H out-of-plane bending ( $\gamma$ ) vibration. In this region the fundamental anharmonic frequencies calculated with 6-311G\*\* basis set deviate by about  $10\text{ cm}^{-1}$  from the observed ones whereas force field fitted frequencies match within  $3\text{ cm}^{-1}$ .

**Table 5.7: Comparison of observed aromatic C-H out-of-plane bending, methyl C-H symmetric<sup>a</sup> and asymmetric<sup>b</sup> stretching and aromatic C-H stretching vibrations in DMPs.**

Mode of vibration	1,9-DMP	2,4-DMP	3,9-DMP
Aromatic C-H out-of-plane	748.3 (1.000)	742.7 (1.000)	754.0 (1.000)
Methyl C-H stretching	2875.3 <sup>a</sup> (0.277)	2882.3 <sup>a</sup> (0.397)	2875.0 <sup>a</sup> (0.310)
	2905.0 <sup>b</sup> (0.067)	2930.8 <sup>b</sup> (0.639)	2908.2 <sup>b</sup> (0.125)
	2933.5 <sup>b</sup> (0.652)	2976.7 <sup>b</sup> (0.425)	2933.5 <sup>b</sup> (0.829)
Aromatic C-H stretching	3069.7 (0.608)	3057.2 (0.880)	3085.7 (0.307)

<sup>a</sup>, <sup>b</sup> *methyl C-H symmetric and antisymmetric stretching vibrations, respectively. The band positions are given in cm<sup>-1</sup> and the intensities in km mol<sup>-1</sup>.*

In Table 5.7, I have listed four characteristic bands of DMPs which may help identification of DMPs in a mixture. The aromatic C-H out-of-plane bending vibration ( $\gamma$ ) is a highly intense band in the DMPs and is easy to identify around 750 cm<sup>-1</sup>. The DMPs are clearly distinguishable from this band. A moderately intense band observed in 2885 - 2870 cm<sup>-1</sup> region is assigned to methyl C-H symmetric stretching vibration in DMPs. Another set of methyl C-H antisymmetric stretching bands observed in the spectral range of (2930 – 2980) cm<sup>-1</sup> and (2900 – 2930) cm<sup>-1</sup>, respectively can also help to identify a particular DMP in a mixture. With respect to this vibration, 2,4-DMP isomer is clearly distinguishable from the other two isomers. DMPs are clearly distinguishable with respect to intense aromatic C-H stretching band observed at 3069.7 cm<sup>-1</sup> in 2,4-DMP, at 3057.2 cm<sup>-1</sup> in 2,6-DMP, and at 3085.7 cm<sup>-1</sup> in 2,7-DMP.

## **5.5 Conclusion**

I have reported the gas phase vibrational spectra of 1,9-DMP, 2,4-DMP, and 3,9-DMP at 0.5 cm<sup>-1</sup> resolution and assigned the spectra using scaled force field frequencies and their PEDs at the B3LYP/6-31G\* and B3LYP/6-311G\*\* levels of theory. The anharmonic frequencies, even calculated with an extended basis set, are less accurate for the assignment of the aromatic C-H and methyl C-H stretching fundamental vibrations. But the error in fitting is within 3 cm<sup>-1</sup> between the observed fundamental vibrations and the scaled force field fitted frequencies emphasizing the need for such calculations in the assignment of the vibrational spectra. I have shown that it is possible to distinguish different isomers of DMPs with the help of the observed intense bands.



## 5.6 References

- [1] (a) Das, P.; Arunan, E.; Das, P. K. *Vibr. Spectrosc.*, **2008**, *47*, 1. (b) Das, P.; Manogoran, S.; Arunan, E.; Das, P. K. *J. Phys. Chem. A*. **2010**, *114*, 8351.
- [2] Kovalenko, L. J.; Maechling, C. R.; Clemett, S. J.; Philipoz, J. M.; Zare, R. N. *Anal. Chem.* **1992**, *64*, 682.
- [3] Clemett, S. J.; Maechling, C. R.; Zare, R. N.; Swan, P. D.; Walker, R. M. *Science* **1993**, *262*, 721.
- [4] Williams, P. T.; Bartle, K. D.; Andrews, G. E. *Fuel* **1986**, *65*, 1150.
- [5] Nelson, P. F. *Fuel* **1989**, *68*, 283.
- [6] Zamperlini, G. C. M.; Silva, M. R. S.; Vilegas, W. *Chromatographia* **1997**, *46*, 655.
- [7] Yu, M. L.; Hites, R. A. *Anal. Chem.* **1981**, *53*, 951.
- [8] Benner, Jr., B. A.; Gordon, G. E.; Wise, S. A. *Environ. Sci. Technol.* **1989**, *23*, 1269.
- [9] Benner, Jr., B. A.; Wise, S. A.; Currie, L. A.; Klouda, G. A.; Klinedinst, D. B.; Zweidinger, R. B.; Stevens, R. K.; Lewis, C. W. *Environ. Sci. Technol.* **1995**, *29*, 2382.
- [10] Rhead, M. M.; Hardy, S. A. *Fuel* **2003**, *82*, 385.
- [11] Barras, E.; Tortajada-Genaro, L. A.; Vazquez, M.; Zielinska, B. *Atmos. Environ.* **2009**, *43*, 5944.
- [12] LaVoie, E. J.; Tulley-Freiler, L.; Bedenko, V.; Hoffman, D. *Cancer Res. (a)* **1981**, *41*, 3441; (b) **1982**, *42*, 4045.
- [13] (a) Allamandola, L. J.; Tielens, A. G. G. M.; Barker, J. R. *Astrophys. J. Suppl. Series* **1989**, *71*, 733 (b) Muizon, M. D.; Geballe, T. R.; Bass, F. *Astrophys. J.* **1986**, *306*, L105 (c) Allamandola, L. J.; Tielens, A. G. G. M.; Barker, J. R. *Astrophys. J. Suppl. Series* **1989**, *71*,

733 (d) Cook, D. J.; Schlemmer, S.; Wagner, D. R.; Steiner, B.; Saykally, R. J. *Nature* **1996**, 380, 270.

[14] Pakdel, H.; Roy, C.; *Energy & Fuels* **1991**, 5, 427.

[15] (a) Cane, E.; Miani, A.; Palmieri, P.; Tarroni, R.; Trombetti, A. *J. Chem. Phys.* **1997**, 106, 9004 (b) Cane, E.; Miani, A.; Palmieri, P.; Tarroni, R.; Trombetti, A. *Spectrochim. Acta Part A* **1997**, 53, 1839.

[16] Sonnefeld, W. J.; Zoller, W. H.; May, W. E. *Anal. Chem.* **1983**, 55, 275.

[17] Calculated using Advanced Chemistry Development (ACD/Labs) software.

[18] Frisch M. J.; et al. Gaussian 09, Revision A.02, Gaussian, Inc., Wallingford CT, **2009**.

[19] (a) Reddy, K. V.; Heller, D. F.; Berry, M. J. *J. Chem. Phys.* **1982**, 76, 2814 (b) McKean, D. C. *Spectrochim. Acta*, **1973**, 29A, 1559.

# **Chapter-6**

**Is there Intramolecular Hydrogen Bonding in Diols?**

**An FT-IR and DFT investigation**

## 6.1 Introduction

In the introduction chapter, I have discussed that diols exist in a mixture of conformers with various possibility of intermolecular and intramolecular interaction between two hydroxyl groups. Electron density topological analysis has not shown a bond critical point (BCP) and atomic bond path corresponding to intramolecular hydrogen bonding (IHB) in 1,2 EG.<sup>1a, b</sup> Further, this has been corroborated by X-ray and neutron diffraction studies in the liquid phase<sup>2</sup>, NMR spectroscopic study in solution<sup>3</sup>, and X-ray study in crystalline form.<sup>4</sup> From the small red-shift in the O–H stretching frequency in the observed mid-IR and their overtone spectrum of 1,2-EG in the gas phase, several author concluded that *gauche* conformers are stabilized by the weak IHB.

An interesting question which arises is that of the extent to which the intramolecular hydrogen bond is found between vicinal hydroxyl groups in 1,2-EG in the gas phase. Infrared red-shifts for the O–H stretching vibration, ranging from a few tens of wavenumbers to many hundred wavenumbers, are frequently used by spectroscopists as an evidence for hydrogen bonding.<sup>5</sup> Combination of theoretical and FT-IR spectroscopic studies of 1,2-EG and 1,4-BD in the gas phase is very limited. A few reports are available in the literature on IR spectroscopic studies of 1,2-EG and 1,4-BD in the gas phase.<sup>6-9</sup> However, experimentally most of these studies are silent about intensity changes which are expected to be there due to intramolecular interaction or IHB formation.

Therefore, my goal of this work is (1) to record the IR spectra of 1,2-EG and 1,4-BD at lowest possible concentrations in the gas phase where intermolecular interaction is minimum/does not exist, (2) to calculate the equilibrium population of each conformers of 1,2-EG and 1,4-BD at experimental temperatures, (3) to identify the conformers of 1,2-EG and

1,4-BD with the help of the simulated population weighted spectrum and the observed spectrum at a particular temperature, and (4) to answer whether intramolecular hydrogen bond (IHB) exist in diols or not by looking at the red-shifts and intensities of the O–H stretching bands in the observed and calculated spectra of 1,2-EG and 1,4-BD. This study is a valuable complement to the computational work which is carried out by Klein for the series of diols.<sup>10</sup>

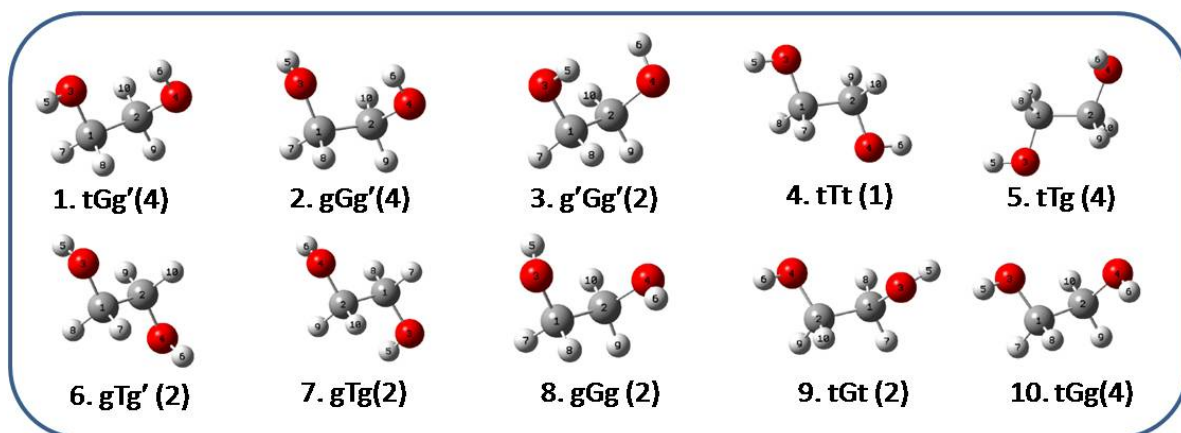
## **6.2 Experimental section**

The sample 1,2-ethylene glycol (HOCH<sub>2</sub>CH<sub>2</sub>OH, LR grade, Ranbaxy) and 1,4-butanediol (HOCH<sub>2</sub>CH<sub>2</sub>CH<sub>2</sub>CH<sub>2</sub>OH, 98%, Merck) were used for this study. Details of the experimental set-up have been described in section 2.3.1 of chapter 2. The sample was placed in a ~2 ml bulb mounted on gas cell and degassed by several freeze-pump-thaw cycles, and subsequently pumped on the vacuum line for an hour to remove dissolved gases. The vacuum was then closed and the sample vapor was allowed to equilibrate throughout the vacuum line and gas cell at 303 K and 313 K for 1,2-EG and 1,4-BD, respectively. The sample vapor was then diluted with 100 mmHg Ar (buffer gas) in order to minimize intermolecular interaction. All spectra were recorded with spectral resolution of 0.5 cm<sup>-1</sup> and averaged over 2048 scans. The spectra were recorded at three different temperatures with the increments of 10 degree Celsius in each stage from the starting temperature to check for existence of intermolecular interaction.

## **6.3 Computational methods**

EG is a typical rotor molecule that can exist in one of the 3<sup>3</sup>=27 conformation. Some of the structures are degenerate due to symmetry, and the number of unique conformations is 10. The 10 conformers are shown in Figure 6.1. In case of 1,4-BD, there are five intramolecular

rotational degrees of freedom with three of them characterizing the backbone structure (OCCC, CCCC and CCCO) and the remaining two are related to the orientation of the two OH groups (HOCC).

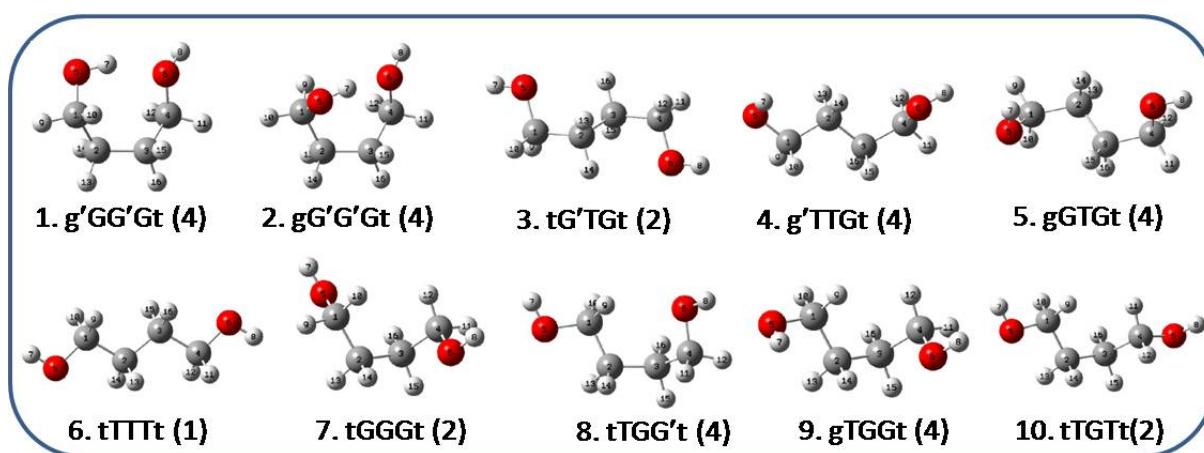


**Figure 6.1.** The 10 unique conformers of 1,2-EG. The structural degeneracy of each conformer is indicated in parentheses.

The existence of three-fold axis around each of the five dihedral angles can result in a total  $3^5 = 243$  conformation that complicates the structural studies of 1,4-BD. However, symmetry considerations reduce this number to 70 unique conformations. Out of these, 10 conformers were chosen based on the backbone family as shown in Figure 6.2. The conformers are defined according to the following rule: assuming three possible minima per torsion, i.e., *trans* ( $180^\circ \pm 30^\circ$ ), *+gauche* ( $60^\circ \pm 30^\circ$ ), and *-gauche* ( $-60^\circ \pm 30^\circ$ ) abbreviated by t or T, g or G and g' or G'. Capital letters refer to the backbone structure while the lower case letters refer to the OH orientation and superscript 'prime' indicates the sense of internal rotation corresponding to the negative dihedral angle.

Geometry optimization and frequency calculations on 10 conformers of 1,2-EG and 1,4-BD were carried out at the B3LYP/6-311++G\*\* level of theory. We have carried out

frequency calculations on 10 conformers of 1,2-EG and 1,4-BD to ensure that we were dealing with the true minima and not the transition states or saddle points. In case of the g'Gg' conformer, however, one imaginary frequency at  $75.1\text{ cm}^{-1}$  indicated the presence of a first-order transition point and not a true minimum. This has been pointed by earlier as well.<sup>10</sup> Graphical examination of the DFT calculated vibrational frequencies using Gauss View 3.0, showed that the single imaginary frequency corresponded to a wagging mode vibration for the pendant OH groups. It has been found that geometry optimization of conformer tGt led to another conformer g'Gg'. Therefore conformer tGt is not a true minimum at this level of theory and, thus, we don't consider for the population analysis. All computations were carried out using the Gaussian 03 set of programs.<sup>11</sup>



**Figure 6.2.** Geometries of the most populated conformers of each of the backbone families of 1,4-BDO. The structural degeneracy of each conformer is indicated in parentheses.

I have performed a statistical thermodynamic population analysis with 9 and 10 conformers of 1,2-EG and 1,4-BD, respectively, at experimental temperatures. The purpose of the theoretical population analysis is to predict which conformers contribute to the vibrational

spectra at that temperature. Standard statistical mechanical relationships were used to calculate the free energies and thus the relative populations of the 9 and 10 conformers of 1,2-EG and 1,4-BD, respectively, in a manner similar to that performed by Cramer and Howard.<sup>8,12</sup> In brief, the electronic energy values obtained after geometry optimization were corrected with the zero-point vibrational energy giving total energy at 0 K ( $E_o = E_{\text{elec}} + \text{ZPE}$ ). Translational, rotational and vibrational thermal energies were added to this value in order to obtain the enthalpy ( $H = E + RT$ , where  $E = E_o + E_{\text{vib}} + E_{\text{rot}} + E_{\text{trans}}$ ) at 298 K for 1,2-EG and 1,4-BD, respectively. From this quantity and that calculated for the entropy, the Gibbs energy ( $G = H - TS$ ) was determined. The relative weight of each conformer in the gas phase was obtained from Boltzmann distribution based on the Gibbs energy.

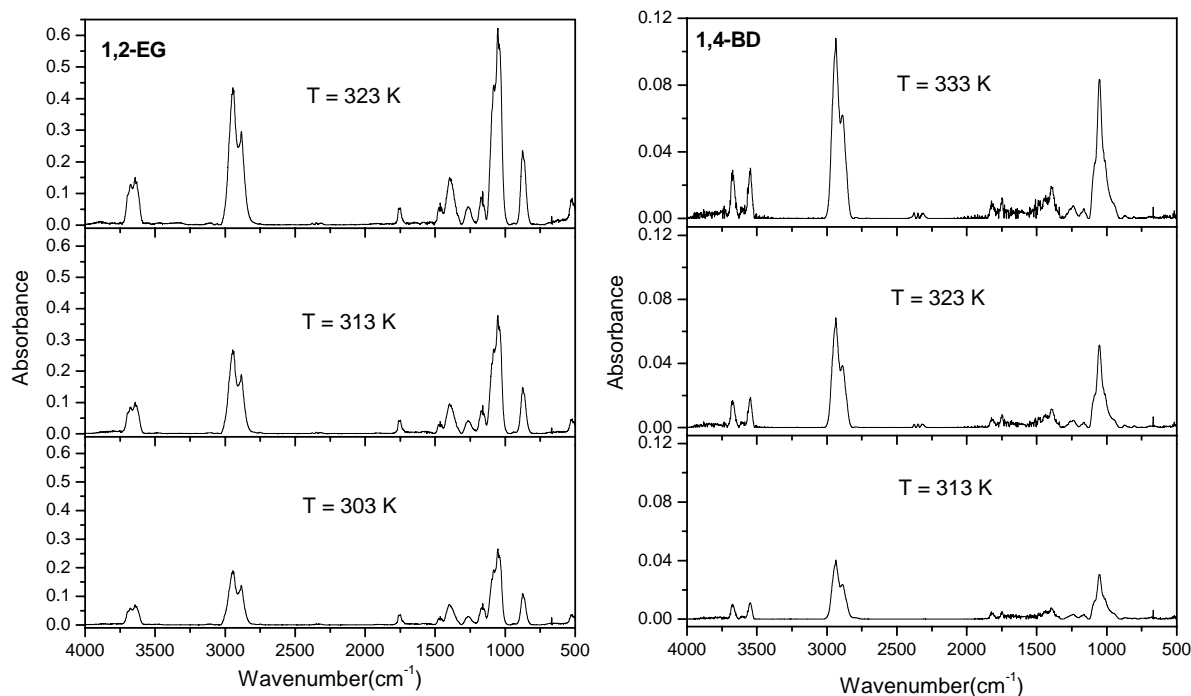
## **6.4 Results and discussion**

### **6.4.1 Gas phase infrared spectra of 1,2-EG and 1,4-BD**

Figure 6.3 shows the experimental IR absorption spectra of 1,2-EG and 1,4-BD at three different temperatures. Frequencies, FWHM and band areas of the O–H stretching vibrations for 1,2-EG and 1,4-BD as a function of temperature are listed in Table 6.1. We note that in the gas phase both the in/free O–H and the out/bound O–H stretching frequencies can be seen at experimental temperatures (in and out abbreviation used for two OH groups in 1,2-EG whereas in 1,4-BD it is free and bound). The frequencies of both of these bands are entirely independent of temperature since the red-shift ( $\Delta\nu$  in  $\text{cm}^{-1}$ ) in O–H stretching frequency is constant as the temperature is increased (see Figure 6.3 and Table 6.1). This implies that there is no intermolecular interaction. If intermolecular interaction is there the interacted O–H



stretching frequency as well as intensity expected to be changed as function of temperature because this interaction is a concentration dependent phenomenon.



**Figure 6.3.** Gas phase IR spectra of 1,2-EG and 1,4-BD at three different temperatures ( $T$ 's). Samples was loaded at the lowest possible temperature, 303 or 313 K for 1,2-EG or 1,4-BD, respectively. Total pressure in the gas cell containing the buffer gas (Ar) and the sample was maintained at 100 mmHg.

Furthermore, it has been found that the ratio of integrated band area ( $R$ ) of  $O-H_{in/bound}$  to the  $O-H_{out/free}$  at higher temperatures of 323 K and 333 K for 1,2-EG and 1,4-BD, respectively, is slightly smaller than those at lower temperatures 303 K and 313 K. This clearly implies that the conformational equilibrium between bound (hydrogen bonded) and free (non-hydrogen bonded) forms is shifted towards free forms by a small extent at higher temperature. Out of these three sets of spectra, we have chosen one set of spectrum measured at 303 K in 1,2-EG

and 313 K in 1,4-BD for the identification of conformers in the gas phase by comparing with the simulated spectrum and for further discussions.

**Table 6.1: Frequency ( $\nu$ ,  $\text{cm}^{-1}$ ), FWHM ( $\nu_{1/2}$ ,  $\text{cm}^{-1}$ ), integrated band area (S) and ratio of integrated band area ( $R = S_{\text{in/bound}}/S_{\text{out/free}}$ ) of O–H absorption bands for 1,2-EG and 1,4-BD observed at three different temperatures.**

System	T/K	O–H <sub>out/free</sub>			O–H <sub>in/bound</sub>			R
		$\nu$	$\nu_{1/2}$	S	$\nu$	$\nu_{1/2}$	S	
1,2-EG	303	3682.8	42.3	1.947	3637.5	41.6	2.582	1.326
	313	3682.2	45.3	3.036	3637.3	41.3	3.551	1.169
	323	3681.1	41.2	3.873	3637.7	40.3	4.959	1.280
1,4-BD*	313	3672.5	27.2	0.272	3606.5	8.6	$8.6 \times 10^{-3}$	0.031
					3548.4	24.0	0.288	1.058
	323	3672.5	27.7	0.471	3606.1	11.3	$2.2 \times 10^{-2}$	0.046
					3548.7	25.0	0.475	1.008
	333	3672.5	28.6	0.859	3605.9	15.9	$4.9 \times 10^{-2}$	0.057
3549.2					26.6	0.799	0.930	

*In 1,2-EG, two O–H stretching vibration is defined as O–H<sub>in</sub> and O–H<sub>out</sub> whereas in 1,4-BD it is defined as O–H<sub>bound</sub> and O–H<sub>free</sub>, respectively.*

*\*In 1,4-BD, bands observed at 3606 and 3549  $\text{cm}^{-1}$  for bound O–H group which correspond to two hydrogen bonded conformers (see text for details).*

#### 6.4.2 Population analysis

The calculated zero point vibrational energy (ZPVE) corrected energies,  $\Delta E_0$  and relative free energies,  $\Delta G$ , of the 9 conformers of 1,2-EG and 10 conformers of 1,4-BD are presented

in Tables 6.2 and 6.3, respectively. Each conformer has a contribution to its free energy of  $-RT \ln \omega$ , where  $\omega$  is the structural degeneracy of conformers listed in Figures 6.1 and 6.2 for 1,2-EG and 1,4-BD, respectively. The fractional gas-phase equilibrium population  $F(M)$  of a conformer M is calculated according to the Boltzmann distribution

$$F(M) = \frac{\exp(-\Delta G_M^0 / RT)}{\sum_i \exp(-\Delta G_i^0 / RT)} \quad (6.1)$$

where  $i$  spans all the 10 conformers. I have used the  $\Delta G^0$  values from Tables 6.2 – 6.3. In tables,  $A(\%) \equiv 100 \times F(M)$ .

Calculated % population of chosen conformers of 1,2-EG and 1,4-BD are listed in Table 6.2 and 6.3, respectively. From Table 6.2 it is clear that conformer tGg' in 1,2-EG is most populated one followed by gGg' and g'Gg' conformers at experimental temperature 303 K. Out of three, the conformers tGg' and gGg' unlikely to have IHB. The experimental spectra of 1,2-EG match well with the simulated spectra (see discussion in next section). It implies that the calculated % populations at a particular temperature agree well with the experimental populations. On the other hand, in 1,4-BD one hydrogen bonded and three non-hydrogen bonded conformers are most populated at experimental temperature 313 K (see Table 6.3). The gas phase equilibrium population calculated to be 26.8 and 8.0 % for the hydrogen bonded conformer g'GG'Gt and gG'G'Gt, respectively and for the non-hydrogen bonded conformers tG'TGt, g'TTGt and gGTGt it is 17.8, 17.7 and 14.6%, respectively. The discrepancy between simulated and observed spectra at 313 K has been found in 1,4-BD (see next section) which clearly indicate that calculated % population of conformers must be different from the experimental one. Therefore, I have varied the calculated A(%) to find the experimental A(%) which is designated by “fitted A” as shown in Table 6.3. Now experimental population found

to be 17.8, 4.0, 21.8, 20.7, 17.6, and 6.8 % for g'GG'Gt, gG'G'Gt, tG'TGt, g'TTGt, gGTGt, and tTTTt, respectively. It implies that in spite of IHB, the hydrogen bonded conformers are less stable than some of the non-hydrogen bonded conformers due to steric hindrance.

**Table 6.2: Symmetry point groups, relative energies (in kJ mol<sup>-1</sup>) and equilibrium gas phase populations of the conformers of 1,2-EG at 298 and 303 K at the B3LYP/6-311++G\*\* level.**

Conformers of 1,2-EG	Sym ( $\omega$ )	$\Delta E_0$	$\Delta G$ at 298 K	A (%) at 298 K	$\Delta G$ at 303 K	A (%) at 303 K	<sup>a</sup> A (%) at 298 K
tGg'	C <sub>1</sub> (4)	0.00	0.00	65.8	0.00	65.2	57.7
gGg'	C <sub>1</sub> (4)	2.34	2.83	20.9	2.84	21.1	25.7
g'Gg'	C <sub>2</sub> (2)	3.27	5.52	7.0	5.55	7.1	10.4
tTt	C <sub>2h</sub> (1)	8.98	10.31	1.0	10.37	1.1	0.5
tTg	C <sub>1</sub> (4)	10.37	8.02	2.6	8.02	2.7	2.2
gTg'	C <sub>i</sub> (2)	10.73	11.19	0.7	11.22	0.7	0.9
gTg	C <sub>2</sub> (2)	11.79	14.00	0.2	14.03	0.2	0.3
gGg	C <sub>2</sub> (2)	10.71	11.12	0.7	11.15	0.7	0.8
tGt <sup>b</sup>	C <sub>2</sub> (2)	---	---	---	---	---	0.8
tGg	C <sub>1</sub> (4)	13.74	10.61	0.9	11.61	0.9	0.8

All energies are relative to the most stable conformer tGg'. Each symmetry point group is associated with the conformational degeneracy ( $\omega$ ) given in the parentheses. Gibbs energies at 298 and 303 K account for the degeneracy by adding an  $-RT \ln(\omega)$  term.

<sup>a</sup>Reported % populations of conformers were obtained using energy calculated at the CCSD (T)/aug-cc-pVTZ level of theory at 298 K.<sup>8</sup>

<sup>b</sup> Not a stationary point at this level of theory.

**Table 6.3: Symmetry point groups, relative energies (in kJ mol<sup>-1</sup>) and equilibrium gas phase populations of the conformers of 1,4-BD at 298 and 313 K at the B3LYP/6-311++G\*\* level.**

Conformers of 1,4-BD	Sym ( $\omega$ )	$\Delta E_o$	$\Delta G$ at 298K	A(%) at 298K	$\Delta G$ at 313K	A (%) at 313K	*A(%) at 298K	A(%) Fitted	$\Delta G_{\text{Expt.}}$ at 313 K
g'GG'Gt	C <sub>1</sub> (4)	0.00	0.00	27.3	0.00	26.7	30.21	17.8	0.53
gG'G'Gt	C <sub>1</sub> (4)	3.78	3.14	7.7	3.14	8.0	17.06	4.0	4.41
tG'TGt	C <sub>i</sub> (2)	5.62	0.97	18.5	1.05	17.8	14.51	21.8	0.00
g'TTGt	C <sub>1</sub> (4)	7.28	1.07	17.7	1.07	17.7	15.55	20.7	0.13
gGTGt	C <sub>1</sub> (4)	7.33	1.58	14.4	1.58	14.5	7.04	17.6	0.56
tTTTt	C <sub>2h</sub> (1)	7.39	4.92	3.7	5.09	3.7	3.54	6.8	3.03
tGGGt	C <sub>2</sub> (2)	9.15	6.90	1.7	6.98	1.8	4.38	1.8	6.49
tTGG't	C <sub>1</sub> (4)	10.79	4.18	5.0	4.18	5.3	3.45	5.4	3.63
gTGGt	C <sub>1</sub> (4)	11.51	5.75	2.7	5.75	2.9	3.32	2.9	5.24
tTGTt	C <sub>2</sub> (2)	12.00	7.90	1.1	7.99	1.2	0.94	1.2	7.54

*All energies are relative to the most stable conformer g'GG'Gt. Each symmetry point group is associated with the conformational degeneracy ( $\omega$ ) given in the parentheses. Gibbs energies at 298 and 313 K account for the degeneracy by adding an  $-RT \ln(\omega)$  term.*

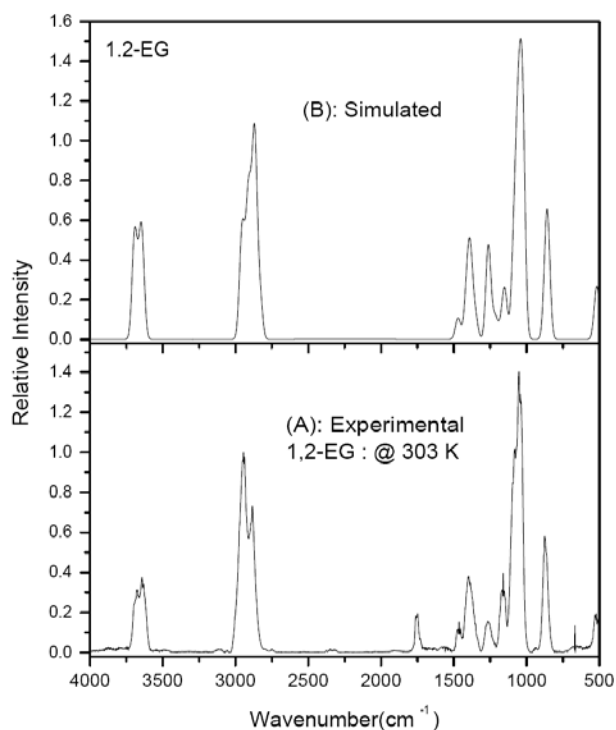
*\*Reported % populations of conformers were obtained using energy calculated at the MP2/6-311G\*\* level of theory at 298 K.<sup>13</sup> For the fitted A(%) value see text.*

*$\Delta G_{\text{Expt.}}$  at 313 K for the chosen 10 conformers were calculated using fitted % population value and equation 6.1.*

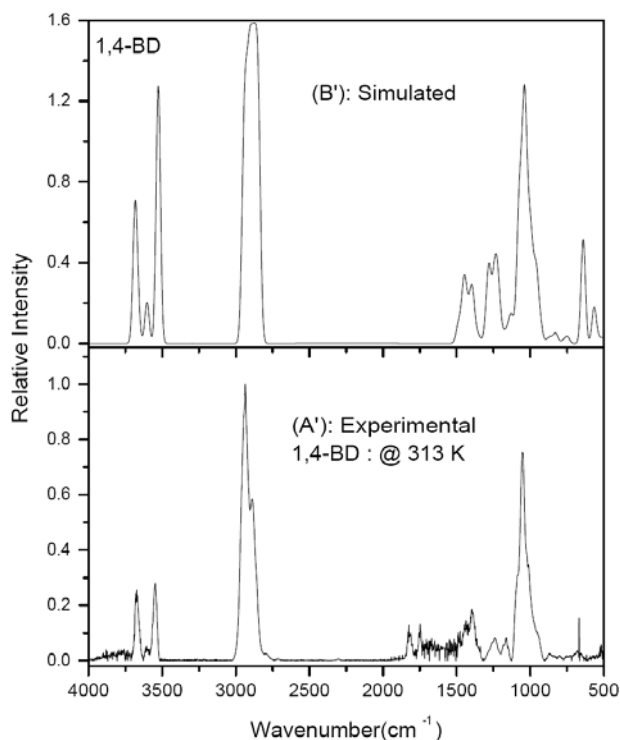
### 6.4.3 Identification of conformers

The comparison between the experimental and simulated spectra allows us to verify the presence of the most stable conformers in the gas phase. In order to interpret the experimental

spectra, we considered 9 conformers out of 27 in 1,2-EG and 10 conformers out of 243 conformers in 1,4-BD. Then we assumed that population of each conformer corresponds to its weight at the experimental temperature. The calculated intensities of the spectra of each conformer were weighted by its population as described in Tables 6.2 – 6.3. The calculated frequencies and their intensities of O–H stretching region of 1,2-EG and 1,4-BD are listed in Table 6.4 and 6.5, respectively.



**Figure 6.4.** Experimental IR absorption spectrum of 1,2-EG in the gas phase at 303 K (A) and stimulated spectrum of a mixture of stable conformers  $tGg'$ ,  $gGg'$  and  $g'Gg'$  (B). The calculated intensities in the individual spectra of conformers were weighted by the population of the respective conformer as described in Table 6.2. The frequencies of the calculated spectra were scaled by two scaling factors: 0.9578 for O–H and methyl C–H stretching frequencies and 0.9824 for frequencies below  $1600\text{ cm}^{-1}$ . The simulated spectrum (B) was obtained using Gaussian functions centered at the scaled frequencies and with a band width at half-height of  $35\text{ cm}^{-1}$ .



**Figure 6.5.** Experimental IR absorption spectrum of 1,4-BD in the gas phase at 313 K (A'), simulated spectrum of a mixture of conformers *g'GG'Gt*, *gG'G'Gt*, *tG'TGt*, *g'TTGt*, *gGTGt*, *tTTTt*, *tGGGt*, *tTGG't*, and *gTGGt* (B'). The calculated intensities in the individual spectra of conformers were weighted by the population of the respective conformer as described in Table 6.3. The frequencies of the calculated spectra were scaled by two scaling factors: 0.9578 for O–H and methyl C–H stretching frequencies and 0.9824 for frequencies below 1600  $\text{cm}^{-1}$ . The simulated spectrum (B') was obtained using Gaussian functions centered at the scaled frequencies and with a band width at half-height of 35  $\text{cm}^{-1}$ .

The experimental and simulated spectra of 1,2-EG and 1,4-BD are presented in Figures 6.4 and 6.5, respectively. The simulated spectrum (at 303 K) of 1,2-EG, a mixture of most stable conformers: *tGg'*, *gGg'* and *g'Gg'* with a contribution of 65.2, 21.1 and 7.1 %, respectively, is shown in Figure 4 (B, upper frame). The simulated spectrum (at 313 K) of 1,4-

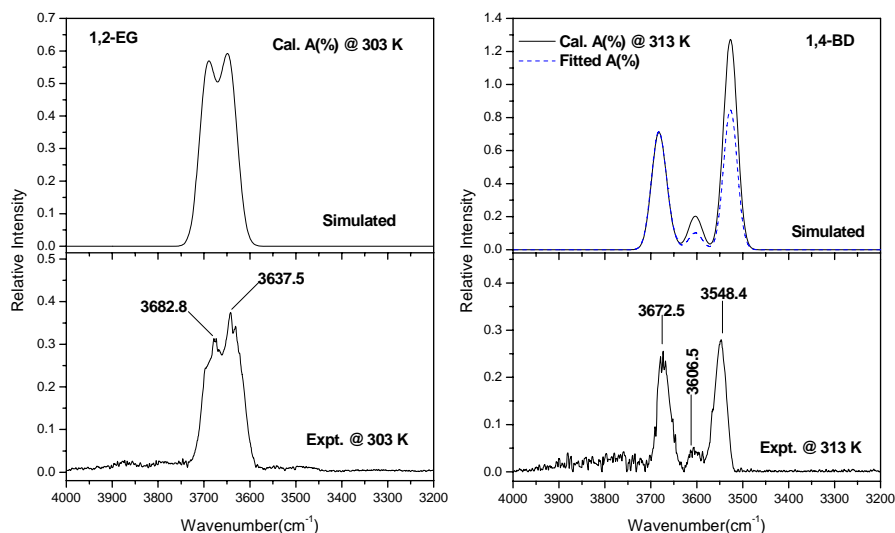
BD derived from a mixture of conformers: g'GG'Gt, gG'G'Gt, tG'TGt, g'TTGt, gGTGt, tTTTt, tGGGt, tTGG't, and gTGGt with weightages of 26.8, 8.0, 17.8, 17.7, 14.6, 3.8, 1.8, 5.4, and 2.9 %, respectively, is shown in Figure 6.4 (B', upper frame). The conformer, tTGTt was not considered for the simulation of calculated spectrum of 1,4-BD since % population is very low compared to other conformers.

In the O–H stretching region, the gas phase IR spectra of the 1,2-EG exhibit two distinct bands, whereas 1,4-BD exhibits three bands. The higher frequency band appears at 3682.8 and 3672.5  $\text{cm}^{-1}$  in 1,2-EG and 1,4-BD, respectively. This band corresponds to the stretching vibration of the out/free O–H group. This absorption band has a contribution of all the conformers which are used for the simulation of the calculated spectra. The second O–H stretching band observed at 3637.5  $\text{cm}^{-1}$  in 1,2-EG is assigned to the O–H<sub>in</sub> stretching vibration. Only two conformers of 1,2-EG (tGg' and gGg') are contributed to this band. In 1,4-BD two bands are observed in this region at 3548.4 and 3606.5  $\text{cm}^{-1}$ . The appearance of two hydrogen bonded O–H stretching bands provide evidence for the existence of two differently hydrogen bonded conformers, namely gG'G'Gt and g'GG'Gt, respectively. One low intense band observed at 1754.7 and 1820.4  $\text{cm}^{-1}$  for 1,2-EG and 1,4-BD, respectively, in the experimental spectrum which is not corresponding to any calculated frequency. Therefore, this band is assigned as a non-fundamental band such overtone or combination band. Detail of the bands assignments have not done in this work since we are interested only to address the question whether IHB exist in vicinal diols or not.

The experimental spectra of 1,2-EG match well with the simulated spectra. It implies that the calculated % populations at particular temperature agree well with experiment. From Figure 6.4 and Table 6.2, it is clear that, in case of 1,2-EG most stable conformers, tGg', gGg'



and  $g'Gg'$  that the *gauche* conformers are present in the gas phase. On the other hand, in 1,4-BD comparison of the experimental spectrum with the simulated spectra reveals that although frequencies match well, the relative intensities of the bound O–H band observed at 3548.4 and 3606.5  $\text{cm}^{-1}$  do not agree well with the simulated spectra (see Figure 6.5). The discrepancy between the observed and calculated relative intensities in 1,4-BD suggests that lowest energy conformers,  $g'GG'Gt$  and  $gG'G'Gt$  do not exist with 26.8 and 8.0 % population in the equilibrium mixture, respectively, rather it is less than that of the calculated population. We then varied the % population of a few conformers having  $\Delta E_0$  value below 8  $\text{kJ mol}^{-1}$  to simulate the spectrum of 1,4-BD in a way to reproduce the experimental spectrum.



**Figure 6.6.** Enlarged view of the O–H stretching regions of observed and simulated spectra of 1,2-EG and 1,4-BD. In 1,4-BD, simulated spectra obtained with the calculated and fitted population is shown by solid line (–) and dash line (----), respectively. See text for the details.

The fitted % population values found by trial and error are 17.8, 4.0, 21.8, 20.7, 17.6, and 6.8 for  $g'GG'Gt$ ,  $gG'G'Gt$ ,  $tG'TGt$ ,  $g'TTGt$ ,  $gGTGt$ , and  $tTTTt$ , respectively, as reported in Table

6.3 whereas % population of the rest of the conformers were not changed. The experimental and simulated spectrum in the O–H stretching region of 1,2-EG and 1,4-BD are shown in Figure 6.6.

#### 6.4.4 Estimation of the hydrogen bond energy

The peak frequency shift,  $\Delta\nu = (\nu_{\text{out/free}} - \nu_{\text{in/bound}})$  is commonly used to evaluate the strength of the hydrogen bond and a correlation between this and the enthalpy of the hydrogen bond formation has been reported by several groups. The HB formation enthalpy can be estimated using the empirical equations proposed by Iogansen<sup>14</sup>

$$\Delta H^f = -0.3312(\Delta\nu - 40)^{1/2} \text{ -- -- -- -- -- (6.2)}$$

with  $\Delta H^f$  in kcal mol<sup>-1</sup> and  $\Delta\nu$  in cm<sup>-1</sup>. This equation is valid only when  $\Delta\nu \geq 40$  cm<sup>-1</sup>. This empirical relation has found a minimum of 40 cm<sup>-1</sup> for a hydrogen bond induced red shift.

The red-shift in O–H stretching vibration of 1,2-EG found to be 45.3 cm<sup>-1</sup> which is slightly higher than previously reported<sup>7</sup> value, 33.0 cm<sup>-1</sup> whereas calculated red-shifts are found to be 47 and 30 cm<sup>-1</sup> for tGg' and gGg' conformers, respectively (see Table 6.4). In calculation, some of the conformers showed very small red-shift of ~2 cm<sup>-1</sup> in such cases coupled vibrations have been observed between O–H<sub>in</sub> and O–H<sub>out</sub> groups (see Table 6.4). In 1,4-BD the red-shift of two bands relative to the O–H<sub>free</sub> stretching band observed at 3672.5 cm<sup>-1</sup> are 124.1 and 66.0 cm<sup>-1</sup> for the g'GG'Gt and gG'G'Gt, respectively. The estimated HB formation enthalpy of the 1,2-EG and 1,4-BD are listed in Tables 6.4 and 6.5, respectively. In 1,2-EG, it is difficult to get HB enthalpy for the individual conformer involved in

intramolecular interaction between two hydroxyl groups from experimental spectrum because bands are not well separated for different conformers.

**Table 6.4: Calculated (B3LYP/6-311++G\*\*) O–H stretching frequencies and their intensities (in km mol<sup>-1</sup>), observed (at 303 K) O–H stretching frequencies (in cm<sup>-1</sup>) and their band areas (in cm<sup>-1</sup>), red shifts (in cm<sup>-1</sup>) between “in” and “out” O–H stretching frequencies, and hydrogen-bond enthalpy in 1,2-EG.**

Conformers of 1,2-EG	O–H <sub>in</sub>		O–H <sub>out</sub>		shift cm <sup>-1</sup>	-ΔH <sup>I</sup> kcal mol <sup>-1</sup>	Rel. Int.
	Freq.	Int.	Freq.	Int.			
tGg'	3647.8	42.43	3694.8	44.65	47.0	0.8	0.95
gGg'	3634.6	44.77	3664.0	28.99	29.4		1.54
g'Gg'	3682.2	15.68	3684.0	56.85			
tTt	3692.8	0.00	3693.2	80.16			
tTg	3672.4	26.85	3690.8	38.17			
gTg'	3670.5	58.31	3671.9	0.00			
gTg	3667.3	27.26	3668.1	24.12			
gGg	3664.5	42.40	3665.4	12.02			
tGt	3682.2	15.61	3684.0	56.76			
tGg	3665.7	21.19	3686.0	35.03			
Observed	3637.5	2.228*	3682.8	1.680*	45.3	0.7	1.3
Reported <sup>a</sup>	3644.0		3677.0		33.3		
Reported <sup>b</sup>	3607.0		3642.8		35.6		
Reported <sup>c</sup>	3624.1		3663.2		39.1		

*DFT calculated frequencies are scaled by a factor 0.9578. <sup>a</sup> Data taken at 47 °C from ref<sup>7</sup>; Data taken from <sup>b</sup>solution phase<sup>15</sup> and <sup>c</sup>matrix-isolation IR spectroscopic study.<sup>16</sup>*

*\*Observed band area weighted by sum of the % population corresponds to conformer tGg' and gGg'.*

**Table 6.5: Calculated (B3LYP/6-311++G\*\*) O–H stretching frequencies and their intensities (in km mol<sup>-1</sup>), observed (at 313 K) O–H stretching frequencies (in cm<sup>-1</sup>) and their band areas (in cm<sup>-1</sup>), red shifts (in cm<sup>-1</sup>) between “free” and “bound” O–H stretching frequencies, and hydrogen-bond enthalpy in 1,4-BD.**

Conformers of 1,4-BDO	O–H <sub>bound</sub>		O–H <sub>free</sub>		Shift cm <sup>-1</sup>	-ΔH <sup>I</sup> kcal mol <sup>-1</sup>	Rel. Int.
	Freq.	Int.	Freq.	Int.			
g'GG'Gt	3526.7	304.68	3678.0	41.22	151.3	3.5	7.4
gG'G'Gt	3603.1	125.31	3686.0	39.70	82.9	2.1	1.5
tG'TGt	3685.9	64.38	3686.0	0.00			
gGTGt	3662.8	23.05	3686.4	33.66			
g'TTGt	3666.8	22.85	3685.6	35.51			
tTGG't	3681.7	31.51	3685.4	28.77			
tTTTt	3681.6	62.47	3681.7	0.000			
tGGGt	3685.9	37.38	3686.0	26.13			
gTGGt	3665.3	23.26	3685.5	35.59			
tTGTt	3682.3	40.10	3682.5	22.31			
Observed	3548.4	0.288	3672.5	0.048*	124.1	3.0	6.0
	3606.5	8.6x10 <sup>-3</sup>		0.011*	66.0	1.7	0.8
Reported <sup>a</sup>					110.0	2.7	
Reported <sup>b</sup>	3474.1		3634.3		160.2	3.6	

*DFT calculated frequencies in the O-H stretching region are scaled by a factor 0.9578. <sup>a</sup>Red-shift value taken from ref<sup>6</sup>; <sup>b</sup>Data taken from IR spectroscopic study in CCl<sub>4</sub>.<sup>17</sup>*

*\*Band observed at 3672.5 cm<sup>-1</sup> in the experimental spectrum corresponds to the free O-H group and its band area has contribution from all the conformers chosen for the calculations. Therefore, observed band area for the hydrogen bonded conformers is obtained by weighted their % population of the total band area at 3672.5 cm<sup>-1</sup>.*

On the other hand, in 1,4-BD, we could calculate the HB enthalpy for two intramolecularly hydrogen bonded conformers since bands are well separated in the experimental spectrum. The HB enthalpy value is more in 1,4-BD compared to that in 1,2-EG as seen in Tables 6.4 and 6.5, respectively. In 1,4-BD, a seven member ring results from the formation of the IHB and energy of formation is maximum whereas in 1,2-EG IHB formation leads to a five member ring whose strain energies nearly cancels out the HB stabilization energy. Another contribution to the enhanced stabilization of the 1,4-BD lies in the possibility of closer approach of the two hydroxyl groups to each other, which is, in turn, reflected in the large O–H stretching frequency shift. From these data we conclude that the intramolecular interaction or intramolecular hydrogen bonding is a major stabilizing factor in the lowest energy conformers for 1,4-BD.

#### **6.4.5 Nature of hydrogen bond in diols**

In general, forming of IHB increases the O–H equilibrium distance and thus the magnitude of the electrical transition dipole moment of the O–H stretching mode, which is the reason for the intensity enhancement. In Table 6.6, the values calculated for structural characteristics related with the hydrogen-bonding manifestations for the lowest energy conformers of 1,2-EG and 1,4-BD are displayed.

In 1,4-BD, the formation of an intramolecular hydrogen-bonded conformation involves the distortion of the carbon chain to a gauche arrangement which helps to bring two hydroxyl groups closer to each other. The O–H bond length and H-bonding parameters listed in Table 6.6 clearly show that the calculated shortest HB donor-acceptor distance (H...O), (1.9 – 2.0 Å) found in 1,4-BD is within the criteria defined for the existence of an intramolecular hydrogen

bond proposed by Desiraju and Steiner.<sup>18</sup> However, the deviation of  $O_A\cdots H-O_D$  angle from the most favorable geometry ( $180^\circ$ ) turns this bond into a weak one. In 1,2-EG, the calculated  $O_A\cdots H$  bond distance and  $O_A\cdots H-O_D$  bond angle lie around  $2.4 \text{ \AA}$  and  $106 - 110^\circ$ , respectively, which is below the criteria of IHB. Furthermore, the  $O_A\cdots H$  distance is less than the sum of *van der Waals* radii of O and H ( $2.6 \text{ \AA}$ ), it is more than the sum of 'hydrogen bond radii' ( $2.0 \text{ \AA}$ ), appropriate for OH ( $0.7 \text{ \AA}$ ) and O ( $1.3 \text{ \AA}$ ), as proposed by Raghavendra et al. in 2006.<sup>19</sup>

**Table 6.6: Calculated (B3LYP/6-311++G\*\*) hydrogen bond parameters of lowest energy conformers in 1,2-EG and 1,4-BD.**

Compound	Conformer	Hydrogen bonding parameters <sup>a</sup>		
		$O_A\cdots H / \text{\AA}$	$O_D-H / \text{\AA}$	$\angle O_A\cdots H-O_D$
1,2-EG	tGg'	2.395	0.964	106.4
	gGg'	2.397	0.965	109.6
	tTt		0.961	
1,4-BDO	g'GG'Gt	1.874	0.970	155.9
	gG'G'Gt	2.063	0.967	141.6
	tTTTt		0.961	

<sup>a</sup>  $O_D$  = donor oxygen: atom number 4 in 1,2-EG (see Figure 1) and 6 in 1,4-BD (see Figure 2);  $O_A$  = acceptor oxygen: atom number 3 in 1,2-EG (see Figure 1) and 5 in 1,4-BD (see Figure 2). One of the non-hydrogen bonded conformers, tTt in 1,2-EG and tTTTt in 1,4-BD listed in the table for the comparison of  $O_D-H$  distance with hydrogen bonded conformers.

In 1,2-EG, the small red-shift is found to be  $45.3 \text{ cm}^{-1}$  (see Table 4). This small red-shift could be due to intramolecular interactions between two hydroxyl groups. It has been predicted by several authors. However, the QCISD/6-311++G\*\* and the B3LYP/6-311G\*\* charge densities of the tGg' and gGg' conformers of 1,2-EG do not present any bond path connecting

H<sub>6</sub> and O<sub>3</sub> (see Figure 6.1) as suggested by Mandado et al.<sup>20</sup> This confirms the conclusion obtained by Klein with several DFT levels of calculation that IHB is absent in this compound.<sup>10</sup>

The findings that the crystal structure for 1,2-EG preserves the *gauche* configuration in the crystalline state and a small red-shift of the bound O–H stretching frequencies without changing intensity for intramolecular hydrogen bonding raise its an important question: What is the driving force that maintains the *gauche* configuration in 1,2-EG in the gas phase if it is not primarily the O–H···O interaction as frequently assumed in the literature? As it has been pointed out by numbers of authors, hyper-conjugative effects such as  $n_o(O_A-LP \text{ electrons}) \Rightarrow \sigma[C-H]^*$  and  $\sigma[C-H] \Rightarrow \sigma[O-H]^*$  are energetically more significant than  $n_o \Rightarrow \sigma[O_D-H]^*$  interaction.<sup>4, 10, 22, 23</sup> This hyper-conjugation effect is likely to be present in molecules containing neighboring C–H and O–H moieties, particularly if the C–H and O–H bonds are in *trans* or in nearly *trans* configurations which is found in tGg' and gGg' conformers of 1,2-EG. The dihedral angle (H<sub>6</sub>-O<sub>4</sub>-C<sub>2</sub>-H<sub>9</sub>, see Figure 6.1) is calculated to be -173.6° and 165.9° in tGg' and gGg', respectively.

The frequency change occurs as a result of the O···H–O interaction, obscuring hyper-conjugative effects on both  $\nu_{out/free}$  and  $\nu_{in/bound}$ .<sup>21</sup> Using hyper-conjugation method, Howard et al. reported experimental  $\Delta\nu$  red-shifts for the two most stable conformers of 1,2-EG (tGg' and gGg') of 285 and 173 cm<sup>-1</sup>, respectively, in the fifth overtone vapor-phase spectra ( $\Delta\nu_{OH=5}$ ).<sup>8</sup> These authors also pointed out that the red-shift within a conformer is not necessarily a measure of hydrogen bonding since the stretching frequency for the 'free' *gauche* O–H in the gGg' is red-shifted by 208 cm<sup>-1</sup> at  $\Delta\nu_{OH=5}$  compared to the 'free' *trans* O–H group in the tGg'

conformer. Rotation of an open-chain 1,2-diol *trans* O–H group to either the  $g^+$  and  $g^-$  (also known as  $g$  and  $g'$ ) configuration with or without the possibility of interaction with the second O–H group, results in a ‘*gauche*’ red-shift of up to 30 - 40  $\text{cm}^{-1}$  for the O–H fundamental. This red-shift is paralleled by an increase in the  $\sigma^*$ [O–H] occupancy. Even larger *trans*  $\Rightarrow$  *gauche* effect found in strained cyclic diols and it gives red-shift of 50  $\text{cm}^{-1}$ . This non-hydrogen bond related red-shifts result from O–H bond weakening due to  $\sigma \Rightarrow \sigma^*$  interactions involving C–C and C–H bond rather than that from interactions with the oxygen lone-pair electrons.<sup>5</sup> As Klein pointed out that increasing the  $\sigma^*$  antibonding orbital occupancy in vicinal diols weakens the O–H bond, reducing the stretching force constant and producing a red-shift associated with bond lengthening.<sup>22</sup>

The analysis of the natural bond orbitals demonstrates the HB acceptor oxygen LP electrons to be of the highest energy and lowest energy occupancy for the LP in 1,4-BD with delocalization into the O–H<sub>D</sub> antibonding orbital.<sup>14,22</sup> Reduction in occupancy for the oxygen LP associated with the increase in occupancy for the O–H antibonding orbital is consistent with the energy stabilization. Increasing stability of the interaction between LP and the O–H antibond is associated with increased delocalization and increased occupancy of the O–H antibond. The percentage of *s*-character of the interacting LP electrons increases markedly in line with the  $n_o \Rightarrow \sigma^*$  delocalization. Based on these results, the IHB in 1,4-BD with seven member ring is the most stable.

In 1,2-EG, the intensity between O–H<sub>in</sub> and O–H<sub>out</sub> is enhanced by a factor of 1.3 for a mixture of conformers (see Table 6.4) in the observed spectrum (see Figure 6.6). From the Table 6.4 we note that the most stable hydrogen bonded conformers of 1,2-EG, *tGg'* has not



shown the intensity enhancement in the O–H<sub>in</sub> with respect to O–H<sub>out</sub> stretching vibrations. Although, the second most populated conformer has shown the intensity enhancement by a factor of 1.5 however red-shift value is very small,  $\sim 30\text{ cm}^{-1}$  which is below the criteria of  $\geq 40\text{ cm}^{-1}$  in order to have hydrogen bond (see equation 6.2). It clearly indicates that intramolecular hydrogen bond interaction does not exist. On the other hand in 1,4-BD, experimentally, we found that there is a red-shift more than  $65\text{ cm}^{-1}$  as well as significant intensity enhancement have been observed between O–H<sub>bound</sub> and O–H<sub>free</sub> stretching vibration in the intramolecularly hydrogen bonded conformers (see Figure 6.6) which is consistent with the calculations (see Table 6.5).

## 6.5 Conclusions

In this work, I have collected the gas phase IR spectra of 1,2-EG and 1,4-BD at three different temperatures. The conformers of 1,2-EG and 1,4-BD have been investigated by means of DFT calculation and experimental methods. The infrared spectra of 1,2-EG and 1,4-BD in the gas phase are found to show a good agreement with a population weighted calculated spectrum. Comparison between the observed and calculated spectra of diols reveals the existence of more than one conformers weighted by the Boltzmann factor in the gas phase. The small red-shift in O–H band position and no significant intensity enhancement compared to the ‘out’ O–H peak do not support the idea of an intramolecular hydrogen bonding in 1, 2-EG. On the other hand, in 1,4-BD, there is a  $124.1\text{ cm}^{-1}$  shift in the O–H stretching frequency and intensity enhancement by a factor of 6.0 (Expt.) for the ‘bonded’ O–H compared to the ‘free’ O–H which strongly support the existence of an intramolecular hydrogen bonding in the compound.

---

**6.7 References**

- [1] (a) Klein, R. A. *J. Comp. Chem.* **2002**, *23*, 585 (b) Klein, R. A. *J. Am. Chem. Soc.* **2002**, *124*, 13931.
- [2] Bako, I.; Grosz, T.; Palinkas, G.; Bellissent-Funel, M. C. *J. Chem. Phys.* **2003**, *118*, 3215.
- [3] Petterson, K. A.; Stein, R. S.; Drake, M. D.; Roberts, J. D. *Magn. Reson. Chem.* **2005**, *43*, 225.
- [4] Chopra, D.; Row, T. N. G.; Arunan, E.; Klein, R. A. *J. Mol. Struct.* **2010**, *964*, 126.
- [5] Klein, R. A. *Chem. Phys. Lett.* **2006**, *429*, 633.
- [6] Fishman, E.; Chen, T. L. *Spectrochim. Acta* **1969**, *25A*, 1231.
- [7] Buckley, P.; Giguere, P. A. *Canad. J. Chem.* **1967**, *45*, 397.
- [8] Howard, D. L.; Jorgensen, P.; Kjaergaard, H. G. *J. Am. Chem. Soc.* **2005**, *127*, 17096.
- [9] Howard, D. L.; Kjaergaard, H. G. *J. Phys. Chem. A* **2006**, *110*, 10245.
- [10] Klein, R. A. *J. Comp. Chem.* **2002**, *23*, 585.
- [11] Frisch, M. J.; Trucks, G. W.; Schlegel, H. B.; Scuseria, G. E.; Robb, M. A.; Cheeseman, J. R.; Montgomery, J. A.; Vreven, T.; Kudin, K. N.; Burant, J. C.; Millam, J. M.; Iyengar, S. S.; Tomasi, J.; Barone, V.; Mennucci, B.; Cossi, M.; Scalmani, G.; Rega, N.; Petersson, G. A.; Nakatsuji, H.; Hada, M.; Ehara, M.; Toyota, K.; Fukuda, R.; Hasegawa, J.; Ishida, M.; Nakajima, T.; Honda, Y.; Kitao, O.; Nakai, H.; Klene, M.; Li, X.; Knox, J. E.; Hratchian, H. P.; Cross, J. B.; Adamo, C.; Jaramillo, J.; Gomperts, R.; Stratmann, R. E.; Yazyev, O.; Austin, A. J.; Cammi, R.; Pomelli, C.; Ochterski, J. W.; Ayala, P. Y.; Morokuma, K.; Voth, G. A.; Salvador, P.; Dannenberg, J. J.; Zakrzewski, V. G.; Dapprich, S.; Daniels, A. D.; Strain, M. C.; Farkas, O.; Malick, D. K.; Rabuck, A. D.; Raghavachari, K.; Foresman, J. B.; Ortiz, J. V.; Cui, Q.; Baboul, A. G.; Clifford, S.; Cioslowski, J.; Stefanov, B. B.; Liu, G.; Liashenko, A.;

Piskorz, P.; Komaromi, I.; Martin, R. L.; Fox, D. J.; Keith, T.; Al-Laham, M. A.; Peng, C. Y.; Nanayakkara, A.; Challacombe, M.; Gill, P. M. W.; Johnson, B. ; Chen, W.; Wong, M. W.; Gonzalez, C.; Pople, J. A. Gaussian 03, Revision D.01; Gaussian Inc.: Pittsburg, PA, 2003.

[12] Cramer, C. J.; Truhlar, D. *J. Am. Chem. Soc.* **1994**, *116*, 3892.

[13] Jesus, A. J. L.; Rosado, M. T. S.; Reva, I.; Fausto, R.; Eusebio, M. E.; Redinha, J. S. *J. Phys. Chem. A* **2008**, *112*, 4669.

[14] Iogansen, A. V. *Spectrochim. Acta Part A* **1999**, *55*, 1585.

[15] Bangal, P. R.; Chakravorti, S. *J. Phys. Chem. A* **1999**, *103*, 8585.

[16] Park, C. G.; Tasumi, M. *J. Phys. Chem.* **1991**, *95*, 2757.

[17] Jesus, A. J. L.; Rosado, M. T. S.; Leitao, M. L. P.; Redinha, J. S. *J. Phys. Chem. A* **2003**, *107*, 3891.

[18] (a) Desiraju, G. R.; Steinner, T. *The Weak Hydrogen Bond In Structural Chemistry and Biology*; Oxford Univeristy Press: New York, **1999** (b) Steiner, T. *Angew. Chem., Int. Ed.* **2002**, *41*, 48

[19] Raghavendra, B.; Mandal, P. K.; Arunan, E. *Phys. Chem. Chem. Phys.* **2006**, *8*, 5276.

[20] Mandado, M.; Grana, A. M.; Mosquera, R. A. *Phys. Chem. Chem. Phys.* **2004**, *6*, 4391.

[21] Ablabugin, I. V.; Manoharan, M.; Peabody, S.; Weinhold, F. *J. Am. Chem. Soc.* **2003**, *125*, 5973.

[22] Klein, R. A. *J. Comp. Chem.* **2003**, *24*, 1120.

[23] Bader, R. F. W. *J. Phys. Chem. A* **1998**, *102*, 7314.

# **Chapter-7**

**Concluding remarks and future directions**

## **7.1 Concluding remarks**

This work has broadly fulfilled the following objectives: First, it has provided an experimental verification of low concentration (up-to ppm level) IR spectroscopic measurement which is essential for the detection of atmospherically and astronomically important PAHs. The low concentration measurement is essential even for the detection of intramolecular hydrogen bonded conformers in a mixture in the gas phase.

Second, this work has established the potential of the FT-IR spectroscopic technique combined with scaled force field calculations for the identification of different PAHs. We have shown a better agreement between experiment and theory can be achieved by scaling the force fields rather than the frequencies which is a common practice. For assigning the fundamental vibration in aromatic molecules particularly in the aromatic and methyl C-H stretching bands scaled force field methods is absolutely necessary for unambiguous assignment. However, clear identification of Fermi resonances in large molecules such as PAHs is still difficult. It will require selective isotope substitution and careful analysis of the spectra of the substituted compounds.

Third, combined experimental and theoretical IR spectroscopic study on diols evidences that intramolecular hydrogen bonding does not exist in small diols, like 1,2-EG.

## **7.2 Future direction: Photochemistry of PAHs and time-resolved FT-IR spectroscopy**

In section 7.1, I have discussed about potential of the FT-IR spectroscopic technique for the identification of neutral PAHs in the gas phase. There is another potential application of this technique is the investigation of photochemical reactions of PAHs which is important in

the area of atmospheric photochemistry. IR spectroscopy may be used to identify reaction intermediates in a time resolved manner.

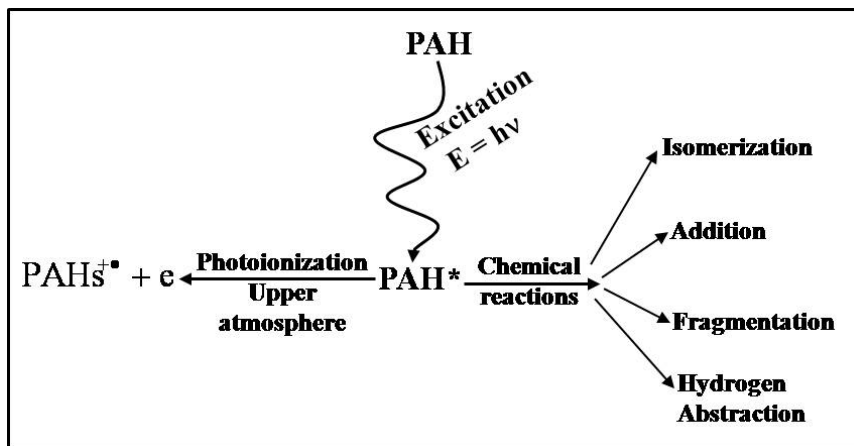


Figure 7.2. Photoionization and some photochemical reactions of PAHs.

Since PAHs cause health hazard it is necessary to destroy them or find some ways to remove them from the atmosphere. There are three effective ways by which PAHs can be removed from the atmosphere: (1) photochemical transformation, (2) photoinduced oxidation (in presence of OH-radicals,  $\text{NO}_3$  or  $\text{O}_3$ ) and (3) biological transformation. PAHs can be converted into less toxic materials by any of the above processes.

PAHs have strong UV absorption at  $\sim 266$  nm which is present in the solar radiation and many of them are readily photo-oxidized. A few photochemical along with photoionization processes are shown in Figure 7.1. The photochemical degradation and photoinduced oxidation occur mostly in the gas phase in the upper atmosphere and in the aquatic environment. PAHs are expected to be photoionized at low intensity of incident light whereas at higher intensity photodestruction channel opens up. Subsequently, suitable techniques are needed for the identification of products generated in the photoionization or photodestruction

## *Chapter 7: Concluding remarks and future direction*

---

of PAHs. The step-scan time-resolved FT-IR spectroscopy is one of the suitable methods to obtain spectral and kinetic information on such chemical reactions. In the near future it will be desirable to couple an UV laser with a step-scan FT-IR spectrometer to study the photochemical reactions of PAHs and to characterize the short lived radical or radical-cation of PAHs in the gas phase in laboratory. The time resolved FT-IR spectroscopy of the PAHs followed by their photochemical degradation under UV irradiation may lead us develop possible scavenging schemes for their removal.

# Appendix

## Symbolic Force constant matrix, unscaled and scaled Force constants in terms of nonredundant local coordinates

TABLE I1: A symbolic Force constant matrix of 2,4-DMQ

```

-----
Symbolic F matrix  nf= 1235ndim 63
=====

```

	1	2	3	4	5	6	7	8	9	10	11
1	1	62	63	65	68	72	77	83	90	98	107
2	62	2	64	66	69	73	78	84	91	99	108
3	63	64	3	67	70	74	79	85	92	100	109
4	65	66	67	4	71	75	80	86	93	101	110
5	68	69	70	71	5	76	81	87	94	102	111
6	72	73	74	75	76	6	82	88	95	103	112
7	77	78	79	80	81	82	7	89	96	104	113
8	83	84	85	86	87	88	89	8	97	105	114
9	90	91	92	93	94	95	96	97	9	106	115
10	98	99	100	101	102	103	104	105	106	10	116
11	107	108	109	110	111	112	113	114	115	116	11
12	117	118	119	120	121	122	123	124	125	126	127
13	128	129	130	131	132	133	134	135	136	137	138
14	140	141	142	143	144	145	146	147	148	149	150
15	153	154	155	156	157	158	159	160	161	162	163
16	167	168	169	170	171	172	173	174	175	176	177
17	182	183	184	185	186	187	188	189	190	191	192
18	198	199	200	201	202	203	204	205	206	207	208
19	215	216	217	218	219	220	221	222	223	224	225
20	215	216	217	218	219	220	221	222	223	224	225
21	234	235	236	237	238	239	240	241	242	243	244
22	253	254	255	256	257	258	259	260	261	262	263
23	253	254	255	256	257	258	259	260	261	262	263
24	275	276	277	278	279	280	281	282	283	284	285
25	296	297	298	299	300	301	302	303	304	305	306
26	318	319	320	321	322	323	324	325	326	327	328
27	341	342	343	344	345	346	347	348	349	350	351
28	365	366	367	368	369	370	371	372	373	374	375
29	390	391	392	393	394	395	396	397	398	399	400
30	416	417	418	419	420	421	422	423	424	425	426
31	443	444	445	446	447	448	449	450	451	452	453
32	471	472	473	474	475	476	477	478	479	480	481
33	500	501	502	503	504	505	506	507	508	509	510
34	530	531	532	533	534	535	536	537	538	539	540
35	561	562	563	564	565	566	567	568	569	570	571
36	593	594	595	596	597	598	599	600	601	602	603



37	626	627	628	629	630	631	632	633	634	635	636
38	660	661	662	663	664	665	666	667	668	669	670
39	695	696	697	698	699	700	701	702	703	704	705
40	733	734	735	736	737	738	739	740	741	742	743
41	772	773	774	775	776	777	778	779	780	781	782
42	0	0	0	0	0	0	0	0	0	0	0
43	814	815	816	817	818	819	820	821	822	823	824
44	853	854	855	856	857	858	859	860	861	862	863
45	896	897	898	899	900	901	902	903	904	905	906
46	939	940	941	942	943	944	945	946	947	948	949
47	0	0	0	0	0	0	0	0	0	0	0
48	0	0	0	0	0	0	0	0	0	0	0
49	0	0	0	0	0	0	0	0	0	0	0
50	0	0	0	0	0	0	0	0	0	0	0
51	0	0	0	0	0	0	0	0	0	0	0
52	0	0	0	0	0	0	0	0	0	0	0
53	0	0	0	0	0	0	0	0	0	0	0
54	0	0	0	0	0	0	0	0	0	0	0
55	0	0	0	0	0	0	0	0	0	0	0
56	0	0	0	0	0	0	0	0	0	0	0
57	0	0	0	0	0	0	0	0	0	0	0
58	0	0	0	0	0	0	0	0	0	0	0
59	0	0	0	0	0	0	0	0	0	0	0
60	0	0	0	0	0	0	0	0	0	0	0
61	0	0	0	0	0	0	0	0	0	0	0
62	0	0	0	0	0	0	0	0	0	0	0
63	0	0	0	0	0	0	0	0	0	0	0

=====

	12	13	14	15	16	17	18	19	20	21	22
--	----	----	----	----	----	----	----	----	----	----	----

-----

12	12	139	151	164	178	193	209	226	226	245	264
13	139	13	152	165	179	194	210	227	227	246	265
14	151	152	14	166	180	195	211	228	228	247	266
15	164	165	166	15	181	196	212	229	229	248	267
16	178	179	180	181	16	197	213	230	230	249	268
17	193	194	195	196	197	17	214	231	231	250	269
18	209	210	211	212	213	214	18	232	232	251	270
19	226	227	228	229	230	231	232	19	233	252	271
20	226	227	228	229	230	231	232	233	19	252	272
21	245	246	247	248	249	250	251	252	252	20	273
22	264	265	266	267	268	269	270	271	272	273	21
23	264	265	266	267	268	269	270	272	271	273	274
24	286	287	288	289	290	291	292	293	293	294	295
25	307	308	309	310	311	312	313	314	314	315	316
26	329	330	331	332	333	334	335	336	336	337	338
27	352	353	354	355	356	357	358	359	359	360	361
28	376	377	378	379	380	381	382	383	383	384	385
29	401	402	403	404	405	406	407	408	408	409	410
30	427	428	429	430	431	432	433	434	434	435	436
31	454	455	456	457	458	459	460	461	461	462	463
32	482	483	484	485	486	487	488	489	489	490	491
33	511	512	513	514	515	516	517	518	518	519	520

34	541	542	543	544	545	546	547	548	548	549	550
35	572	573	574	575	576	577	578	579	579	580	581
36	604	605	606	607	608	609	610	611	611	612	613
37	637	638	639	640	641	642	643	644	644	645	646
38	671	672	673	674	675	676	677	678	678	679	680
39	706	707	708	709	710	711	712	713	714	715	716
40	744	745	746	747	748	749	750	751	752	753	754
41	783	784	785	786	787	788	789	790	790	791	792
42	0	0	0	0	0	0	0	810	-810	0	811
43	825	826	827	828	829	830	831	832	832	833	834
44	864	865	866	867	868	869	870	871	872	873	874
45	907	908	909	910	911	912	913	914	915	916	917
46	950	951	952	953	954	955	956	957	957	958	959
47	0	0	0	0	0	0	0	981	-981	0	982
48	0	0	0	0	0	0	0	988	-988	0	989
49	0	0	0	0	0	0	0	996	-996	0	997
50	0	0	0	0	0	0	0	1005	-1005	0	1006
51	0	0	0	0	0	0	0	1015	-1015	0	1016
52	0	0	0	0	0	0	0	1026	-1026	0	1027
53	0	0	0	0	0	0	0	1038	-1038	0	1039
54	0	0	0	0	0	0	0	1051	-1051	0	1052
55	0	0	0	0	0	0	0	1065	-1065	0	1066
56	0	0	0	0	0	0	0	1080	-1080	0	1081
57	0	0	0	0	0	0	0	1096	-1096	0	1097
58	0	0	0	0	0	0	0	1113	-1113	0	1114
59	0	0	0	0	0	0	0	1131	-1131	0	1132
60	0	0	0	0	0	0	0	1150	-1150	0	1151
61	0	0	0	0	0	0	0	1170	-1170	0	1171
62	0	0	0	0	0	0	0	1191	-1191	0	1192
63	0	0	0	0	0	0	0	1213	-1213	0	1214

=====

	23	24	25	26	27	28	29	30	31	32	33
--	----	----	----	----	----	----	----	----	----	----	----

-----

23	21	295	316	338	361	385	410	436	463	491	520
24	295	22	317	339	362	386	411	437	464	492	521
25	316	317	23	340	363	387	412	438	465	493	522
26	338	339	340	24	364	388	413	439	466	494	523
27	361	362	363	364	25	389	414	440	467	495	524
28	385	386	387	388	389	26	415	441	468	496	525
29	410	411	412	413	414	415	27	442	469	497	526
30	436	437	438	439	440	441	442	28	470	498	527
31	463	464	465	466	467	468	469	470	29	499	528
32	491	492	493	494	495	496	497	498	499	30	529
33	520	521	522	523	524	525	526	527	528	529	31
34	550	551	552	553	554	555	556	557	558	559	560
35	581	582	583	584	585	586	587	588	589	590	591
36	613	614	615	616	617	618	619	620	621	622	623
37	646	647	648	649	650	651	652	653	654	655	656
38	680	681	682	683	684	685	686	687	688	689	690
39	717	718	719	720	721	722	723	724	725	726	727
40	755	756	757	758	759	760	761	762	763	764	765
41	792	793	794	795	796	797	798	799	800	801	802

42	-811	0	0	0	0	0	0	0	0	0	0
43	834	835	836	837	838	839	840	841	842	843	844
44	875	876	877	878	879	880	881	882	883	884	885
45	918	919	920	921	922	923	924	925	926	927	928
46	959	960	961	962	963	964	965	966	967	968	969
47	-982	0	0	0	0	0	0	0	0	0	0
48	-989	0	0	0	0	0	0	0	0	0	0
49	-997	0	0	0	0	0	0	0	0	0	0
50	-1006	0	0	0	0	0	0	0	0	0	0
51	-1016	0	0	0	0	0	0	0	0	0	0
52	-1027	0	0	0	0	0	0	0	0	0	0
53	-1039	0	0	0	0	0	0	0	0	0	0
54	-1052	0	0	0	0	0	0	0	0	0	0
55	-1066	0	0	0	0	0	0	0	0	0	0
56	-1081	0	0	0	0	0	0	0	0	0	0
57	-1097	0	0	0	0	0	0	0	0	0	0
58	-1114	0	0	0	0	0	0	0	0	0	0
59	-1132	0	0	0	0	0	0	0	0	0	0
60	-1151	0	0	0	0	0	0	0	0	0	0
61	-1171	0	0	0	0	0	0	0	0	0	0
62	-1192	0	0	0	0	0	0	0	0	0	0
63	-1214	0	0	0	0	0	0	0	0	0	0

=====

	34	35	36	37	38	39	40	41	42	43	44
--	----	----	----	----	----	----	----	----	----	----	----

-----

34	32	592	624	657	691	728	766	803	0	845	886
35	592	33	625	658	692	729	767	804	0	846	887
36	624	625	34	659	693	730	768	805	0	847	888
37	657	658	659	35	694	731	769	806	0	848	889
38	691	692	693	694	36	732	770	807	0	849	890
39	728	729	730	731	732	37	771	808	812	850	891
40	766	767	768	769	770	771	38	809	813	851	892
41	803	804	805	806	807	808	809	39	0	852	893
42	0	0	0	0	0	812	813	0	40	0	894
43	845	846	847	848	849	850	851	852	0	41	895
44	886	887	888	889	890	891	892	893	894	895	42
45	929	930	931	932	933	892	934	935	936	937	938
46	970	971	972	973	974	975	976	977	0	978	979
47	0	0	0	0	0	983	984	0	985	0	986
48	0	0	0	0	0	990	991	0	992	0	993
49	0	0	0	0	0	998	999	0	1000	0	1001
50	0	0	0	0	0	1007	1008	0	1009	0	1010
51	0	0	0	0	0	1017	1018	0	1019	0	1020
52	0	0	0	0	0	1028	1029	0	1030	0	1031
53	0	0	0	0	0	1040	1041	0	1042	0	1043
54	0	0	0	0	0	1053	1054	0	1055	0	1056
55	0	0	0	0	0	1067	1068	0	1069	0	1070
56	0	0	0	0	0	1082	1083	0	1084	0	1085
57	0	0	0	0	0	1098	1099	0	1100	0	1101
58	0	0	0	0	0	1115	1116	0	1117	0	1118
59	0	0	0	0	0	1133	1134	0	1135	0	1136
60	0	0	0	0	0	1152	1153	0	1154	0	1155

61	0	0	0	0	0	1172	1173	0	1174	0	1175
62	0	0	0	0	0	1193	1194	0	1195	0	1196
63	0	0	0	0	0	1215	1216	0	1217	0	1218

=====

45	46	47	48	49	50	51	52	53	54	55
----	----	----	----	----	----	----	----	----	----	----

-----

45	43	980	987	994	1002	1011	1021	1032	1044	1057	1071
46	980	44	0	0	0	0	0	0	0	0	0
47	987	0	45	995	1003	1012	1022	1033	1045	1058	1072
48	994	0	995	46	1004	1013	1023	1034	1046	1059	1073
49	1002	0	1003	1004	47	1014	1024	1035	1047	1060	1074
50	1011	0	1012	1013	1014	48	1025	1036	1048	1061	1075
51	1021	0	1022	1023	1024	1025	49	1037	1049	1062	1076
52	1032	0	1033	1034	1035	1036	1037	50	1050	1063	1077
53	1044	0	1045	1046	1047	1048	1049	1050	51	1064	1078
54	1057	0	1058	1059	1060	1061	1062	1063	1064	52	1079
55	1071	0	1072	1073	1074	1075	1076	1077	1078	1079	53
56	1086	0	1087	1088	1089	1090	1091	1092	1093	1094	1095
57	1102	0	1103	1104	1105	1106	1107	1108	1109	1110	1111
58	1119	0	1120	1121	1122	1123	1124	1125	1126	1127	1128
59	1137	0	1138	1139	1140	1141	1142	1143	1144	1145	1146
60	1156	0	1157	1158	1159	1160	1161	1162	1163	1164	1165
61	1176	0	1177	1178	1179	1180	1181	1182	1183	1184	1185
62	1197	0	1198	1199	1200	1201	1202	1203	1204	1205	1206
63	1219	0	1220	1221	1222	1223	1224	1225	1226	1227	1228

=====

56	57	58	59	60	61	62	63
----	----	----	----	----	----	----	----

-----

56	54	1112	1129	1147	1166	1186	1207	1229
57	1112	55	1130	1148	1167	1187	1208	1230
58	1129	1130	56	1149	1168	1188	1209	1231
59	1147	1148	1149	57	1169	1189	1210	1232
60	1166	1167	1168	1169	58	1190	1211	1233
61	1186	1187	1188	1189	1190	59	1212	1234
62	1207	1208	1209	1210	1211	1212	60	1235
63	1229	1230	1231	1232	1233	1234	1235	61

=====

TABLE I2: The complete force field in terms of unscaled and scaled nonredundant local coordinate force constants of 2,4-DMQ

Loc. Force constants according to Symf (unscaled)

1	6.2781	2	7.9180	3	6.1247	4	8.6614	5
6.8128								
6	6.0318	7	6.4057	8	7.7489	9	6.5595	10
7.7964								
11	6.4571	12	4.7106	13	5.5552	14	4.6790	15
5.6384								
16	5.6059	17	5.6068	18	5.6669	19	5.2264	20
5.4524								
21	5.2348	22	5.3579	23	0.9949	24	0.5643	25
0.9542								
26	0.5694	27	0.5568	28	0.5565	29	0.5272	30
1.5533								
31	1.4426	32	1.7053	33	1.5177	34	1.4453	35
1.5539								
36	0.5912	37	0.6574	38	0.6739	39	0.5967	40
0.5978								
41	0.5954	42	0.6686	43	0.6984	44	0.6125	45
0.6065								
46	0.5912	47	0.4569	48	0.5892	49	0.4478	50
0.4619								
51	0.4699	52	0.4749	53	0.2660	54	0.2089	55
0.2540								
56	0.3188	57	0.2715	58	0.3126	59	0.4172	60
0.0177								
61	0.0571	62	0.6588	63	-0.5063	64	0.6956	65
0.2421								
66	-0.4048	67	0.9636	68	-0.3319	69	0.2595	70
0.5256								
71	0.6727	72	0.6662	73	-0.3012	74	0.0353	75
0.3336								
76	0.8205	77	0.7051	78	-0.1671	79	0.0098	80
0.2013								
81	0.0829	82	0.6410	83	-0.1587	84	0.1605	85
0.0866								
86	0.0798	87	-0.2227	88	-0.2895	89	0.6653	90
0.0171								
91	-0.0852	92	0.2281	93	-0.0990	94	0.0109	95
0.1252								
96	-0.4621	97	0.7390	98	-0.2163	99	0.0697	100
0.0780								
101	0.1828	102	-0.1621	103	-0.3054	104	0.2307	105
0.4124								
106	0.7518	107	0.0606	108	-0.1965	109	0.0231	110
0.1959								
111	0.9327	112	0.6357	113	-0.3351	114	0.2151	115
0.4550								
116	0.6561	117	0.3259	118	0.2930	119	-0.0149	120
0.0721								

121	-0.0503	122	-0.0171	123	-0.0049	124	0.0246	125	-
0.0180									
126	0.0042	127	-0.0100	128	-0.0095	129	0.0983	130	
0.0847									
131	-0.0046	132	-0.0166	133	-0.0088	134	0.0036	135	
0.0009									
136	-0.0022	137	0.0006	138	0.0021	139	0.0029	140	-
0.0474									
141	-0.0397	142	0.3212	143	0.5043	144	0.0300	145	-
0.0753									
146	-0.0105	147	0.0102	148	-0.0132	149	0.0144	150	-
0.0067									
151	0.0027	152	0.0081	153	-0.0862	154	-0.0022	155	
0.0272									
156	0.0323	157	0.0127	158	-0.0598	159	0.0630	160	
0.1092									
161	0.0180	162	0.0083	163	-0.0135	164	0.0025	165	
0.0021									
166	0.0017	167	0.0051	168	0.0006	169	-0.0039	170	-
0.0004									
171	0.0037	172	-0.0134	173	-0.0046	174	0.1070	175	
0.1008									
176	-0.0049	177	-0.0169	178	0.0003	179	0.0011	180	
0.0005									
181	0.0110	182	0.0008	183	-0.0020	184	-0.0035	185	
0.0008									
186	0.0147	187	-0.0118	188	-0.0164	189	-0.0054	190	
0.1006									
191	0.1103	192	-0.0089	193	0.0003	194	0.0006	195	
0.0014									
196	0.0035	197	0.0103	198	-0.0021	199	0.0176	200	
0.0098									
201	0.0038	202	-0.0240	203	-0.0265	204	-0.0189	205	-
0.0041									
206	0.0028	207	0.0976	208	0.0675	209	0.0013	210	
0.0002									
211	0.0012	212	0.0015	213	0.0022	214	0.0100	215	-
0.0124									
216	0.0098	217	-0.0016	218	0.0191	219	0.0069	220	-
0.0024									
221	0.0039	222	-0.0030	223	0.0018	224	-0.0005	225	
0.0013									
226	0.0009	227	0.0055	228	0.0943	229	0.0005	230	
0.0002									
231	0.0003	232	0.0002	233	0.0516	234	0.0108	235	-
0.0035									
236	0.0006	237	-0.0229	238	-0.0010	239	0.0041	240	-
0.0006									
241	0.0009	242	-0.0022	243	0.0014	244	-0.0001	245	
0.0017									
246	-0.0016	247	0.0421	248	-0.0001	249	0.0002	250	
0.0001									
251	0.0003	252	0.0342	253	-0.0227	254	-0.0054	255	
0.0046									

256	0.0054	257	-0.0051	258	-0.0001	259	0.0064	260	-
0.0052									
261	0.0024	262	0.0045	263	0.0013	264	0.1090	265	-
0.0016									
266	0.0005	267	0.0099	268	0.0000	269	-0.0001	270	
0.0000									
271	0.0002	272	0.0000	273	0.0004	274	0.0511	275	-
0.0049									
276	-0.0012	277	0.0026	278	-0.0014	279	0.0077	280	-
0.0045									
281	-0.0095	282	0.0022	283	0.0020	284	0.0010	285	
0.0007									
286	0.0532	287	0.0132	288	0.0012	289	-0.0030	290	
0.0005									
291	0.0005	292	0.0009	293	0.0004	294	-0.0001	295	
0.0402									
296	-0.3937	297	0.2570	298	0.0371	299	0.0572	300	
0.0086									
301	-0.0692	302	-0.0640	303	-0.0214	304	0.0422	305	
0.0512									
306	0.0011	307	0.0417	308	-0.0320	309	0.0084	310	
0.0543									
311	-0.0006	312	-0.0006	313	-0.0037	314	0.0002	315	
0.0025									
316	0.0467	317	-0.0664	318	-0.0108	319	-0.2034	320	
0.1600									
321	0.0218	322	-0.0217	323	0.0187	324	-0.0096	325	-
0.0040									
326	0.0057	327	0.0022	328	0.0021	329	0.0173	330	
0.0043									
331	-0.0028	332	0.0001	333	-0.0008	334	0.0001	335	-
0.0007									
336	0.0033	337	-0.0048	338	0.0011	339	-0.0084	340	-
0.0097									
341	-0.0374	342	0.0090	343	-0.2290	344	0.4550	345	
0.0345									
346	-0.0234	347	0.0078	348	-0.0085	349	0.0057	350	-
0.0033									
351	0.0139	352	-0.0107	353	0.0103	354	0.0391	355	
0.0016									
356	0.0000	357	0.0010	358	0.0008	359	0.0422	360	-
0.0864									
361	-0.0023	362	-0.0005	363	-0.0150	364	0.0000	365	
0.0324									
366	0.0056	367	-0.0001	368	-0.0185	369	0.0026	370	
0.0130									
371	0.1833	372	-0.1736	373	-0.0180	374	0.0074	375	-
0.0205									
376	0.0247	377	0.0003	378	0.0005	379	-0.0238	380	
0.0087									
381	-0.0082	382	-0.0001	383	0.0003	384	-0.0004	385	
0.0028									
386	-0.0023	387	-0.0391	388	0.0002	389	0.0013	390	
0.0082									

391	0.0042	392	-0.0053	393	-0.0011	394	-0.0024	395	-
0.0160									
396	0.0117	397	0.1778	398	-0.1710	399	-0.0128	400	
0.0181									
401	-0.0001	402	0.0010	403	0.0002	404	-0.0090	405	-
0.0013									
406	0.0071	407	-0.0074	408	0.0000	409	0.0001	410	
0.0001									
411	0.0003	412	0.0000	413	-0.0012	414	-0.0002	415	
0.0079									
416	0.0022	417	0.0030	418	0.0055	419	-0.0054	420	-
0.0156									
421	0.0113	422	-0.0197	423	0.0136	424	0.1713	425	-
0.1723									
426	-0.0085	427	-0.0012	428	-0.0003	429	-0.0006	430	
0.0085									
431	-0.0070	432	0.0007	433	0.0074	434	-0.0001	435	-
0.0001									
436	-0.0005	437	0.0001	438	-0.0002	439	-0.0002	440	-
0.0012									
441	-0.0125	442	0.0096	443	-0.0052	444	-0.0112	445	-
0.0108									
446	-0.0012	447	0.0350	448	0.0199	449	0.0198	450	-
0.0265									
451	-0.0016	452	0.1656	453	-0.1422	454	-0.0022	455	
0.0004									
456	-0.0003	457	0.0001	458	0.0079	459	-0.0090	460	-
0.0191									
461	0.0003	462	-0.0003	463	0.0001	464	-0.0008	465	
0.0046									
466	0.0010	467	0.0004	468	-0.0020	469	-0.0121	470	
0.0088									
471	0.1817	472	0.0471	473	-0.0070	474	-0.2611	475	-
0.4031									
476	0.0120	477	0.2375	478	0.0972	479	0.0005	480	-
0.0825									
481	-0.2615	482	-0.1799	483	0.1228	484	-0.1822	485	-
0.0199									
486	0.0076	487	-0.0074	488	0.0143	489	-0.0099	490	-
0.0019									
491	-0.0099	492	-0.0028	493	-0.0630	494	0.0014	495	-
0.0317									
496	0.0184	497	0.0132	498	0.0122	499	-0.0041	500	
0.2037									
501	0.0342	502	-0.2990	503	0.3485	504	0.5235	505	-
0.0434									
506	0.1596	507	-0.0459	508	-0.1603	509	-0.0288	510	
0.1707									
511	-0.2473	512	0.0546	513	0.1093	514	-0.0131	515	
0.0073									
516	0.0064	517	-0.0171	518	0.0041	519	-0.0042	520	-
0.0095									
521	0.0019	522	-0.0285	523	-0.0758	524	0.0872	525	-
0.0140									



526	0.0076	527	-0.0073	528	0.0155	529	-0.0071	530
0.0033								
531	0.2797	532	0.0865	533	-0.2976	534	-0.0183	535
0.0818								-
536	0.2656	537	0.1049	538	-0.0127	539	-0.0896	540
0.3169								-
541	0.0257	542	-0.0949	543	0.2166	544	-0.0466	545
0.0034								
546	-0.0071	547	0.0248	548	0.0138	549	-0.0080	550
0.0079								-
551	-0.0049	552	-0.0352	553	-0.0495	554	0.0278	555
0.0341								
556	0.0117	557	0.0127	558	-0.0122	559	0.2020	560
0.0034								-
561	0.3114	562	0.1053	563	-0.0064	564	-0.1094	565
0.3799								-
566	-0.0020	567	0.1646	568	0.0540	569	-0.0138	570
0.0476								-
571	-0.1684	572	0.0084	573	0.0067	574	-0.0062	575
0.1393								-
576	0.1081	577	-0.1089	578	0.1181	579	-0.0018	580
0.0001								
581	-0.0031	582	0.0011	583	-0.0814	584	-0.0133	585
0.0119								-
586	0.0228	587	0.0035	588	0.0032	589	-0.0121	590
0.3554								
591	-0.0199	592	0.4026	593	0.2072	594	-0.0528	595
0.1904								-
596	-0.0308	597	0.2733	598	-0.0301	599	0.2450	600
0.0578								
601	-0.3666	602	0.0785	603	0.2257	604	-0.0039	605
0.0075								
606	0.0086	607	-0.1222	608	0.0522	609	0.0508	610
0.1095								-
611	0.0005	612	0.0021	613	0.0011	614	-0.0029	615
0.0284								-
616	-0.0082	617	0.0032	618	0.0077	619	0.0744	620
0.0756								-
621	0.0129	622	-0.0180	623	0.2823	624	-0.0267	625
0.0115								-
626	-0.3593	627	-0.1102	628	0.0218	629	0.1076	630
0.3980								
631	-0.0391	632	0.0272	633	-0.2696	634	0.0214	635
0.2658								
636	0.0165	637	-0.0169	638	-0.0030	639	0.0122	640
0.0440								
641	0.0854	642	-0.0839	643	-0.0236	644	0.0026	645
0.0002								
646	0.0095	647	-0.0009	648	0.1262	649	0.0118	650
0.0116								
651	0.0521	652	-0.0483	653	-0.0486	654	0.0965	655
0.3733								-
656	0.0283	657	-0.4179	658	-0.2510	659	0.0138	660
0.0008								-

661	0.0000	662	0.0263	663	0.0194	664	0.0200	665	-
0.0095									
666	-0.0009	667	0.0008	668	-0.0040	669	0.0043	670	-
0.0017									
671	0.0015	672	0.0064	673	0.3046	674	0.0004	675	
0.0001									
676	0.0005	677	0.0004	678	-0.0693	679	-0.0539	680	
0.0001									
681	0.0004	682	0.0020	683	0.0029	684	-0.0063	685	
0.0001									
686	0.0000	687	-0.0001	688	-0.0003	689	-0.0251	690	
0.0166									
691	0.0205	692	-0.0017	693	0.0033	694	0.0040	695	
0.0010									
696	-0.0070	697	-0.0174	698	0.0282	699	0.0091	700	-
0.0036									
701	-0.0001	702	0.0001	703	-0.0009	704	0.0019	705	-
0.0003									
706	-0.0015	707	0.0033	708	-0.0126	709	0.0005	710	
0.0000									
711	0.0004	712	0.0001	713	0.0946	714	-0.0513	715	-
0.0480									
716	-0.0004	717	-0.0005	718	0.0002	719	-0.0028	720	
0.0021									
721	0.0713	722	0.0004	723	-0.0001	724	-0.0002	725	
0.0005									
726	0.0050	727	0.0078	728	-0.0049	729	-0.0021	730	
0.0010									
731	0.0029	732	0.0010	733	0.0018	734	-0.0121	735	-
0.0302									
736	0.0488	737	0.0157	738	-0.0062	739	-0.0002	740	
0.0001									
741	-0.0016	742	0.0034	743	-0.0006	744	-0.0025	745	
0.0057									
746	-0.0218	747	0.0008	748	0.0001	749	0.0006	750	
0.0001									
751	-0.0046	752	0.0796	753	-0.0831	754	-0.0008	755	-
0.0007									
756	0.0004	757	-0.0049	758	0.0036	759	0.1235	760	
0.0007									
761	-0.0001	762	-0.0003	763	0.0008	764	0.0087	765	
0.0134									
766	-0.0085	767	-0.0036	768	0.0017	769	0.0051	770	
0.0017									
771	0.0143	772	0.0089	773	-0.0118	774	0.0107	775	-
0.0209									
776	-0.0012	777	-0.0016	778	-0.0032	779	0.0021	780	-
0.0030									
781	0.0025	782	-0.0027	783	-0.0005	784	0.0029	785	-
0.0431									
786	0.0000	787	-0.0002	788	-0.0001	789	-0.0001	790	
0.0683									
791	-0.1043	792	-0.0002	793	0.0002	794	0.0000	795	
0.0036									

796	-0.0373	797	-0.0001	798	0.0000	799	0.0000	800	-
0.0001									
801	0.0029	802	0.0001	803	-0.0066	804	0.0002	805	
0.0007									
806	0.0010	807	-0.0054	808	0.0047	809	0.0082	810	-
0.1082									
811	-0.0002	812	0.0013	813	-0.0007	814	0.0269	815	
0.0168									
816	0.0060	817	-0.0130	818	-0.0071	819	0.0052	820	
0.0116									
821	0.0050	822	-0.0062	823	0.0020	824	-0.0012	825	
0.3320									
826	0.0081	827	0.0014	828	0.0011	829	0.0003	830	
0.0000									
831	0.0005	832	0.0004	833	0.0006	834	-0.0708	835	-
0.0711									
836	0.0136	837	-0.0038	838	-0.0031	839	0.0082	840	
0.0003									
841	-0.0005	842	-0.0006	843	-0.0228	844	-0.0335	845	
0.0046									
846	0.0044	847	0.0031	848	-0.0041	849	0.0004	850	-
0.0004									
851	-0.0007	852	-0.0001	853	-0.0041	854	0.0150	855	-
0.0016									
856	-0.0061	857	0.0021	858	0.0063	859	0.0161	860	
0.0021									
861	-0.0078	862	-0.0032	863	-0.0028	864	-0.0228	865	-
0.0038									
866	0.0002	867	-0.0063	868	-0.0002	869	0.0000	870	-
0.0005									
871	-0.0001	872	0.0000	873	0.0005	874	0.0907	875	-
0.0512									
876	-0.0409	877	0.0376	878	0.0021	879	-0.0023	880	
0.0060									
881	-0.0001	882	-0.0001	883	0.0010	884	0.0134	885	
0.0068									
886	0.0199	887	0.0038	888	0.0062	889	-0.0076	890	
0.0001									
891	-0.0011	892	-0.0006	893	-0.0002	894	-0.0007	895	-
0.0070									
896	-0.0071	897	0.0259	898	-0.0027	899	-0.0105	900	
0.0036									
901	0.0109	902	0.0279	903	0.0037	904	-0.0135	905	-
0.0056									
906	-0.0048	907	-0.0395	908	-0.0065	909	0.0004	910	-
0.0108									
911	-0.0003	912	0.0000	913	-0.0010	914	0.0000	915	-
0.0001									
916	0.0009	917	-0.0068	918	0.0752	919	-0.0708	920	
0.0652									
921	0.0037	922	-0.0039	923	0.0103	924	-0.0003	925	-
0.0001									
926	0.0017	927	0.0233	928	0.0118	929	0.0344	930	
0.0066									

931	0.0107	932	-0.0132	933	0.0001	934	-0.0018	935	-
0.0004									
936	0.0004	937	-0.0121	938	0.0259	939	0.0283	940	-
0.0046									
941	-0.0061	942	-0.0102	943	0.0003	944	0.0027	945	
0.0053									
946	0.0028	947	-0.0097	948	-0.0036	949	-0.0020	950	-
0.0377									
951	0.0033	952	-0.0013	953	-0.0034	954	-0.0002	955	-
0.0003									
956	0.0000	957	-0.0001	958	-0.0002	959	0.0636	960	-
0.1186									
961	-0.0416	962	-0.0010	963	0.0002	964	0.0102	965	
0.0001									
966	-0.0005	967	0.0000	968	0.0068	969	-0.0009	970	
0.0119									
971	0.0097	972	0.0077	973	-0.0123	974	-0.0003	975	
0.0000									
976	0.0001	977	0.0001	978	-0.0014	979	0.0070	980	
0.0121									
981	-0.0002	982	-0.1105	983	-0.0001	984	0.0000	985	-
0.0001									
986	-0.0088	987	0.0051	988	0.0006	989	-0.0313	990	
0.0033									
991	-0.0019	992	0.0031	993	-0.0994	994	0.0574	995	-
0.0140									
996	0.0071	997	0.0067	998	0.0027	999	-0.0016	1000	
0.0026									
1001	0.0185	1002	-0.0107	1003	-0.0082	1004	-0.1036	1005	-
0.0309									
1006	0.0007	1007	-0.0927	1008	0.0535	1009	0.0001	1010	
0.0045									
1011	-0.0026	1012	-0.0010	1013	-0.0190	1014	-0.0364	1015	
0.0000									
1016	0.0033	1017	-0.0002	1018	0.0001	1019	-0.0001	1020	
0.0040									
1021	-0.0023	1022	0.0096	1023	0.0071	1024	0.0074	1025	
0.0020									
1026	-0.0002	1027	0.0003	1028	-0.0003	1029	0.0002	1030	
0.0001									
1031	-0.0007	1032	0.0004	1033	-0.0002	1034	0.0052	1035	-
0.0010									
1036	0.0011	1037	-0.0872	1038	0.0001	1039	0.0003	1040	
0.0007									
1041	-0.0004	1042	-0.0002	1043	-0.0004	1044	0.0002	1045	
0.0001									
1046	0.0006	1047	0.0032	1048	-0.0016	1049	0.0051	1050	-
0.0530									
1051	0.0000	1052	0.0000	1053	-0.0009	1054	0.0005	1055	-
0.0002									
1056	-0.0006	1057	0.0003	1058	0.0000	1059	0.0028	1060	
0.0006									
1061	0.0037	1062	-0.0221	1063	0.0059	1064	-0.0889	1065	
0.0098									

1066	0.0091	1067	0.0259	1068	-0.0150	1069	-0.0022	1070	
0.0314									
1071	-0.0181	1072	0.0007	1073	-0.1379	1074	0.1575	1075	-
0.1290									
1076	0.0137	1077	-0.0092	1078	0.0071	1079	-0.0190	1080	-
0.0096									
1081	0.0028	1082	-0.0279	1083	0.0161	1084	-0.0002	1085	
0.0103									
1086	-0.0059	1087	0.0073	1088	-0.0407	1089	-0.0408	1090	
0.1376									
1091	0.0116	1092	-0.0080	1093	-0.0036	1094	-0.0205	1095	-
0.0323									
1096	0.0001	1097	-0.0094	1098	0.0168	1099	-0.0097	1100	-
0.0018									
1101	-0.0354	1102	0.0204	1103	0.0006	1104	0.1528	1105	-
0.1565									
1106	-0.0456	1107	0.0060	1108	0.0051	1109	0.0052	1110	-
0.0107									
1111	-0.0587	1112	-0.0253	1113	0.0009	1114	0.0011	1115	
0.0024									
1116	-0.0014	1117	-0.0005	1118	0.0039	1119	-0.0022	1120	
0.0047									
1121	-0.0082	1122	0.0119	1123	-0.0089	1124	0.1472	1125	-
0.1583									
1126	0.1552	1127	-0.1544	1128	0.0382	1129	0.0078	1130	
0.0021									
1131	0.0004	1132	0.0016	1133	-0.0006	1134	0.0003	1135	-
0.0003									
1136	0.0037	1137	-0.0021	1138	0.0049	1139	-0.0039	1140	
0.0085									
1141	-0.0005	1142	0.0442	1143	0.0616	1144	-0.1646	1145	
0.1192									
1146	0.0056	1147	-0.0123	1148	-0.0175	1149	-0.0732	1150	
0.0004									
1151	-0.0011	1152	0.0023	1153	-0.0014	1154	-0.0002	1155	-
0.0005									
1156	0.0003	1157	-0.0027	1158	-0.0059	1159	-0.0051	1160	-
0.0086									
1161	-0.1528	1162	0.1534	1163	0.0202	1164	-0.1267	1165	
0.0043									
1166	-0.0137	1167	0.0123	1168	-0.0414	1169	-0.0348	1170	
0.0015									
1171	-0.0013	1172	0.0032	1173	-0.0018	1174	-0.0009	1175	
0.0070									
1176	-0.0040	1177	0.0044	1178	-0.0386	1179	-0.0217	1180	-
0.0204									
1181	-0.0292	1182	-0.0182	1183	-0.0220	1184	-0.0483	1185	
0.0088									
1186	0.0378	1187	-0.0423	1188	0.0047	1189	-0.0276	1190	
0.0565									
1191	-0.0143	1192	0.0003	1193	0.0148	1194	-0.0085	1195	-
0.0322									
1196	0.0010	1197	-0.0006	1198	-0.0001	1199	-0.0034	1200	-
0.0048									

1201	0.0294	1202	-0.0002	1203	0.0004	1204	0.0004	1205	
0.0001									
1206	-0.0089	1207	0.0098	1208	-0.0008	1209	-0.0005	1210	-
0.0008									
1211	0.0004	1212	-0.0033	1213	0.0001	1214	-0.0253	1215	
0.0005									
1216	-0.0003	1217	-0.0001	1218	0.0133	1219	-0.0077	1220	-
0.0063									
1221	0.0221	1222	-0.0117	1223	-0.0021	1224	0.0110	1225	-
0.0008									
1226	-0.0007	1227	-0.0007	1228	-0.0039	1229	0.0067	1230	
0.0045									
1231	0.0077	1232	0.0076	1233	0.0005	1234	0.0093	1235	
0.0001									

Fitting with nfit= 1(Pulay's method)

Force constants according to Symf 1235 (scaled)

1	5.8185	2	7.4194	3	5.7031	4	7.8897	5	
6.4993									
6	5.8089	7	5.8958	8	7.5018	9	6.2178	10	
7.3547									
11	6.1504	12	4.4130	13	4.8871	14	4.6767	15	
5.1915									
16	4.8935	17	5.0700	18	5.1815	19	4.6878	20	
4.7713									
21	4.6815	22	4.7828	23	0.9307	24	0.5325	25	
0.9201									
26	0.5285	27	0.5320	28	0.5139	29	0.4942	30	
1.5125									
31	1.3571	32	1.6062	33	1.4390	34	1.3914	35	
1.4324									
36	0.5454	37	0.6483	38	0.6645	39	0.5535	40	
0.5641									
41	0.5638	42	0.6317	43	0.6599	44	0.5821	45	
0.5567									
46	0.5530	47	0.4285	48	0.5140	49	0.4409	50	
0.4413									
51	0.4185	52	0.4743	53	0.2486	54	0.1968	55	
0.2446									
56	0.3066	57	0.2656	58	0.3025	59	0.3930	60	
0.0162									
61	0.0535	62	0.6140	63	-0.4704	64	0.6497	65	
0.2224									
66	-0.3740	67	0.8875	68	-0.3120	69	0.2454	70	-
0.4954									
71	0.6271	72	0.6294	73	-0.2861	74	0.0334	75	-
0.3125									
76	0.7865	77	0.6512	78	-0.1552	79	0.0091	80	-
0.1843									
81	0.0777	82	0.6035	83	-0.1504	84	0.1529	85	-
0.0822									

86	0.0749	87	-0.2141	88	-0.2796	89	0.6280	90	-
0.0160									
91	-0.0803	92	0.2143	93	-0.0920	94	0.0104	95	
0.1196									
96	-0.4316	97	0.7079	98	-0.2022	99	0.0655	100	-
0.0731									
101	0.1694	102	-0.1538	103	-0.2911	104	0.2150	105	-
0.3941									
106	0.7109	107	0.0570	108	-0.1857	109	0.0218	110	-
0.1825									
111	0.8891	112	0.6088	113	-0.3137	114	0.2065	115	-
0.4323									
116	0.6219	117	0.3037	118	0.2745	119	-0.0139	120	-
0.0666									
121	-0.0475	122	-0.0162	123	-0.0046	124	0.0234	125	-
0.0170									
126	0.0040	127	-0.0095	128	-0.0086	129	0.0892	130	
0.0767									
131	-0.0041	132	-0.0152	133	-0.0081	134	0.0033	135	
0.0008									
136	-0.0020	137	0.0005	138	0.0019	139	0.0027	140	-
0.0456									
141	-0.0384	142	0.3098	143	0.4812	144	0.0293	145	-
0.0739									
146	-0.0101	147	0.0101	148	-0.0129	149	0.0140	150	-
0.0066									
151	0.0026	152	0.0076	153	-0.0796	154	-0.0020	155	
0.0252									
156	0.0296	157	0.0119	158	-0.0563	159	0.0580	160	
0.1031									
161	0.0169	162	0.0077	163	-0.0126	164	0.0023	165	
0.0019									
166	0.0016	167	0.0046	168	0.0005	169	-0.0035	170	-
0.0004									
171	0.0033	172	-0.0123	173	-0.0042	174	0.0984	175	
0.0917									
176	-0.0044	177	-0.0154	178	0.0003	179	0.0010	180	
0.0005									
181	0.0099	182	0.0008	183	-0.0018	184	-0.0032	185	
0.0007									
186	0.0137	187	-0.0110	188	-0.0149	189	-0.0051	190	
0.0931									
191	0.1019	192	-0.0083	193	0.0002	194	0.0005	195	
0.0013									
196	0.0032	197	0.0092	198	-0.0019	199	0.0163	200	
0.0090									
201	0.0034	202	-0.0224	203	-0.0249	204	-0.0173	205	-
0.0038									
206	0.0026	207	0.0906	208	0.0630	209	0.0012	210	
0.0002									
211	0.0011	212	0.0014	213	0.0020	214	0.0091	215	-
0.0113									
216	0.0090	217	-0.0015	218	0.0173	219	0.0064	220	-
0.0022									

221	0.0035	222	-0.0028	223	0.0016	224	-0.0004	225
0.0012								
226	0.0009	227	0.0049	228	0.0893	229	0.0005	230
0.0001								
231	0.0003	232	0.0002	233	0.0463	234	0.0097	235
0.0032								-
236	0.0005	237	-0.0204	238	-0.0009	239	0.0038	240
0.0005								-
241	0.0008	242	-0.0020	243	0.0013	244	-0.0001	245
0.0016								
246	-0.0014	247	0.0394	248	-0.0001	249	0.0002	250
0.0001								
251	0.0002	252	0.0303	253	-0.0207	254	-0.0050	255
0.0042								
256	0.0049	257	-0.0047	258	-0.0001	259	0.0058	260
0.0048								-
261	0.0022	262	0.0041	263	0.0012	264	0.0998	265
0.0015								-
266	0.0004	267	0.0090	268	0.0000	269	-0.0001	270
0.0000								
271	0.0001	272	0.0000	273	0.0004	274	0.0457	275
0.0044								-
276	-0.0011	277	0.0024	278	-0.0012	279	0.0071	280
0.0042								-
281	-0.0086	282	0.0021	283	0.0018	284	0.0009	285
0.0006								
286	0.0486	287	0.0117	288	0.0011	289	-0.0027	290
0.0004								
291	0.0004	292	0.0008	293	0.0004	294	-0.0001	295
0.0359								
296	-0.3666	297	0.2406	298	0.0346	299	0.0528	300
0.0082								
301	-0.0657	302	-0.0594	303	-0.0204	304	0.0397	305
0.0481								
306	0.0010	307	0.0391	308	-0.0290	309	0.0081	310
0.0504								
311	-0.0005	312	-0.0005	313	-0.0034	314	0.0002	315
0.0022								
316	0.0428	317	-0.0607	318	-0.0101	319	-0.1913	320
0.1500								
321	0.0202	322	-0.0206	323	0.0178	324	-0.0089	325
0.0038								-
326	0.0054	327	0.0021	328	0.0020	329	0.0163	330
0.0039								
331	-0.0027	332	0.0001	333	-0.0008	334	0.0001	335
0.0006								-
336	0.0031	337	-0.0043	338	0.0011	339	-0.0077	340
0.0091								-
341	-0.0354	342	0.0085	343	-0.2170	344	0.4264	345
0.0331								
346	-0.0225	347	0.0074	348	-0.0082	349	0.0055	350
0.0031								-
351	0.0133	352	-0.0102	353	0.0095	354	0.0384	355
0.0015								



356	0.0000	357	0.0009	358	0.0007	359	0.0392	360	-
0.0794									
361	-0.0021	362	-0.0005	363	-0.0143	364	0.0000	365	
0.0301									
366	0.0052	367	0.0000	368	-0.0170	369	0.0024	370	
0.0123									
371	0.1694	372	-0.1646	373	-0.0169	374	0.0069	375	-
0.0193									
376	0.0230	377	0.0002	378	0.0005	379	-0.0220	380	
0.0078									
381	-0.0075	382	-0.0001	383	0.0002	384	-0.0003	385	
0.0026									
386	-0.0021	387	-0.0364	388	0.0002	389	0.0012	390	
0.0077									
391	0.0040	392	-0.0050	393	-0.0010	394	-0.0023	395	-
0.0154									
396	0.0110	397	0.1710	398	-0.1627	399	-0.0121	400	
0.0172									
401	-0.0001	402	0.0009	403	0.0002	404	-0.0085	405	-
0.0012									
406	0.0066	407	-0.0069	408	0.0000	409	0.0001	410	
0.0001									
411	0.0003	412	0.0000	413	-0.0012	414	-0.0002	415	
0.0074									
416	0.0021	417	0.0028	418	0.0051	419	-0.0049	420	-
0.0146									
421	0.0107	422	-0.0182	423	0.0129	424	0.1602	425	-
0.1608									
426	-0.0079	427	-0.0011	428	-0.0002	429	-0.0005	430	
0.0078									
431	-0.0063	432	0.0007	433	0.0068	434	-0.0001	435	-
0.0001									
436	-0.0005	437	0.0001	438	-0.0001	439	-0.0002	440	-
0.0011									
441	-0.0116	442	0.0090	443	-0.0049	444	-0.0105	445	-
0.0101									
446	-0.0011	447	0.0331	448	0.0189	449	0.0184	450	-
0.0253									
451	-0.0015	452	0.1558	453	-0.1343	454	-0.0020	455	
0.0004									
456	-0.0003	457	0.0001	458	0.0072	459	-0.0083	460	-
0.0176									
461	0.0003	462	-0.0003	463	0.0001	464	-0.0007	465	
0.0043									
466	0.0010	467	0.0004	468	-0.0019	469	-0.0115	470	
0.0082									
471	0.1726	472	0.0450	473	-0.0067	474	-0.2459	475	-
0.3885									
476	0.0116	477	0.2248	478	0.0943	479	0.0005	480	-
0.0791									
481	-0.2519	482	-0.1718	483	0.1136	484	-0.1797	485	-
0.0188									
486	0.0070	487	-0.0069	488	0.0135	489	-0.0093	490	-
0.0018									

491	-0.0092	492	-0.0026	493	-0.0601	494	0.0013	495	-
0.0307									
496	0.0175	497	0.0127	498	0.0115	499	-0.0039	500	
0.1902									
501	0.0321	502	-0.2798	503	0.3226	504	0.4960	505	-
0.0413									
506	0.1485	507	-0.0438	508	-0.1513	509	-0.0271	510	
0.1616									
511	-0.2322	512	0.0497	513	0.1060	514	-0.0122	515	
0.0067									
516	0.0059	517	-0.0159	518	0.0038	519	-0.0038	520	-
0.0087									
521	0.0017	522	-0.0268	523	-0.0714	524	0.0831	525	-
0.0131									
526	0.0072	527	-0.0068	528	0.0146	529	-0.0068	530	
0.0031									
531	0.2628	532	0.0810	533	-0.2756	534	-0.0173	535	-
0.0779									
536	0.2473	537	0.1002	538	-0.0120	539	-0.0845	540	-
0.3002									
541	0.0242	542	-0.0864	543	0.2102	544	-0.0434	545	
0.0030									
546	-0.0065	547	0.0231	548	0.0126	549	-0.0073	550	-
0.0073									
551	-0.0045	552	-0.0331	553	-0.0467	554	0.0264	555	
0.0319									
556	0.0111	557	0.0119	558	-0.0115	559	0.1934	560	-
0.0032									
561	0.2919	562	0.0992	563	-0.0060	564	-0.1017	565	-
0.3613									
566	-0.0019	567	0.1537	568	0.0517	569	-0.0131	570	-
0.0450									
571	-0.1600	572	0.0079	573	0.0061	574	-0.0060	575	-
0.1301									
576	0.0983	577	-0.1008	578	0.1100	579	-0.0016	580	
0.0001									
581	-0.0029	582	0.0010	583	-0.0767	584	-0.0126	585	-
0.0113									
586	0.0214	587	0.0034	588	0.0030	589	-0.0114	590	
0.3415									
591	-0.0188	592	0.3804	593	0.1957	594	-0.0501	595	-
0.1803									
596	-0.0288	597	0.2619	598	-0.0289	599	0.2307	600	
0.0558									
601	-0.3502	602	0.0748	603	0.2161	604	-0.0037	605	
0.0069									
606	0.0085	607	-0.1150	608	0.0478	609	0.0474	610	-
0.1028									
611	0.0005	612	0.0020	613	0.0010	614	-0.0027	615	-
0.0270									
616	-0.0078	617	0.0031	618	0.0073	619	0.0714	620	-
0.0713									
621	0.0123	622	-0.0174	623	0.2686	624	-0.0255	625	-
0.0110									

626	-0.3321	627	-0.1024	628	0.0202	629	0.0986	630	
0.3732									
631	-0.0368	632	0.0251	633	-0.2547	634	0.0200	635	
0.2478									
636	0.0155	637	-0.0157	638	-0.0027	639	0.0117	640	
0.0405									
641	0.0766	642	-0.0766	643	-0.0217	644	0.0024	645	
0.0002									
646	0.0086	647	-0.0009	648	0.1172	649	0.0110	650	
0.0110									
651	0.0482	652	-0.0454	653	-0.0449	654	0.0897	655	-
0.3537									
656	0.0263	657	-0.3894	658	-0.2347	659	0.0130	660	-
0.0007									
661	0.0000	662	0.0244	663	0.0178	664	0.0188	665	-
0.0089									
666	-0.0008	667	0.0008	668	-0.0038	669	0.0040	670	-
0.0016									
671	0.0014	672	0.0058	673	0.2925	674	0.0004	675	
0.0001									
676	0.0005	677	0.0004	678	-0.0630	679	-0.0484	680	
0.0001									
681	0.0004	682	0.0019	683	0.0027	684	-0.0060	685	
0.0001									
686	0.0000	687	-0.0001	688	-0.0002	689	-0.0238	690	
0.0154									
691	0.0191	692	-0.0016	693	0.0031	694	0.0037	695	
0.0010									
696	-0.0067	697	-0.0167	698	0.0267	699	0.0088	700	-
0.0035									
701	-0.0001	702	0.0001	703	-0.0009	704	0.0019	705	-
0.0003									
706	-0.0014	707	0.0031	708	-0.0125	709	0.0005	710	
0.0000									
711	0.0004	712	0.0000	713	0.0890	714	-0.0483	715	-
0.0446									
716	-0.0004	717	-0.0004	718	0.0002	719	-0.0027	720	
0.0020									
721	0.0695	722	0.0004	723	-0.0001	724	-0.0002	725	
0.0004									
726	0.0049	727	0.0075	728	-0.0047	729	-0.0020	730	
0.0010									
731	0.0028	732	0.0010	733	0.0017	734	-0.0117	735	-
0.0289									
736	0.0463	737	0.0153	738	-0.0061	739	-0.0002	740	
0.0001									
741	-0.0015	742	0.0032	743	-0.0005	744	-0.0024	745	
0.0053									
746	-0.0217	747	0.0008	748	0.0001	749	0.0006	750	
0.0001									
751	-0.0044	752	0.0749	753	-0.0772	754	-0.0007	755	-
0.0007									
756	0.0004	757	-0.0047	758	0.0035	759	0.1204	760	
0.0007									

761	-0.0001	762	-0.0003	763	0.0008	764	0.0086	765	
0.0129									
766	-0.0082	767	-0.0035	768	0.0017	769	0.0049	770	
0.0017									
771	0.0141	772	0.0083	773	-0.0110	774	0.0100	775	-
0.0192									
776	-0.0011	777	-0.0015	778	-0.0030	779	0.0020	780	-
0.0028									
781	0.0023	782	-0.0025	783	-0.0005	784	0.0026	785	-
0.0415									
786	0.0000	787	-0.0001	788	-0.0001	789	-0.0001	790	
0.0623									
791	-0.0940	792	-0.0002	793	0.0002	794	0.0000	795	
0.0033									
796	-0.0353	797	-0.0001	798	0.0000	799	0.0000	800	-
0.0001									
801	0.0028	802	0.0001	803	-0.0062	804	0.0002	805	
0.0007									
806	0.0009	807	-0.0050	808	0.0045	809	0.0078	810	-
0.0996									
811	-0.0001	812	0.0012	813	-0.0007	814	0.0252	815	
0.0158									
816	0.0056	817	-0.0121	818	-0.0067	819	0.0049	820	
0.0108									
821	0.0048	822	-0.0059	823	0.0018	824	-0.0012	825	
0.3128									
826	0.0074	827	0.0013	828	0.0010	829	0.0003	830	
0.0000									
831	0.0004	832	0.0003	833	0.0005	834	-0.0651	835	-
0.0654									
836	0.0128	837	-0.0035	838	-0.0029	839	0.0077	840	
0.0003									
841	-0.0004	842	-0.0006	843	-0.0219	844	-0.0317	845	
0.0043									
846	0.0042	847	0.0030	848	-0.0038	849	0.0004	850	-
0.0004									
851	-0.0007	852	-0.0001	853	-0.0038	854	0.0141	855	-
0.0015									
856	-0.0056	857	0.0020	858	0.0060	859	0.0150	860	
0.0020									
861	-0.0074	862	-0.0030	863	-0.0026	864	-0.0215	865	-
0.0034									
866	0.0002	867	-0.0058	868	-0.0001	869	0.0000	870	-
0.0005									
871	-0.0001	872	0.0000	873	0.0005	874	0.0834	875	-
0.0471									
876	-0.0376	877	0.0354	878	0.0020	879	-0.0022	880	
0.0056									
881	-0.0001	882	0.0000	883	0.0009	884	0.0129	885	
0.0064									
886	0.0187	887	0.0036	888	0.0059	889	-0.0071	890	
0.0000									
891	-0.0011	892	-0.0005	893	-0.0002	894	-0.0007	895	-
0.0066									

896	-0.0066	897	0.0244	898	-0.0025	899	-0.0098	900	
0.0034									
901	0.0104	902	0.0260	903	0.0035	904	-0.0128	905	-
0.0053									
906	-0.0046	907	-0.0372	908	-0.0060	909	0.0003	910	-
0.0101									
911	-0.0002	912	0.0000	913	-0.0009	914	0.0000	915	-
0.0001									
916	0.0008	917	-0.0062	918	0.0691	919	-0.0651	920	
0.0613									
921	0.0035	922	-0.0037	923	0.0097	924	-0.0002	925	-
0.0001									
926	0.0016	927	0.0223	928	0.0111	929	0.0325	930	
0.0062									
931	0.0102	932	-0.0124	933	0.0001	934	-0.0017	935	-
0.0004									
936	0.0004	937	-0.0115	938	0.0244	939	0.0265	940	-
0.0044									
941	-0.0057	942	-0.0095	943	0.0003	944	0.0026	945	
0.0050									
946	0.0027	947	-0.0092	948	-0.0034	949	-0.0019	950	-
0.0356									
951	0.0030	952	-0.0013	953	-0.0032	954	-0.0002	955	-
0.0003									
956	0.0000	957	0.0000	958	-0.0002	959	0.0587	960	-
0.1093									
961	-0.0393	962	-0.0009	963	0.0002	964	0.0096	965	
0.0001									
966	-0.0005	967	0.0000	968	0.0066	969	-0.0008	970	
0.0113									
971	0.0092	972	0.0074	973	-0.0115	974	-0.0003	975	
0.0000									
976	0.0001	977	0.0001	978	-0.0013	979	0.0066	980	
0.0114									
981	-0.0002	982	-0.1001	983	-0.0001	984	0.0000	985	-
0.0001									
986	-0.0082	987	0.0048	988	0.0006	989	-0.0286	990	
0.0031									
991	-0.0018	992	0.0029	993	-0.0935	994	0.0540	995	-
0.0130									
996	0.0065	997	0.0061	998	0.0026	999	-0.0015	1000	
0.0024									
1001	0.0174	1002	-0.0101	1003	-0.0076	1004	-0.0971	1005	-
0.0274									
1006	0.0006	1007	-0.0860	1008	0.0497	1009	0.0000	1010	
0.0041									
1011	-0.0023	1012	-0.0009	1013	-0.0172	1014	-0.0329	1015	
0.0000									
1016	0.0031	1017	-0.0002	1018	0.0001	1019	-0.0001	1020	
0.0038									
1021	-0.0022	1022	0.0091	1023	0.0068	1024	0.0071	1025	
0.0019									
1026	-0.0002	1027	0.0003	1028	-0.0003	1029	0.0001	1030	
0.0001									

1031	-0.0007	1032	0.0004	1033	-0.0002	1034	0.0049	1035	-
0.0009									
1036	0.0010	1037	-0.0845	1038	0.0001	1039	0.0003	1040	
0.0007									
1041	-0.0004	1042	-0.0002	1043	-0.0003	1044	0.0002	1045	
0.0001									
1046	0.0005	1047	0.0029	1048	-0.0014	1049	0.0048	1050	-
0.0489									
1051	0.0000	1052	0.0000	1053	-0.0009	1054	0.0005	1055	-
0.0002									
1056	-0.0006	1057	0.0003	1058	0.0000	1059	0.0027	1060	
0.0006									
1061	0.0034	1062	-0.0219	1063	0.0057	1064	-0.0839	1065	
0.0090									
1066	0.0083	1067	0.0249	1068	-0.0144	1069	-0.0021	1070	
0.0295									
1071	-0.0170	1072	0.0007	1073	-0.1289	1074	0.1474	1075	-
0.1165									
1076	0.0131	1077	-0.0087	1078	0.0064	1079	-0.0183	1080	-
0.0088									
1081	0.0026	1082	-0.0269	1083	0.0155	1084	-0.0001	1085	
0.0097									
1086	-0.0056	1087	0.0068	1088	-0.0382	1089	-0.0383	1090	
0.1248									
1091	0.0112	1092	-0.0076	1093	-0.0033	1094	-0.0199	1095	-
0.0304									
1096	0.0001	1097	-0.0087	1098	0.0164	1099	-0.0095	1100	-
0.0017									
1101	-0.0338	1102	0.0195	1103	0.0006	1104	0.1451	1105	-
0.1488									
1106	-0.0418	1107	0.0059	1108	0.0048	1109	0.0048	1110	-
0.0105									
1111	-0.0557	1112	-0.0241	1113	0.0008	1114	0.0011	1115	
0.0023									
1116	-0.0013	1117	-0.0005	1118	0.0037	1119	-0.0021	1120	
0.0044									
1121	-0.0078	1122	0.0113	1123	-0.0082	1124	0.1432	1125	-
0.1517									
1126	0.1436	1127	-0.1513	1128	0.0362	1129	0.0074	1130	
0.0021									
1131	0.0003	1132	0.0015	1133	-0.0006	1134	0.0003	1135	-
0.0003									
1136	0.0035	1137	-0.0020	1138	0.0046	1139	-0.0038	1140	
0.0082									
1141	-0.0005	1142	0.0434	1143	0.0596	1144	-0.1536	1145	
0.1178									
1146	0.0053	1147	-0.0118	1148	-0.0170	1149	-0.0710	1150	
0.0004									
1151	-0.0010	1152	0.0023	1153	-0.0013	1154	-0.0002	1155	-
0.0005									
1156	0.0003	1157	-0.0025	1158	-0.0056	1159	-0.0049	1160	-
0.0079									
1161	-0.1491	1162	0.1475	1163	0.0188	1164	-0.1245	1165	
0.0041									

1166	-0.0131	1167	0.0119	1168	-0.0400	1169	-0.0339	1170
0.0014								
1171	-0.0012	1172	0.0031	1173	-0.0018	1174	-0.0008	1175
0.0066								
1176	-0.0038	1177	0.0040	1178	-0.0362	1179	-0.0204	1180
0.0185								-
1181	-0.0281	1182	-0.0173	1183	-0.0201	1184	-0.0469	1185
0.0083								
1186	0.0356	1187	-0.0403	1188	0.0045	1189	-0.0265	1190
0.0540								
1191	-0.0130	1192	0.0003	1193	0.0141	1194	-0.0081	1195
0.0299								-
1196	0.0009	1197	-0.0005	1198	-0.0001	1199	-0.0032	1200
0.0044								-
1201	0.0263	1202	-0.0002	1203	0.0003	1204	0.0004	1205
0.0001								
1206	-0.0083	1207	0.0091	1208	-0.0007	1209	-0.0004	1210
0.0007								-
1211	0.0004	1212	-0.0031	1213	0.0001	1214	-0.0232	1215
0.0005								
1216	-0.0003	1217	-0.0001	1218	0.0125	1219	-0.0072	1220
0.0058								-
1221	0.0207	1222	-0.0110	1223	-0.0019	1224	0.0106	1225
0.0007								-
1226	-0.0006	1227	-0.0007	1228	-0.0036	1229	0.0063	1230
0.0043								
1231	0.0074	1232	0.0073	1233	0.0005	1234	0.0087	1235
0.0001								

## List of Publications

1. Infrared spectra of dimethyl naphthalenes in gas phase, **Prasanta Das**, E. Arunan, Puspendu K. Das, *Vibr. Spectrosc.* **2008**, *47*, 1-9.
2. Production of paclitaxel by *Fusarium solani* isolated from *Taxus celebica*, B.V.S.K Chakravarthi, **Prasanta Das**, Kalpana Surendranath, Anjali A. Karande and Chelliah Jayabaskaran, *J. Biosci.* **2008**, *32*, 259–267.
3. Infrared Spectra of Dimethylquinolines in the Gas Phase: Experiment and Theory, **Prasanta Das**, S. Manogaran, E. Arunan and Puspendu K. Das, *J. Phys. Chem. A* **2010**, *114*, 8351-8358.
4. Isomeric identification of methylated naphthalenes using gas phase infrared spectroscopy, Shubhadip Chakraborty, **Prasanta Das**, and Puspendu K. Das, **Accepted** in *Ind. J. Phys.* **2010**.
5. Is there Intramolecular Hydrogen Bonding in Diols? An FT-IR and DFT investigation, **Prasanta Das**, Puspendu K. Das and E. Arunan, *Manuscript ready for submission in J. Phys. Chem. A* **2010**.
6. An Experimental and Theoretical investigation of IR spectra of dimethylphenanthrenes in the gas phase, **Prasanta Das**, E. Arunan and Puspendu K. Das, *Manuscript under correction*.